Optimisation for serviceability of fabric-formed concrete structures

Tayfur, Yadgar

Award date:
2017

Awarding institution:
University of Bath

Optimisation for serviceability of fabric-formed concrete structures

Yadgar Rafiq Tayfur

A thesis submitted for the Degree of Doctor of Philosophy

University of Bath
Department of Architecture and Civil Engineering

December 2016

[Blank]

Abstract

Concrete is one of the most widely used materials in the world. According to new research, as much as 40% of concrete used in conventional buildings does not serve a function (in carrying the applied loads) but does add extra selfweight to the structure. Such an inefficient use of concrete not only plays a role in increasing structural costs but also increases embodied energy. This is because cement production is shown to contribute around 5% of total global CO_2 emissions. A way to challenge this inefficiency (underutilisation of concrete material) is to structurally optimise concrete members so that their geometry reflects their performance requirements. The optimised concrete member shapes can then be realised using flexible formwork. Considering concrete beams, optimisation for strength is straightforward as it simply involves removing concrete from where it is unnecessary. However, strength-optimised concrete members show a significant loss in stiffness compared to an equivalent prismatic beam and this may make them fail to satisfy the equally important serviceability limit states (including deflections and cracking).

The optimisation of a beam to satisfy both strength *and* serviceability requirements simultaneously is much more complex than strength alone as it is not obvious where material should be added or removed along the member in order to satisfy the chosen serviceability criteria. In this thesis, research has been undertaken to develop numerical methods to optimise fabric-formed concrete structures for both ultimate and serviceability limit states. The theoretical part of this work has been implemented in two phases. In phase one, new numerical methods have been developed to predict the behaviour of both statically determinate and indeterminate beams. In the second phase, shape and topology optimisation methods have been developed to iteratively optimise those members for both strength and serviceability.

Laboratory experiments were carried out to verify the proposed methods, and the test results are shown to be in good agreement with the model prediction and optimisation criteria. A parametric study was conducted to investigate optimisation of statically determinate and indeterminate concrete beams and showed that up to about 30% reduction in concrete material can be successfully achieved without compromising strength and serviceability conditions. This work transforms flexible-formwork research into the realms of fully optimised form-found structures which satisfy both strength and serviceability. This is the first time that this research has been conducted, and it opens up the possibility for fabric-formed concrete structures to be used with confidence.

Declaration

The author wishes to declare that, except for commonly understood and accepted ideas, or where specific reference is made to the works of others, the content of this dissertation is his own work. This dissertation has not been submitted previously to any university of institution for any degree, diploma or other qualification.

Acknowledgement

Firstly, I would like to express my sincere gratitude to my supervisors Dr. Antony Darby, Prof. Tim Ibell, Dr. John Orr and Dr. Mark Everndon for the continuous support of my PhD study and related research, for their patience, motivation, and immense knowledge. Their guidance helped me in all the time of research and writing of this thesis. I could not have imagined having a better supervisors and mentor for my PhD study.

I am using this opportunity to express my gratitude to everyone who supported me throughout the course of this project, especially the kind and helpful staff of the labs in the department of Architecture and Civil engineering. I am thankful for my parents, my sisters and brothers and my friends, for their aspiring guidance, invaluably constructive criticism and friendly advice during the project work. I am sincerely grateful to them for sharing their truthful and illuminating views on a number of issues related to the project.

[Blank Page]

[Blank Page]

Table of contents

[Blank page]

[Blank page]

List of Figures

Chapter One

Chapter Two

Chapter Three

Chapter Four

Chapter Five

Chapter six

Chapter 7

[Blank page]

List of Tables

[Blank page]

Chapter One

Introduction

1.1 Introduction:

The construction industry is now confronted with a number of challenges among which are reduction in the energy consumption, efficient use of natural resources and reduction of carbon dioxide emissions (Zhong and Wu, 2015). The materials used in construction significantly contribute to the global embodied CO2 and embodied energy. Concrete is by far the most widely used material in the world with a total annual usage of more than 10 billion tons globally (Meyer, 2009). As can be seen in Figure 1.1, which presents the global usage for different families of materials, concrete significantly outweighs the other materials. This is mainly due to the numerous durability and mechanical advantages which concrete has over the other construction materials. Concrete is also generally low cost and readily available. It can be engineered to take any type of conceivable shape and have any set of rational performance specifications (Meyer, 2009, Ashby, 2013).

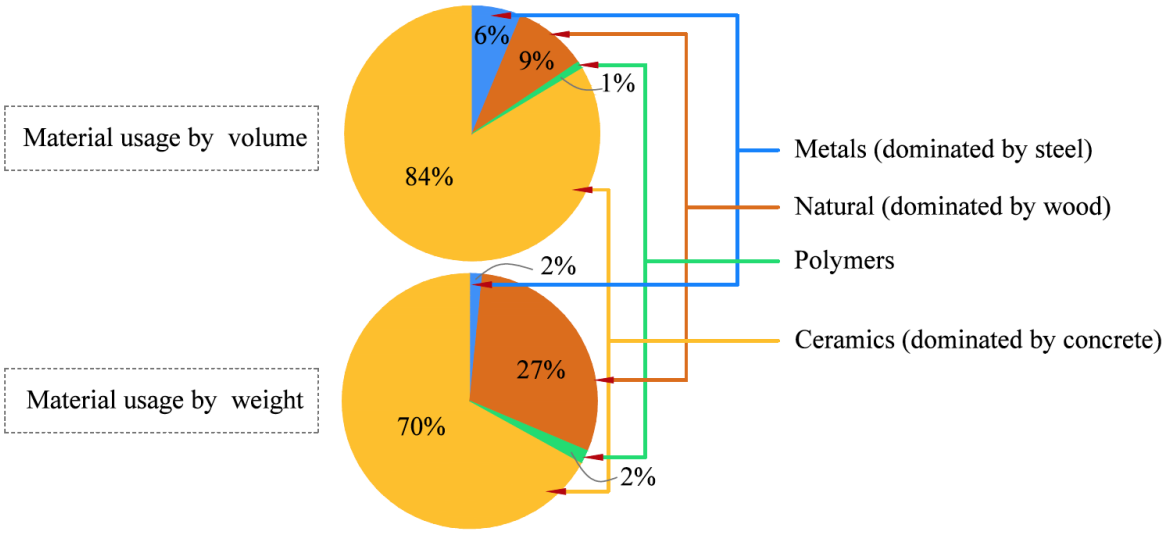

Figure 1.1: Global material usage by family (After Ashby, 2013)

Cement, as the key constituent of concrete, is produced from raw materials collected from the natural environment. Extracting, grinding and burning large volumes of such materials consumes a high amount of energy and that makes cement manufacturing responsible for 10% of total global man-made CO2 emissions (Long et al., 2015). This leaves serious environmental impact in terms of using up natural material resources, energy consumption and air pollution. Therefore, research interests have recently moved towards greener construction and sustainable development of concrete not only from a standpoint of cutting costs in building construction but also with a view towards a cleaner environment (Long et al., 2015, Landry, 2012, Sakai and Noguchi, 2012).

Structural designers are now faced with tremendous challenges. Among them is designing environmentally friendly structures through sustainable usage of concrete material. This can be done by putting only the necessary quantity of concrete material to the right place within the geometric boundaries of a single member or the whole structural system.

The shape of elements in a typical structural system usually reflects the desire for an easier construction process rather than performance requirements. This can clearly be seen in flexural members, for instance, beams are usually designed with a constant cross-section along their length as a prismatic form. The cross-section is designed for the critical case, whereas the magnitude of the applied stresses varies and hence the required resistance varies along the length.

Therefore, concrete structures can potentially be designed to be more material-efficient by using structural optimisation. The members in an ordinary structural system can be shaped based on the requirements of the loading envelope to use less material but serve the same purpose, resist the same loads, and provide the same levels of comfort to the occupants as a conventional prismatic structural system (Thirion, 2012).

Optimisation of concrete structures which results in consumption of less material and which offers opportunities to reduce embodied carbon may have been difficult in past due to the complicated computational work involved and difficulties in casting unusual optimised shapes using conventional formwork. When computers became widely available, the complicated calculations needed to design and analyse structural members with exceptional geometric properties became easier to perform. Combined with the availability of strong and cost-effective polyolefin textiles, this has made optimised non–prismatic structural members easy to design and cast in flexible fabric forms. This suggested reconsidering design and construction of reinforced concrete structures (West, 2001, Orr et al., 2011).

1.2 Structural optimisation

Structural optimisation can be used to design concrete members with the minimum possible amount of material for given loading and boundary conditions. This is done by designing structural components for maximum efficiency and by minimising the amount of under-utilised material in each member.

Optimisation methods can be classified by three categories as shown in Figure 1.2; 1) size optimisation, 2) shape optimisation and 3) topology optimisation. Size optimisation chooses an optimum size, shape optimisation tries to find the optimum shape among a number of possible shapes and topology optimisation attempts to find the best layout of a structure within a specific domain (or best material layout within the geometric boundaries of a member) (Bendose and Sigmound, 2003).

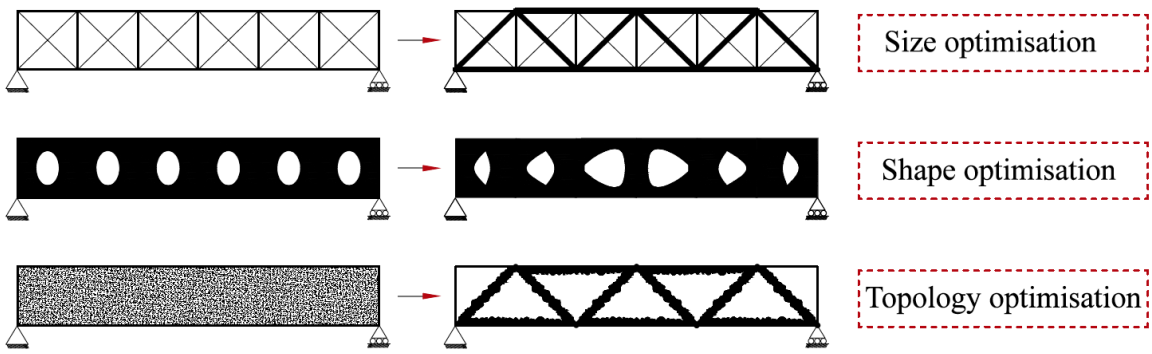

Figure 1.2: Categories of structural optimisation (After Bendose and Sigmound, 2003)

It is the purpose of this thesis to optimise concrete beams which satisfy ultimate and serviceability limit states while meeting buildability criteria when these members are cast in flexible fabric forms. All three optimisation categories are therefore necessary to optimise concrete beams. Size optimisation is applicable when the right amount of material is used for a member and any unnecessary and under-utilized material is taken away. Shape optimisation is necessary to optimise the member for the ultimate limit state by allowing the shape of the member to follow the shape of

the applied bending moment. Finally, topology optimisation is required to find the right layout of material to produce a member that satisfies the serviceability limit state criterion and meets buildability requirements imposed by fabric formwork technique.

1.3 Fabric formwork

Fabric formwork is a technique by which sophisticated shapes of concrete members to be cast in fabric membranes instead of rigid timber or steel forms. Due to high flexibility, the material deforms under static pressure applied by the wet concrete and takes a predictable shape. Apart from the advantage of using fabric formwork to cast optimised concrete members and from which saving of up to 40% of concrete material can be achieved (Orr et al., 2011), fabric formwork offers the following benefits:

- *Inexpensive, light weight and widely available formwork:* The light weight feature of geotextile fabrics often used in flexible forming system provides a great reduction in storage, handling and transportation costs and efforts. Suitable fabrics for construction applications are cheap and available worldwide, their cost is at least ten times less than that of plywood. The fabric can also be reused many times as it does not adhere to the surface of concrete (West, 2001, Kostova et al., 2013).

- *Stronger, more durable and sustainable concrete:* when wet concrete is poured into a permeable fabric form, the selfweight of the concrete causes the surface air and water to be pushed through the openings of the fabric. This results in decreasing the water/cement ratio of the cover concrete. Consequently, a concrete surface with higher compressive strength and less porosity is produced. This brings about reduced rate of carbonation and chloride penetration, better surface quality and improved durability as shown in Figure 1.3, (Kostova et al., 2013, Orr et al., 2011).

- *A new form of architecture for concrete structures:* architecturally elegant concrete structures are possible to be produced with fabric formwork. The combination of woven fabric membrane delivers texture and form. It is the limitation from the edges and pressure points that expresses a new language of architecture as shown in Figure 1.3, (Chandler and Pedreschi, 2007).

Figure 1.3: Fabric-formed concrete (CAST, 2007)

1.4 Problem

The main objective of designing a concrete structure is that it should fulfil the functions for which it was designed. It is hence crucial to ensure that the structure is both safe and serviceable through its lifetime. In order to satisfy ultimate and serviceability limit states, the structure should be strong enough to carry all the applied loads. Deflections should not be large enough to influence the appearance of structural components nor impact their functionality. The number and width of cracks under service loads should be kept below allowable limits so that they do not affect the durability of the concrete or make the structure aesthetically undesirable.

When a concrete beam is designed for ultimate limit state only, its shape represents the requirements imposed by the applied moments and shear stresses. Therefore, the cross-section size varies along the length of the beam and in all but a few locations the cross-section size is smaller than that of an equivalent prismatic beam as illustrated in Figure 1.4.

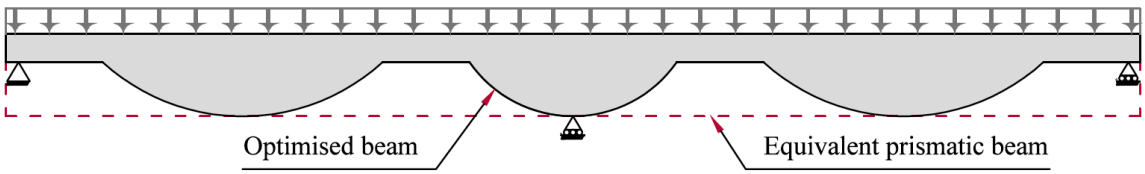

Figure 1.4: Variable section depth in optimised beams

However, compared to an equivalent strength prismatic beam, an optimised beam experiences considerable reduction in flexural stiffness for two reasons. First, optimised concrete beams use a smaller amount of material, have smaller cross-sectional dimensions (Figure 1.4) and hence exhibit lower flexural stiffness values than unoptimised beams. Second, optimised concrete beams are

designed in such a way that the capacity of each section represents the applied bending moment and therefore the ratio of the applied moment to the cracking moment capacity is approximately constant along the beam. This allows cracks to form and propagate over a much longer region of the beam at earlier stages of loading than that of a prismatic beam reducing overall stiffness. These two reasons coupled together make the optimised beam less stiff and likely to fail to satisfy serviceability limit states. Therefore, it is necessary to optimise fabric-formed concrete beams for both ultimate and serviceability limit states.

The existing work on optimising fabric-formed concrete beams in the literature mainly deals with optimisation of simply supported beams for ultimate limit state only. No research work has yet been carried out on optimising simply supported fabric-formed beams for serviceability. Moreover, continuous concrete beams, are commonly used in structural systems yet no study has examined optimising continuous fabric-formed concrete beams for both ultimate and serviceability limit states.

1.5 Aims and objectives

The main objectives of the work carried out in this thesis are briefly outlined below:

1. To develop computational models to predict the behaviour of fabric formed concrete beams at both ultimate and serviceability limit states.
2. To develop numerical techniques to optimise statically determinate and indeterminate fabric-formed concrete beams for both ultimate and serviceability limit states.
3. To examine the parameters which affect the performance of the optimisation models for beams with different sizes, section shapes, reinforcement ratio and layout and loading types.

The thesis begins in Chapter Two with a review of literature related to work performed on fabric formwork and structural optimisation. Chapter Three deals with the theoretical models developed in this thesis to predict the behaviour of both statically determinate and indeterminate non-prismatic concrete beams. The models developed in this work to optimise concrete beams for both strength and serviceability are presented in Chapter four. Chapters Five and Chapter Six detail the experimental program carried out to verify the theoretical models and discuss the results respectively. Chapter Seven features a parametric study undertaken to assess the optimisation models.

Publications

Journal papers

- Tayfur, Y. R, Darby, A., Ibell, T., Evernden, M. and Orr, J. (2016), *Serviceability of Fabric-formed Concrete Structures*, World Academy of Science, Engineering and Technology International Journal of Civil, Environmental, Structural, Construction and Architectural Engineering, Vol: 10, No: 5.

Others:

- Poster presenter at '*Young Researchers conference*', The Institution of Structural Engineers, 2015.
- [Best Paper Award], Speaker at ICCBE 2016: *18th International Conference on Civil and Building Engineering*, Montreal, Canada May 16 - 17, 2016

[Blank Page]

Chapter Two

Literature Review

2.1 Preface

In this chapter, a review of previous work related to fabric-formwork, structural optimisation and analysis of behaviour of reinforced concrete beams is presented. Firstly, historical background and development, properties and construction and analysis methods of fabric-formed concrete as a technique to cast optimised concrete members are surveyed. Secondly, historical development and methods of structural optimisation are reviewed with a focus on shape optimisation technique which is used to design fabric-formed flexural concrete members. Finally, existing methods to analyse and predict the behaviour of reinforced concrete members including statically determinate and indeterminate members are reviewed, in particular the methods which can possibly be applied to non-prismatic fabric-formed concrete members.

2.2 Fabric formwork

2.2.1 Historical background

Fabric formwork is a method of forming concrete members in flexible fabric membranes which has been used for many years. Going far back to Roman times, some basic use of fabric formwork can be noticed in works of the Roman architect and engineer Vitruvius in construction of cofferdams by filling woven reed baskets with clay (Veenendaal et al., 2011b). The more significant development in this area however occurred in the second part of the 18th century and 19th century when different types of cost-effective fabrics became widely available due to the new technologies introduced by the Industrial Revolution.

Lilienthal (1899) invented a fabric-formed suspended floor system which is shown in Figure 2.1. This was formed by using a relatively impermeable type of fabric which was stretched over parallel timber joists. A wire mesh was then placed on the fabric to function as internal reinforcement and finally concrete was poured in successive layers.

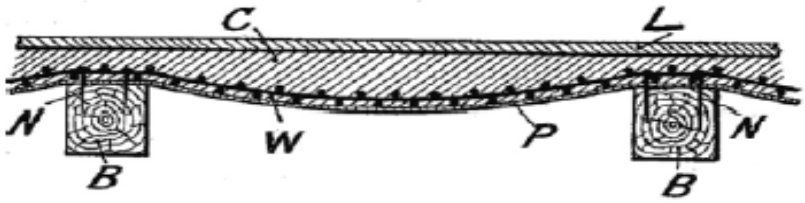

Figure 2.1: Fabric-formed floor system (Lamberton, 1968)

A patent application by Waller (1934) considers a similar floor system but with some addition to the idea. A canvas or woven fabric which is made from vegetable fibres is stretched as tightly as possible over a temporary wooden frame and then plastered with a slurry of cement mortar or any plastering material on both sides. Waller (1934) applied this concept to other building elements such as floor systems, walls, circular columns and tubular building members as shown in Figure 2.2.

Another application for a patent by Lamberton (1968) presents a new method of forming elongated concrete members such as bridge piers, caissons, shaft linings or tanks.

According to his method, a cementitious grout with a water cement ratio more than 0.45 is pumped into a permeable fabric form until excess water is pushed out through the pores of the fabric reducing the water cement ratio to about 0.3 and the fabric is fully inflated. At this point, the grout sets and it will no longer be flowable. Figure 2.3 shows details of the inflatable fabric form and a tubular concrete body.

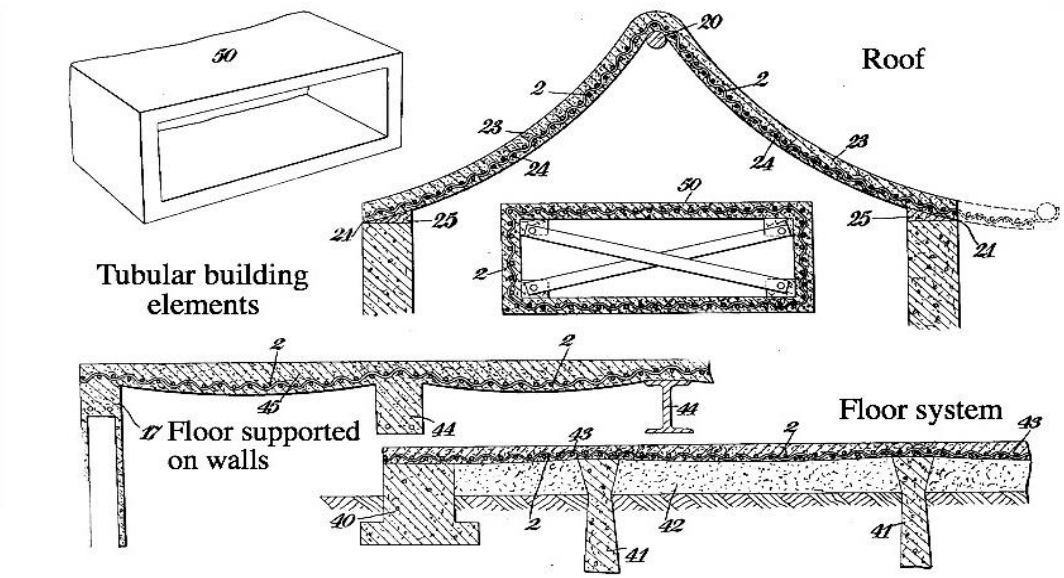

Figure 2.2: Patented fabric-formed building elements by (Waller, 1934)

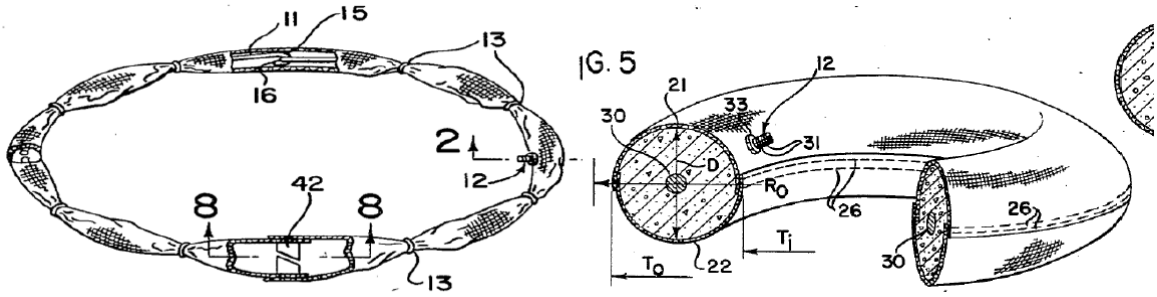

Figure 2.3: Tubular fabric form (left), cylindrical fabric-formed concrete body (right) (Lamberton, 1968)

The first architectural use of fabric formwork dates back to 1969 when the Spanish architect Miguel Fisac used smooth and flexible polyethylene lamina to give an attractive texture to concrete surface in the project Centro de Rehabilitación para la MUPAG in Madrid and later in Ybarra Hotel Tres Islas as shown in Figure 2.4.

In 1990's, Mark West of the University of Manitoba in Winnipeg, Canada, founded the Centre for Architectural and Structural Technology (CAST). This is considered to be an important turning point in using fabric formwork for casting concrete structures with the intention of discovering architectural and structural possibilities of this technique. Their work then led to international cooperation with other architects like Rick Fearn and Kenzo Unno and increasing awareness in the history of fabric-forming. Figure 2.5 shows fabric-formed panels cast by Kenzo and the formwork used. The experiments carried out by CAST combined structural and architectural functions of fabric formwork together. A variety of fabric-formed concrete members were cast, as shown in Figure 2.6, including highly expressive columns, beams and floor slabs with various shapes, highly optimized concrete trusses and double-curvature thin shells (Veenendaal et al., 2011b).

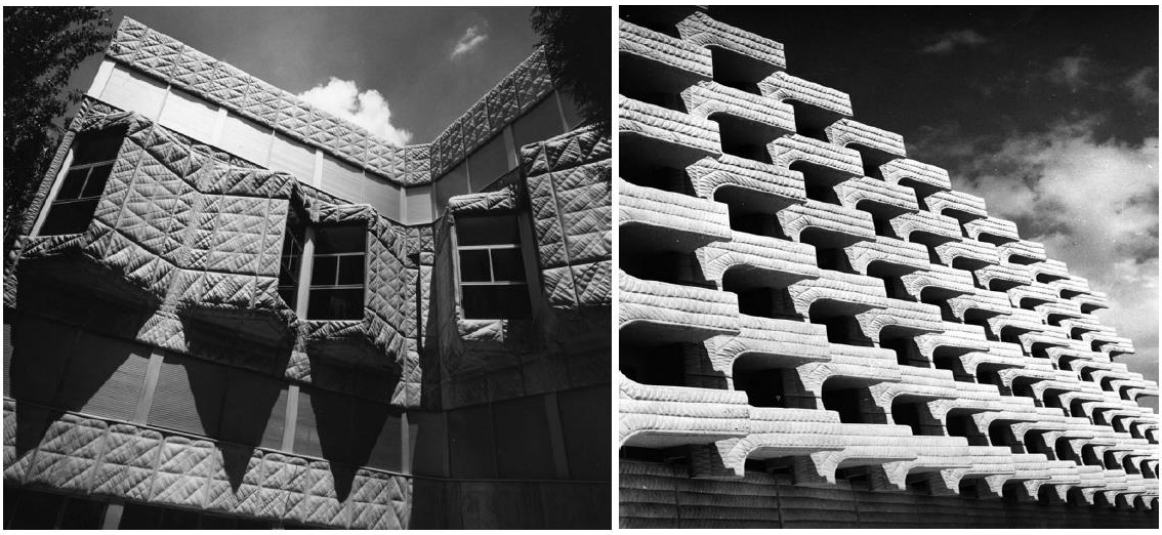

Figure 2.4: Centro de Rehabilitación para la MUPAG in Madrid (left), Ybarra Hotel Tres Islas (right) (Veenendaal et al., 2011b)

Figure 2.5: Zero-waste formwork (left), fabric formed concrete wall by Kenzo Unno (right) (Veenendaal et al., 2011b)

Figure 2.6: Fabric-formed wall Panels by CAST (Veenendaal et al., 2011b)

2.2.2 Properties of fabric-formed concrete

2.2.2.1 Durability

Decay in concrete members occur mainly due to existence of porosity in the concrete surface which allows for humidity and environmental penetration into the concrete surface (Orr, 2012).When concrete is cast in permeable fabric forms, excess surface mix water and air bubbles are pushed out through the openings of the membrane resulting in a reduction in the water cement ratio, porosity leading to a stronger and more durable concrete (Lamberton, 1968) (Provided that the right type of fabric with appropriate pore size is chosen as mentioned later in §2.2.2.2).

Orr (2012) conducted a number of accelerated durability tests on fabric cast concrete in terms of rate of carbonation, resistance to chloride ingress and surface hardness. Orr (2012) also tested concrete specimens cast against conventional steel moulds and fabric moulds in order to see the surface quality improvements achieved in fabric cast concrete compared to that of steel cast concrete. The experimental results indicated that, a 50% improvement in durability against carbonation and chloride ingress into concrete and a 13% improvement in concrete surface hardness were achieved when fabric forms are used to cast concrete instead of conventional moulds.

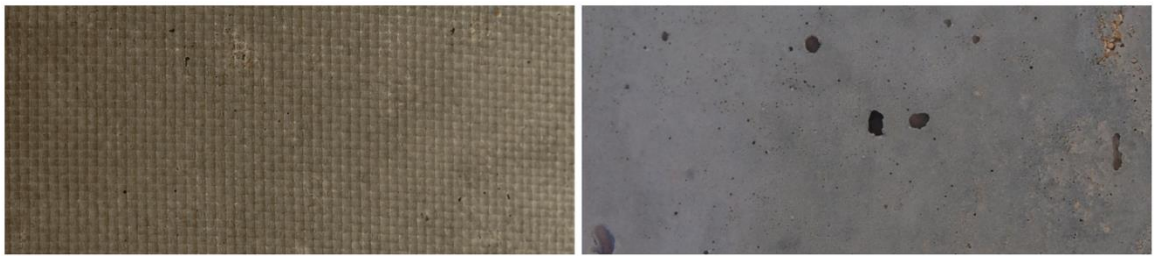

Figure 2.7: Fabric-formed concrete surface (left), timber-formed concrete surface (right) (Orr, 2012)

The surface quality of fabric cast and timber cast concrete samples are shown in Figure 2.7.

2.2.2.2 Compressive strength

When designing fabric-formed concrete members, it is vital to choose the right type of fabric for a specific concrete mix. The pore sizes of the fabric affect the amount of water and cement content discharged through the surface of the formwork which may eventually affect the compressive strength of the surface concrete.

Ghaib and Gorski (2001) studied the influence of fabric type and concrete mix on the compressive strength of concrete. They tested twelve sets of cubes (232 samples) cast in four different types of textiles with different pore sizes. The cubes were then subjected to destructive tests. Their results showed that, the compressive strength of fabric cast concrete samples was a function of the pore size of the fabric. For very small pore sizes, the compressive strength decreased probably due to

clogging of the fabric pore that prevents the surface free water from escaping. For larger pore sizes on the other hand, the compressive strength again decreased which, according to them, may be attributed to loss of cement content. They found the optimum fabric pore size to be 0.35 x 10^{-3} to obtain the highest compressive strength.

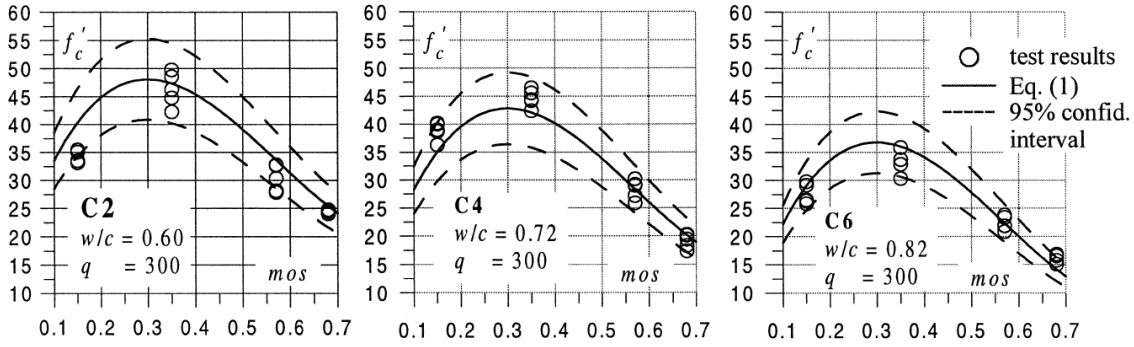

Figure 2.8: Graphical interpretation for concrete mixes with different water cement ratio (Ghaib and Gorski, 2001)

Figure 2.8 shows the relationship between 28 days compressive strength of concrete mixes, water cement ratio and fabric pore size.

2.2.3 Form finding

Fabric formwork usually consists of two parts, a flexible textile and a rigid frame that carries the load of the concrete-filled fabric container. When wet concrete is poured into a highly flexible form, the form deflects under the fluid static pressure and takes a shape that is defined by the fabric and rigid formwork constraints. Various researchers have been able to successfully predict the shape of fluid-filled membrane in a number of ways which are explained in the following sections.

2.2.3.1 Empirical methods

Bailiss (2006) used test data to develop a number of empirical equations representing the relationship between the perimeter, top breadth and depth of a fabric envelope filled with a fluid. This was done through a number of tests on a strip of hanging fabric enclosed in a glass-sided box shown in Figure 2.9. The fabric was then filled with a viscous fluid to model the hydrostatic shape of a concrete-filled form. The length of the fabric strip and the width of the top opening were varied and in each stage the measurements of top breadth, perimeter of the fabric and depth of the liquid were recorded. Photographs of cross-sections were taken in order to calculate the area of the envelope.

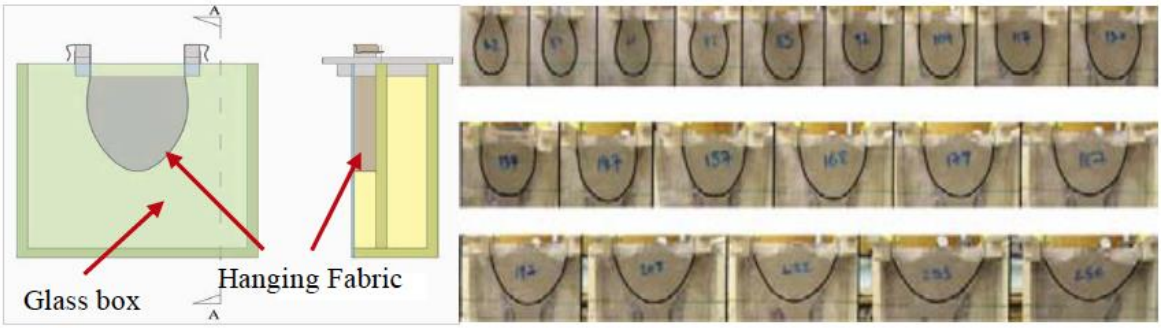

Figure 2.9: Rig with hanging fabric in glass box (left), hydrostatic shapes (right) (Bailiss, 2006)

Finally, Equations 2.2, 2.3 and 2.4 were developed to find the perimeter of the fabric P, and the cross-section area of the fabric mould A if the top breadth B and the liquid depth D are known.

$$\frac{B}{D} = -0.49\left[\frac{B}{D}\right]^2 + 0.212\left[\frac{B}{D}\right] + 0.396 \quad for \quad \left(\frac{B}{D} > 0.1\right) \tag{2.1}$$

$$P = \frac{-(0.212B - D) \pm \sqrt{(0.212B - D)^2 - 4{\times}0.396{\times}(-0.49B^2)}}{2{\times}0.396} \tag{2.2}$$

$$A = \left[\left\{\frac{\left[\frac{B}{P}\right] - 0.05}{0.65}\right\}^{-0.3} - 0.34\right]{\times}(B{\times}D) \quad for \quad \left(\frac{A}{(B{\times}D)} > 0.1\right) \tag{2.3}$$

The above equations allow sufficiently accurate calculation of area and perimeter but do not indicate how material over the section is distributed which is often necessary for optimisation. Garbett et al. (2008) further investigated the test data collected by Bailiss (2006) and derived equations to determine the maximum width of the cross-section W and its location within the depth H as follows.

$$W = \left(3.2016{\times}\left(\frac{B}{D}\right)^2 - 5.7721{\times}\left(\frac{B}{D}\right) + 3.6111\right){\times}B \tag{2.4}$$

$$H = \left(-0.3263{\times}\left(\frac{B}{D}\right)^2 + 0.6659\right){\times}D \tag{2.5}$$

Equations 2.4 and 2.5 help defining the cross-section of the fluid-filled fabric mould more comprehensively. However, the exact deformed shape of the fabric can still not be accurately plotted using the above equations.

2.2.3.2 Mathematic approach

Iosilevskii (2010) produced a closed-form solution to find the hydrostatic shape of a flexible container filled with fluid from a mathematical perspective.

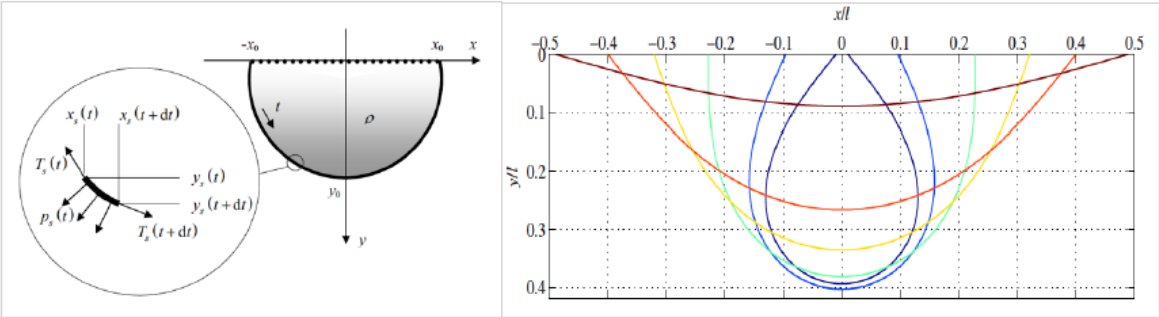

Figure 2.10: Free body diagram of an element on a fabric mould filled with liquid (left), variable cross-sections (Iosilevskii, 2010)

Equilibrium of a small element on the perimeter of the fabric envelope was considered as shown in Figure 2.10. Iosilevskii's method included solving a set of deferential equations and solved by using incomplete elliptic integrals. Finally, a set of equations are given to create the shape of the envelope as a function of maximum depth and breadth of the fabric mould as given below:

$$\frac{x_s}{l} = \frac{E(\theta_s, k)}{K(k)} - \frac{1}{2}\frac{F(\theta_s, k)}{K(k)} \tag{2.6}$$

$$\frac{y_s}{l} = \frac{k}{K(k)}\, cos\theta_s \tag{2.7}$$

$$\frac{t}{l} = \frac{1}{2}\left(1 + \frac{F(\theta_s, k)}{K(k)}\right) \tag{2.8}$$

$$V = l^2 \frac{k\sqrt{1-k^2}}{K^2(k)} \tag{2.9}$$

Where x_s *and* y_s are coordinates on the cross-section, l is the width of the fabric, $E(\theta_s, k)$is an incomplete elliptic integral of the second kind, $F(\theta_s, k)$ is an incomplete elliptic integral of the first kind, $K(k)$ is respective complete integral, θ_s is an auxiliary function on $[0, l]$, t is the distance measured from one edge along the fabric perimeter, V is the area of the cross-section.

Using the above equations given by Iosilevskii (2010) the exact shape of cross-sections of fabric formed concrete members can be found. Predicting the exact shape and knowing where the material is located within the cross-section is important, especially when optimisation for section shape is conducted to find an optimum material layout that produces the best section performance for the minimum area of material.

2.2.3.3 Pseudo-dynamic approach

A finite element analysis based on dynamic relaxation method was used by Veenendaal (2008) to form-find a fabric mould filled with wet concrete. Dynamic relaxation is a pseudo-dynamic process that combines static solution of a given problem with the properties of damped structural motion. In

this method, the fabric shape is discretized into a number of triangular two dimensional elements connected by nodes as shown in Figure 2.11(left), the nodes are then set in motion by applying an external load that is converted to acceleration of the loaded nodes. The movements of nodes continue until static equilibrium between the external and internal elastic stresses is reached due to kinetic damping.

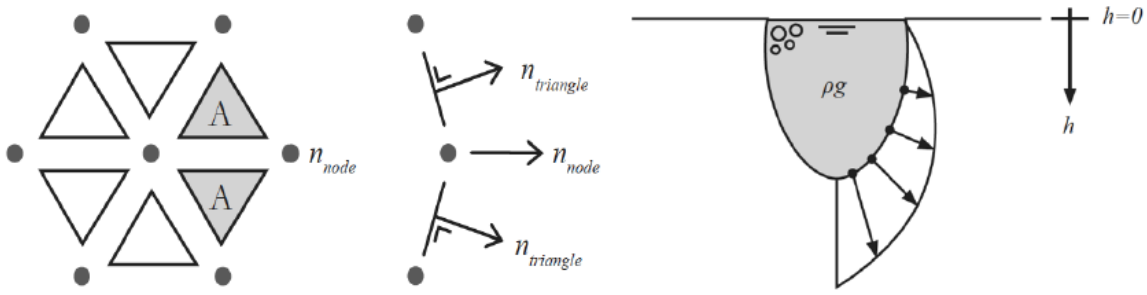

Figure 2.11: Discretized fabric and applied nodal and elemental forces (left), the fabric mould under hydrostatic forces (right) (Veenendaal, 2008)

The perpendicular force applied by the hydrostatic pressure of the wet concrete is found on each element and translated to nodal motion in Figure 2.11(right). The area of each element is found according to:

$$A = \sqrt{s(s-a)(s-b)(s-c)} \tag{2.10}$$

$$s = \frac{a+b+c}{2} \tag{2.11}$$

Each triangle is then represented by vectors u, v and w with length a, b and c respectively, the normal vector is then given as below:

$$n_{triangle} = u \times v = \begin{bmatrix} u_y v_z & u_z v_y \\ u_z v_x & u_x v_z \\ u_x v_y & u_y v_x \end{bmatrix} \tag{2.12}$$

the normal vector of each node is then calculated as weighted sum of all triangle normals connected by the node:

$$n_{node} = \sum \frac{n_{triangle}}{A_{triangle}} \tag{2.13}$$

The unit vector is determined and from this the load applied to the node by the wet concrete is calculated as below:

$$\hat{n}_{node} = \frac{n_{node}}{\|n_{node}\|} \tag{2.14}$$

$$q_c = \rho g h . \hat{n}_{node} \tag{2.15}$$

Veenendaal (2008) added the interaction effects between the fabric and the edges of the rigid frame to his analysis by employing specific checks to control folding of the fabric along the edges of the supporting frame. Temporary nodes are inserted in those elements that fold over an edge in order to allow for the correct length of the element to be calculated, as shown in Figure 2.12.

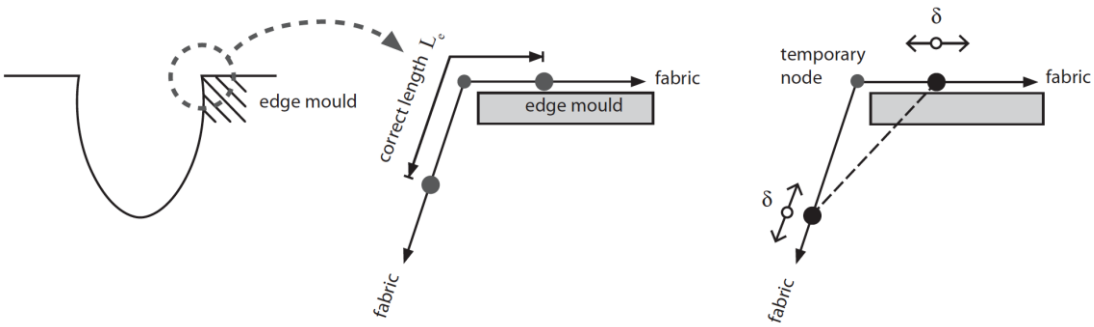

Figure 2.12: Check and correction for elements that span across an edge (Veenendaal, 2008)

This method can give a fairly accurate indication of a three-dimensional mould shape and it was successfully applied to form-find concrete beams. However, it needs relatively high computational effort compared to other form-finding methods and its application requires a finite element software.

2.2.3.4 Static approach

Foster (2010) developed a step-wise analysis procedure to solve the form-finding problem of fabric formed concrete beams. Equilibrium condition of in-plane forces resulting from the hydrostatic pressure of wet concrete and the tensile resistance of the fabric form is considered. Foster divides the beam into a number of sections and analyses each two-dimensional transverse section to find the curvature of the fabric at any level within the depth. All out-of-plane forces and displacements are assumed to be negligible.

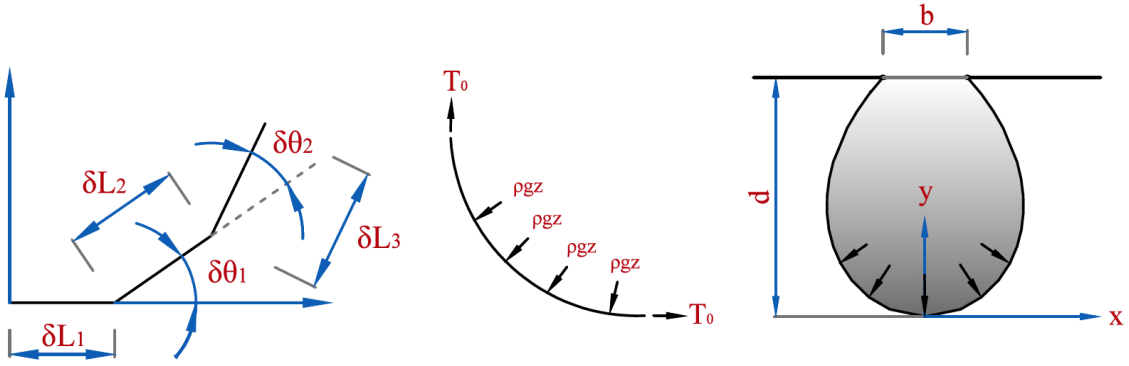

Figure 2.13: Applied forces and coordinates of fabric mould filled with concrete (Foster, 2010)

The fabric is assumed to be vertical at the hanging nodes and its self-weight and stiffness are neglected. It is also assumed that the tensile force in the fabric is constant along its perimeter and can be found from equilibrium as follows:

$$T_0 = \frac{\rho g z}{k} \qquad (2.16)$$

Where ρ is the density of the filling liquid, g is the gravitational acceleration, z is hydraulic height and k is variation in curvature.

A walking-out procedure is carried out from the point of origin (very bottom point of the concrete-filled fabric mould) along the perimeter according to the relationship between the curvature and hydrostatic depth. Depending on the value of an assumed coefficient K, a group of curves can be created. The correct curve is then chosen according to the boundary conditions. In this case, the boundary conditions are $y \approx d$ and $x \approx 0.5b$, where x and y are coordinates, d is the total depth and b is the top breadth as shown in Figure 2.13.

The trial cross-section shape of the fabric that is deflected under the fluid pressure can be created using the following expression:

$$(x_n, y_n) = \left(\delta L \sum_{i=1}^{n} cos \sum_{j=1}^{i-1} \delta\theta_j \, , \delta L \sum_{i=2}^{n} sin \sum_{j=1}^{i-1} \delta\theta_j \right) \qquad (2.17)$$

Where:

$$z_n = z - y_n \qquad (2.18)$$

$$\delta\theta_n = k z_n \qquad (2.19)$$

Foster (2010) revisited the form-finding equations proposed by Bailiss (2006) and Iosilevskii (2010) which were mentioned in §2.2.3.1 and §2.2.3.2 respectively and found a good agreement between the predictions made by these methods and the walking-out procedure proposed. An improved version of equation (2.1) was then suggested as below:

$$\frac{D}{P} = -2.0424\left(\frac{B}{P}\right)^5 + 3.9928\left(\frac{B}{P}\right)^4 - 2.8385\left(\frac{B}{P}\right)^3 + 0.5239\left(\frac{B}{P}\right)^2 + 0.0328\left(\frac{B}{P}\right) + 0.3935 \qquad (2.20)$$

Once the cross-section shape is found at each section along the length of a fabric-formed concrete beam, they are connected together in order to find the full shape of the beam.

This method is quite accurate and simple to apply. The calculations can easily be made in Excel spread sheets or any programming software such as Matlab. Since this method relies on a section-based procedure, it is easy to implement the data in a sectional analysis procedures carried out on

fabric-formed beams. For these reasons, this method was used in the analysis and optimisation procedure of fabric formed beams carried out in this thesis and explained further in §4.8.

2.2.4 Construction techniques

Available construction methods for fabric-formed concrete beams are limited to a few methods depending on the desired cross-section shape. What defines the form and eventual shape of the beam are the elastic modulus and the dimensions of the fabric sheet, the restrictions applied by the rigid edges of the temporary framework holding the fabric, pretensioning applied to the fabric and the unit-weight of the wet concrete.

2.2.4.1 Freely hung fabric method

This method consists of simply hanging the fabric between two parallel rigid supports (usually a timber frame) without applying pretensioning or restrictions to the fabric anywhere between the supporting edges. However, the fabric is stretched while stitched to the formwork panels in order to avoid wrinkles. The concrete mix is then poured into the fabric mould and the fabric is allowed to freely bulge under the hydrostatic pressure of wet concrete.

This method was used by Bailiss (2006) and Garbett et al. (2008) to cast simply supported fabric-formed beams (Figure 2.14).

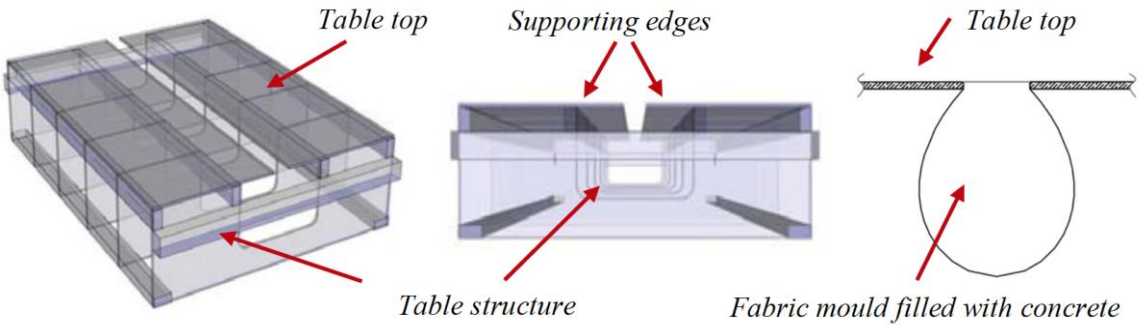

Figure 2.14: Table form (Bailiss, 2006)

Due to simplicity and minimal labour required compared to the other methods, this method was used to cast a continuous fabric formed beam in the work carried out for this thesis which is further described in Chapter Five.

2.2.4.2 Spline mould method

In this method, the fabric is fixed on a timber forming table in a way similar to the previous method. Then a metal bar is used to vertically pretension the fabric sheet in order to reduce the area of tensile concrete (Orr, 2012). Figure 2.15 shows the forming details. This method was first used by the Centre for Architectural and Structural Technology (CAST) as shown in Figure 2.16.

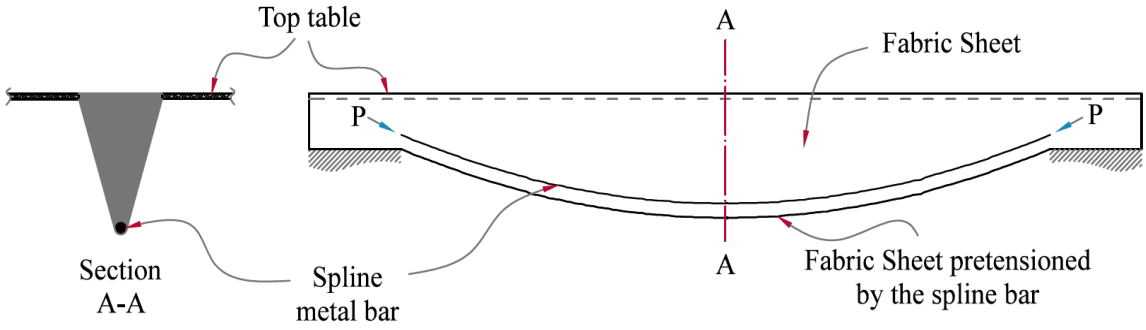

Figure 2.15: Spline mould method

Figure 2.16: Spline mould (left), concrete beam cast in spline mould by CAST (right)

2.2.4.3 Keel mould method

The required fabric-formed beam profile is achieved in this method by cutting two sheets of plywood referred to as keel to the longitudinal desired beam shape as shown in Figure 2.17. Two fabric sheets are supported at the top of parallel supporting rigid timber frames and restrained on the bottom by the keel which defines the bottom boundary of the beam. This method was used by Orr (2012) to form fabric-formed double T-beams shown in Figure 2.18. CAST also built a number of beams using this method; the forming method and the final beam shape are shown in Figure 2.19.

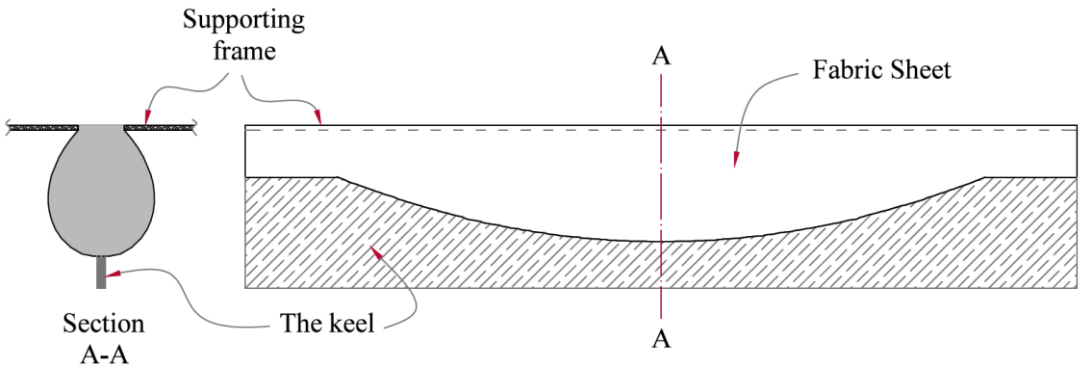

Figure 2.17: Keel mould method

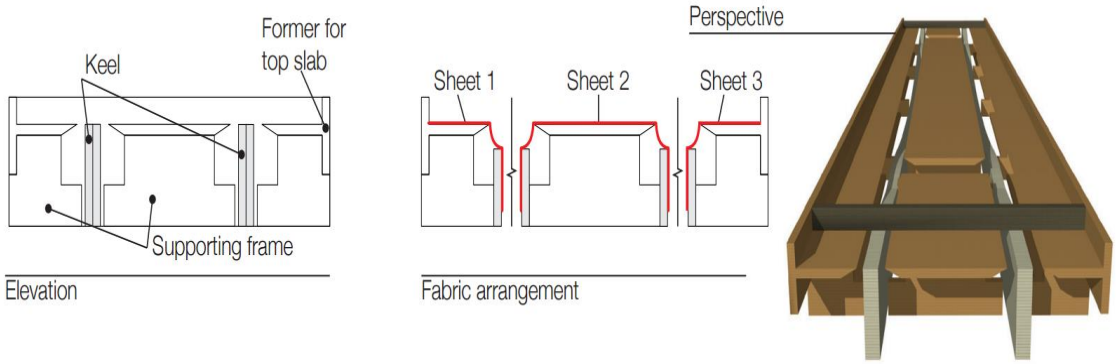

Figure 2.18: Keel mould used to cast fabric-formed double T-beams by (Orr, 2012)

Figure 2.20: Fabric-formed beam cast in keel mould by CAST

2.2.4.4 Pinch mould method

This method is more sophisticated and requires more labour compared to the other forming methods, but the beam shapes achieved by this method are more exciting and offer a significant reduction in the amount of material used. It is mainly used to cast reinforced concrete trusses by putting openings in the web of a beam with the desired sizes and at the desired locations.

Figure 2.20: Pinch mould method (left), fabric-formed concrete truss (right) by CAST

This method uses two fabric sheets sandwiched by wooden panels that have protruding elements. These elements "pinch" the fabric mould together to form openings in the beam as illustrated in Figure 2.20. A wide range of plaster models, as well as larger concrete specimens, were created by CAST towards discovering possible benefits of pinch moulding.

2.2.4.5 Keyhole mould method:

This method was used by (Garbett et al., 2008) aiming to reduce the width of concrete beam webs in the tensile region. This was done by applying timber web formers on both sides of the beam thus restricting this part of the web to a desired size. Details of this method are shown in Figure 2.21.

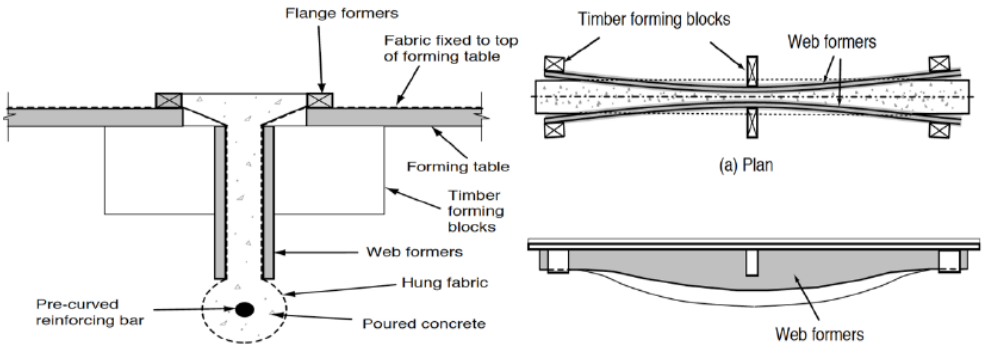

Figure 2.21: Details of key mould method use by Garbett et al. (2008)

2.3 Structural optimisation

2.3.1 Historical background

Structural optimisation and attempting to reduce the amount of material used in structures has always been a point of interest for designers, since the time of the Pantheon in Rome, 126 AD, where a shell was created with variable thickness and density along its span (Thirion, 2012). Perhaps, the first successful attempt to optimise a beam dates back to the time of Galileo (1638) when he predicted the shape of a cantilever beam required to resist an applied bending moment from the selfweight and a load hanging at its tip (Figure 2.22).

Galileo (1638) explains how one can diminish about one-third of the size of a beam like this without diminishing its strength. His primary intension was to reduce the weight of the beam as lightness according to him is of prime importance especially in manufacturing structures like the deck of large vessels.

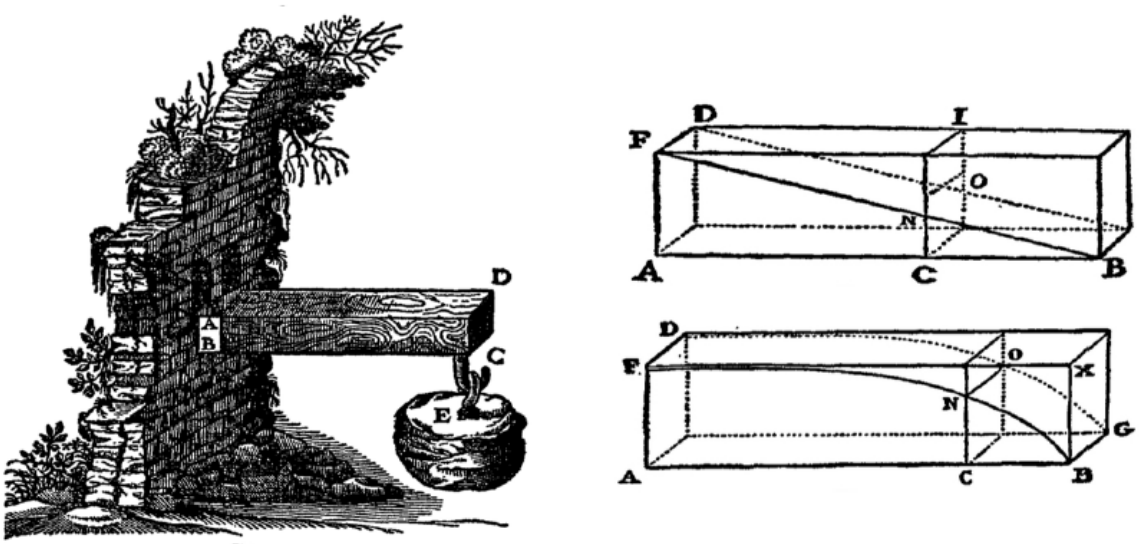

Figure 2.22: Cantilever beam considered in Galileo's Dialogues (Galileo, 1638)

In the last few decades, various structural optimisation methods have been developed and applied to a wide domain of problems. Such optimisation methods have been mostly aimed at finding an optimal cost or an optimal weight of a given structure. Depending on the algorithms used in searching for an optimum solution, optimisation methods can be divided into deterministic and probabilistic methods (Kripka et al., 2015). However, depending on the optimisation parameter which need to be optimised within a given design domain, optimisation problems can be classified as size optimisation, shape optimisation and topology optimisation.

2.3.2 Deterministic method:

Deterministic methods are used to solve problems that have continuous variables for which the derivative can be found. These methods are relatively simple and straightforward and do not require high computational effort (Kripka et al., 2015, Degertekin, 2007). Deterministic optimisation problems always converge to the same solution regardless of the initial conditions and starting points providing that optimisation parameters are fixed. This method is unable to find the global optima when a number of local optima exists (Thirion, 2012). However, problems with continuous variables can mathematically be directed towards finding the global optima as explained later in chapter five.

2.3.3 Probabilistic Method:

Probabilistic methods, which are often referred to as heuristic or stochastic methods, deal with discontinuous variables and directly search for solution in a given design space without need for calculating derivatives. Probabilistic methods use a large number of algorithms and therefore are expensive and time-consuming in terms of computational effort required (Thirion, 2012, Kripka et al., 2015). These methods are usually used when a high number of variables exist in the design space and the optimisation model is expected to find the best combination of these variables to achieve a certain objective function. For example, the process of optimising reinforced concrete frames for minimum cost involve a considerable number of parameters that can be width and depth of structural members, reinforcement ratio, layout, material grade and so on.

The most popular examples of this type of optimisation are simulated annealing and genetic algorithms. The variables in optimising concrete structures are usually discrete variables. For instance, size of reinforcing bars is subject to availability of standard sizes. The behaviour of concrete is non-linear due to occurrence of cracks and therefore derivatives of such behaviour cannot be calculated. Hence for most practical structural design problems heuristic methods are considered.

2.3.4 Size optimisation

The goal in a typical size optimisation problem is to find an optimum size of an element or a number of elements that return a maximum or minimum physical quantity such as deflections or maximum stress (Bendose and Sigmound, 2003). In optimising concrete structures, the design variable is often the size of its components and the state variable can be one of the limit states. Previous work on this type of optimisation for reinforced concrete structures has mostly been carried out to find the depth and width of prismatic concrete members.

Kripka et al. (2015) formulated a numerical procedure to optimise reinforced concrete beams in a structural system for minimum cost. The cross-sectional size of the beams was taken as the major optimisation problem variable. They used the simulated annealing method to govern the optimisation procedure by taking both the ultimate and serviceability limit states into account.

Simulated annealing is a method that simulates the heating and cooling process of metals, as its name indicates, in order to arrive at a minimum energy state provided that the cooling process is sufficiently slow. Quick cooling however, leads to faster crystallization and a weak and brittle structure.

They also applied a grouping technique to unify the size of groups of beams in order to simplify the construction process. According to their results, the simulated annealing method provides a significant reduction in the total costs and the amount of concrete material used.

Mehta et al. (2013) used bi-direct exhaustive search method to find an optimum size and material grade for reinforced concrete beams that produces cost-optimum beam design. Exhaustive direct search method is an optimisation technique that is assessing design and objective function for each set of discrete decision variables and chooses a combination that yields a low cost feasible design.

Mehta et al. (2013) only considered discrete values of the optimisation parameters. For example, the width b and depth d of the concrete beams were selected according to the size of the formwork. Both doubly and singly reinforced concrete beams were considered, allowing a single design zone at a critically loaded section for which the reinforcement layout was designed and extended throughout the length of the beam. They presented charts to demonstrate the variation of optimum cost and feasibility of design according to codified limitations for different beam sizes b & d.

Mehta et al. (2013) classifies optimisation parameters in designing reinforced beams by three categories:

a) Independent decision variables: there variables are independently chosen by the optimisation procedure for a feasible and cost-optimum design. Discrete values for each parameter are pre-assigned first and the optimisation procedure is allowed to choose the best combination. The depth, width, compressive strength of concrete and tensile strength of concrete belong to this category.

b) Pre-assigned design decision variables: These values are pre-assigned for any individual optimisation procedure prior to design and they can be dependent on independent decision variables. Examples of this type of parameters are length of the beam, design loads, section layout type (i.e. singly or doubly reinforced).

c) Dependent design decision variables: these are values which are dependent on independent decision and pre-assigned design decision parameters but are also based on strict code defined values. Minimum and maximum areas of steel reinforcement and maximum allowable concrete shear resistance are examples of these types of variables.

2.3.5 Shape optimisation

Shape optimisation tries to find an optimal shape of an element that produces maximum performance in terms of the state variables defined in the optimisation process (Bendose and Sigmound, 2003). The upper and lower bound shapes are defined in the optimisation process along with limitations on displacement and stresses. Some of the successful practical applications of shape optimisation are seen in designing bridges, dams, pressure vessels, torque arms,…etc., (Ding, 1986). This class of optimisation has extensively been used and investigated for steel-made elements because manufacturing complicated geometries, which are the usual outcome of shape optimisation procedure, is easier compared to forming shape-optimised concrete members.

2.3.5.1 Simply supported beams

Thirion (2012) shape optimised steel I-beams in order to arrive at the minimum weight and minimum embodied CO2 design under a uniformly distributed loading condition. Considering both the ultimate and the serviceability limit states, Thirion (2012) carried out the optimisation procedure by using Sequential Quadratic Programming (SQP) algorithm which is a deterministic gradient-based method that works on problems where the objective and constraint functions are multi-variable non-linear functions (but they are continuous and have continuous first derivatives).

The analysis was conducted by dividing the beams into a number of equal segments and carrying out sectional analysis to check the performance of the beam in each optimisation step. His results indicated that shape optimisation can produce optimised beams with up to 40% of saving in material compared to their equivalent catalogue sized counterparts.

In spite of the fact that concrete cannot be considered homogenous, as steel is, the results achieved by Thirion (2012) are important as they may indicate that concrete beams can similarly be shape optimised using a sectional analysis method to save a considerable amount of material without compromising performance. The aving in material for a concrete member can potentially be more compared to steel members because concrete can take any conceivable shape unlike steel members which are prefabricated with a limited range of standard sizes.

Rath et al. (1999) used a rather sophisticated method to shape optimise simply supported reinforced concrete beams by using finite element modelling. They used the Sequential Quadratic Programming technique to find the optimal shape of the beams and genetic algorithms to find the reinforcement topology (number and diameter of longitudinal steel bars). The objective function of the main optimisation problem was the total cost of the beam, however, the cross-sectional area was taken as the objective function in optimising the shape of the sections. A limit state design method was employed to design for flexure and shear using sectional analysis procedures. Serviceability deflections were also checked based on effective second moment of area. Manufacturability

constraint in terms of minimum specified spacing between the reinforcing bars and adequate cover was also included. The optimisation started from a rectangular prismatic beam as a reference point and final outcome was an I-shaped variable section depth beam with nearly 40% saving of material compared to the reference beam.

Although serviceability deflection was taken into consideration, strength criteria governed the designs. It is not indicated how serviceability criteria was handled in the optimisation problem when the maximum deflection value exceeds the allowable limit.

Using commonly used rigid forms to cast concrete members limit their shape to prismatic shapes. Fabric formwork, as a technique for casting curvaceous optimised concrete members, has recently led to an increase in research work in the area of shape optimisation in concrete structures. The shape of fabric-cast concrete members can be accurately predicted and simple form-finding techniques can be implemented into the commonly used optimisation methods.

Bailiss (2006) shape optimised four fabric-formed concrete beams based on different loadings and construction methods. The beams were designed for five loading points and the final shapes were enclosed in parabolas so as to simplify the construction processes. Plastic theory and a sectional analysis procedures were used to optimise the beams subjected to both symmetrical and asymmetrical loading arrangements.

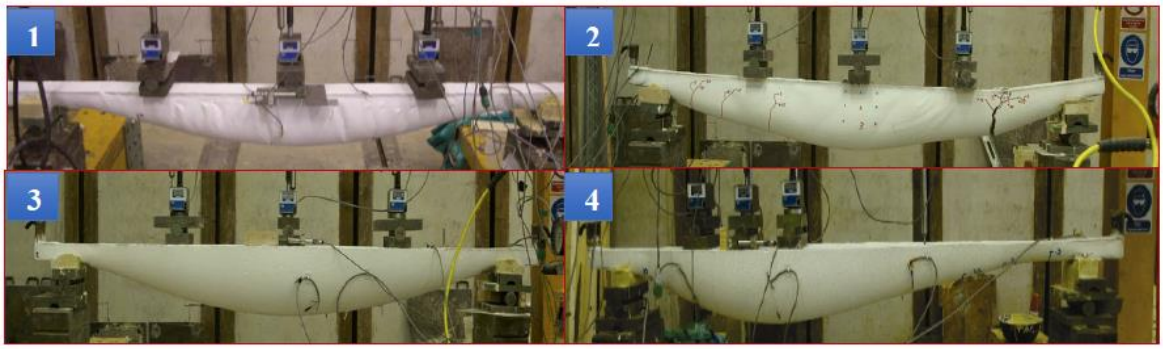

Figure 2.23: Fabric-formed bending moment-shaped beams (Bailiss, 2006)

The main challenge facing the manufacturing processes of shape optimised concrete members is dealing with the constraints in the construction process caused by the reinforcement and the unusual curved shape. Bailiss (2006) tried different types of fabric to construct the shapes produced by the optimisation procedure and there were issues relating to attaining the designed depth, a smooth outer face and the correct reinforcement layout especially in beam one and beam two as shown in Figure 2.23. Therefore, premature shear failure occurred in the beams and the theoretical capacity of the failed sections had to be re-calculated according to as-built cross-section layout. Although the plastic analysis underestimated the failure load of all the beams, this study can be seen as one of the very

first studies into structural optimisation of fabric formwork as a concrete casting technique that was previously used predominantly for architectural purposes.

Garbett et al. (2008) used a sectional analysis procedure to optimise fabric-formed concrete beams for bending moment and shear stresses. The cross-sections along the beams were designed according to the limit state design provisions of BS 8110-1 (1997). The goal was to minimize the amount of material used through 1) varying the depth of the beam as per the requirements of the applied loading and 2) optimising the cross-section shape by considering different sectional parameters shown in Figure 2.24.

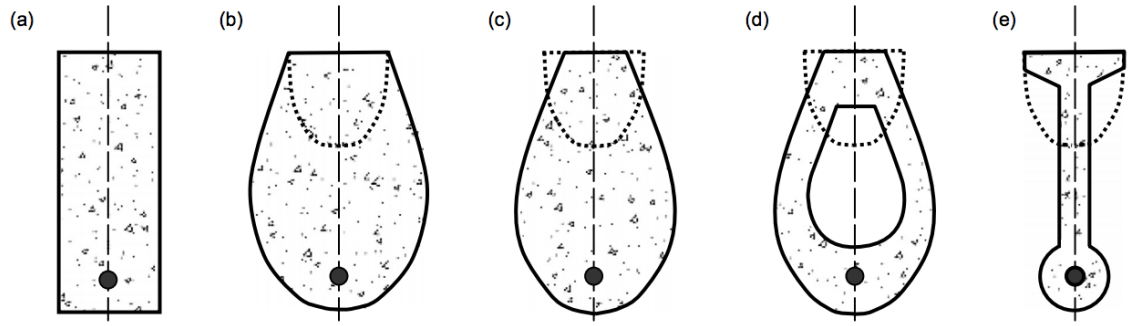

Figure 2.24: Optimisation process of cross-sections of fabric-formed beams (Garbett et al., 2008)

They fabricated and tested two beams, one of which was optimised by allowing the depth and the top breadth to vary along the length as shown in 2.24 (c) and Figure 2.25 (right) and the other one was a keyhole shaped beam shown in Figure 2.24 (e) and Figure 2.25 (left).

Compared to an equivalent prismatic beam shown in Figure 2.24 (a), their results showed 25% of saving in concrete material for the beam with variable depth and top breadth and 55% of material saving for the keyhole shaped beam.

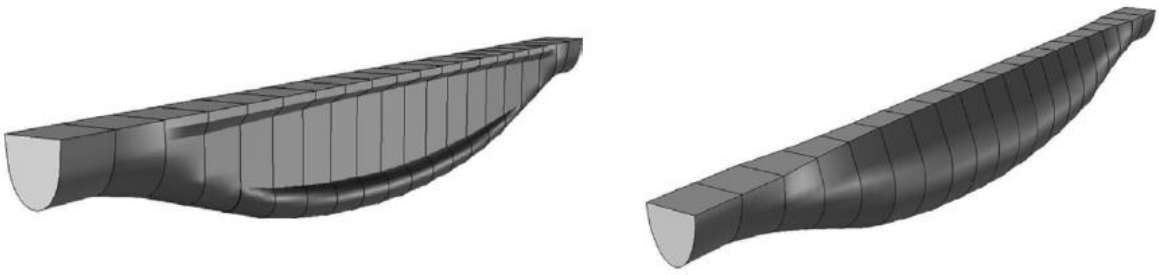

Figure 2.25: Shape optimised fabric-formed beams by (Garbett et al., 2008)

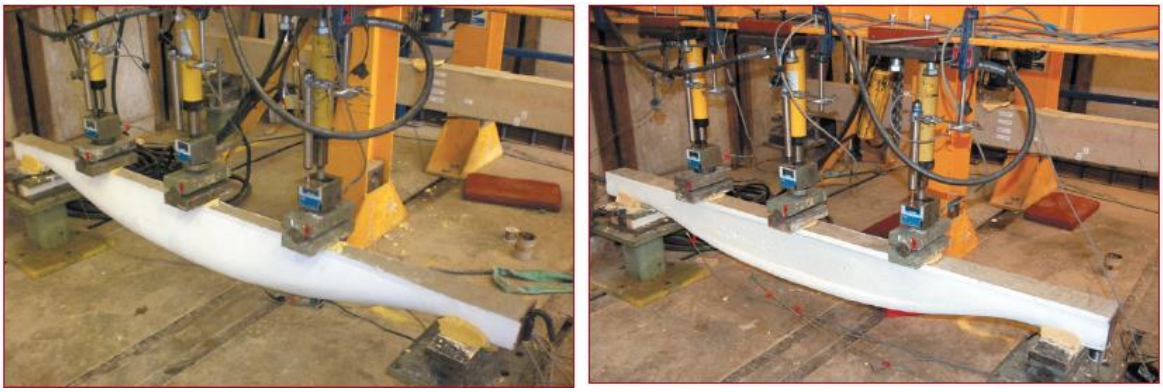

Figure 2.26: Test-set up of the beams designed by (Garbett et al., 2008)

Unlike steel members, reinforced concrete members are made from two types of material (reinforcement and concrete) which have very different strength and stiffness characteristics. Reinforced concrete beams are conventionally reinforced with longitudinal bars and transverse shear links which make the behaviour of the beam less dependent on its shape. Rather, reinforcement type, ratio and layout are crucial parameters to be optimised parallel with shape of beams defined in order to achieve the desired performance.

Orr (2012) optimised and built four geometrically identical fabric-formed T-beams using sectional analysis methods. The beams had different transverse and longitudinal reinforcement layouts and apart from the reinforcement the total depth varied along the beam. Two of the beams were designed assuming to have additional shear resistance from the inclined longitudinal bars, while the other two beams were designed without accounting for this contribution.

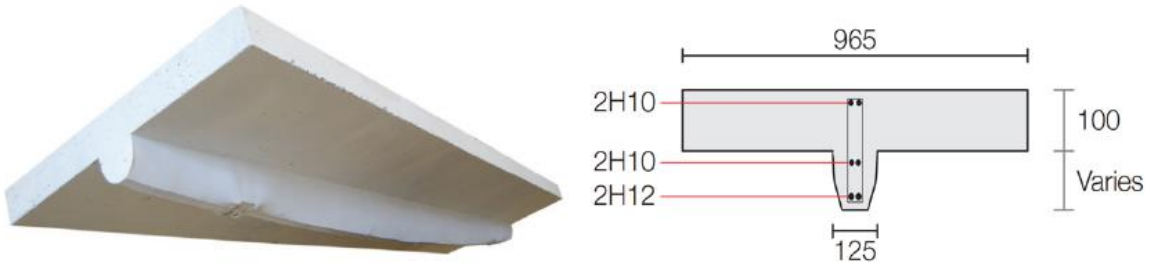

Figure 2.27: Fabric-formed single T-beams (Orr, 2012)

Compared to an equivalent strength prismatic beam and considering the webs of the beams only, the beams provided about 35% of saving in concrete material. The results of the tests showed that all beams failed in flexure and satisfied the failure capacity they had been designed for, despite some overestimation.

Orr (2012) also optimised and tested another series of 4m fabric-formed double T-beams shown in Figure 2.28. The flexural and shear design of all beams were carried out by using the provisions of BS EN 1992-1-1 (2004) and a sectional analysis procedure that ensures the applied bending moment and shear stresses are satisfied at any section.

Figure 2.28: Fabric-formed double T-beams (Orr, 2012)

Beam one was two meters long and was designed without transverse reinforcement. Beams two and three were four meters long and designed with different shear reinforcement arrangements and they were identical in shape. The vertical component of the force in the longitudinal bars were assumed to contribute in enhancing shear resistance near the supports and the horizontal component was used in calculating the moment capacity.

The main motivation behind this serious of tests was to introduce a feasible construction technique and reliable methods of analysis for fabric-formed concrete beams leading to significant savings in material and sustainable concrete structures.

The results of the tests showed successful prediction of failure loads for both shear and flexure modes. A significant amount of material of up to 26% (67% when considering the webs only) was saved compared to an equivalent strength prismatic double T-beam.

It is worth noting from the studies carried out by Orr (2012) that analysis and design methods developed for prismatic members before can successfully be applied to non-prismatic concrete beams, especially the sectional analysis procedure to find the moment capacity of the sections, considering only the horizontal component of the reinforcement force.

Although considerable reduction in the amount of material can potentially be achieved by adopting fabric-form work and shape optimising techniques for concrete members, cost-efficiency of such members is also of importance. Extra costs from special construction techniques involved in manufacturing shape optimised members should not overshadow the benefit of material saving obtained.

Orr (2012) encountered difficulties in casting the double T-beams due to the presence of a high number of shear links that each had a different size due to the variable section depth of the beams. Therefore, Orr optimised and tested another set of fabric cast single and double T-beams by using

ultra high performance fibre reinforced concrete (UHPFRC) aimed at facilitating the removal of shear links due to existence of steel fibres.

Orr designed and tested a total of 5 two meter beams without shear reinforcement. Beams 1, 2 and 3 were single T-beams and were geometrically identical. Beams 4 and 5 were double T-beams and were also identical in shape.

Figure 2.29: Graphic representation of fabric-formed UHPFRC beams (left), actual beams (right) (Orr, 2012)

According to the test results achieved by Orr (2012), beams one and two were successfully produced using fabric-form work method to cast UHPFRC as shown in 2.29. The failure load of beam three was considerably underestimated as the contribution of steel fibres in enhancing the tensile strength of concrete was neglected in calculating the design load. However, the failure load of beams four and five were quite accurately predicted.

So far, research work carried out on shape optimisation of fabric-formed concrete beams have been reviewed. The methods used to analyse and design those members can be classified as three-dimensional finite element methods or two dimensional sectional analysis methods. Among those studies mentioned, only the work that adopted sectional analysis method have been verified by experiments. The results obtained by using this method were fairly accurate and the calculations were relatively simple.

2.3.5.2 Continuous beams

Continuous reinforced concrete beams are commonly used in concrete structures. However, research work on shape optimisation of continuous concrete beams is very limited. This might be attributed to the complicated analysis and design procedures invoked by static indeterminacy and non-linear behaviour of reinforced concrete which often necessitates finite element analysis or highly computational methods.

Rath et al. (1999) used finite element analysis to optimise two span continuous concrete beams in order to arrive at minimum cost and minimum volume of material used. They used a deterministic method to find the optimal shape of cross-sections by using the Sequential Quadratic Programming (SQP) algorithm. They used a probabilistic method by employing a genetic algorithm to optimise for a number of design variables such as reinforcement ratio and layout and design constraints like flexural and shear strength, serviceability deflections and codified manufacturability constraints.

The optimisation initiated by discretizing a prismatic rectangular section beam into a number of finite elements. The beam was 6 meters long (3m each span) and had the cross-sectional dimensions of 300x600mm subjected to a uniformly distributed loading of 80 N/mm^2. The beam was optimised both sectionwise and longitudinally in order to remove understressed material in both section and span directions. The optimisation model was therefore designed to converge to an I section continuous beam with a longitudinal profile similar to the bending moment diagram. Compared to the initial design, their optimisation procedure yielded an equivalent strength optimised continuous beam with about 57% saving in the amount of concrete material used.

A minimum weight shape optimisation procedure for statically indeterminate beams was carried by Karihaloo and Kanagasundaram (1987). The beams were assumed to have been made from isotropic material with linearly elastic behaviour and a deterministic analysis approach was used based on mathematical derivations. The optimisation problem was simplified to be solved by a sequence of a linear programming technique by representing variation in stiffness with splines of order zero, one and two. The considered member was divided into a number of rectangular sections for which the geometric variables were changed along the length in order to achieve the required flexural stiffness for the minimum possible cross-sectional area. Different loading and supporting conditions were taken as constraints of the design procedure.

Although the optimisation procedure carried out by Karihaloo and Kanagasundaram (1987) resulted in continuous beams with up to about 50% reduction in material compared to their prismatic counterpart, the linear analysis procedure they used cannot be applied to non-linear optimisation problems.

For beams with non-linear material properties such as reinforced concrete beams, a non-linear problem solving approach is needed, especially when minimisation of serviceability constraints is required. The optimisation techniques and the analysis methods for non-prismatic members proposed by Rath et al. (1999) and Karihaloo and Kanagasundaram (1987) were only developed theoretically and were not applied to practical examples.

Moreover, from the review undertaken in this section, the following constraints and conditions related to continuous concrete beams are yet to be investigated.

a) Optimising for the ultimate and serviceability limit states simultaneously.

b) Construction constraints by using a special forming techniques such as fabric formwork.

c) Simplicity in the analysis and design procedure to assure that the benefits of material saving is not outweighed by expensive and time consuming computational work.

2.3.6 Topology optimisation

Topology optimisation is a term in structural design that has been defined differently by researchers depending on the objective of optimisation and size of the problem. At structure level, Bendose and Sigmound (2003) define topology optimisation as a technique that finds the best structural layout with regard to the geometric variables, material properties, loading and support conditions of a structural system. At member level, topology optimisation is defined by Shepherd and Richens (2012) as the method of redistributing material with in a given design space in order to achieve the maximum member performance, i.e. an optimum material layout that produces the desired strength and stiffness characteristics subject to certain manufacturing constraints.

There is a wide range of research work relating to material topology optimisation of structural steel members. Finite element modelling is mostly used to handle the numerical calculations. The linear elastic behaviour of steel up to yield point greatly simplifies the optimisation procedure. The area of topologically optimising structural systems such as reinforced concrete frames has also been extensively researched. However, there has been very little work on optimising material layout of reinforced concrete members. Part of the work carried out in this thesis deals with topology optimisation of fabric-formed concrete beams for serviceability limit states. Therefore, only the work conducted on optimising material layout is considered relevant to the scope of this thesis and has been reviewed in this section.

Veenendaal et al. (2011a) used finite element analysis and genetic algorithms to find optimal shapes of 9m fabric-formed beams by considering the construction constraints imposed by the fabric-formwork method. They used the Differential Evolution method which is an optimisation technique that mimics biological evolution to find an optimal shape or topology. In order to assess the

performance of the optimised model, they calculated the total strain energy and volume of the beam in terms of a performance index for optimised shapes. High performance for any optimised beam shape was obtained by achieving highest stiffness possible for the lowest possible volume of the beam. They optimised the beams for strength and stiffness without including the non-linear behaviour of concrete due to high computational demands.

Although the fabric-formed beam shapes produced by Veenendaal et al. (2011a) consumed 58% less concrete material than a prismatic beam equivalent in strength and stiffness, the final shapes taken from their optimisation model are not very optimal due to inclusion of linear material behaviour only. Additionally, their optimisation procedure converged to beam shapes with openings in the web and this could add difficulty to manufacturing process.

Shepherd and Richens (2012) used a specialized procedure to design and cast optimised shapes using fabric formwork techniques. The method included using a topology optimisation algorithm that returns optimised shapes which can be cast in fabric forms. The algorithm was based on the Bi-directional Structural Optimisation method in which convergence towards optimal shapes can be achieved by gradually removing unutilized material from the design domain and adding material back to where it is necessary. The constraints of the fabric formwork were then found by digitally draping the fabric over the optimised shape. Their work was intended to correlate digital optimisation and manufacturability by considering understanding of computational structural analysis, optimisation algorithms, fabric simulation and the practical casting techniques of fabric formwork.

They validated their customized algorithm by presenting performance graphs for a concrete slab simply supported at its centre by a square column with a uniformly distributed loading on the top of the slab. They produced plaster scale models from the initial results of the computational optimisation and form-finding. They found that, when non-prestressed fabric was used, a shape closer to the optimised shape was produced but there were some creasing problems in the fabric. When prestressed fabric was used in the casting procedure, the shape was a poorer approximation of the optimised shape but less creasing was noticed. Finally, they concluded that, for better approximation, a better fabric material model should be used along with introducing the hydrostatic force applied to the fabric by the wet concrete.

2.4 Prediction of behaviour

The behaviour of reinforced concrete structures is mainly governed by material stress-strain properties of the main components (reinforcement and concrete) and the interaction between these materials. Therefore, analysis of such structures can be complicated. With the aid of computers today and in parallel with our improved understanding of material properties, research work in the area of structural analysis has increased (Kwak and Kim, 2002). In the following sections, the main methods developed to analyze statically determinate and indeterminate concrete members are reviewed.

2.4.1 Analysis of statically determinate reinforced concrete beams

Statically determinate members are those elements in a structural system that can be analysed by applying equations of static equilibrium only (Ghali and Neville, 1997). It is usually practical and sufficient to use hand computation in order to find forces and moments acting on these members. The magnitude and direction of deformations, depend on the stiffness characteristics of the member and stiffness depends on material and geometric properties. For the sake of construction process, reinforced concrete members are conventionally cast in prismatic moulds and take a prismatic shape with a constant cross-section along the member's length. For this reason, the vast majority of the research work conducted on analysis of concrete members deal with prismatic members. However, shape optimised non-prismatic concrete beams, have recently received increasing interest and therefore there has been some studies aiming at predicting the behaviour of non-prismatic members using the analysis methods developed for prismatic members.

2.4.1.1 Serviceability of prismatic beams

Deflection of reinforced concrete elements is complicated because of the stress-strain characteristics of concrete and the reinforcement, cracking behaviour, tension-softening, tension-softening, and bond slip between the reinforcement bars and the concrete. Different formulas are provided by design codes in order to predict deflection of concrete members. There have been some studies carried out to find the accuracy of these code equations. Despite the fact that code methods intend to guarantee a safe design, they do not in general represent the actual stress-strain behaviour of structures after cracking (Gribniak et al., 2013).

Conventional methods for evaluating short-term serviceability displacement of concrete structures can be divided by two categories: analytical and numerical methods. Analytical methods can either be the equations taken from basic engineering mechanics derived by elastic analysis or empirical equations, both of which have certain limitations. Numerical methods on the other hand, involve discretizing the member into a number of elements. The global behaviour of the member is then found through simulation of the behaviour of (and interaction between) these smaller elements.

The main numerical methods used in structural analysis are finite element methods and sectional analysis methods. Both areas of research are reviewed in the following sections with a focus on sectional analysis as it was used in the theoretical part of the work carried out for this thesis.

2.4.1.1.1 Semi-empirical effective moment of inertia method

ACI Committee 435 (2000) suggests a method to predict instantaneous deflection of reinforced concrete members using Branson's formula to find effective moment of inertia based on transition between gross and cracked moment of inertia. The member is assumed to have a constant value of effective moment of inertia along the length. Branson's method has been widely used and is found to be adequately accurate in calculating deflections for reinforced and prestressed concrete structural elements. Branson's formula is as follows:

$$I_e = \left(\frac{M_{cr}}{M_a}\right)^3 I_g + \left[1 - \left(\frac{M_{cr}}{M_a}\right)^3\right] I_{cr} \leq I_g \qquad (2.21)$$

Where M_{cr} is the cracking moment, M_a is the unfactored service load moment, I_g is the gross moment of inertia and I_{cr} is the moment of inertia of the cracked transformed section.

The gross and cracked moments of inertia are taken from a bilinear moment-curvature relationship of the cracked section. The value of the effective second moment of area I_e which lies between the lower and upper limits of I_{cr} and I_g, depends on the level of cracking which is represented by M_{cr}/M_a. Once the value I_e is calculated, the moment-area method or similar can be used to find deflections.

Kalkan (2010) examined Branson's effective moment of inertia method for reinforced concrete beams with high steel ratios ($0.024 < \rho < 0.034$). The load-deflection data collected from testing eleven steel reinforced concrete beams was compared to those calculated using Branson's approach. Kalkan's results indicated that Branson's method closely predicts load-deflection behaviour of reinforced concrete beams with medium to high steel ratios ($\rho > 1\%$) and generally overpredicts the cracking moments of the beams.

The cracking moment used in Branson's formula significantly affects the load-deflection values calculated. Therefore, Kalkan (2010) suggests using experimental cracking moments, if known, in order to obtain a better prediction of deflections.

2.4.1.1.2 Empirical methods

BS EN 1992-1-1 (2004) suggests an empirical equation to calculate curvature using interpolation formula for values taken from uncracked and totally cracked states. When the section is uncracked, both the steel and concrete behave elastically and participate in load-bearing capacity, while for the

cracked state, the reinforcement carries all the tensile force on the section. The average curvature is given as:

$$k = (1 - \zeta)k_1 + \zeta k_2 \qquad (2.22)$$

Where k_1 and k_2 stand for uncracked and cracked curvatures respectively. A coefficient ζ which is equal to 1- β $(\mathbf{M_{cr}}/\mathbf{M_a})^2$, indicates how close the stress-strain condition is to cause cracking, it is equal to zero at the cracking moment and approaches unity with increase of load. β is equal to 1.0 when short-term loading is applied $\mathbf{M_{cr}}$ and $\mathbf{M_a}$ are cracking and applied moments respectively.

(Gribniak et al., 2013) carried out a statistical investigation to assess the accuracy of the methods proposed by Branson and BS EN 1992-1-1 (2004) to predict short-term deflections of reinforced concrete beams. The effects of three parameters; reinforcement ratio, load intensity and shrinkage, on prediction results were considered. They used data of nine test programs reported by other researchers with a total number of 80 specimens. Most of the beams were rectangular and reinforced with deformed bars. Eight specimens were inverted T-beams with their flange in the tensile region and were reinforced with smooth bars.

According to their results, both prediction methods showed reasonable accuracy for the beams with reinforcement ratio of (ρ >0.8%) under service loads. Less accurate predictions were noticed at lower levels of load and for lower reinforcement ratios. For beams with a lower reinforcement ratio (ρ>0.4%), prediction techniques returned a variation of results which made comparison unimportant.

They also noticed that, for the effective moment of inertia method suggested by Branson, the matter of accuracy becomes unrelated if time-dependent deformations resulting from creep and shrinkage are not modelled properly. For this reason, when a high degree of precision is required, they suggest that shrinkage should be considered in the analysis.

2.4.1.1.3 Sectional analysis method (full-interaction approach)

Sectional analysis aims at finding moment-curvature behaviour of beam sections based on the assumption that perfect bond exists between the concrete and reinforcing bars. The analysis involves calculating sum of compression and tension forces in a section and solving the equilibrium and strain compatibility conditions. The overall depth of the section can be divided into a number of reinforcement and concrete strips. Each strip is assumed to a have constant value of stress and strain. The sectional equilibrium condition is then imposed and internal forces and moment of resistance are found (Kwak and Kim, 2010).

This method has been widely used by researchers to determine the moment-curvature relationship of reinforced concrete sections from which the ultimate flexural capacity of the concrete beam and the deflected shape can be found. Unlike the effective moment of inertial and empirical methods,

one of the advantages of this method is that the load-deflection behaviour of concrete beams can be followed through the whole loading cycle up to failure of the member. The non-linear material behaviour can also be implemented in this method and so, tension and compression softening of concrete and yielding and strain hardening of steel reinforcement can be modelled.

Kwak and Kim (2002) introduced an analytical model for the material nonlinear analysis of reinforced concrete beams by using sectional analysis to obtain moment-curvature relations of reinforced concrete sections and by considering bond-slip effect and tension-softening. The results of numerical calculations were compared to experimental load-displacement and moment-curvature behaviours of steel reinforced concrete beams reported by other researchers.

Two of the beams were underreinforced and one was overreinforced. Comparison between numerical and experimental results showed that, for underreinforced concrete beams, bond-slip and tension-softening effects have a large effect at the cracking range, whereas for overreinforced concrete beams the influence of tension-softening can be ignored. In the case of considering tension-softening in the analysis, the load-deflection behaviour was a little stiffer than that of the experiments for underreinforced concrete beams. Additionally, the bond-slip effect can also be ignored for overreinforced concrete beams. They finally state that the analytical model based on sectional analysis and moment-curvature relations can effectively be used in the nonlinear analysis for reinforced concrete beams.

Type of reinforcement significantly affects the sectional behaviour of concrete beams, especially after cracking when the reinforcement behaviour dominates. A trilinear moment-curvature relationship was developed by He et al. (2007) for glass fibre reinforced polymer (GFRP) reinforced concrete beam sections. Complete non-linear moment-curvature analysis was conducted on five cross-sections with different reinforcement ratios and concrete strength. From this analysis, a clear unloading process was noticed due to sudden decline in flexural stiffness after cracking and then, when the member restored its flexural strength, it behaved approximately linearly up to failure. Based on these characteristics, the new trilinear moment-curvature relationship was proposed. They also carried out an experimental program on five GFRP reinforced concrete beams so as to validate the developed trilinear moment-curvature relationship. The beams were all overreinforced with shear and flexural reinforcement so that failure due to concrete crushing is assured.

Their test results indicated that a significant increase in sectional curvature caused by the low elastic modulus of FRP rebars should not be neglected in the analysis of the moment-curvature relationship. Due to the limited plasticity of concrete and brittleness of FRP bars, beams behave almost linearly until they fail. Based on the comparison they made between the results of the proposed trilinear moment-curvature model and the experimental data, a simplified tri-linear moment-curvature model can effectively be used to represent sectional response of FRP reinforced concrete beams.

Bazant and Oh (1984) offered a consistent model for analyzing curvature and displacements of reinforced concrete beams at progressive cracking state. The model was derived from fundamental material properties, as shown in Figure 2.30. The concrete was assumed to have a non-zero tensile strength, characterized by a uniaxial stress-strain diagram which has a progressive microcracking feature owing to strain-softening.

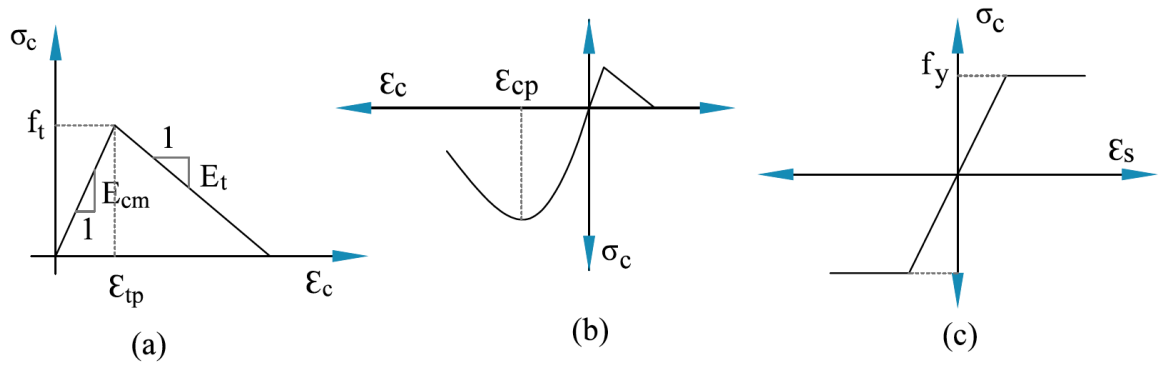

Figure 2.30: (a) tensile stress-strain model of concrete, compressive stress-strain model of concrete, (c) idealized stress-strain model of steel (Bazant and Oh, 1984)

Their model was developed using sectional analysis to find the moment-curvature and load-deflection relationships. The effect of tension-softening was suggested to be replaced by an equivalent tensile concrete area at the level of the tensile steel. They made a comparison between prediction results of their model and Branson's effective moment of inertia model. Their theoretical data agreed well with Branson's formula within the range the formula was suggested for (i.e. before concrete reaches compression softening). However, their sectional analysis model has a more general validity and is applicable to a wide range of situations including long-term deformation of concrete elements.

Tensile strength of concrete is often neglected in analysis of concrete beams, but the study carried through by Bazant and Oh (1984) implies that, neglecting concrete tensile strength leads to considerable underestimation of stiffness for singly reinforced concrete beams.

The sectional analysis method assumes that cracks are smeared along the region of the beam where cracking moment capacity is exceeded. Therefore, explicit information about cracking pattern, crack spacing and crack width cannot be obtained using this method. Models based on bond-slip phenomena between concrete and reinforcement have been developed to simulate cracking behaviour of concrete. The partial-interaction method is one of the methods which has been successfully applied to reinforced concrete beams.

2.4.1.1.4 Segmental-sectional analysis (Partial-interaction approach)

The partial-interaction approach was developed by Visintin et al. (2013) to evaluate moment-rotation of any section layout developing a numerical procedure that finds the relationship between the applied reinforcement force *P* and the slip Δ value between reinforcing bars and the concrete. This sectional-segmental method models the formation and propagation of cracks through application of a bond-slip model to find the stresses built up in the concrete to form primary, secondary and tertiary cracks. A primary crack is a crack which forms where the full-interaction boundary conditions are met, which is where the slip and slip-strain values are zero at the same point. A secondary crack is crack that occurs between two existing cracks where the slip value is zero but slip-strain has a non-zero value. At higher stages of loading and if the reinforcement–concrete bond is strong enough, tertiary cracks form between two secondary cracks.

A segmental moment-rotation analysis was carried out by Visintin et al. (2013) to evaluate short-term deflections and cracking behaviour of reinforced concrete beams. They used a numerical procedure to find load-slip characteristics of cracked sections by considering a segment of the beam with has a length equal to half crack spacing as shown in Figure 2.31. The segments were assumed to rigidly rotate around the crack locations causing the beam to deflect.

The concrete-reinforcement load-slip mechanism was simulated by considering reinforcing bars embedded in a concrete prism which has a depth equal to twice the concrete cover and the width equal the width of the beam (Figure 2.31). The considered segment was then sub-divided into a number of small elements and on each element the values of slip, slip-strain, concrete force and reinforcement force were found as shown in Figure 2.32.

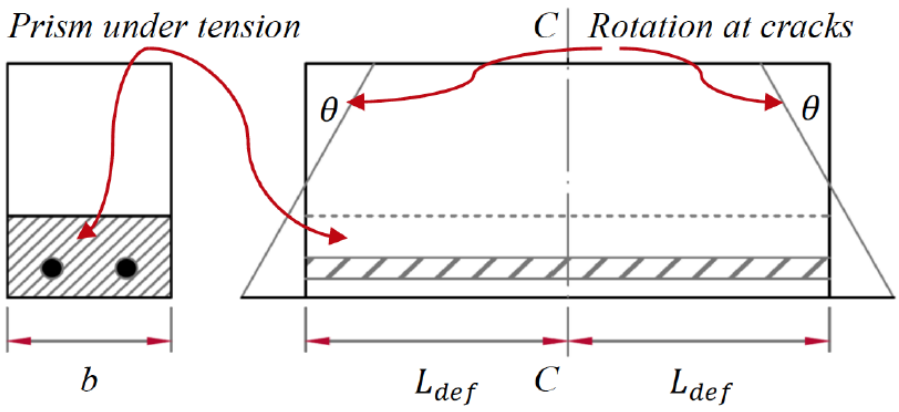

Figure 2.31: Moment-rotation Analysis (Visintin et al., 2013)

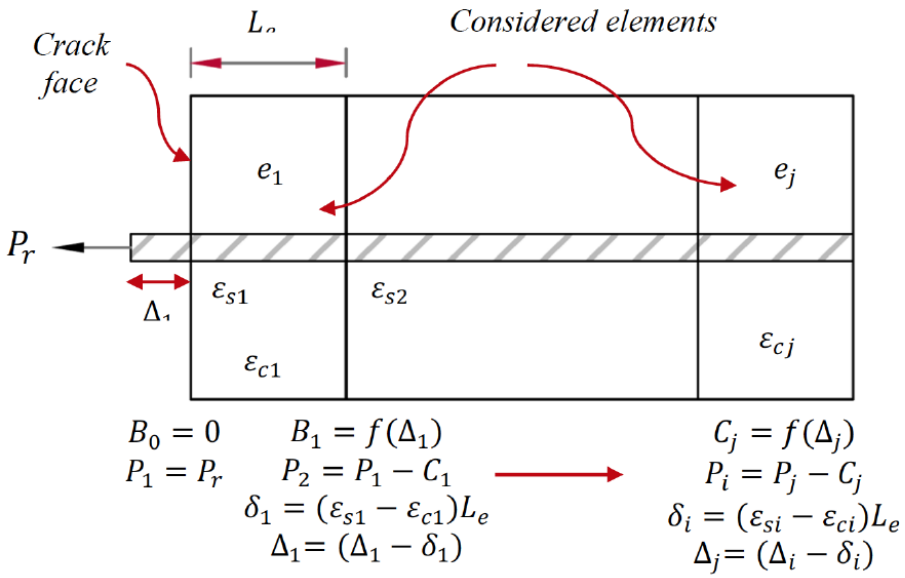

Figure 2.32: Numerical partial-interaction procedure (Visintin et al., 2013)

The procedure starts with an assumed value for the reinforcement force P_r and an increment of slip at the crack face (element 1). The force transferred to the surrounding concrete through bond slip B_1 is then found from a known bond-slip model. The slip value of this element (which is equal to the algebraic difference between the strain in the concrete and the reinforcing bar) is found and this procedure is repeated for subsequent elements to find the slip variation and the correct value of P_r. This $P - \Delta$ analysis is ultimately used to find moment-rotation $M - \theta$ behaviour of the cracked sections. This method is used in this thesis to simulate the cracking behaviour of optimised concrete beams and is further explained in §3.3.2.

Closed form solutions of the partial-interaction mechanism were derived by Oehlers et al. (2013) to find non-time dependent deflections of reinforced concrete beams. Similar to the previous work, the length L_{def} (equal to half crack spacing) and area A_c of the concrete prism were taken into consideration. Rigid body rotation at any crack was assumed to induce a displacement D in the compression part of the beam. They assumed the variation in deformation in the concrete to be linear because the analysis is carried out at serviceability.

The moment at a cracked section is found as follows:

$$M_t = P_r\left(d - \frac{d_c}{3}\right) \qquad (2.23)$$

Where d is the effective depth and d_c is the distance from the extreme compression fibre to the crack tip.

The rotation θ which is directly proportional to slip at the crack face, Δ_r, can be found as:

$$\theta = \frac{\Delta_r}{h_{cr}} \qquad (2.24)$$

Where Δ_r is the value of sleep at the crack and h_{cr} is the distance from the crack tip to the reinforcement lever.

They considered two types of bond-slip characteristic, linear ascending and parabolic bond-slip relationship. The partial-interaction equations were derived by taking the free body diagram of the bonded joints of the concrete-reinforcement prism.

Oehlers et al. (2013) used the test data of 12 GFRP reinforced simply supported concrete beams to validate the closed form expressions they developed. The beams had different cross-section sizes, reinforcement ratios, concrete cover, concrete compressive strength and surface characteristics of the reinforcing bars. The specimens were tested under a four-point loading regime to allow a constant moment region of 600 mm. The results implied that the choice the prism depth A_c plays a crucial role in finding the onset of primary and secondary cracks and consequently the serviceability behaviour of the beams. Generally, the partial-interaction method showed reasonable predictions of load-deflection relationships. However, the prediction improved when a smaller prism area than that suggested by codes was assumed.

Visintin et al. (2013) used partial-interaction theory to derive closed form solutions in order to quantify effective flexural stiffness value EI of reinforced concrete beams to be then used in Branson's formula. They replaced EI of cracked sections with partial-interaction EI to eliminate the necessity of finding effective EI from testing.

They made a comparison between deflection and effective EI values found from Branson's method (which is based on a full-interaction approach) and the partial-interaction approach. An example of a simply supported beam was used. In order to investigate the effect of reinforcement modulus and bond slip characteristics, one of the beam was assumed to be reinforced with steel bars with $E_r = 200GPa$ and bond stiffness $k_e = 13.7\ N/mm$ and a second one reinforced with FRP bars with $E_r = 40GPa$ and $k_e = 92.7\ N/mm$. The influence of reinforcement ratio was also studied by considering two reinforcement ratios of 1.11% and 0.74%. Loading system influence was also investigated by considering a one-point load and a four-point load case.

Based on the results of their comparison, the partial-interaction approach showed a slightly stiffer response especially in the case where the beams were reinforced with steel bars. This might be due to the effect of tension-stiffening which is ignored in the full-interaction approach (Branson's method). Reinforcement ratios seemed to have only slight effect on the serviceability behaviour of the beams. However, loading system considerably affected the results of the partial-interaction

analysis, whilst having no effect on the results of Branson's method because this method does not account for bending moment distribution shape.

Since different results were achieved by both methods in the theoretical analysis carried out above, the experimental data of two FRP reinforced simply supported beams were also used for the comparison and validation purposes. The beams had a span of 1800mm and total depth equal to 190mm. Both beams were reinforced with 2 16mm ribbed GFRP bars. The width, concrete cover and compressive strength were 140mm, 20mm and 56MPa respectively for beam one and those values were 160mm, 40mm and 62MPa correspondingly for beam two. The beams were both tested under a four-point load system.

It was concluded that the assumed crack spacing largely affects the load-deflection behaviour and the moment at which subsequent cracks form. It might therefore be better to analytically find crack spacing rather than using assumed values.

The partial-interaction theory modifies existing procedures to find the load-deflection behaviour of reinforced concrete beams with different types of reinforcement, such as FRP, with different bond-slip characteristics. Minimum crack spacing can be predicted by using this partial-interaction theory from which a closed form solution for the serviceability displacement can be derived. One unexpected result of their approach is that the flexural rigidity and the load to cause successive cracking is not affected by bond-slip stiffness at serviceability. This is useful when considering FRP reinforced members where a variety of FRP with different material properties exist.

2.4.1.1.5 Finite Element methods

Finite element analysis has been commonly used to evaluate the behaviour of concrete members. Moreover, the complex non-linear behaviour of concrete structures makes finite element analysis a real challenge for engineers. Accurate prediction of cracking mechanisms is one of the most challenging issues associated with finite element analysis of reinforced concrete members. What lies behind precise prediction of crack propagation is an accurate modelling of a fracture process zone (FPZ) that can account for gradual energy dissipation during cracking. This is done by considering non-linear fracture mechanics rather than linear elastic fracture mechanics (Yang and Chen, 2005).

Two of the most commonly used crack models to simulate FPZ are smeared and discrete crack models. For the case of modelling a single tensile crack propagation in plain concrete beams, both smeared and discrete methods have been able to satisfactorily predict load-deflection behaviour and crack paths. However, only limited success has been attained in applying these methods to model multiple distributed crack propagation of concrete structures. Computational efficiency has made the smeared crack model much more popular. However, discrete crack models are preferred when

comprehensive information about cracks, such as detailed crack trajectory, crack spacing and width, are desired (Yang and Chen, 2005).

In the smeared crack approach, the fracture is simulated such that an infinite number of parallel cracks are infinitely distributed over the finite element. However, in the discrete crack approach a strain discontinuity in the finite element mesh is applied. This method involves certain re-meshing and/or refinement techniques when the crack propagates (Sancho et al., 2007).

Malvar and Fourney (1990) used a smeared crack approach referred to as the Crack Band Model (CBM) to model the fracture zone of concrete. They simulated the tensile strain softening by modifying non-linear concrete elements in the cracking tensile zone. A full Newton-Raphson formula was implemented to converge to equilibrium in all loading increments. In order to accurately represent changes in stiffness in the cracked elements, the stiffness matrix was updated occasionally during crack propagation. They implemented the CBM approach in two and three dimensional nonlinear concrete elements and the model was evaluated by comparing load-deflection results of a series of beam tests to the numerical results. The testing program consisted of 12 single edge notched beams with cross-section dimensions 102 mm x 102 mm and length 838 mm and they were all tested under three-point bending.

To represent the tension-softening behaviour of concrete in the model, nonlinear and linear elastic concrete elements were used in combination. For comparison purposes, they used results from other researchers who used linear elastic elements, linear softening elements and Fictitious Crack Model (FCM). From the load-deflection responses of different models compared to the experimental data, they found that FCM and CBM approaches yield similar results and the 3D elements showed stiffer behaviour than the 2D elements.

The results of the above research work indicate how the meshing method affects the results in the finite element analysis. Suitable element sizes and element types (2D or 3D) can vary depending on the type of concrete mix.

Using the discrete crack approach, a finite element model for fully automatic simulation of multi-crack propagation in reinforced concrete beams was developed by Yang and Chen (2005). Four-node interface elements are used to model the cohesive cracks based on fictitious crack concept with bilinear concrete tensile softening constitutive laws. The bond-slip behaviour between the reinforcement bars and the surrounding concrete was modelled by using a two-node tension-softening element adopting bilinear elastic-perfectly plastic truss elements for the rebars and with considering the effect of localized secondary cracks. Perfect and weak bond models were also used for comparison purposes.

Their model was able to efficiently simulate multiple crack propagation and the experimental load-deflection response of the beam was accurately predicted up to the point where the beam compression cracking becomes dominant. However, the assumption of strong and weak steel-concrete bond caused overestimation and underestimation in stiffness respectively.

The two previously mentioned approaches to simulate tensile fracture (smeared crack model and discrete crack model) have been combined in the past years by applying a new approach referred to as the Strong Discontinuity Approach (SDA). This model is different from the smeared crack model by representing the fracture zone as a discontinuous displacement surface and is different from the discrete crack model by the fact that the crack geometry is not restricted to inter-element lines, as the displacement jumps are embedded in the corresponding finite element (Sancho et al., 2007).

Sancho et al. (2007) used the SDA approach to model fracture of concrete and they compared crack width and load-deflection results with experiment data. The main aim of their work was to describe concrete cracking in a two dimensional finite element modelling by numerically implementing cohesive cracks as discontinuity in a classical finite element. At the crack level, the crack width was calculated; this resulted in avoiding the necessity of carrying out a static condensation at the element level. They presented the results of well-known experiments compared to their numerical simulation to validate their proposed model and to check its accuracy in describing fracture of concrete.

They used different meshes to analyze a simply supported notched beam under three-point-bending. This test was to check, the capability of their model to trace a straight vertical crack without crack tracking in structured and unstructured meshes and it was also to check the effect of mesh size on computations. Another test of a single edge notched beam subjected to four-point-shear was analysed. They claim that the numerical simulations show that the previous mixture of simple ingredients leads to a technique in which the cohesive crack automatically propagates without the necessity for a tracking algorithm or exclusion zones. Therefore, the embedded cohesive crack method seems to be an efficient and simpler alternative to other more sophisticated methods for the simulation of concrete damage and fracture.

The above review on the finite element methods to predict the behaviour of concrete beams indicates how the method used to model the FPZ, the meshing method, size and type of elements considered affect the accuracy of predictions. This parallel with the high amount of computational time and effort needed makes finite element analysis a challenging tool to use. Therefore, in this work, the sectional analysis methods were used to develop both prediction and optimisation methods.

2.4.1.2 Serviceability of non-prismatic beams

Despite the vast amount of work that exist in literature on serviceability analysis of prismatic concrete beams, there has been little work on predicting serviceability behaviour of non-prismatic beams. Most of this work has been carried out on prediction of load-deflection behaviour by applying Euler-Bernoulli's beam principle (plane sections remain plane after bending deformation). The sectional analysis procedure mentioned in §2.4.1.1.3 was applied by Orr (2012) to determine moment-curvature behaviour of fabric-formed non-prismatic concrete beams presented in §2.3.5.1. Orr used the method of integration of curvatures to predict the load-deflection relationships as follows:

$$\theta = \int_{x=0}^{x=L} k d_x \qquad (2.35)$$

$$D = \int_{x=0}^{x=L} \theta d_x \qquad (2.36)$$

Where θ, k and D are rotation, curvature and deflection respectively, and L is the total length of the beam.

Orr found that, the calculated load-deflection response was in a good agreement with experimental data.

Orr also used Branson's effective moment of inertia method to find deflection of fabric-formed Double and single T-beams. This was done by subdividing the member into a number of sections and the gross and cracked moment of inertia were found for each section using the transformed sections approach. Orr then found the curvature value at each section using the following equation:

$$k = \frac{M}{EI_e} \qquad (2.37)$$

Where M is the applied moment at the section under consideration, E is the elastic modulus of section and I_e is the effective moment of inertia found from Branson's formula.

The predicted load-deflection results were in excellent agreement with the test. The work carried out by Orr may suggest that both the sectional analysis and the effective moment of inertia methods can successfully be applied to find serviceability behaviour of non-prismatic concrete beams. However, it is worth noting that the beams tested by Orr had large flange sizes compared to their webs and the behaviour of these beams may be dominated by the behaviour of their prismatic flanges. This, therefore, may make the beams act more like slabs than non-prismatic beams.

2.4.2 Analysis of statically indeterminate reinforced concrete beams

Statically indeterminate members are members which cannot be analysed by static equilibrium alone and so deformation compatibility conditions are also needed. The vast majority of structures seen in practice are statically indeterminate structures (Ghali and Neville, 1997).

Various methods have been used by researchers and designers to analyse continuous concrete beams primarily comprising *stiffness* and *flexibility* methods. Stiffness methods are far more frequently used due to simplicity and lower computational effort needed, compared to flexibility methods (Reynolds et al., 2007).

2.4.2.1 Codified approximate methods

Design codes of practice have provided simplified analysis methods to analyse continuous reinforced concrete beams. Depending on load and spanning conditions, coefficients are suggested to determine bending moment and shear stresses at mid-spans and supports. These coefficients are usually based on elastic analysis with an allowance of certain ratios of moment redistribution.

El-Mogy et al. (2009) used elastic analysis for two double span continuous beams to find maximum hogging and sagging moments. The beams were symmetric about the middle support and were loaded by a point load at each mid-span. One of the beams was reinforced with GFRP bars and the other beam was steel reinforced. The elastic moments at the central support and each mid-span were $0.188Pl$ and $0.188Pl$ respectively with 20% moment redistribution assumed, this changed the moments to $0.175Pl$ and $0.15Pl$. The flexural design of the critical section was then carried out based on the assumed values of redistributed moments. The test results indicated that elastic analysis overestimated the middle support moment value by 23% and therefore underestimated mid-span moments by the same ratio owing to neglecting moment redistribution in elastic analysis.

Du et al. (2016) applied Branson's formula to find effective moment of inertia of unbonded partially prestressed continuous concrete beams and used it in an elastic deflection equation to predict load-deflection behaviour of the beams. They developed a model to transform the area of prestressed tendon to equivalent reinforcing steel area. The deflection equation for a two-span continuous beam with a point load on each mid-span is given as below:

$$\delta = \frac{7Pl^3}{768E_cI_e} \qquad (2.38)$$

Where P is the point load acting on span l, I_e is effective moment of inertia calculated by from Branson's equation and E_c is the elastic modulus of concrete given by ACI 318-08 (2008) as:

$$E_c = 4700\sqrt{f_c'} \qquad (2.39)$$

They used experimental data from other researchers of prestressed continuous concrete rectangular and T-beams in order to assess the validity of their model in predicting load-deflection behaviour. The prediction results were satisfactory before the non-prestressed steel yielded, when a considerable moment redistribution has not yet occurred.

The results achieved by El-Mogy et al. (2009) and Lou et al. (2016) indicate that elastic analysis for continuous concrete beams can result in satisfactory result at serviceability, but when failure starts to happen at the middle support, moment redistribution significantly affects the overall behaviour of the beam. Therefore, elastic analysis and the assumption of uniform flexural stiffness can only be used for indeterminate concrete beams with constant section properties along the beam and under service loads. For shape optimised non-prismatic continuous concrete beams, geometric non-linearity and non-uniform flexural stiffness characteristics along the beam makes elastic analysis infeasible.

2.4.2.2 Stiffness Methods

Owing to moment redistribution in continuous concrete beams, the analysis method of such beams should be able to implement material non-linear behaviour so as to allow for an accurate prediction of behaviour. The majority of research work involved in non-linear analysis of indeterminate concrete beams fall in one of two categories; 1) segmental analysis in which the beam is discretized into a number of segments and the flexural stiffness of these segments are determined in each loading stage using a sectional analysis procedure, 2) finite element analysis where changing in flexural stiffness is accommodated by updating the global stiffness matrix in each loading step.

Lou et al. (2016) used the stiffness matrix method to analyze two-span continuous prestressed concrete beams with internal unbonded fibre reinforced polymer (FRP) and steel tendons, considering geometric and material non-linearities. A one-dimensional finite element analysis was used in which the beams was divided into a number of smaller beam elements connected by nodes. The global stiffness matrix was created by assembling the stiffness matrix of the beam elements. They used the principal of virtual work to create the tangent equilibrium equation for beam elements as follows:

$$\boldsymbol{dP}^{e} = \boldsymbol{K}_{t}\boldsymbol{du}^{e} \qquad (2.40)$$

in which, $\boldsymbol{u}^{e}$, $\boldsymbol{P}^{e}$ and $\boldsymbol{K}_{t}$ are the nodal displacements, equivalent nodal forces and stiffness matrix of the beam element respectively. Their analysis procedure was established based on the assumptions that, plane sections remain plane after deformation and perfect bond exists between the concrete and the FRP bars. The contribution of shear deformation was neglected. They used experimental load-deflection data of two continuous beams to validate their proposed model. Comparison of the experimental and predicted load-deflection relationships showed that their model

was accurate in modelling the behaviour of such beams that have a high degree of non-linearity due to cracking in concrete, post-tensioning and the concrete-FRP bars bond-slip characteristics.

Dundar et al. (2015) used a non-linear stiffness method to evaluate deflection of multi-span steel and FRP reinforced members. Flexural stiffness values at the cracking state were implemented in the stiffness matrix so as to account for moment redistribution at any stage of loading. Two methods were used to calculate flexural stiffness of concrete sections, sectional moment-curvature analysis and a semi-empirical method. The member was divided into two uncracked and three cracked regions. For each region the stiffness matrix was created and then the global stiffness matrix was assembled. They used the virtual work method in order to create the displacement matrix for the member with considering the contribution of shear strains as follows:

$$f_{ij} = \int_0^L \frac{M_i M_j}{E_c I_{eff}} dx + \int_0^L \frac{V_i V_j}{G_c A} dx \qquad (2.41)$$

Where f_{ij} is the displacement in the ith direction due to the application of unit loads in jth direction. $(M_i V_i)$ and $(M_j V_j)$ are the bending moments and shear forces due to the application of unit loads in the ith and jth directions, E_c is the elastic modulus of concrete, G_c is the shear modulus and A is the section area.

In continuous concrete beams, variation in flexural strength and effective shear modulus due to cracking can be tracked by using an iterative loading procedure so that the effect of moment redistribution on the cracking state of section can accurately be accounted for. Dundar et al. (2015) developed an iterative procedure to predict load-deflection response of a number of continuous slabs and beams tested by other researchers. The specimens were reinforced with FRP and steel bars. The results they achieved from comparing the experimental and analytical data shows that finding flexural stiffness values from sectional moment-curvature analysis offers a better prediction than finding effective flexural stiffness values from semi-empirical methods.

2.5 Conclusions

In this chapter, previous work in the areas of fabric formwork, structural optimisation and analysis of behaviour of reinforced concrete beams has been surveyed. This was aimed at the following points:

1. Clarifying the gaps which exist in the area of serviceability of fabric-formed concrete.
2. Finding and developing appropriate optimisation techniques for design of fabric-formed concrete beams.
3. Finding and developing suitable prediction and analysis methods to be used in optimisation procedures and behaviour analysis of fabric-formed concrete members.

Despite the fact that fabric formwork is a relatively new area of research, there has been a good deal of work conducted recently towards better understanding of the properties, construction methods, structural behaviour and possible benefits of this new forming technique. There is also ongoing work in different universities attempting to fully establish the vocabulary of fabric formwork. As mentioned in this chapter, fabric-formed concrete beams have been optimised for the ultimate limit state and certain analysis methods have been successfully applied to understand the behaviour of these members. However, serviceability, as an important aspect of design and lifetime of fabric-formed concrete members, is yet to be investigated. Very little work is available to study the load-deflection of simply supported fabric-formed concrete beams, with limitations mentioned in §2.4.1.2.

No research work has so far been carried out on the cracking behaviour of fabric-formed concrete beams.

Continuous beams are more commonly seen in concrete structures, but there is still no research work on load-deflection behaviour of continuous fabric formed concrete beams. Cracking behaviour (another equally-important serviceability criteria) of simply supported and continuous fabric-formed concrete beams has not yet been investigated.

Unlike prismatic concrete members, non-prismatic fabric-formed concrete beams can be designed by employing optimisation techniques in order to achieve maximum possible saving in material which is the current objective behind using fabric formwork. Methods for shape optimisation of simply-supported concrete beams for the ultimate limit state based on sectional analysis have been developed as described in §2.3.5. Optimisation of continuous beams for strength is more complicated owing to indeterminacy, moment redistribution due to change in the beam shape and stiffness in each optimisation step and material non-linearity. No research work has yet been carried out on optimising continuous fabric-formed beams to satisfy the ultimate limit states.

Optimising for serviceability (deflection and cracking), which might govern the design of fabric-formed beams in many cases, as discussed in Chapter One, is not seen so far in literature for either simply supported or continuous fabric-formed concrete beams.

In the next chapters, numerical models developed to help filling the gaps which exist in this area are presented. Chapter Three deals with the models developed to analyse the behaviour of non-prismatic beams in general and fabric-formed concrete beams in particular. Chapter Four presents the numerical models developed to optimise non-prismatic concrete beams for strength and serviceability with focus on fabric-formed concrete beams. Experimental program to verify the numerical models and discussion of the test results are presented in Chapter Five and Chapter Six.

[blank page]

[blank page]

Chapter Three

Analysis of behaviour

3.1 Introduction

The design process of flexibly-formed concrete members in this work involves an iterative procedure which consists mainly of two parts. Part one is analysis methods which allow the prediction of behaviour of non-prismatic concrete beams, and part two is optimisation methods. In each design loop, prediction methods assess the performance of the member and identify possible design problems such as exceeding a certain limit state, then the optimisation method is used to improve the design. This prediction-improvement procedure continues until all limit states are satisfied and a robust design is achieved.

This chapter presents part one of the theoretical work carried out for this thesis which addresses the analytical and numerical methods developed to analyse and predict the behaviour of non-prismatic concrete beams at both ultimate and serviceability limit states. Chapter Four presents part two of the design associated with optimisation of flexibly-formed concrete members.

Since beams are assumed to be under gravity and applied vertical loads only in this work, the ultimate limit states considered are limited to bending moment and shear stresses. The serviceability limit states considered are deflections, crack widths and a compressive stress limitation on concrete. All methods developed here were automated by writing MATLAB programs.

3.2 Prediction of behaviour

The behaviour of concrete beams is complicated owing to the non-linear stress-strain relationship of concrete, cracking, tension-stiffening, tension-softening and bond-slip between the reinforcing bars and concrete (Gribniak et al., 2013). Shape optimised flexibly-formed concrete beams have variable section size along their length which leads to geometric non-linearity and adds another degree of complexity in calculations. Therefore, methods with broad applicability are needed to simulate the behaviour of optimised concrete beams. The methods adopted in this section are used in combination with the form-finding method described later in Chapter Four and the structural optimisation methods described in Chapter Four in order to develop a numerical method that can be used to efficiently design flexibly-formed concrete beams optimised for both the ultimate and serviceability limit states.

For the sake of simplicity and feasibility of the analysis procedure, data compatibility between the methods should be assured, i.e. all methods of prediction, form-finding and optimisation should be well-suited to each other. Therefore, in every stage of the numerical method, a section-based analysis method was used. Sectional analysis reduces the three-dimensional beam problem to a two-dimensional problem and modelling reinforced concrete beams based on two-dimensional analysis is found to be fairly accurate as reviewed in Chapter Two. The behaviour of discrete sections can straightforwardly be combined to establish the overall behaviour of concrete beams. The optimisation task can be performed by directly modifying the properties of those sections to bring about maximum possible improvement in the behaviour of the whole beam. The final layout of all sections produced from the optimisation procedure are then passed to the sectional form-finding method to create two-dimensional shape of each section. Those section shapes are finally connected to define the full three-dimensional form of the concrete beam.

This parallel procedure of passing data from one model to another on sectional bases helps to save a significant amount of computation time and produces an intuitive design procedure for flexibly-formed concrete members.

3.3 Statically determinate beams

3.3.1 Full-interaction analysis

A full-interaction method was initially used in a sectional analysis procedure and applied to find the moment-curvature behaviour of reinforced concrete beams in this thesis. The method relies on the assumptions that 1) the reinforcing bars and the surrounding concrete are perfectly bonded (no slip occurs between the reinforcement and the concrete), 2) plain sections remain plain after bending 3), concrete beams deflect due to flexural curvature only 4), the tension side of the concrete beam cracks when its tensile strain exceeds capacity and 5) cracks are smeared over the cracked region of the

member. In this method, the concrete beam is discretized into a number of sections, the moment-curvature relationship of each section is determined and the deflected shape of the beam is found by using method of integration of curvatures as explained in the following sections.

3.3.1.1 Moment-curvature analysis

Based on the full-interaction method, the moment-curvature response of discrete sections along a concrete beam can be developed by using material stress-strain methods and the conditions of equilibrium and strain compatibility. In this procedure, the cross-section is first divided into a number of concrete and reinforcement strips as shown in Figure 3.1(a).

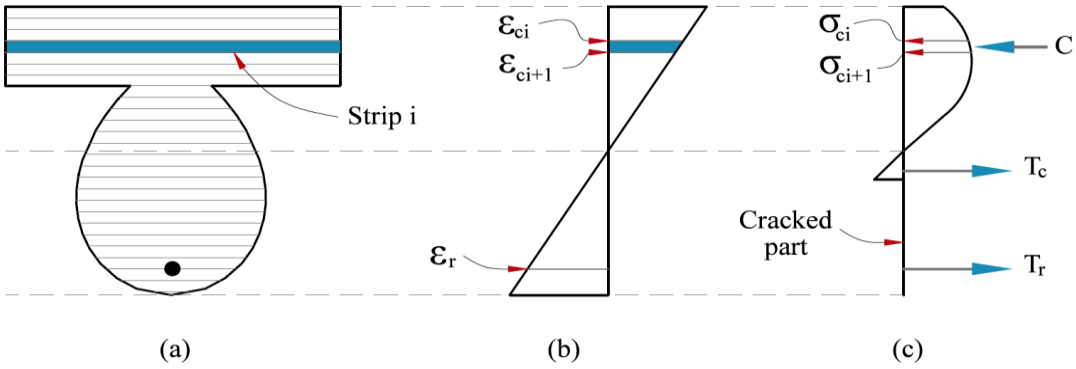

Figure 3.1: (a) discretised beam section, (b) Strain distribution, (c) stress distribution

The depths of strips are equal and intentionally taken to be small so that stress distribution over them can be assumed to be constant. A value of curvature is assumed, driven by an assumed value of strain in the extreme compression fibre of the section and an assumed value of neutral axis depth. From the compatibility condition of sectional deformations, the strain distribution on the section is found, as shown in Figure 3.1(b). The strain values on each strip ε_{ci} and $\varepsilon_{ci+1}$are then substituted into the material constitutive laws to determine the corresponding stress values and consequently the stress profile across the section can be found as shown in Figure 3.1(c).

Sectional equilibrium of the tension and compression forces is then examined and the initially estimated value of the neutral axis is iterated (keeping the curvature constant) until the equilibrium condition is met.

Next, the moment capacity of the section for the particular curvature value is calculated by taking the summation of internal moments around the neutral axis. This concept is repeated for ever-increasing curvature values until the full moment-curvature behaviour of the section is determined. Figure 3.2 shows the procedure in a flow chart which was implemented in a MATLAB program to numerically find the moment-curvature relationship for any specific section layout.

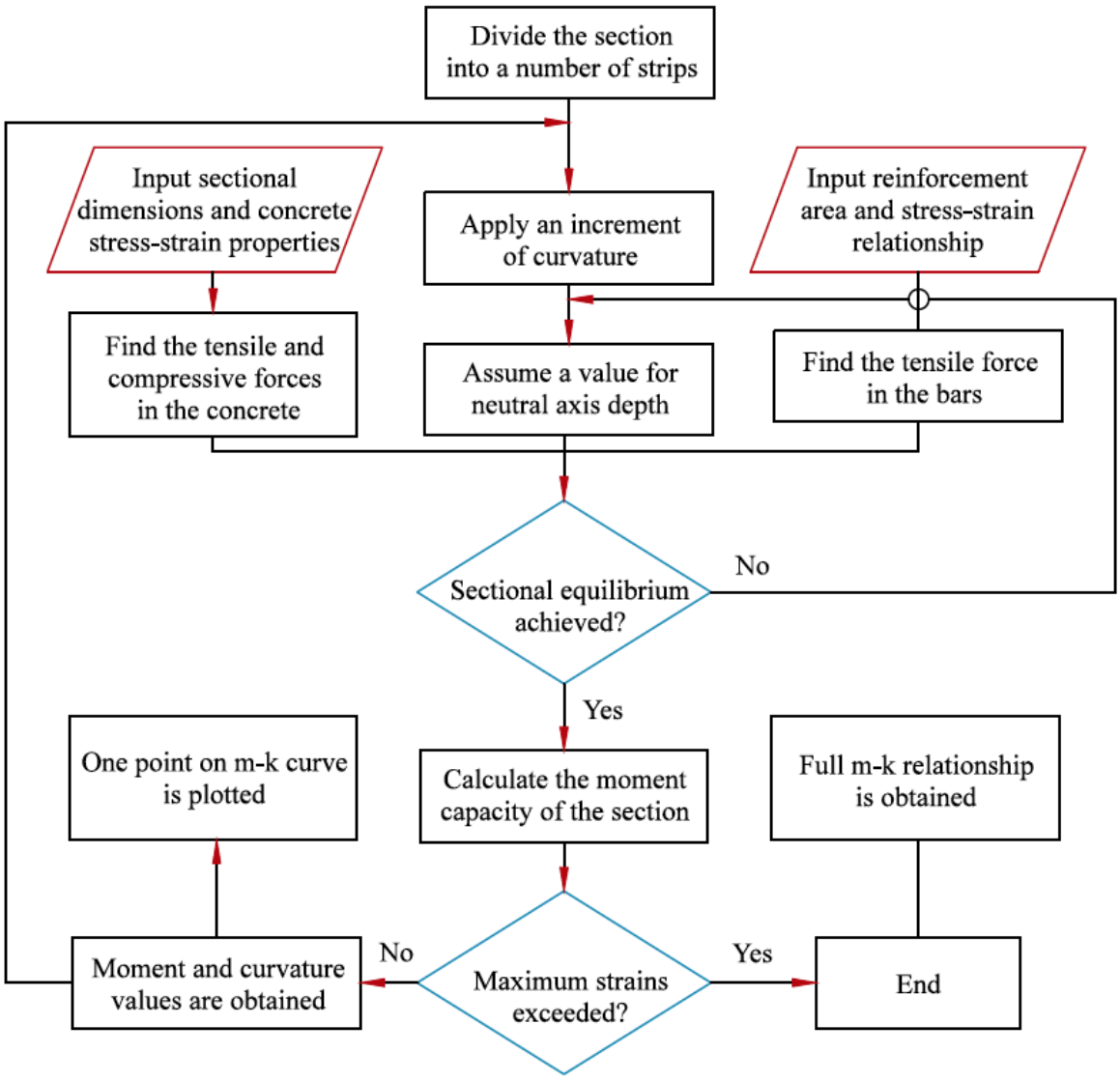

Figure 3.2: Procedure of developing moment-curvature relationship for a section

3.3.1.1.1 Material constitutive laws

3.3.1.1.1.1 Concrete

A model provided by BS EN 1992-1-1 (2004) was used in this thesis to represent the stress-strain relationship of concrete under short-term uniaxial compressive stresses. The model has an ascending part that represents the strain-hardening property of concrete and a descending part which represents the strain-softening characteristics, 3.3(a).

The relation between absolute values of compressive stress σ_c and strain ε_c is given by expression the following:

$$\sigma_c = \frac{k\eta - \eta^2}{1 + (k-2)\eta} f_{cm} \qquad (3.1)$$

where

$$\eta = \frac{\varepsilon_c}{\varepsilon_{c1}} \qquad (3.2)$$

$$k = 1.05E_{cm} \times \frac{|\varepsilon_{c1}|}{f_{cm}} \qquad (3.3)$$

$$E_{cm} = 22\left[{}^{(f_{cm})}/_{10}\right]^{0.3} \qquad (3.4)$$

Where f_{cm} and E_{cm} are the mean value cylinder compressive strength and the secant modulus of elasticity of concrete respectively. This expression is valid for $0 < |\varepsilon_c| < |\varepsilon_{cu1}|$, where ε_{c1} is the strain at peak stress and $|\varepsilon_{cu1}|$ is the nominal ultimate strain.

The tensile stress-strain behaviour of concrete, shown in Figure 3.3(b), was modelled as a linear relationship with the tangent modulus equal to E_{cm} up to the peak tensile stress f_{ctm} (mean value of the axial tensile strength of concrete).

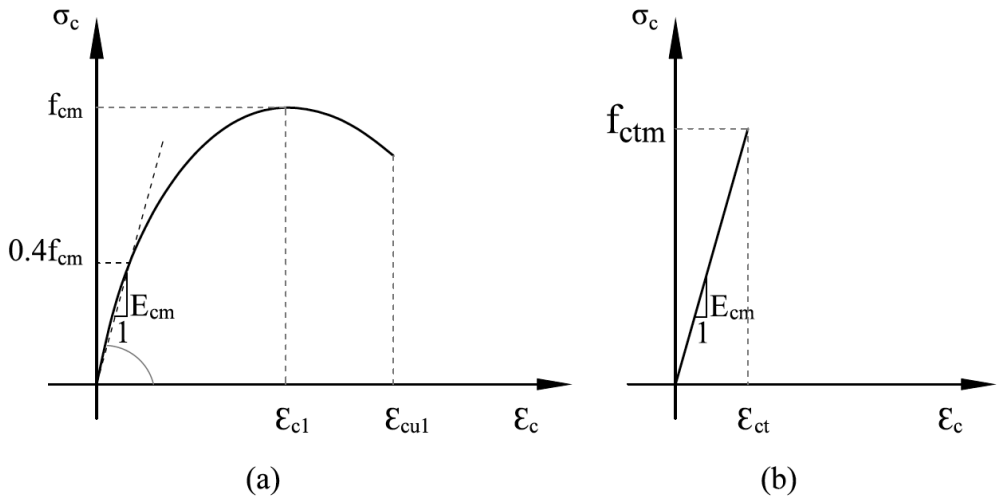

Figure 3.3: Schematic representation of concrete stress-strain relationships, (a) in compression, (b) in tension

3.3.1.1.1.2 Reinforcing steel

An idealized bi-linear stress-strain model provided by BS EN 1992-1-1 (2004) was used to model the behaviour of reinforcing steel bars under both tension and compression. The model includes a linear elastic behaviour up to the yielding point of the steel bar and a linear strain-hardening portion after yielding up until the full failure.

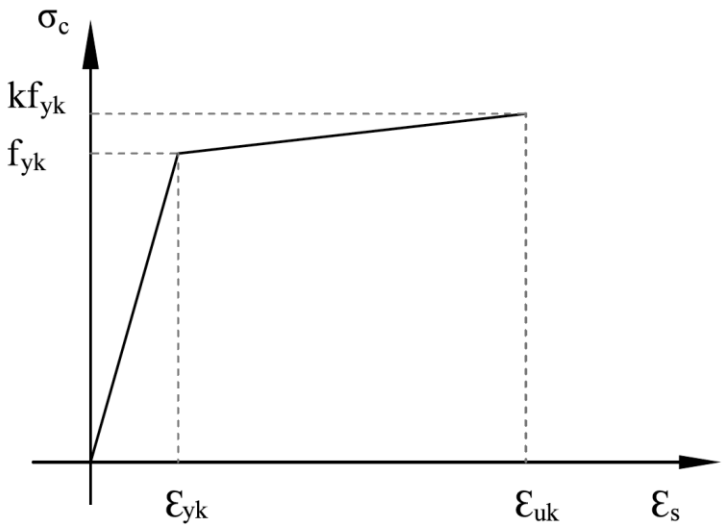

Figure 3.4: Idealized stress-stress strain diagram for reinforcing steel under tension and compression

In Figure 3.4, f_{yk} and ε_{yk} is the characteristic yield strength and strain of steel, kf_{yk} is the ultimate strength, k is the coefficient equal to $\left(f_t/f_y\right)_k$, f_t is the ultimate tensile strength and ε_{uk} is the ultimate strain.

3.3.1.2 Integration of curvatures

The method of integration of curvatures was used in this thesis to find deflections of statically determinate concrete beams based on the moment-curvature relationships. In this method, the geometry of the member is defined and the beam is divided into a number of vertical sections. The applied moment value at each section is then calculated and from the moment-curvature relationship of each section (as described in §3.3.1.1) the curvature distribution along the beam is found. Next, a numerical integration method is used to integrate the curvature distribution once in order to find rotations along the member. The constant of integration produced from the numerical integration process can be found by considering the boundary conditions of the statically determinate beams. These boundary conditions for simply supported beams are the zero value of deflection at the supports. Finally, the rotations are integrated to find the deflected shape of the beam, as described in Equations (3.5) and (3.6):

$$\theta = \int_{x=0}^{x=L} k d_x \qquad (3.5)$$

$$D = \int_{x=0}^{x=L} \theta d_x \qquad (3.6)$$

where L is the total length of the beam, k is curvature, θ is rotation and D is deflection.

Figure 3.5 shows the procedure used to find the load-deflection response in reinforced concrete beams. The procedure was automated using a MATLAB program and was used in conjunction with

the program created to develop moment-curvature relationship for reinforced concrete beam sections.

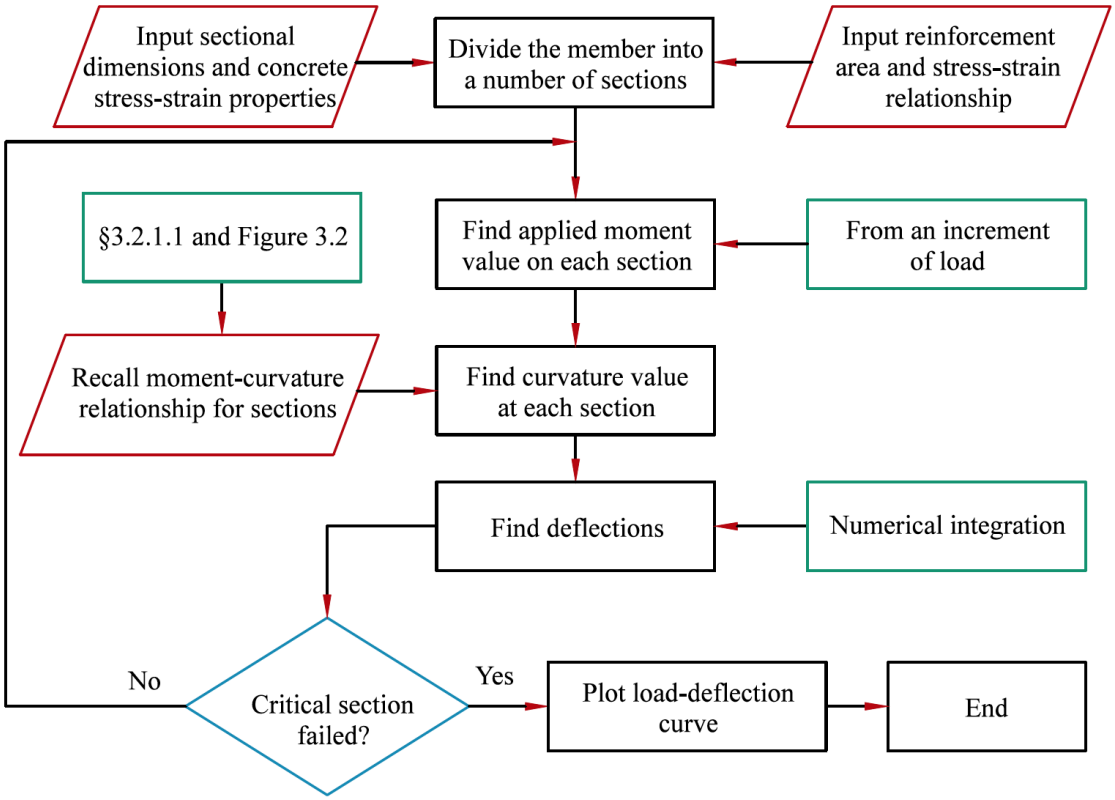

Figure 3.5: Finding load-deflection behaviour of concrete beams

3.3.2 Partial-interaction analysis

The partial-interaction method described in §2.4.1.1.4 was used to simulate cracking behaviour of reinforced concrete beams. The method is only applicable to the post-cracking stage because the equations used are derived from the equilibrium and compatibility conditions of a crack face. The full-interaction analysis is used first to find the location of an initial crack and the moment at which the beam cracks at that point, then the partial-interaction method can be used to predict the formation of subsequent cracks for prismatic concrete beams. This method makes the following assumptions:

1. Slip may occur between the reinforcement and the surrounding concrete.
2. Cracks form when the stress transferred to the concrete from the reinforcing bars through bond-slip exceeds the concrete tensile strength.
3. The beam deflects due to rigid body rotation at discrete cracks.
4. The value of curvature is zero in the cracked region (i.e. all deformation occurs due to rotation at crack locations).

A numerical modelling procedure which was previously developed by Visintin et al. (2013) is used to simulate crack-widening behaviour of cracked sections. In this procedure, the tension side of the beam is modelled as a prism which is subjected to uniaxial tension. The width of the prism, w, is equal to the width of the beam and the depth of the prism d_p is taken as twice the clear cover of the beam (Oehlers et al., 2013).

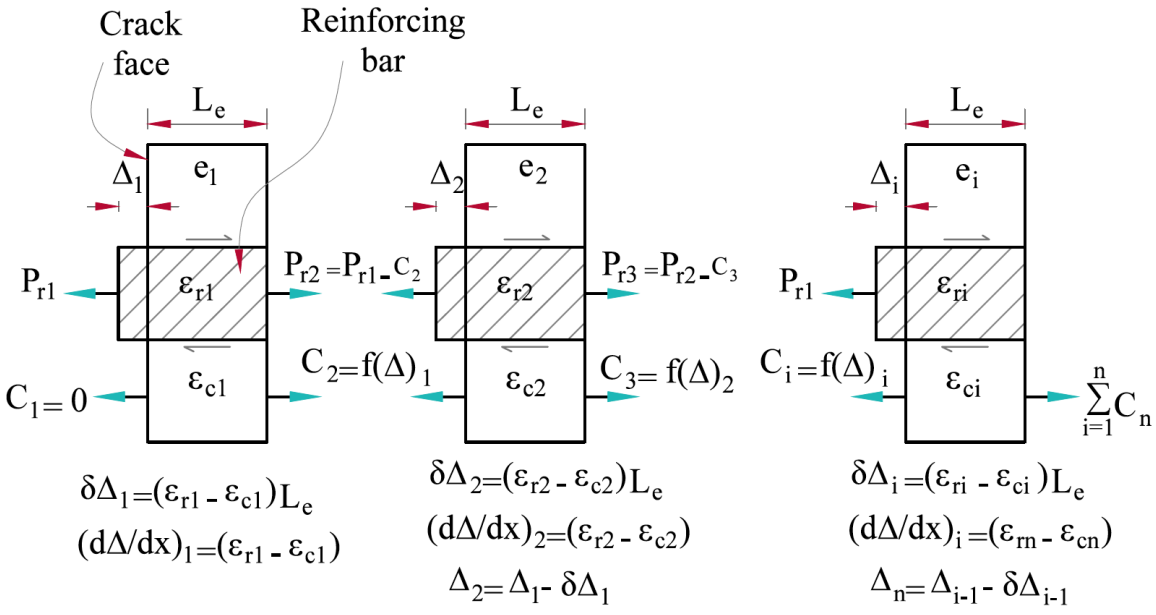

Figure 3.6: Numerical partial-interaction method

In this numerical analysis procedure and as shown in Figure 3.6, a portion of the beam of length L_t (transfer length) to the right or left of the initial crack is considered and divided into a number of elements. The width of each element L_e is taken to be very small so that the slip value can be assumed to be constant over the length of each element. It is now assume that the left hand side of element one (e_1) is the face of the initial crack. In order to plot the first point on the load-slip ($P-\Delta$) curve, an initial value of total slip at the crack face Δ_1 is assumed and the value of the reinforcement force P_{r1} is guessed. Considering element one and from a bond-slip $\tau - s$ method (presented later in §3.3.2.1), the amount of force in the concrete C_1 built up at the right end of element one can be determined as follows:

$$C_1 = L_p L_e \tau_1 \qquad (3.7)$$

Here, L_p is the total perimeter of the bars and bond stress τ_1 is dependent on the value of Δ_1. As the value of stress in the concrete at the left side of element one (crack face) is zero and on the right side is C_1, the mean stress value can approximately be taken as $0.5C_1$. In this stage, the area of the concrete prism A_c and the elasticity of the concrete E_c are known, so the mean concrete strain value ε_{c1} can be calculated. Furthermore, the value of the reinforcement force at the right end of element one is decreased by C_1 and from this, the value of reinforcement strain ε_{s2} can also be found. Knowing the strain values of the reinforcement and the concrete, the value of slip-strain ds/dx, the slip δ in element one can be determined. Slip in the elements is denoted as δ to distinguish it from Δ which is the total slip accumulated at the crack face:

$$\frac{d_s}{d_x} = \varepsilon_{s1} - \varepsilon_{c1} \qquad (3.8)$$

$$\delta = \int \frac{d_s}{d_x} = (\varepsilon_{s1} - \varepsilon_{c1}) L_e \qquad (3.9)$$

Once all values related to element one are known, the same analysis can be applied to subsequent elements and slip-strain and slip values can be calculated. At this stage, the initial guess of P_{r1} should be trialled until full interaction boundary conditions are met, i.e. slip and slip-strain are equal to zero at the same point. If this is not satisfied, the value of P_{r1} should be adjusted and the procedure is repeated. The initially assumed value of Δ_1 and the correct value of P_{r1} plot one point on the $P-\Delta$ curve. The whole procedure is then repeated for higher values of Δ_1 until the total stress built up in the concrete exceeds the tensile strength of the concrete and a primary crack forms at a distance known as the primary crack spacing S_p (Figure 3.7).

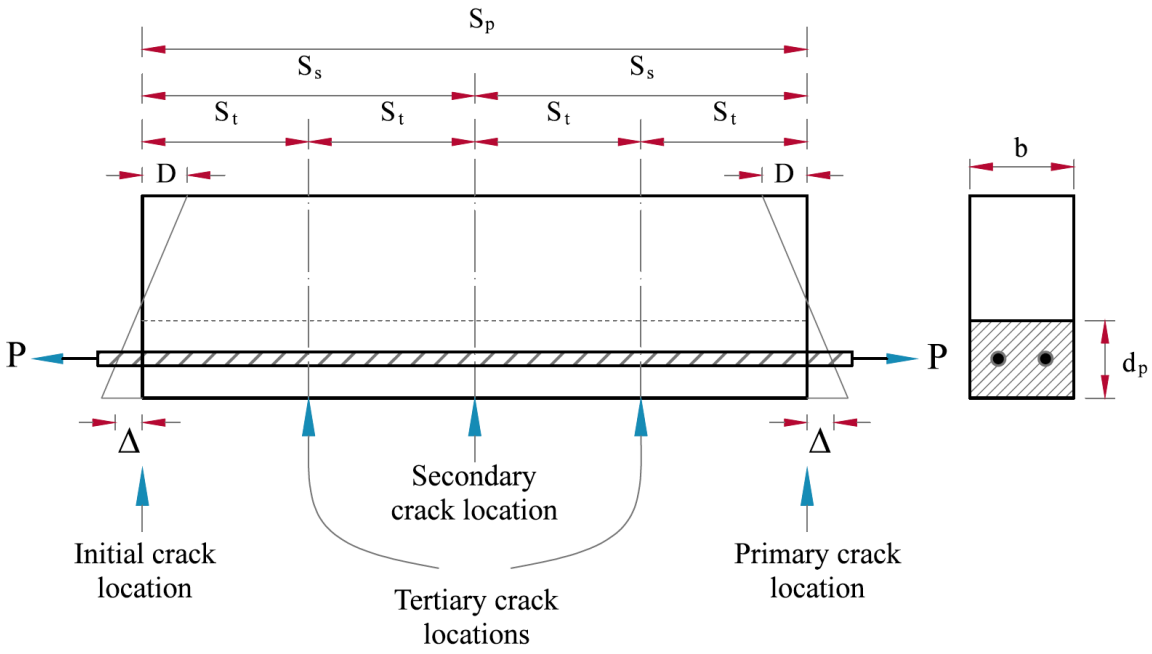

Figure 3.7: Cracking sequence in partial-interaction method

The same procedure is repeated to predict the reinforcement force and the slip value at which secondary and tertiary cracks form (should the bond be strong enough to allow the tertiary cracks to form) when the following boundary conditions are met:

$$\Delta = 0 \text{ and } ds/dx \neq 0 \text{ at } x = S_s = S_p/2 \quad \text{(for secondary cracks)}$$

$$\Delta = 0 \text{ and } ds/dx \neq 0 \text{ at } x = S_t = S_p/4 \quad \text{(for tertiary cracks)}$$

As shown in Figure 3.7, S_s is the secondary crack spacing and S_t is the tertiary crack spacing. It is worth noting that, the longer the bond stress transfer length, the larger the slip value. Therefore, a smaller value of reinforcement force is needed to cause a certain value of slip where cracks are spaced S_p apart from each other compared to the case where the crack spacing is equal to S_s or S_t.

3.3.2.1 Bond-slip method

The bond-slip model used in this thesis is that proposed by CEB-FIP (2010a) shown Figure 3.8. The model is for steel ribbed bars in unconfined concrete and has a parabolic ascending branch up to the ultimate bond stress τ_{bmax}, a horizontal plateau of constant bond stress value, a linear descending branch during which the bond stress decreases to τ_{bf} when the slip value increases, and the final branch where the bond stress remains constant for increasing slip values purely due to friction between the cracked concrete and the reinforcing bar.

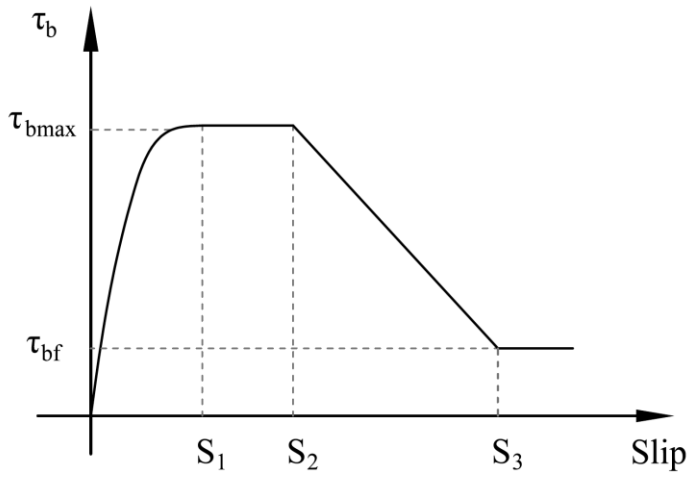

Figure 3.8: Bond-slip relationship under monotonic loading condition

The bond-slip expressions are given below:

$$\tau_b = \tau_{bmax}\left(\frac{S}{S1}\right)^{\alpha} \qquad 0 \le S \le S_1 \qquad (3.10)$$

$$\tau_b = \tau_{bmax} \qquad S_1 \le S \le S_2 \qquad (3.11)$$

$$\tau_b = \tau_{bmax} - \left(\tau_{bmax} - \tau_{bf}\right)\frac{(S-S_2)}{(S_3-S_2)} \qquad S_2 \le S \le S_3 \qquad (3.12)$$

$$\tau_b = \tau_{bf} \qquad S_3 \le S \qquad (3.13)$$

where τ_b is bond stress and S is slip. The values of τ_{bf}, S_1, S_2, S_3 and τ_{bmax} are given by CEB-FIP (2010b) for different bond and concrete confinement conditions.

3.3.2.2 Moment-rotation analysis

After finding $P-\Delta$ relationship for cracked sections as per §3.3.2, a sectional analysis procedure can be employed to find the moment-rotation relationship based on partial-interaction theory. As presented in Figure 3.9, formation of a crack induces a rigid-body rotation 2θ at the cracked region due to a crack widening equal to 2Δ and a displacement in the compression part of the concrete equal to $2D$. The variation of deformation in the compression part of the concrete is assumed to be linear and D is proportional to the value of slip at the crack (Oehlers et al., 2013).

To find the moment-rotation relationship of a section, it is assumed that the section has cracked and an increment of slip is applied. The load in the reinforcement corresponding to that value of slip is found from the $P-\Delta$ analysis described in §3.3.2.

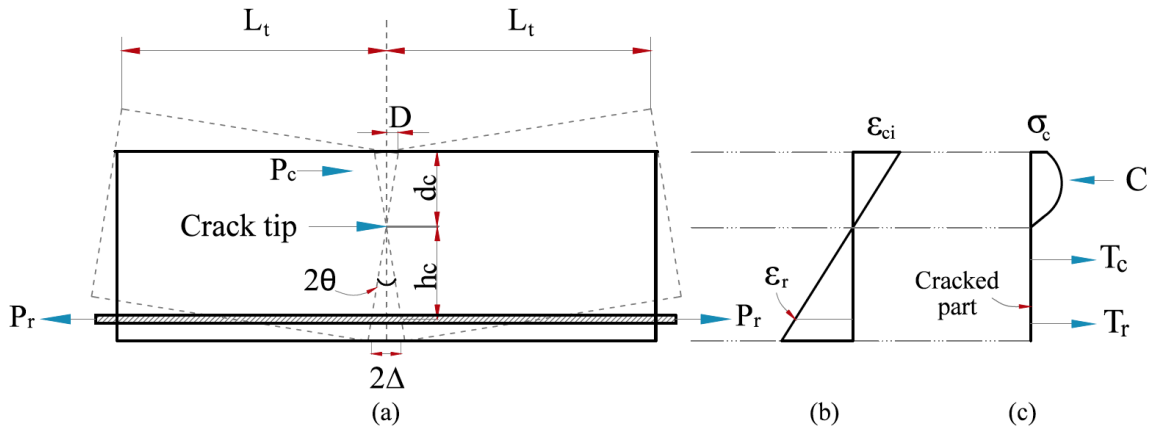

Figure 3.9: (a) rigid body rotation at a crack, (b) strain profile, (c) stress profile

Next, the value of d_c is guessed, and the deformation in the concrete D is calculated from the geometry of the rigid body deformation as:

$$D = \frac{\Delta}{(d - d_c)}\, d_c \qquad (3.14)$$

Where d is the effective depth. The deformation in the concrete D can be converted to a strain profile shown in Figure 3.9(b) by dividing by the deformation length (bond stress transfer length via partial bond interaction) L_t which is equal to half crack spacing (i.e. $S_p/2$ if primary crack spacing is considered).

$$\varepsilon_c = \frac{D}{L_t} \qquad (3.15)$$

Once the strain profile is obtained, the same sectional analysis procedure defined previously for full-interaction analysis in §3.3.1 can be applied (considering the equilibrium of the tension and compression forces) to find the correct value of the initially guessed d_c and subsequently to determine the value of moment M induced by the slip Δ. The crack width value at any crack is simply equal to 2Δ as shown in Figure 3.9(a) and rotation can be found as follows:

$$\theta = \frac{\Delta}{h_c} \qquad (3.16)$$

3.3.2.3 Discrete crack rotation

Deflections can be found using the partial-interaction method through rotation of discrete cracks a long a concrete beam. In the pre-cracking stage, full-interaction analysis is used to find the deflected shape by using the method of integration of curvatures.

However, in the post-cracking stage deflections are found from 1) the contribution of deflection due to curvatures in the non-cracked region, D_f, and 2) the contribution of deflection due to crack rotations in the cracked region, D_t according to Oehlers et al. (2013), as shown as below:

$$D_t = D_f + D_p \qquad (3.17)$$

where D_t is the total deflection value.

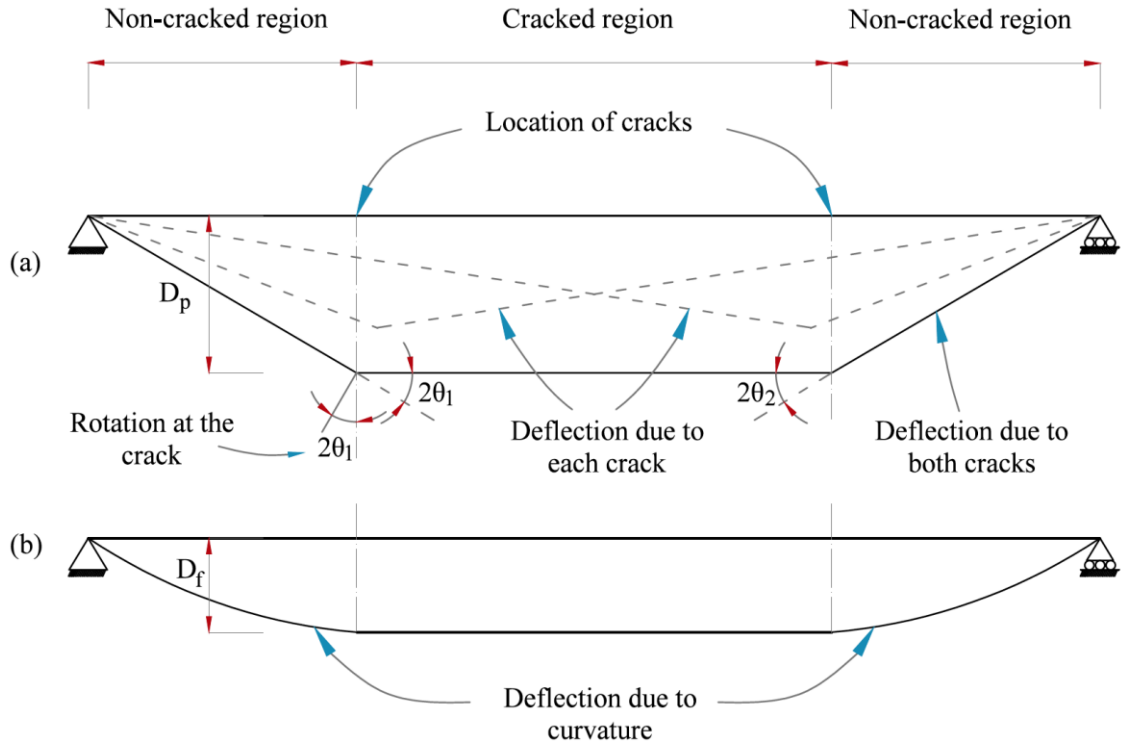

Figure 3.10: Deflections due to (a) discrete crack rotations, (b) curvature

D_f is determined from equations (3.5) and (3.6), and D_p is found as below:

$$D_p = \frac{\theta_i L_1 L_2}{L} \qquad (3.18)$$

where L_1 and L_2 are distances from the crack to the supports, and θ_i is the rotation induced by the crack. When calculating D_f, it is important to note that the beam has non-zero curvature values in the full-interaction (non-cracked) regions only.

Figure 3.10 illustrates the method by which deflection is found using partial-interaction method for a beam that has two cracks as an example. Figure 3.11 shows the procedure of applying partial-interaction method in a flowchart. This procedure was only used in this thesis to check the validity of the partial-interaction method for non-prismatic concrete beams. However, the following section explains that using partial-interaction alone cannot return a valid prediction for the cracking pattern in non-prismatic concrete beams.

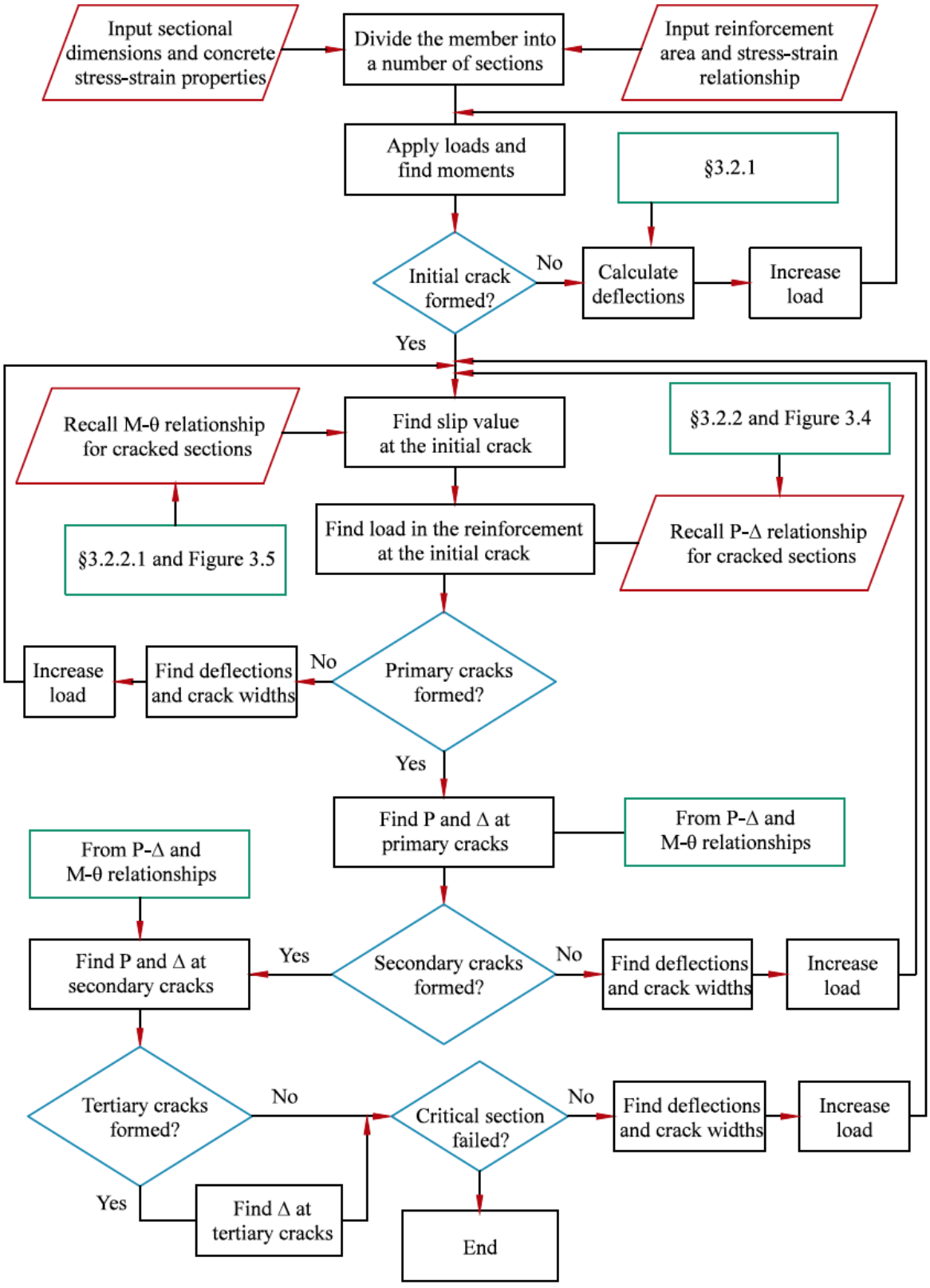

Figure 3.11: Partial-interaction analysis for prismatic beams

3.3.3 Combined-interaction Method

The partial-interaction method (PI) described in §3.3.2 has only been applied to prismatic concrete beams in previous studies. Prismatic concrete beams with a constant section layout along their length and a variable applied moment will crack first at the location of maximum moment. When load increases, the slip value increases at the initial crack location and the force transferred form the reinforcing bars to the surrounding concrete through bond-slip increases. At some point, the stress built up in the concrete exceeds the tensile capacity and another crack forms. As demonstrated in Figure 3.12, this crack forms when the full-interaction (FI) region starts (points *b* and *c*) because the applied moment decreases when moving away from this point into the full-interaction region but the cracking moment capacity stays constant. Therefore, both full and partial interaction methods indicate points *b* and *c* as critical cracking points. For this reason, the occurrence of subsequent cracks can be predicted solely using the PI method for prismatic beams.

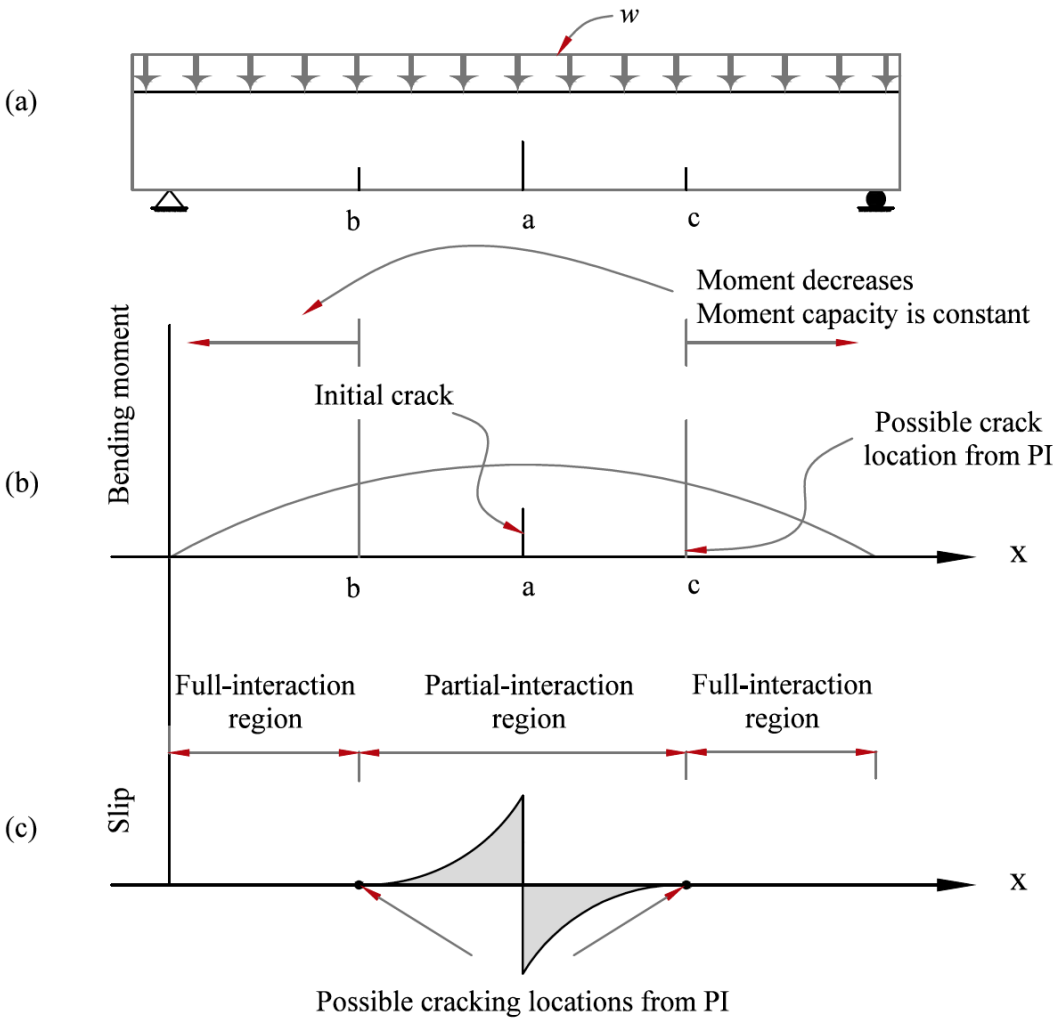

Figure 3.12: Cracking process for prismatic beams according to PI

In the case of non-prismatic concrete beams, sectional cracking capacity is variable along the beam. Once an initial crack formed based on FI mechanism, a PI region forms with a slip distribution shown in Figure 3.13(b). Anywhere outside this region is a FI region and a crack may form at any point where the ratio of the applied moment M_A to the cracking moment capacity M_{Crf} is greatest (according to the full-interaction theory). Therefore, FI and PI methods do not converge to the same cracking locations at a certain stage of loading.

This is explained further in Figure 3.13. Assuming that an initial crack forms at point *a*, there are two points at which the next crack may form due to the PI mechanism. However, there are also two possible cracking regions where an unknown number of cracks may form owing to FI mechanism. In other words, the next crack occurs either 1) when the applied bending moment at the initial crack results in a stress transferred to the concrete (via bond-slip and partial-interaction mechanism) to cause a crack at the primary crack spacing distance S_p; or 2) when the applied bending moment exceeds the cracking moment capacity anywhere in the full-interaction region where slip value is zero.

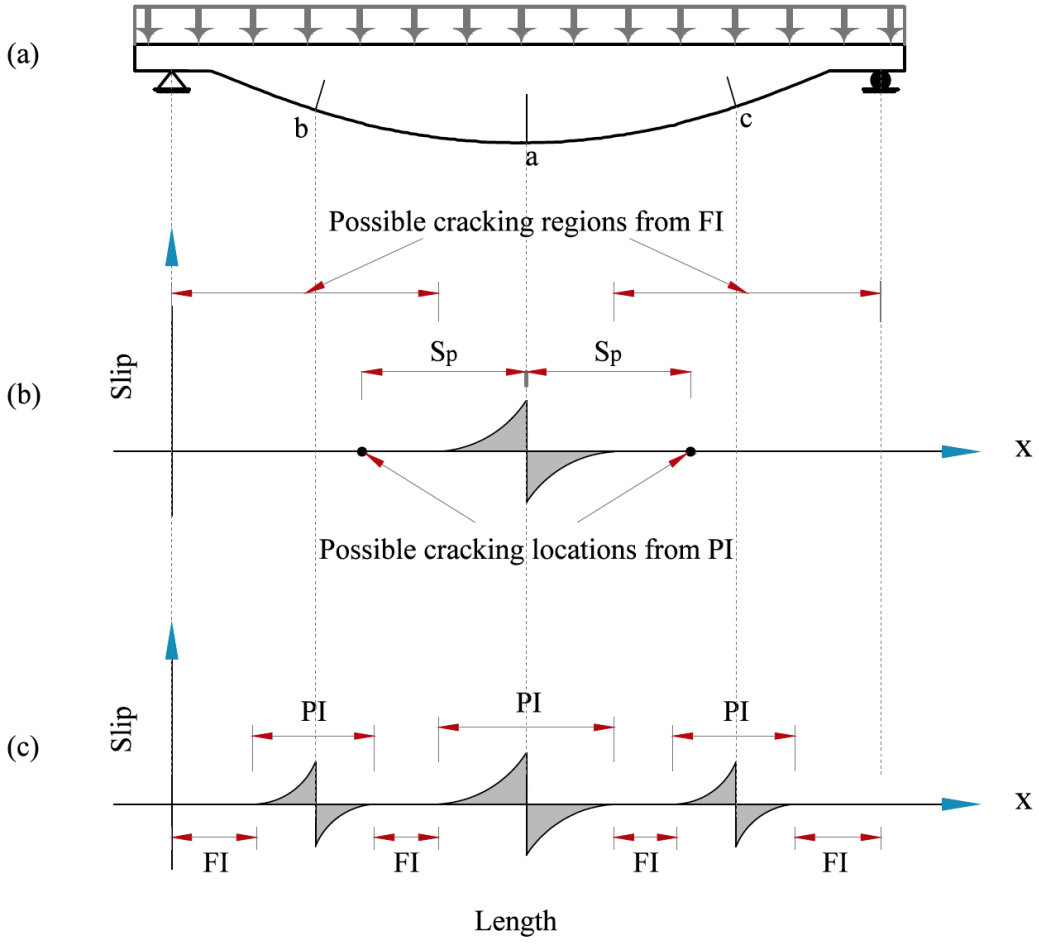

Figure 3.13: Cracking process in non-prismatic beams

Similarly, in Figure 3.13(c), the next crack may occur somewhere in the full-interaction regions marked as FI where the ratio M_A/M_{crf} is largest, or in the partial-interaction regions marked as PI where the applied moment at one of the cracked sections exceeds the moment required to cause another crack through bond-stress transfer.

It is clear from the points mentioned above that, neither of the interaction methods are capable of accurately predicting the location of subsequent cracks for non-prismatic beams. The FI method assumes that cracks are smeared along the length and so discrete locations of cracks are unknown. The PI method on the other hand neglects the cracks that may form through FI mechanism.

The FI method does not account for bond-slip, and therefore, the tension-stiffening effect which will affect predictions of deflections is neglected (Ng et al., 2011). On the other hand, neglecting cracks that may form in FI regions by the PI method makes this method simply invalid to find deflections in non-prismatic beams.

What is seen in reality is a combination of both interaction mechanisms in cracked and non-cracked regions of a concrete beam. Therefore, a new combined-interaction method is developed in the theoretical work carried out for this thesis to predict the deflections and cracking behaviour of non-prismatic concrete beams.

The new combined-interaction method combines the full- and partial-interaction methods in such a way that smeared and discrete crack approaches are applied to different regions of the same beam based on the bond-slip value. The combined-interaction method is established on the following assumptions:

1. The FI method is applied to find deflections in the pre-cracking stage.
2. A combination of FI and PI is applied in the post-cracking stage to find deflections and cracking behaviour.
3. When a crack forms in a FI region at any stage of loading, a new PI region forms in the vicinity of the crack. Slip distribution on the left and right hand sides of the crack is found by using the $P-\Delta$ analysis described in §3.3.2. This eliminates the smeared crack assumption in the FI method (which does not represent reality).
4. At any stage of loading, cracks may form in PI regions when bond-stress transferred to the surrounding concrete exceeds the capacity or in FI regions when cracking curvature is exceeded.
5. Possible crack locations from both interaction methods are found first, only some of them are actual cracks based on the highest possibility of occurrence (represented by a cracking index, explained later) and certain boundary conditions. The boundary conditions are for

example that no FI cracks are allowed to form in the vicinity of other existing cracks where slip has a non-zero value.

3.3.3.1 Register-eliminate algorithm

A numerical 'register-eliminate' algorithm was developed to predict the cracking process of non-prismatic concrete beams based on the combined-interaction method. In this procedure, a generation of possible cracks were found (smeared cracks from FI analysis and discrete cracks from PI analysis) in each step of loading. A goal-seeking algorithm was designed to iteratively eliminate less possible cracks in the calculations and register actual cracks among these possible cracks based on highest possibility. The term "actual crack" here is used for cracks which are predicted to occur.

A MATLAB program was written to automate the procedure. In the first step, the concrete beam is divided into a number of sections. The moment-curvature and load-slip relationship for each section is found based on FI and PI methods respectively. In the PI method mentioned earlier, subsequent cracks are assumed to form at a certain distance from an existing crack. These distances are limited to the primary, secondary or tertiary crack spacing. However, in the combined-interaction method, since crack locations are predicted by both interaction methods rather than just PI, crack spacing can vary. Therefore, the $P-\Delta$ relationship is developed for each section based on a range of possible crack spacing, from closet to farthest possible crack spacing. The closest possible crack spacing is found based on the smallest slip distribution length possible once a crack forms. This is because theoretically no crack will form within the close neighbourhood of an existing crack where slip is not zero. The farthest possible crack spacing is taken as the maximum bond-slip development length because if a crack is farther than this distance from an existing crack, it will have no effect on the $P-\Delta$ relationship of the existing crack.

In the next step, increments of load are applied to the member gradually and the deflection profile is calculated based on FI method up until the onset of the initial crack. The vicinity length (the length of slip distribution region on the left and right hand sides of the crack) of the initial crack is then found. Anywhere outside this region, locations of possible cracks are found using FI analysis. This can be done by introducing a cracking index which is equal to the ratio of the applied moment M_A to the cracking moment capacity M_{crf} at each section. Any section with a FI cracking index M_A/M_{crf} larger than unity accommodates a possible crack. Possible cracks based on the PI method are also found (if any) by finding the applied moment M_A at the cracked section and also the moment needed at the crack to cause another crack to form through PI mechanism M_{crp}. If the PI cracking index M_A/M_{crp} is larger than one then a possible crack location is indicated.

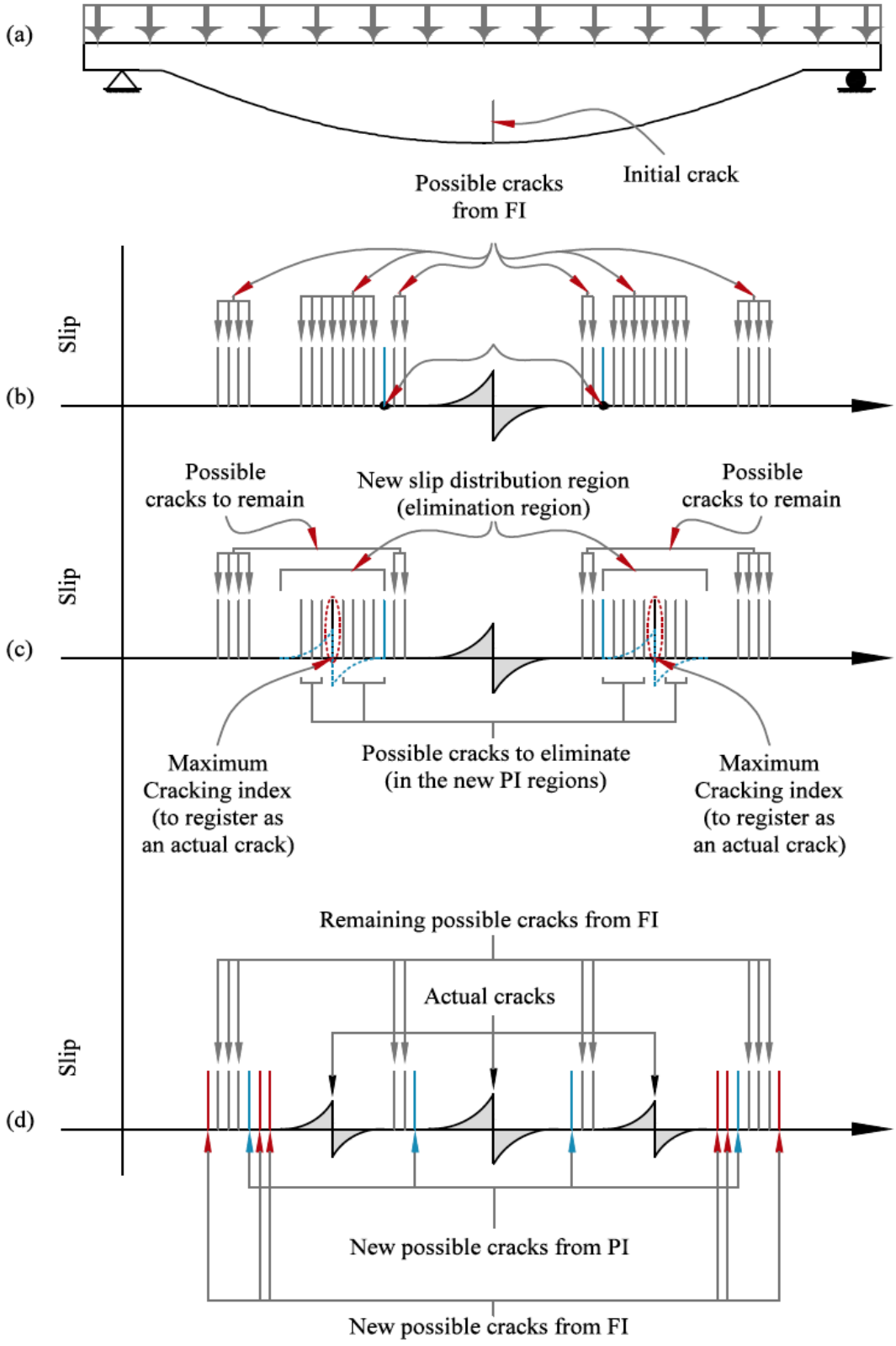

Figure 3.14: Register-eliminate method (a) loading step I, (b) loading step i+1

Figure 3.14 shows the procedure of eliminating possible cracks and registering actual cracks at two consecutive post-cracking loading stages.

Next, actual crack(s) are selected among the possible cracks. The full- and partial-interaction cracking indexes are compered. The first modelled crack forms at a section which has highest cracking index. Slip distribution around this crack is determined using PI method. All possible cracks falling within the vicinity of the newly formed crack are cancelled (eliminated). Furthermore, the section with the second highest cracking index among the remaining possible cracks is selected as another actual crack and again all possible cracks in its neighbourhood (slip distribution region) are eliminated.

This procedure is continued until all possible cracks are either indicated as actual cracks or eliminated from the calculation. In other words, the calculation stops where there is no possibility for other cracks to form at this stage of loading apart from the actual cracks that are already registered. For later stages of loading, the same register-eliminate procedure is applied to find subsequent cracks.

The deflection profile is found by summing the contribution to deflections of, 1) applying method of integration of curvatures to the FI regions where curvature has a non-zero value but slip is zero and 2) by applying discrete crack rotation approach at the actual cracks.

In the early post-cracking stage, deflection from curvatures dominates since there are fewer cracks and full-interaction regions are wider than partial-interaction region. At later stages of cracking however, deflection value mainly governed by rotation discrete cracks rather than curvature.

The procedure used to apply the combined-interaction method in conjunction with the register-eliminate algorithm is illustrated in a flowchart in Figure 3.15.

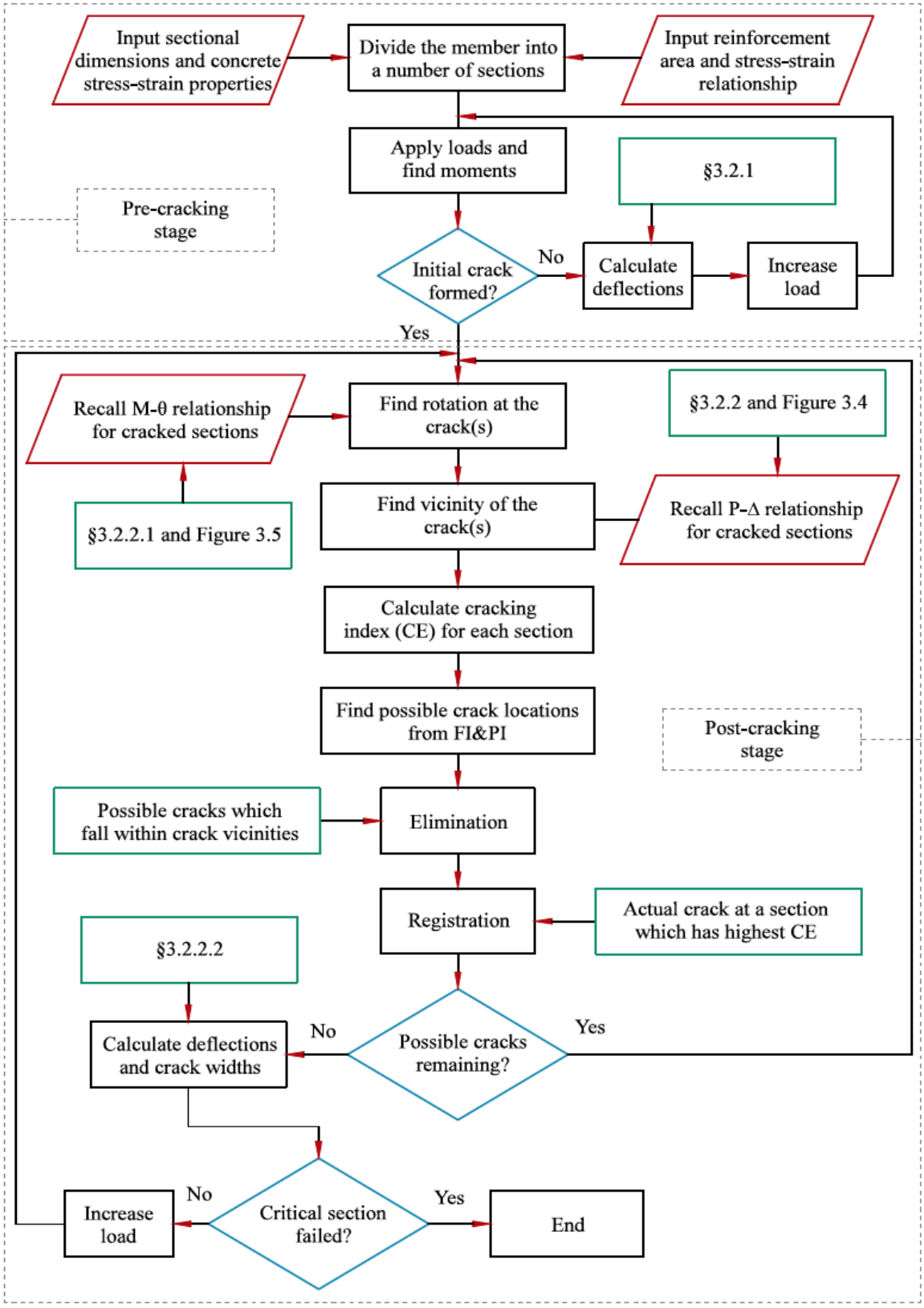

Figure 3.15: The combined-interaction method

3.4 Analysis of statically indeterminate beams

3.4.1 Stiffness matrix method

As discussed earlier in Chapter Two, analysis methods used for statically indeterminate concrete beams can be divided into three main categories; 1) elastic analysis in which reinforced concrete sections are assumed to have linear elastic behaviour for simplicity allowing equations of engineering mechanics to be directly used to find deflections, 2) non-linear segmental analysis, where the concrete beam is discretized into a number of beam elements and either the flexibility or stiffness method is applied to analyse the member, 3) Finite element methods.

Due to material and geometric non-linearity of non-prismatic continuous concrete beams, elastic analysis is not suitable. Besides, optimisation for the ultimate limit state creates beams shaped like the bending moment diagram. If an elastic bending moment distribution is used in the optimisation method, the resulting shape of the beam would not match the real bending moment because of the high degree of moment redistribution within a continuous beam which occurs when the beam shape is changed from prismatic to non-prismatic after optimisation.

The limitation of finite element analysis for non-prismatic concrete beams may arise mainly due to two points, 1) the underlying mathematics such as the partial differential equations that may make predicting cracking hard and 2) the use of empirical relationships that have been calibrated on tests of prismatic beams.

In this work, a new sectional-segmental analysis procedure has been developed. This procedure is based on a standard stiffness and displacement method given in numerous structural analysis textbooks (Ghali and Neville, 1997). The stiffness method was preferred to flexibility method in this work because the stiffness matrix is much easier to construct than the flexibility matrix for the kind of structure considered. Creating the flexibility matrix involves careful selection and introduction of a high number of redundant forces (according to the number of sections taken a long a beam) and finding displacements caused by each of these redundant forces. However, creating the stiffness matrix is simpler as it only involves assembling the standard stiffness matrices of the constituting elements of the beam.

This method of analysis is used in conjunction with two interaction methods in two phases: 1) it was used with the full-interaction method to optimise continuous concrete beams for strength and find deflections for the purpose of comparison with the deflection values predicted by the combined-interaction method and 2) it was used in combination with the combined-interaction method to predict deflections and cracking behaviour of statically indeterminate concrete beams. Since the partial-interaction method has been developed to simulate the serviceability behaviour of simply supported beams only, it is not suitable to be applied to continuous beams as it is, because: 1) the

interaction between hogging and sagging cracking regions affect the results when applied to continuous beams. Clearly, this has not been considered in analysing simply supported beams using this method.

2) The procedure used in this method to find deflections from crack rotations is applicable to continuous beams with some modifications (which is outside the scope of this work).

Generally, regardless of the interaction method chosen, this analysis procedure consists of the following fundamental steps:

Step 1: the main beam is divided into a number of sections and the segments between these sections are treated as smaller beam elements. To address the current analysis problem, the following assumptions are made:

- The beam elements are assumed to be rigidly connected to each other.
- Out-of-plane deformations such as shear and torsion strains are neglected.
- When this procedure is used in combination with the discrete crack method (the combined-interaction method), the cracks are allowed to form at sections only and the beam elements rigidly rotate about cracks the end sections.
- When this procedure is combined with the full-interaction method, the cracks were assumed to be smeared along the beam elements.
- Since the beam is assumed to deform in the xz plane only (vertical deflections and rotations), the kinematic degree of indeterminacy of the beam is equal to twice the number of sections minus the number of supports (restraining forces).

Step 2: the flexural stiffness value of each beam element is found by determining the flexural stiffness at the end sections. The value of the flexural stiffness of the beam element is taken as the average of the values of flexural stiffness of the end sections as illustrated in Figure 3.16.

Step 3: a stiffness matrix is created for each beam element and the global stiffness matrix of the main beam is created by assembling the stiffness matrices of the beam elements.

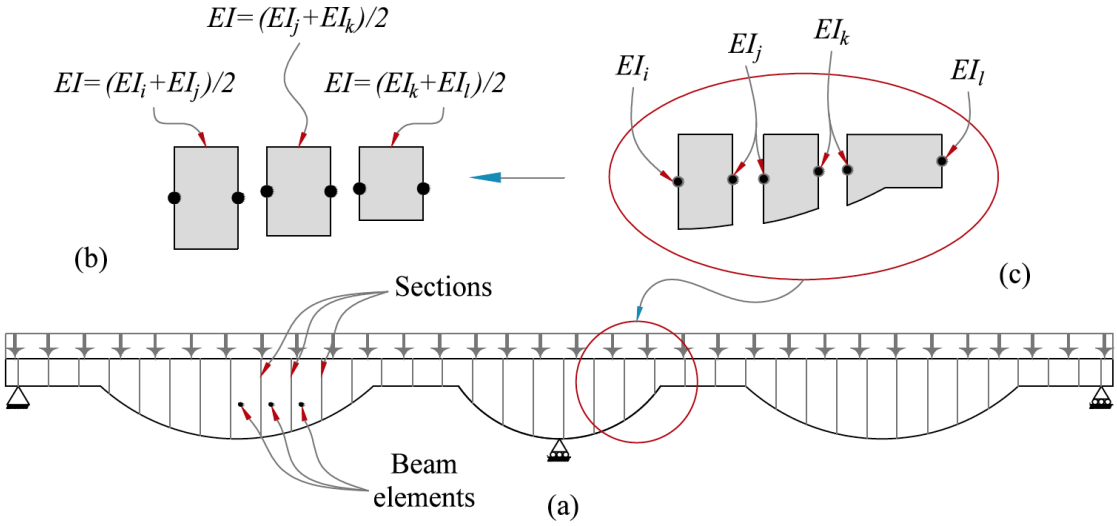

Figure 3.16: Sectional-segmental analysis method

The standard stiffness matrix for rigidly supported beams under flexural loads only is as follows:

$$k_e = \begin{bmatrix} 12EI/L^3 & 6EI/L^2 & -12EI/L^3 & 6EI/L^2 \\ 6EI/L^2 & 4EI/L & -6EI/L^2 & 2EI/L \\ -12EI/L^3 & -6EI/L^2 & 12EI/L^3 & -6EI/L^2 \\ 6EI/L^2 & 2EI/L & -6EI/L^2 & 4EI/L \end{bmatrix} \quad (3.19)$$

Where k_e is the stiffness matrix of a beam element, EI is the average flexural stiffness of the element and L is the length of the element. The global stiffness matrix S of the main beam is given in the form below:

$$S = \begin{bmatrix} k_{e12} & \cdot & \cdot & \cdot & \cdot & \cdot & \cdot & \cdot \\ \cdot & k_{e23} & \cdot & \cdot & \cdot & \cdot & \cdot & \cdot \\ \cdot & \cdot & k_{e33} & \cdot & \cdot & \cdot & \cdot & \cdot \\ \cdot & \cdot & \cdot & k_{e43} & \cdot & \cdot & \cdot & \cdot \\ \cdot & \cdot & \cdot & \cdot & \cdot & \cdot & \cdot & \cdot \\ \cdot & \cdot & \cdot & \cdot & \cdot & \cdot & \cdot & \cdot \\ \cdot & \cdot & \cdot & \cdot & \cdot & \cdot & \cdot & \cdot \\ \cdot & \cdot & \cdot & \cdot & \cdot & \cdot & \cdot & k_{e(n-1)n} \end{bmatrix} \quad (3.20)$$

This method is an incremental method in which the loads are applied incrementally and the flexural stiffness values of the sections are found in each step of loading. In order to account for material and geometric non-linearity (and eventually moment redistribution in the beam), the global stiffness matrix is updated in each step of loading. This is done by finding the flexural stiffness of each section at each stage of loading as below:

$$EI = \frac{M}{k} \quad (3.21)$$

Where M is the applied moment at the section and k is the curvature corresponding to the applied moment.

Step 4: the relationship between the displacements and applied load which is driven from global equilibrium of the beam is then expressed in matrix form as the following:

$$[D] = [S]^{-1}[F] \tag{3.22}$$

$$[F] = [Q] - [FEM] \tag{3.23}$$

Where $[D]$ is the displacement matrix, $[S]$ is the global stiffness matrix, $[F]$ is the global force matrix, $[Q]$ is the applied moments and shear forces matrix and $[FEM]$ is the fixed end forces and moments matrix.

Equation (3.22) can be expanded and written as below:

$$\begin{bmatrix} \delta_1 \\ \theta_1 \\ \delta_2 \\ \theta_2 \\ . \\ . \\ \delta_n \\ \theta_n \end{bmatrix} = \begin{bmatrix} k_{e12} & . & . & . & . & . & . \\ . & k_{e23} & . & . & . & . & . \\ . & . & . & . & . & . & . \\ . & . & . & . & . & . & . \\ . & . & . & . & . & . & . \\ . & . & . & . & . & . & . \\ . & . & . & . & . & . & . \\ . & . & . & . & . & . & k_{e(n-1)n} \end{bmatrix}^{-1} \left(\begin{bmatrix} V_1 \\ M_1 \\ V_2 \\ M_2 \\ . \\ . \\ V_n \\ M_n \end{bmatrix} - \begin{bmatrix} F_1 \\ MF_1 \\ F_2 \\ MF_2 \\ . \\ . \\ F_n \\ MF_n \end{bmatrix} \right) \tag{3.24}$$

Where δ_i and θ_i are values of deflection and rotation at section i, $k_{ei(i+1)}$ is the stiffness matrix of a beam element between sections i and i+1, V_i and M_i are the applied shear force and moment values at section i, and F_i and MF_i are fixed end forces and moments on section i.

Equation (3.24) can be solved numerically to find the deflection profile of the beam for a given loading increment and rotations.

Step 5: Once the displacement values are found at each section, the beam elements can be analysed separately and the forces and moments on each beam element can eventually be found from the following equation:

$$[f] = [s][d] + [fem] \tag{3.25}$$

where $[f]$, $[s]$, $[d]$ and $[fem]$ respectively, are the force matrix, stiffness matrix, displacement matrix and fixed-end forces matrix of a beam element.

At this stage, new values of flexural stiffness are found for the beam elements. These values are used in the next step of loading to perform the above calculations again and find the forces and deformations.

Since the state of the beam in terms of cracking and deformations changes from one step of loading to another, the values of EI at a certain stage of loading may not accurately represent the stiffness of the beam at the next stage of loading. Indeed, if the loading steps are large, a considerable change may occur in the overall value of EI when the state of a high number of sections changes from uncracked to cracked.

Therefore, in order to find accurate values of EI and applied moments in each step of loading, a sub-loop is implemented to iterate the above procedure until a predefined accuracy limit is achieved.

In this sub-loop, once the new values of EI are found at a certain loading step, they will be used to find new values of moments, then the new moment values are used to find another set of new EI values from the moment-curvature relationship of each section. The new values of moments are compared to the old values and this procedure continues until the maximum difference between moment values of two consecutive iterations falls below an acceptable limit according to the following equation:

$$|M_{\max(i)} - M_{\max(i+1)}| < Lim \qquad (3.26)$$

where $M_{max(i)}$ and $M_{max(i+1)}$ are maximum applied moment values in the iteration i and i_1 respectively and Lim is the acceptable accuracy limit.

3.4.1.1 Stiffness method with the full-interaction method

The stiffness method is used with the full-interaction method, in which the cracks were assumed to be smeared along the beam elements, by following the procedure described in the previous section. The flexural stiffness values at each section is determined from previously-developed moment-curvature relationship of the section layout (§3.3.1.1) using equation 3.21. As for the statically determinate beams, this method predicts deflections and sectional flexural strength of the beam only. Therefore, this method (in the part dedicated to the analysis of behaviour in this thesis) is used to find load-deflection relationships of continuous concrete beams and assess the performance of the full-interaction method against the combined-interaction method.

3.4.1.2 Stiffness method with the combined-interaction method

The proposed combined-interaction method and the stiffness method are used to find both cracking behaviour and deflections of continuous concrete beams. In order to follow the formation of the cracks, the register-eliminate algorithm presented in §3.3.3.1 is employed in combination with the five step segmental-sectional analysis procedure described previously.

For every increment of load, the indeterminate concrete beam is analysed and the applied moments are found. Then for the given moment distribution the combined-interaction method was used to find the location and width of cracks in the post-cracking stage. To find the flexural stiffness values

at each section (in the cracked region), which was essential to employ the stiffness method, the deformation in the concrete compression fibre of the section at cracks is converted into curvature. Using equation 3.15, the value of compressive strain in the extreme compression concrete fibre is found and from which curvature is calculated by dividing it by crack tip depth d_c (Figure 3.9) as follows:

$$\kappa = \frac{\varepsilon_c}{d_c} \qquad (3.27)$$

The curvature along the bond-stress transfer length is then assumed to vary proportional to the slip value. Finally, equation 3.21 is used to find the flexural stiffness for any section along the PI region. In the FI regions, the curvature and flexural stiffness values are found according to the procedure described in §3.4.1.1.

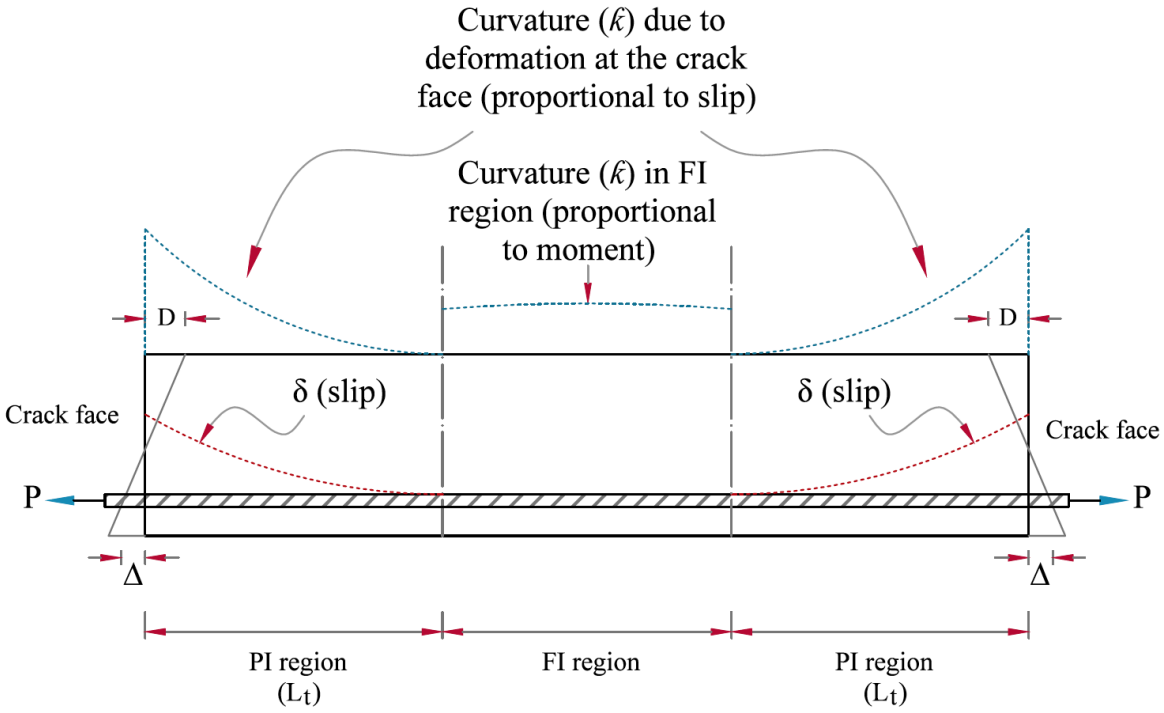

Figure 3.17: Finding curvature in the combined-interaction method

The above analysis procedure is presented in a flowchart in Figure 3.18.

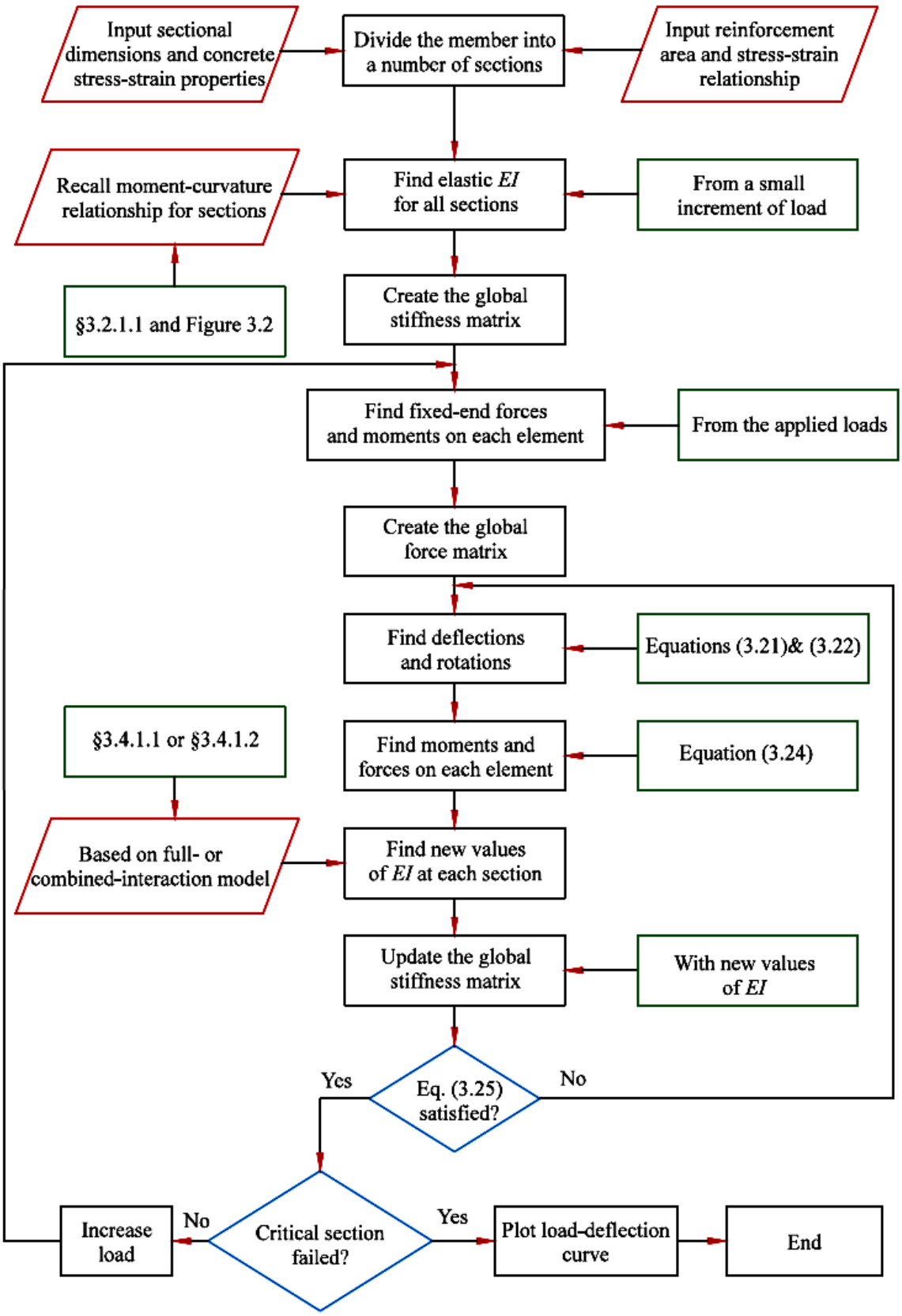

Figure 3.18: Automation of the stiffness analysis procedure combined with the full- or combined-interaction method

3.5 Conclusions

In this chapter, methods developed to predict the behaviour of non-prismatic statically determinate and indeterminate concrete beams are presented. The main conclusions are as follows:

1- A sectional analysis procedure is found to be the most appropriate to use for the purposes of this thesis as it is relatively simple, reasonably accurate and provides a good data compatibility across the main design models (prediction of behaviour, optimisation and form-finding) of flexibly-formed concrete beams.

2- Neither of the full- nor partial-interaction methods are capable of predicting the cracking behaviour of non-prismatic beams when applied alone.

3- A new combined-interaction method is developed to simulate different interaction conditions (between the reinforcing bars and the surrounding concrete) in different regions of a concrete beam. This method combines the full- and partial-interaction methods and finds the actual cracks among the possible cracks predicted by both methods based on highest possibility of occurrence.

4- A new register-eliminate algorithm was developed to find the cracking pattern of concrete beams based on highest possibility of occurrence of cracks according to the full- and partial-interaction mechanisms.

In the next chapter, the theoretical methods developed to optimise flexibly-formed concrete beams for both the ultimate and serviceability limit states are presented along with the form-finding method used to generate the correct beam shape using fabric formwork.

[Blank Page]

Chapter Four

Optimal design and form-finding

4.1 Preface

This chapter presents the methods developed in this thesis to optimise reinforced concrete beams for ultimate and serviceability limit states with the goal of maximum feasible reduction in the volume of concrete used based upon shapes derived using flexible fabric concrete formwork. The ultimate limit states taken into account are flexural and shear capacities. In regard to serviceability, deflection, crack width and stress limitation were considered as the criteria. The methods developed in this chapter were all automated by writing MATLAB programs.

4.2 Choice of optimisation parameter

The behaviour of structural concrete members is dependent on a number of parameters. These parameters are material properties (concrete and reinforcement), cross-section shape and dimensions and reinforcement ratio and layout. In structural optimisation, any of these parameters can be selected as an optimisation variable. However, in order to establish an efficient optimisation procedure, create a feasible design and produce a buildable concrete member shape, there are some factors which need to be considered when selecting optimisation variables. One of these factors is the dependence level of the overall performance of the member on a particular parameter. For instance, the behaviour of a flexural concrete member is more dependent on the cross-section depth than the width. Buildability is another important factor. For example, allowing the cross-section shape to vary along a member is likely to add complications to the fabrication procedure. Moreover, it is not practical to take the reinforcement ratio as an optimisation variable along the member, because bar sizes are constant along their length and curtailing bars is often neither practical nor economical.

For the above reasons, the cross-section depth was taken as the optimisation parameter and all other parameters mentioned above were kept constant along the beam in the optimisation methods developed in this work.

4.3 Objective function

The objective function of an optimisation problem is the function that is to be minimized or maximized according to the targets of structural design. The main aim of this work is to design concrete beams with less carbon footprint compared to conventional prismatic beams through the use of minimum possible amount of concrete material. Therefore, the function which is sought to be minimized here is the total volume of concrete beam V_m, which, in the sectional analysis procedure used, is found as below:

$$V_m = \sum_{i=1}^{n} A_i \, v \qquad (4.1)$$

Where A_i is the area of section i, n is the number of sections taken along a beam, v is the distance between consecutive sections.

4.4 Optimisation constraints

The constraints considered in developing the optimisation methods here are a number of pre-set design code-defined limits used to keep the outcomes of the optimisation procedure within the allowable limits. The optimisation constraints used here are limits on reinforcement ratio and

concrete stress. These constraints are selected because their values vary along the length of variable depth concrete members.

4.4.1 Reinforcement ratio

Limitations on maximum and minimum reinforcement ratios provided by BS EN 1992-1-1 (2004) were incorporated as optimisation constraints in the optimisation procedure. The minimum allowable flexural reinforcement area was taken as the smaller of the following values:

$$A_{s,min} = 0.26\frac{f_{ctm}}{f_{yk}}b_t d \qquad (4.2)$$

$$A_{s,min} = 0.0013 b_t d \qquad (4.3)$$

Where $A_{s,min}$ is the minimum longitudinal reinforcement area, f_{ctm} is the mean value of tensile strength of concrete, f_{yk} is the characteristic yield strength of reinforcing bars, b_t is the mean width of the tension zone and d is the effective depth of the beam.

In order to ensure a ductile failure mode, the maximum reinforcement are $A_{s,max}$ for a given cross-sectional area $A_c$was limited to:

$$A_{s,max} = 0.04 A_c \qquad (4.4)$$

Since the reinforcement area is taken to be constant along the member length, the limitations of the minimum and maximum reinforcement areas were respectively applied to the largest and smallest cross-sections along the beam only.

4.4.2 Stress limitation

In order to avoid high levels of creep, longitudinal cracks and microcracks, the compressive stress in concrete should be kept below allowable limits under service loads according to BS EN 1992-1-1 (2004). Creep in concrete members plays an important role in cracking tendency, durability and long-term excessive deformations (Ghasemzadeh et al., 2016). Longitudinal cracks which may form due to a characteristic combination of applied stresses exceeding the critical value and may lead to reduction in durability (BS EN 1992-1-1, 2004). The inequality below is provided by BS EN 1992-1-1 (2004) used to limit the compressive stress:

$$\sigma_c < 0.6 f_{ck} \qquad (4.5)$$

For those sections that exceed the value in equation (4.5) at serviceability, the section depth is increased until this limit is satisfied.

4.5 Choice of optimisation method

4.5.1 Choice of algorithm

Two main categories of optimisation are described in Chapter Two; deterministic methods and stochastic or probabilistic methods. Deterministic algorithms are mathematically simpler algorithms and always return the same certain outputs for the same initial set of inputs. Probabilistic algorithms, as their name implies, are based on probability and so different starting points of the same problem may not lead to the same solution (Kripka et al., 2015). Considering the objective function, optimisation constraints and optimisation parameters taken into account in this work, a given starting set of parameters and boundary conditions will always converge to the same results regardless of the initial assumptions. For instance, an increase in depth, width or steel ratio will lead to an increase in stiffness and reduction in deflections by a specific amount directly proportional to the increase in the design variable. For a specific change in the input, always a certain change in output is achieved. Furthermore, the objective function, as well as the optimisation constraints, are all continuous functions of the optimisation parameter.

Consequently, a deterministic algorithm is appropriate for the purpose of the work undertaken in this research. The deterministic algorithms rely on direct 'improve-check' routines in which performance is improved and checked iteratively until the optimum solution is reached. However, deterministic methods are not able to find a global optimum among a number of local optima. In order to avoid convergence to a local optimum, theoretical and mathematical derivations to find the correct route towards the global optimum were developed along with specially designed deterministic algorithms to carry out the optimisation procedure. This is explained in detail in the succeeding sections.

4.5.2 Choice of interaction method

Optimisation of structural members usually involves two main tasks: 1) an improvement of properties task which consists of changing design parameters in favour of reaching a desired target, and 2) an assessment of performance task which consists of assessing the behaviour of structural member corresponding to the change made in its properties. As explained in Chapter Three, the combined-interaction method is seen to be more appropriate to be used to predict the behaviour of non-prismatic concrete beams as it mimics what is seen in reality. For optimisation however, methods that use a discrete crack approach, such as the partial-interaction method and the combined-interaction method, are not suitable candidates. This is due to the non-linear behaviour of reinforced concrete members. These methods would allow identification of cracked sections as candidates to improve (by adding material to them as explained in the following sections) at every stage of the procedure. This is attributable to the fact that, cracked sections are weakest sections along the beam

because the flexural stiffness significantly decreases after cracking. Improving those sections would result in maximum improvement in performance of the whole member but adding material to the cracked sections at every step would convert the optimisation procedure into a 'healing' process, and material would be added to the same points repeatedly. It is obvious such an optimisation procedure will not produce a smoothly curved buildable beam shape.

The full-interaction method, which is based on a smeared crack approach, eliminates local discontinuity in the behaviour of concrete beams due to cracking and so is an appropriate method to base the optimisation method on. Therefore, in every design iteration of the proposed methods, the full-interaction method is used to find where best to add material, all the while optimising for ultimate and serviceability limit states (the improvement of property task). The combined-interaction method is then used to predict the performance of the optimised shapes in order to decide on whether further optimisation is required (the assessment of performance task).

4.6 Optimisation of simply supported beams

4.6.1 Optimisation for strength (Shape optimisation)

A sectionwise analysis procedure is adopted in both prediction methods and optimisation methods. The proposed shape optimisation routine directly chooses a shape that resists the applied moments and shear forces at each vertical section. The final shape, of a strength optimised concrete beam, looks like the bending moment diagram with minimum permissible depth near the supports to account for higher shear stresses and minimum allowable section depth.

4.6.1.1 Calculating selfweight

Self-weight may have a significant impact on the behaviour of concrete beams at serviceability, especially for beams with larger spans. In order to account for the variable selfweight of the beam accurately, an iterative procedure is carried out in this stage. In the first iteration, zero selfweight is assumed along with other imposed and variable loads on the member. Once the initial shape is found from the imposed loads, the selfweight can be found and used in the calculations. An increase in the applied moments owing to addition of selfweight occurs and a new shape corresponding to the new moments is then found. This procedure is continued until the difference between the selfweight of the beam at two subsequent iterations is negligible.

4.6.1.2 Bending resistance

Bending resistance of every section along the beam should withstand the applied bending moment on that section. What defines the initial shape of the beam under consideration is the applied bending moment and the shape is modified later to satisfy the other optimisation constraints. The moment-curvature analysis described in §3.3.1.1 was used to find the ultimate bending resistance of every

section. For statically determinate beams, the ultimate failure of the section was considered to be due to yielding of the tensile bars. However, for statically indeterminate beams different modes of failure can be assumed due to moment-redistribution capacity in indeterminate beams.

Optimisation for bending moment is simple and straightforward. At any section, the cross-sectional depth is varied until its bending moment capacity is equal to, or just larger than, the applied bending moment. This is repeated across all sections until the full shape of the beam is found. This is explained in later sections of this Chapter.

4.6.1.3 Shear resistance

Optimisation of shear capacity was carried out based on relatively simple expressions suggested by CEB-FIP (2010) where the total applied shear force at any section is resisted by the shear capacity of the concrete $V_{Rd,c}$ and the shear capacity of the links $V_{Rd,s}$ as follows:

$$V_{Rd} = V_{Rd,c} + V_{Rd,s} \tag{4.6}$$

$$V_{Rd,s} = \frac{A_{sw}}{S_w} Z f_{ywd} cot\theta \tag{4.7}$$

$$V_{Rd,c} = k_v \frac{\sqrt{f_{ck}}}{\gamma_c} b_w \tag{4.8}$$

$$k_v = \frac{180}{1000 + 1.25Z} \tag{4.9}$$

Where b_w and d is the width and the effective depth of the beam respectively, A_{sw} is the area of shear reinforcement within spacing S_w, and f_{ywd} is the yield strength of the shear links, Z is the lever arm taken as $0.9d$, θ is the angle of compression field assumed to be 40 degrees, f_{ck} is the characteristic compressive strength of concrete, γ_c is the partial safety factor for concrete (taken as 1.0 in this work).

For each section, the shear capacity contribution from the concrete was first found, then necessary shear reinforcement ratio was calculated. To simplify the construction process, the shear link spacing was unified over multiple regions by choosing the minimum spacing found in each region. For sections that required a higher shear reinforcement than the maximum allowable shear reinforcement ratio, the section depth was increased until the required sectional shear capacity is achieved.

4.6.2 Optimisation for serviceability (Topology optimisation)

BS EN 1992-1-1 (2004) indicates deflection control, crack width control and compressive stress limitation in the concrete as the main serviceability limit states and prescribes limits for each that must be satisfied in design. For a concrete structure to satisfy serviceability limit states, large deflections should not affect appearance and duty of the structure, crack widths should not be large

enough to cause durability problems and make the structure aesthetically undesirable (Gilbert, 2011). The compressive stress in the concrete shall not be above a limit that results in longitudinal cracks, micro-cracks or considerable levels of creep (BS EN 1992-1-1, 2004). The limitation on compressive stress is dealt with by taking stress in concrete as an optimisation constraint, as explained in §4.4.2.

In order to optimise for the ultimate limit state, the depth of a reinforced concrete beam follows the requirements of the stress resultants at any section. This is straightforward. However, in considering further optimisation to satisfy the serviceability limit states of cracking and deflection it is not immediately obvious where material should be added (if deemed necessary) in order to have greatest effect on reducing cracking or deflection at specific locations. This problem is more complicated than the simple sectional strength-related approach to optimisation, and requires an overall topology optimisation procedure, which accounts for cracking in the reinforced-concrete structure.

The whole serviceability optimisation procedure can be divided into two parts, 1) a theoretical derivation where the best locations to which to add material are identified, 2) a deterministic algorithm that iteratively adds material to these locations and assesses the performance of the member until the designated optimisation targets are reached.

4.6.2.1 Deflection

Considering the deflection limit state, adding material (increasing depth) to any section would result in an increase in flexural stiffness and a reduction in deflections. The role of the topology optimisation procedure here is to find the best location to which material should be added so that maximum reduction in deflection is achieved. This will ensure quickest possible convergence to an optimum shape in terms of computational time and more importantly minimum possible usage of material for the member.

Finding the best locations to which to add material in each optimisation loop can be done in three ways. First, by simply adding material to each section then comparing the performance of the beam in each step and finally choosing the section for which adding material resulted in maximum reduction in deflections. Second, by employing a probabilistic goal-seeking algorithm (such as those methods reviewed in Chapter Two) which uses a technique that results in a smaller number of attempts compared to the first method to find the best candidate location to add material. Third, by theoretical analysis to identify the locations to which adding material would lead to an optimal design.

Method one needs a considerable computation time because this procedure has to be repeated in every optimisation loop. Method two may be computationally less time-consuming than method one but still requires a significant amount of time due to the complexity of the method. The third method

improves computational time and simplifies the whole optimisation procedure as explained in the following section.

4.6.2.1.1 Theoretical derivation

In order to gauge how a change in depth of any section reflects a change in maximum deflection of the beam as a whole, the full-interaction method and numerical integration of curvatures is used. A typical simply supported beam under uniformly distributed loading with its schematic representation of curvature distribution at serviceability is considered as shown in Figure 4.1. Points a and d indicate the boundaries of the cracked region and the sections located within this region are all assumed to have cracked according to FI theory (smeared cracks). Points b and c represent the boundaries of a region where curvature is inversely proportional to the value of the applied moment. In this way, equations (3.5) and (3.6) are solved as shown below:

$$\theta_n = \kappa_1 v + \kappa_2 v + \kappa_3 v \dots\dots\dots \kappa_n v + C_1 \tag{4.10}$$

$$D_n = n\kappa_1 v + (n-1)\kappa_2 v + (n-2)\kappa_3 v \dots\dots\dots \big(n-(n-1)\big)\kappa_n v + C_2 \tag{4.11}$$

that is:

$$D_n = l_1\left(\frac{M_{A1}}{EI_1}\right)v + l_2\left(\frac{M_{A2}}{EI_2}\right)v + l_3\left(\frac{M_{A3}}{EI_3}\right)v \dots\dots\dots l_i\left(\frac{M_{An}}{EI_n}\right)k_n v + C_2 \tag{4.12}$$

where k_n, θ_n, D_n, M_{An} and EI_n are values of curvature, rotation, deflection, applied bending moment and flexural stiffness at section n respectively, C is the coefficient of integration, l_i is the distance between section i and section n, and v is the distance between two successive sections as shown in Figure 4.1. For the purposes of illustration, it is assumed that section n is at mid-span, where maximum deflection occurs (although this is not a necessary assumption). Section i is a candidate section for the addition of material for which an increase in depth of Δd increases the flexural stiffness by ΔEI_i. It can be seen from equation (4.13) that reduction in maximum deflection ΔD_n is proportional both to distance from this point to the point of maximum deflection, l_i and the applied moment M_{Ai} at section i but inversely proportional to the change in flexural stiffness ΔEI_i of section i. Therefore:

$$\Delta D_n \propto \frac{l_i M_{Ai}}{\Delta EI_i} \tag{4.13}$$

It can readily be seen that the reduction factor $l_i M_{Ai}/\Delta EI_i$ for any section plays a decisive role in choosing a section as a candidate to which to add material. That is, the section with the maximum reduction factor results in maximum reduction in mid-span deflection, and therefore it is the prime candidate section to which to add material.

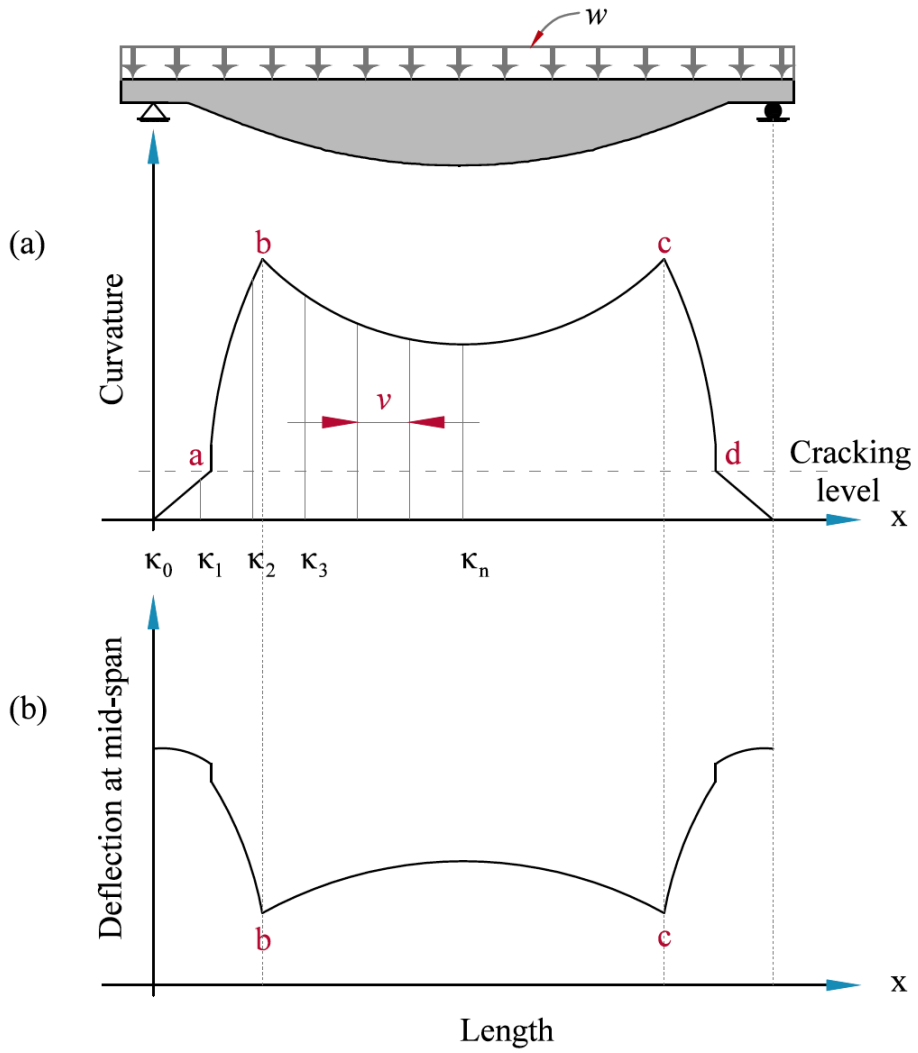

Figure 4.1: (a) schematic curvature distribution of a strength-optimised simply supported beam under uniformly distributed loading, (b) schematic influence line for mid-span deflection based on a unit amount material moving along the beam

With regard to deflections, the maximum reduction factor $l_i M_{Ai}/\Delta EI_i$ (which is equal to $l_i \Delta\kappa_i$) can be achieved by adding material to the section with maximum curvature as explained below:

The amount of reduction in curvature for a section after adding depth is proportional to the original value of curvature at that section before adding material (for a given value of moment on that section) as follows:

$$\Delta\kappa_i \propto \kappa_i \qquad (4.14)$$

Moreover, for sections between point *b* and *c* in Figure 4.1, curvature is seen to increase when moving away from mid-span:

$$\kappa_i \propto l_i \qquad (4.15)$$

From equations (4.11) & (4.12):

$$\kappa_i \propto l_i \Delta\kappa_i \qquad (4.16)$$

According to equation (4.16), within that region (between point *b* and *c*), the higher the curvature value, the higher the reduction factor $l_i\Delta\kappa_i$. However, outside that region, curvature value decreases when moving away from mid-span and equation (4.16) changes to:

$$\kappa_i \propto \frac{1}{l_i} \qquad (4.17)$$

The rate at which $l_i\Delta\kappa_i$ changes when moving from point b towards the supports depends on the changing rate of Δk_i and l_i. It can be seen from Figure 4.1(a) that curvature value (and so $\Delta\kappa_i$) decreases rapidly when moving from point *b* towards point *a* but distance from mid-span l_i steadily increases because distance between two successive sections is constant. Therefore, the reduction factor for those sections is smaller than the reduction factor of the section of maximum curvature.

In order to further demonstrate this, the principal of influence lines for a moving unit load is applied. Instead of a moving unit load however, a unit amount of material is moved along the length of the member (i.e. a set amount of additional depth is added to sections) to create an influence line of mid-span deflections, as shown in Figure 4.1(b). It can be seen how adding material to each section in turn along the member changes the maximum deflection value at mid-span. It is clear from Figure 4.1(b) that increasing the depth of sections at b and c, which have maximum curvature values, results in smallest mid-span deflections (i.e. greatest reduction in mid span deflections).

4.6.2.2 Crack width

Optimisation for crack widths is a more complicated process due to a large localised reduction in flexural stiffness at a cracked section which must be accounted for. One way to decrease crack widths of a beam is to allow a higher number of cracks to form within the cracking region right at the onset of cracking. This ensures shorter bond stress transfer length between the cracks, smaller slip values and therefore smaller crack widths.

Similar to optimisation for deflections, this can be achieved by adding material gradually to the sections that have maximum curvature value in each optimisation loop.

This can be illustrated by considering examples of two concrete beams, one of them optimised for strength only and denoted as T-OS-S, the other is optimised for both strength and stiffness (by adding depth to the location of maximum curvature) and denoted as T-OSS-S. These beams were designed and tested to validate the numerical methods developed in this thesis and their full details are given in Chapter Five. In Figure 4.2, the curve CC-T-OS-S represents the curvature values at which each section cracks, for a beam optimised for strength only, and the curve CD-T-OSS-S is

the curvature distribution of the same beam under loading at the onset of cracking (when first cracks appear in the beam).

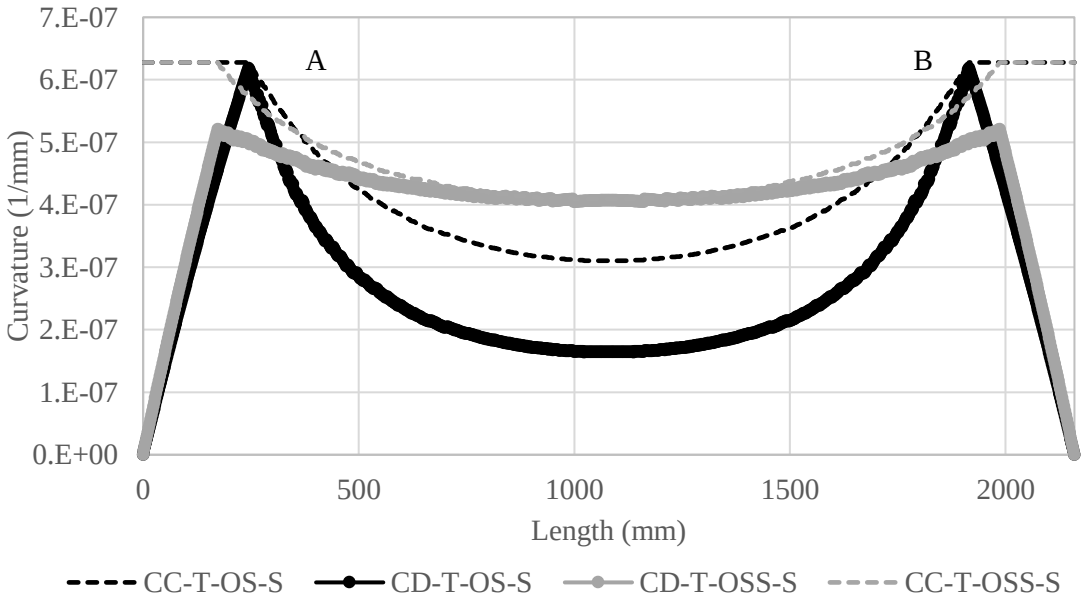

Figure 4.2: Curvature distribution and cracking curvature curves of simply supported concrete beams optimised for strength and serviceability limit states

It can be seen from the plots that cracks start to form at the sections which have maximum curvature values at points A & B (where the two curves meet). These cracks tend to be relatively wide local cracks because subsequent neighbouring cracks take longer to form under increasing load when the curves CC-T-OS-S and CD-T-OS-S gradually converge towards the mid-span (the two curves rapidly diverge when moving away from point A and B). The cracks are forced to scatter over a wider region, leading to higher concrete-reinforcement bond stress transfer at each crack, larger slip values and eventually wider cracks.

When material is added to the section of maximum curvature, the cracking capacity of that section increases. If material is added iteratively in this manner, the cracking moment capacity of regions A and B in Figure 4.2 increases until at some point the optimised beam shape will be liable to crack first at mid-span rather than at points A and B. Such a procedure delays the cracking process and produces a final beam shape that has as wide a possible cracking region at the time of cracking compared with a beam optimised for strength only. In order to illustrate this further, another example is considered of a beam which is optimised for strength and serviceability by adding material to the point of maximum curvature, denoted as T-OSS-S. The cracking curvature distribution (curvature at cracking is calculated for each section) of this beam is denoted by CC-T-OSS-S in Figure 4.2, while CD-T-OSS-S is the curvature distribution at the beginning of cracking of the whole beam.

Compared with the T-OS-S plots, there are longer regions of match between the two curves CC-T-OSS-S and CD-T-OSS-S. The initial crack and subsequent full-interaction cracks form at a faster rate than in the case of beam T-OS-S.

This allows for multiple full-interaction cracks to form at small distances from each other before the cracks widen due to bond-slip under service loads.

It should also be noted that a delay in cracking initiation has been achieved. In these examples, cracking in beam T-OSS-S initiated at a loading level equal to 21% of the failure load, compared with beam T-OS-S in which cracking started at 19% of the failure load.

It is evident now that an effective way to optimise simply supported concrete beams for serviceability is to add material gradually to the sections that have maximum curvature until the optimum beam shape is produced.

4.6.3 Buildability

Due to the non-linear behaviour of reinforced concrete, using a theoretical method to optimise concrete beams for deflection can produce an irregular beam shape which is difficult to reinforce and build, rather than a smoothly curved beam shape as shown in Figure 4.1 (which is a typical simply-supported beam shape optimised for strength only). Buildability therefore must be taken into account as an important constraint in the optimisation procedure as explained below.

Considering buildability, once material is added to the section that experiences the maximum curvature, the curvature value decreases and one of the neighbouring sections will possess the maximum curvature value in the next optimisation step. In this manner, material is added gradually over a distributed region, as an iterative process, without resulting in sudden discontinuities, but rather a smooth beam geometry.

4.7 Optimisation of continuous beams

4.7.1 Optimisation for strength (Stable state method)

Optimisation of statically indeterminate beams for strength is not a direct and simple procedure as that of determinate beams for two reasons: 1) Flexural stiffness (EI) values should initially be assumed (because the geometric and reinforcement properties of the beam are not yet known) in order to analyse the indeterminate beam and therefore, the calculated values of the applied moments and shear forces do not represent the actual values; and 2) Moment distribution along the beam changes significantly after optimisation for strength is carried out because the shape of the member and so flexural stiffness distribution along the beam changes.

In this work, an incremental optimisation procedure is developed (referred to as stable state method) in which a number of analysis and optimisation iterations for the same loading arrangement are carried out. The output of a certain iteration (shape) is used as the input (stiffness distribution) of the next iteration until a stable state between the output and input data of an iteration is achieved. The procedure employs the sectional-segmental analysis method described in §3.4 in which the whole beam is divided into a number of smaller beam elements and the forces and moments are found on each element. After analysing the beam, a suitable section layout is selected (using the moment-curvature analysis) that has a moment capacity equal to or just larger than the applied moment in each section.

There are three main factors affecting the ability of the strength optimisation procedure to converge to an acceptable solution and the computational time needed. These factors are the initial input values (i.e. the initially assumed EI distribution), the choice of failure region (negative or positive moment region) and the choice of failure mode.

The initial EI distribution results in a bending moment diagram and a particular beam shape upon which the calculation time of the optimisation procedure depend. The optimisation problem of a statically indeterminate beam reaches solution when two conditions are satisfied: 1) the moment capacity at each section is equal to or slightly larger than the applied moment at that section, and 2) the flexural stiffness values at two successive optimisation loops are nearly equal. This ensure that the moment distribution at two consecutive loops does not change.

Two different indexes were introduced to aid the optimisation method and to direct the problem towards convergence to an optimum solution. The capacity-stiffness index I_{cs} is the representation of stiffness distribution at failure EID_f of a beam shape (stiffness of sections at failure) corresponding to the moment capacity MD_f values across all sections (moment capacity distribution).

$$EID_f = \{EI_{f1}, EI_{f2}, EI_{f3}, EI_{f4} \dots \dots \dots \dots \dots \dots \dots EI_{fn}\} \quad (4.18)$$

$$MD_f = \{M_{f1}, M_{f2}, M_{f3}, M_{f4} \dots \dots \dots \dots \dots \dots \dots M_{fn}\} \quad (4.19)$$

I_{cs} is found for all sections along the beam as follows:

$$I_{cs} = \frac{MD_f}{EID_f} \quad (4.20)$$

The moment-stiffness index I_{sm} represents the flexural stiffness distribution EID_a corresponding to the applied moment distribution MD_a and is found as below:

$$EID_a = \{EI_{a1}, EI_{a2}, EI_{a3}, EI_{a4} \dots \dots \dots \dots \dots \dots \dots EI_{an}\} \quad (4.21)$$

$$MD_a = \{M_{a1}, M_{a2}, M_{a3}, M_{a4} \dots \dots \dots \dots \dots \dots \dots M_{an}\} \quad (4.22)$$

$$I_{ms} = \frac{MD_a}{EID_a} \quad (4.23)$$

Where n is the number of sections taken along the beam. These indexes represent the state of the optimisation procedure and the rate of convergence to a solution at any given loop. At the first loop, an assumed EID_{a1} is used to find the initial moment distribution MD_{a1}. A beam shape and cross-section layout(s) are then found according to MD_{a1}. The new shape has a stiffness distribution EID_{a2} found from the applied moments MD_{a1} using (equation 3.20). The analysis of the beam based on the new stiffness distribution EID_{a2} produce a new moment distribution MD_{a2} which does not match with moment capacity distribution MD_f. Therefore, the optimisation should continue and a new shape should be found from MD_{a2} . The final loop and the optimum shape is reached when the capacity-stiffness index of the optimised beam shape is nearly equal to the moment-stiffness index of the previous loop as follows:

$$I_{cs,j} \approx I_{ms,j+1} \quad (4.24)$$

Such a condition indicates that, the stiffness values of the optimum shape under the given loading arrangement produce applied moment values equal to the moment capacity of this shape at any section. The closer these index values are at any two consecutive optimisation loops, the closer the optimisation procedure to an optimum solution.

During the optimisation cycle, for every new beam shape a new EI distribution along the beam and a new moment distribution is achieved. Unlike simply supported beams, using a single-looped shape optimisation method for strength for continuous beams produces a shape that is not capable of resisting the applied loads. Before arriving at an optimum shape, there is an unstable state between the applied and capacity moment distribution curves in which the curves exceed each other in different regions. This is illustrated by considering a typical double-span beam shown in Figure 4.3.

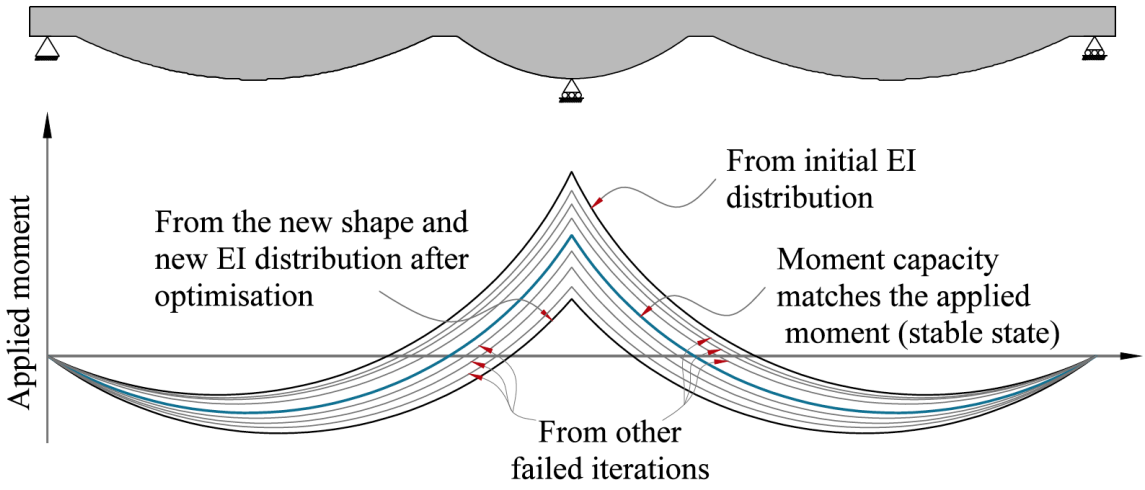

Figure 4.3: Optimisation procedure of a double span continuous beam

4.7.1.1 Upper and lower bound optimum solutions

Depending on the cross-section properties of a beam and the applied loadings, any optimisation problem for statically indeterminate concrete beams converge to only one possible optimum solution. An upper bound solution is reached when the cross-sections in the hogging region have a low capacity-stiffness index relative to that of the sagging region as presented in Figure 4.4. Low I_{cs} values in a region means selected sections that have a moment capacity to resist the applied moment have high stiffness values and high stiffness values attract high values of applied moment which eventually results in further growth of shape in that region.

In contrast, a lower bound solution is achieved when the I_{cs} in the sagging regions is low compared to that of the hogging region. The value of I_{cs} depends entirely on the cross-section geometry, reinforcement layout and reinforcement ratio. Therefore, a desired optimum shape in terms of appearance and the amount of saving in concrete material can be attained by carefully selecting cross-section layout(s) for sagging and hogging regions.

For example, selecting cross-sections that have low I_{cs} in the hogging region results in a higher maximum hogging moment value as illustrated in Figure 4.4. Optimising for this moment distribution brings about a beam shape which has larger cross-section sizes in the hogging region than the sagging region. This therefore produces higher EI values, greater moment values and eventually even larger cross-section sizes in the hogging region. Continuing this procedure yields shape one shown in Figure 4.4.

The upper and lower bound solutions (shape one and shape two in Figure 4.4) are reached when the optimisation process comes to a stable state. Therefore, these beam shapes are capable of carrying the applied loads used in the optimisation. However, an optimum shape in terms of minimum volume of concrete material may fall within the interval between these two bound shapes. For a given beam

problem under defined loading conditions, tuning the values of $I_{cs,hogging}$ and $I_{cs,sagging}$ by trying different cross-section layouts helps finding an optimum shape using the proposed optimisation procedure.

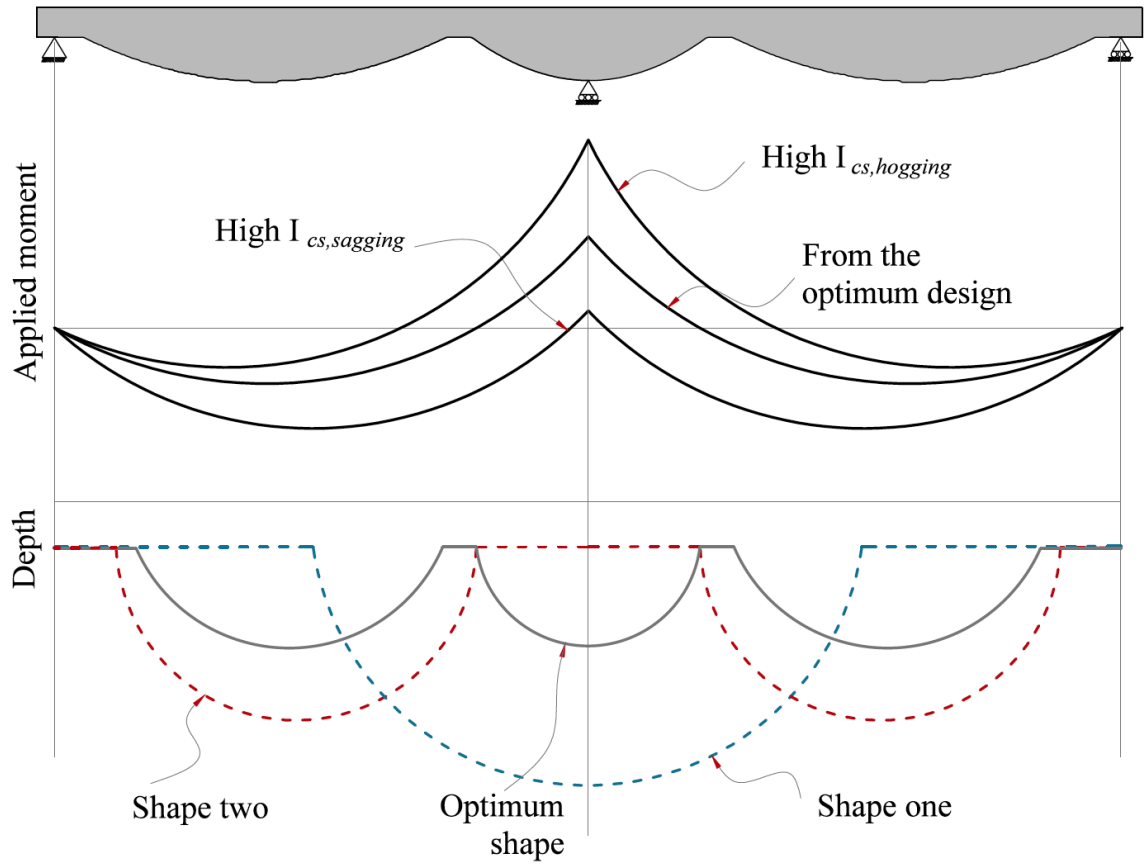

Figure 4.4: Effect of initial flexural stiffness distribution

4.7.1.2 Failure modes

In steel reinforced continuous concrete beams, when the steel yields in a section, stiffness decreases considerably in that section and the applied moment is redistributed to the stiffer sections, (Bagge et al., 2014). This continues until complete failure of the beam occurs by rupture of the steel bars or crushing of the concrete at the initially yielded section.

In non-prismatic continuous concrete beams, depending on whether moment redistribution is considered in the design or not and depending on the direction of moment redistribution (from which region to which), four modes of failure are possible:

1) The yield of tensile steel bars is assumed to be the failure point of any section (point b in Figure 4.6(a)) in both hogging and sagging regions. The tensile steel bars in all sections along the beam yield theoretically at the same time and so no moment redistribution due to yield of steel bars can be considered.

2) The failure point of all sections in the hogging region is assumed to be the crushing point of the concrete (point c in Figure 4.6) but for sections in the sagging region yield of the steel bars dictate the maximum capacity (partial moment redistribution is considered).

3) The failure point of all sections in the sagging region is assumed to be the crushing point of the concrete but for sections in the hogging region the sections are assumed to fails when the bars yield (partial moment redistribution is considered).

4) The sections in both hogging and sagging regions are assumed to fail when the concrete crushes (point c in Figure 4.5) (Full moment redistribution is considered).

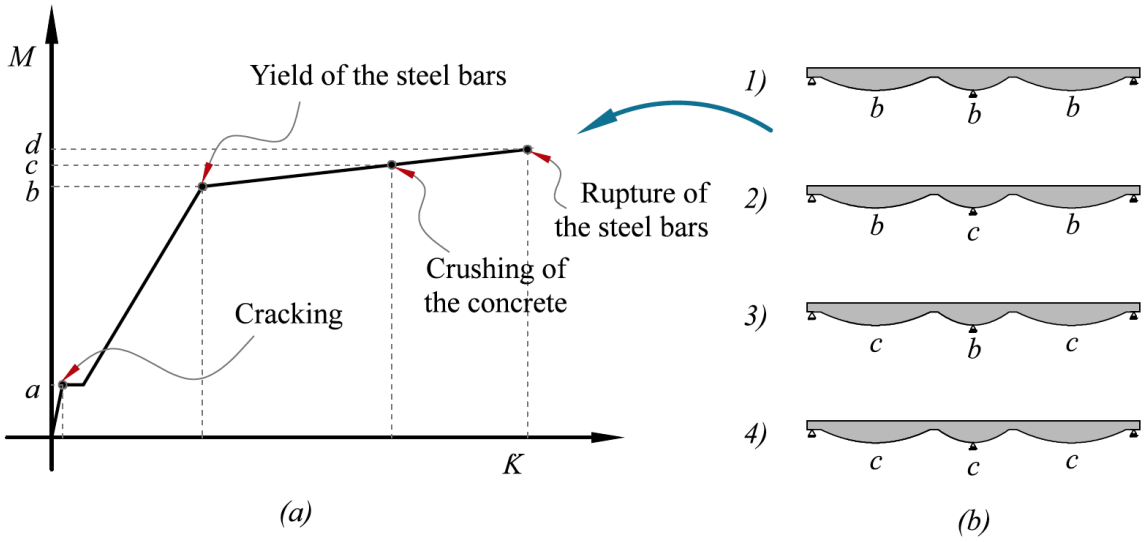

Figure 4.5: (a) Idealized moment-curvature relationship of a typical steel reinforced section, (b) failure modes

The choice of failure mode has a direct influence on the outcome of the optimisation because the capacity-stiffness index changes significantly for the same section layout when different failure modes are considered. On the other hand, the direction of flow of the redistributed moment (from the hogging region to the sagging region or vice versa), which is decided by the choice of the failure mode and cross-sectional properties, has a direct effect on the final shape of the beam.

In the following sections, the optimisation method developed is explained according to assumed modes of failure and consideration of moment redistribution. An example of a steel reinforced cross-section layout was considered here to clarify all possible optimisation solutions. The cross-section properties are the same as those of beam T-OSS-C which was part of the test program undertaken to verify the methods developed in this thesis and its details are given in Chapter Five.

First of all, choosing sections based on the applied loadings produces a final shape similar to the resulting bending moment diagram as explained for simply supported beams. In the hogging region, the angular shape of the bending moment diagram produces a shape that is not feasible to reinforce

and construct. To tackle this problem, a parabolic shape is defined which encloses the hogging region as shown in Figure 4.6.

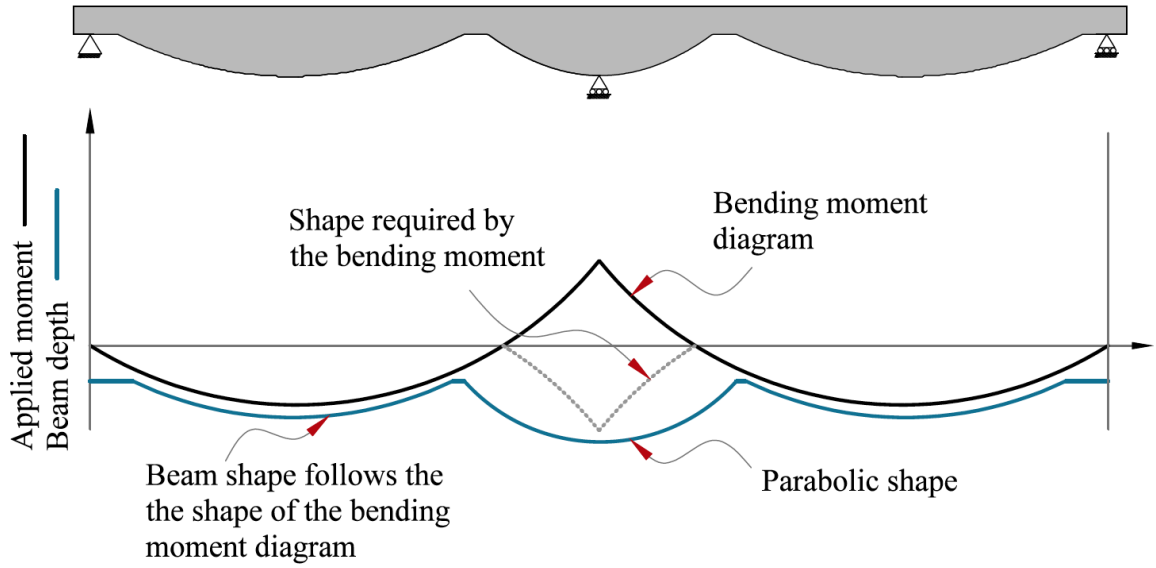

Figure 4.6: Shape correction technique used for optimised continuous beams

4.7.1.2.1 No moment redistribution

If yield of the tensile steel bars is considered to occur at every section along the beam, no moment redistribution occurs (aside from minor moment redistribution due to cracking). The sectional stiffness values EI_f in this case are high as they consist of pre-yielding stiffness of the sections. This is because the sections selected to resist the applied moments have a yield moment capacity slightly larger than the corresponding applied moment. So the values of $I_{cs,hogging}$ and $I_{cs,sagging}$ are both small values relatively.

In this case one of the regions (the hogging region for the example cross-section layout considered here) tends to attract greater applied moment than the sagging region. This causes gradual increase in depth and further increases in the stiffness of the hogging region during the optimisation procedure until the stable state between applied moment distribution and the moment capacity distribution is reached. As presented in Figure 4.8, the optimised beam shape consists of a large curved hogging region and flat sagging regions set at a minimum allowable depth indicated in the optimisation procedure.

Notwithstanding the fact that such a shape might not be feasible to construct in a real structure, the amount of material used for this specific example is 6.8% larger than an equivalent strength prismatic beam. It is obvious that, a prismatic beam is a better option if this mode of failure is selected in this case. On the other hand, this result proves that selection of appropriate cross-section layouts are essential to make optimisation for strength beneficial and meaningful.

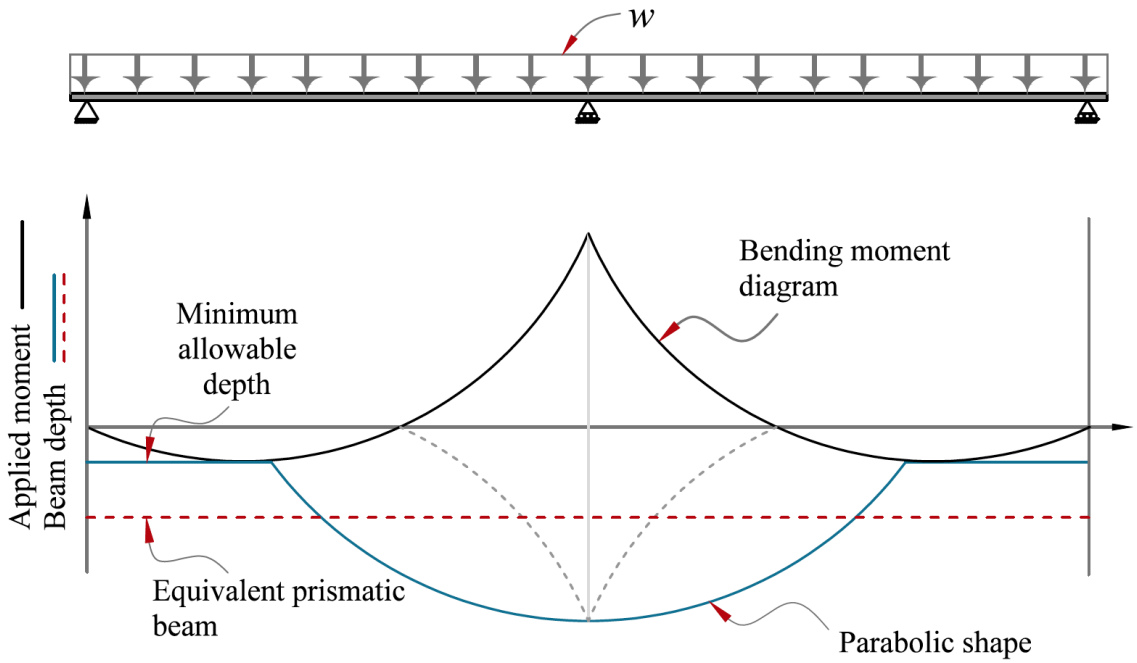

Figure 4.7: Double span continuous beam optimised according to mode one of failure and compared to an equivalent strength prismatic beam

4.7.1.2.2 Partial moment redistribution

When case two or three are considered in Figure 4.5 in the optimisation procedure, partial moment redistribution is allowed to occur. Considering mode two of failure first, sections in the hogging region are designed to resist moments beyond the yield of the steel bars and fail when concrete in the extreme compression fibre of the section crushes (high $I_{cs,hogging}$ and low $I_{cs,saging}$). This allows moments to redistribute from the hogging region to the sagging region since the flexural stiffness values drop by a significant amount when the steel bars yield.

During the strength optimisation procedure, regardless of the assumed initial EI distribution, the sagging regions gradually increase in depth and the hogging region decreases until a stable state is achieve. Similarly, if mode three of failure is considered, the hogging region undergoes gradual growth of shape while the sagging regions decay.

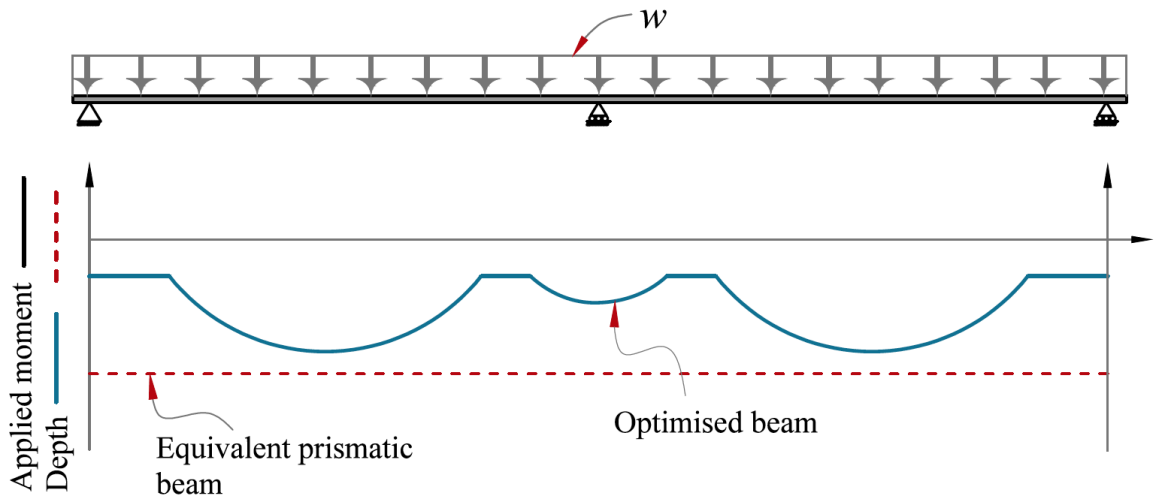

Figure 4.8: Continuous beam optimised for strength according to second failure mode and compared to an equivalent strength prismatic beam

Presented in Figure 4.8 is a continuous beam with the example cross-section layout optimised for the second failure mode indicated in Figure 4.5 and an equivalent strength prismatic beam.

4.7.1.2.3 Full moment redistribution

Considering the fourth mode of failure and allowing the tensile steel bars to yield in both hogging and sagging regions before ultimate failure of the beam, ensures moment redistribution from one region to the other in the post-yielding stages of loading up until failure of the beam. The first region to yield loses stiffness first and redistributes moment to the unyielded region. When the steel bars in second region yield too, reverse moment redistribution may occur to the initially yielded region (providing that strain-hardening has already started in the initially yielded region). This allows full moment redistribution (highest possible ratio) and high utilisation of material.

Figure 4.9 shows the continuous prismatic beam considered and the continuous beam optimised for mode four of failure. The total volume of the optimised beam is less than the volume of the equivalent prismatic beam but with smaller safety margins than the case when other modes of failure are used in design. It should be noted that, the prismatic continuous beam should also be iteratively designed to find a cross-section layout for sagging and hogging regions that resist the actual moment distribution as explained further in the following section.

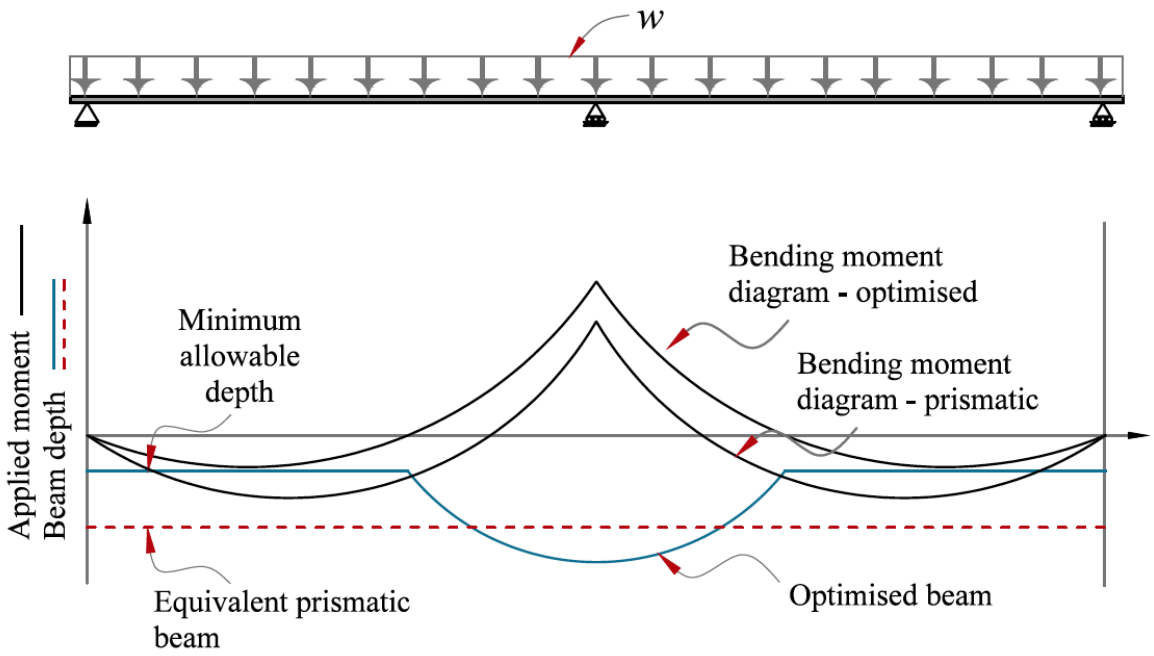

Figure 4.9: Continuous concrete beam optimised for strength based on fourth mode of failure and compared to an equivalent strength prismatic beam

4.7.1.3 Optimisation of prismatic continuous concrete beams

Optimisation for prismatic beams in this section is referred to designing for the actual moment distribution. To design the equivalent strength prismatic beams for the continuous beams optimised in for the purpose of a reasonable comparison, a numerical procedure was carried out to iteratively optimise prismatic continuous concrete beams. The initial design has to be carried out first based on the elastic moment distribution. Depending on the mode of failure considered in design, the actual moment distribution may vary from the moments for which a beam was initially designed. In any of the subsequent steps of the design procedure, the flexural stiffness value at any section is found (from the moment values of the previous iteration) and the stiffness matrix is updated. A new moment distribution was then determined and a suitable section layout was selected for the maximum negative and positive moment values (with constant section geometry along the beam but reinforcement layout may vary). This procedure is repeated until the design and the actual moment distribution match.

The optimisation method developed here iterates possible sectional layouts for hogging and sagging regions based on the selected mode of failure to find the optimum continuous prismatic beam design. A beam denoted as T-N-C was designed according to the second failure mode and constructed to be tested in an experimental program carried out to verify the theoretical methods developed in this thesis. The details of them beam and test results are presented in Chapter Five and Six respectively.

4.7.2 Optimisation for serviceability

Once a statically indeterminate beam is optimised for strength, further optimisation for serviceability, if needed, can be carried out by incrementally adding material to certain points until serviceability limit states are satisfied. As explained previously, adding material to any section changes the shape, EI distribution and therefore, the applied moment distribution. This necessitates further optimisation for strength in parallel with optimisation for serviceability to ensure that the moment capacity at any section is matched with the new applied moment value.

Finding where is best to add material while optimising for serviceability is complicated because the considerable size of the force, deformation and stiffness matrices make it extremely difficult to theoretically find correct paths towards an optimum design.

Two methods have been developed in this thesis to undertake serviceability optimisation for statically indeterminate concrete beams.

4.7.2.1 Optimising for serviceability at the ultimate limit state (shape optimisation)

The dependence of moment distribution on stiffness distribution of continuous concrete beams can be used as a beneficial property to produce buildable and optimised beam shapes.

Flexible formwork technique works best with smoothly curved beam shapes as explained in Chapter Two. Bending moment-shaped beams lead themselves to this. The method developed here combines the optimisation for serviceability and strength in order to achieve a bending moment shaped beam that satisfies both ultimate and serviceability limit states.

This procedure includes choosing one zone (sagging or hogging) depending on the capacity-stiffness index (I_{sc}) value to gradually add material (increase depth) until the optimum shape for both limit states is obtained. The region selected is one with a high I_{sc} value where the depth has been reduced during the strength optimisation procedure. Within the selected region, the choice of a section to which to add material does not have any effect on the final results but rather affects the number of iterations needed to achieve the optimum shape. After any increase in stiffness in the selected region, the moment distribution changes and strength optimisation method reshapes the entire beam. To ensure convergence to the solution, the proposed method chooses a section to add material which offer highest increase in flexural stiffness within the selected region.

The serviceability optimisation procedure may hit its targets by adding material to one region only, but if the selected region to add material reached a maximum allowable depth and the serviceability limits are still unsatisfied, then the opposite region(s) is selected to undertake further optimisation. Figure 4.11 shows example beam shapes optimised for strength and serviceability in two phases. In the first phase, the hogging region has a small capacity-stiffness index relative to the sagging

regions. Therefore, the hogging region is selected to add material. Once the hogging region reaches its maximum allowable depth, the beam is only partially optimised for serviceability, so further optimisation is needed in a second phase.

In phase two, the sagging regions are candidates to add material. In this manner the optimisation procedure continues until a fully optimised shape is achieved.

Due to the reshaping performed by the strength optimisation method in each optimisation loop, individual sections cannot be improved separately. For this reason, optimisation for crack widths and deflection is performed simultaneously by stiffening (adding material to) the selected region(s) until both limit states are satisfied.

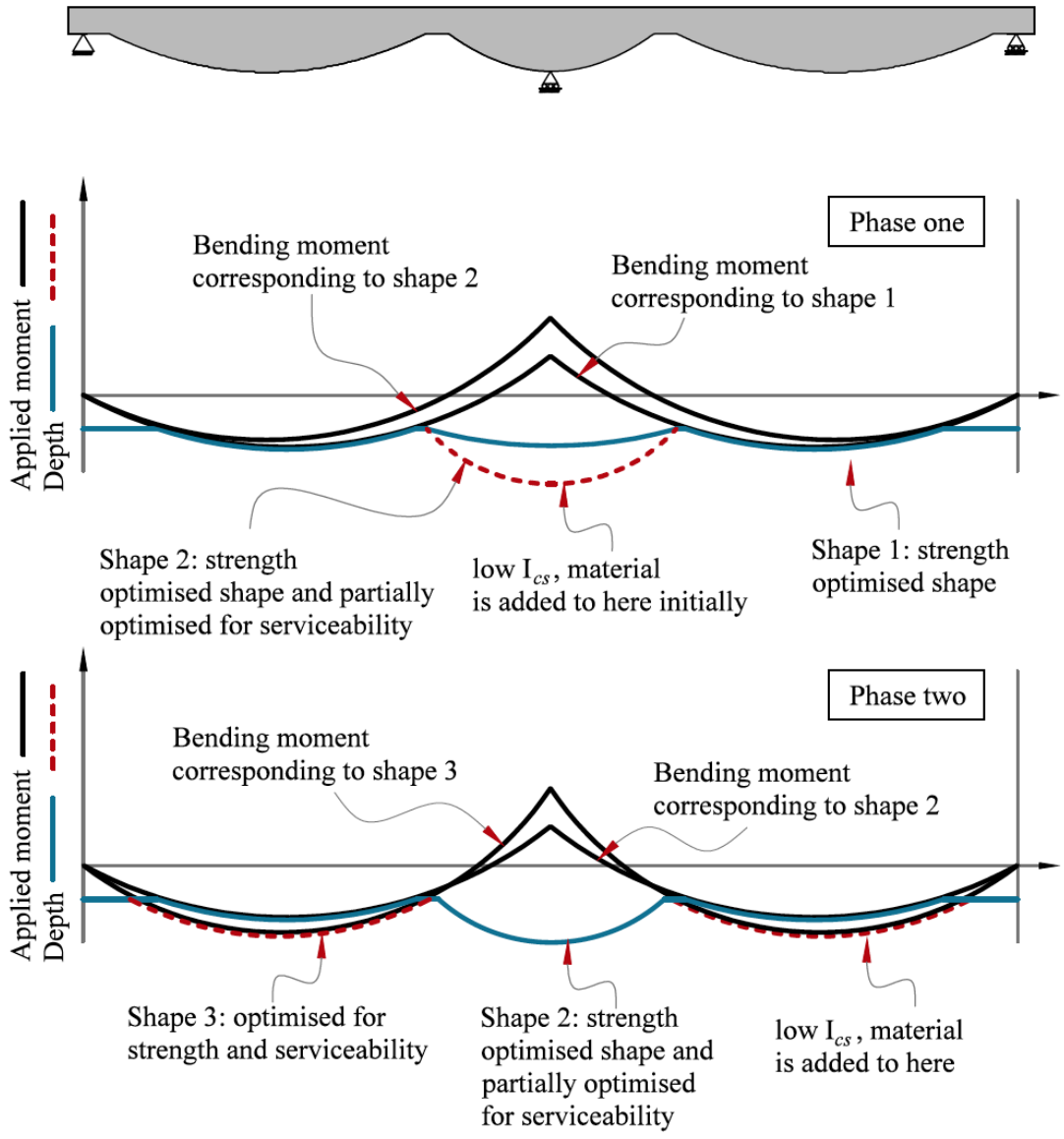

Figure 4.10: Optimisation for serviceability in two phases

4.7.2.2 Point of maximum influence method (topology optimisation)

This method was developed to optimise continuous concrete beams at the serviceability limit states. Once a concrete beam is optimised for strength, it will be subjected to service loads in this method and further serviceability optimisation, if deemed essential, is carried out without running any further optimisation for strength. The candidate sections to which to add material are selected based on their maximum influence in reducing crack widths and deflections when their depth is increased. This is not straightforward due to a high degree of material and geometric non-linearity a shape optimised continuous concrete beam possesses.

4.7.2.2.1 Principle of influence line

Finding where best to add material not only ensures a high degree of utilisation of material but also a quicker convergence to an optimum shape. In this method, the principle of influence line of loads was used to find the section of maximum influence to which adding depth results in maximum reduction in crack widths or deflection. This is similar to that done for simply supported beams (see § 4.6.2.1.1) but in the case of continuous beam, since moment distribution changes in every step of optimisation, the influence line shape changes too. Therefore, in every optimisation loop, a new influence line is created.

Figure 4.12 shows the influence lines of added material for maximum reduction in crack widths and deflections for the beam example taken in §4.7.1.2. for a strength optimised shape and in the first step of serviceability optimisation.

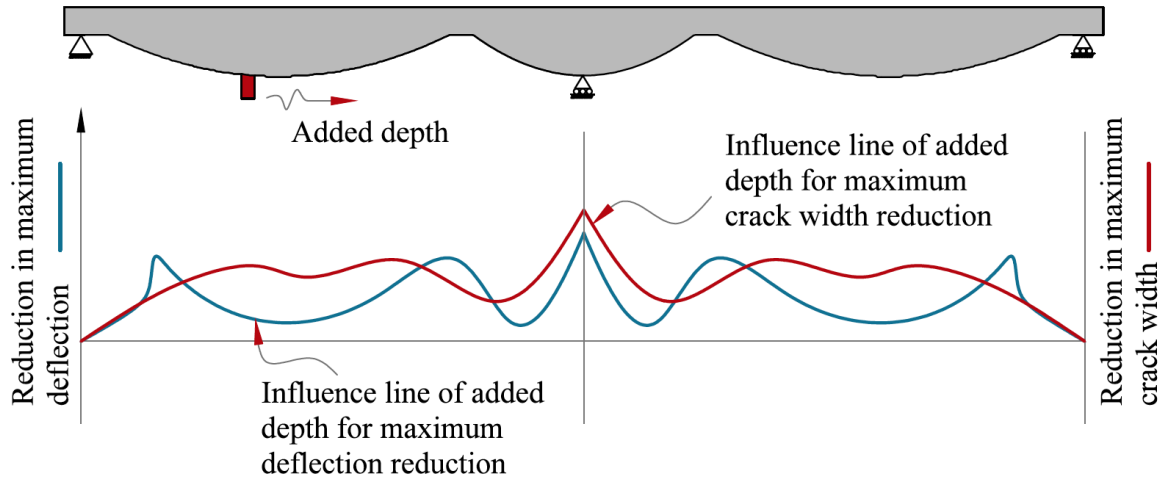

Figure 4.11: Using the principle of influence line to choose the candidate point to add material (schematic representation)

4.7.2.3 Choice of serviceability optimisation method

The two methods developed here to optimise continuous concrete beams for serviceability which are shape and topology optimisation methods, may converge to different results for the same optimisation problem. The shape achieved from the first method is a bending moment shaped beam, while the second method produces a curved beam shape which depends on the final material layout. In both cases, the optimal beam has a moment capacity higher than that required by the applied moment. The choice of any of these two proposed methods and the amount of material saved depends entirely on the section layouts selected, loading and span conditions and the failure mode considered. This is further explained with an example in Chapter Six.

4.8 Form-finding

A sectionwise form-finding procedure is adopted to create a two-dimensional shape of vertical sections along an optimised beam. The method was presented by Foster (2010) as explained in Chapter Two. The optimisation methods described before are used to calculate the total depth distribution of the optimised beam along the length the other sectional properties are defined prior to optimisation. Then the form-finding model finds the cross-section shape from the known depth and breadth values. Along the member, the vertical cross-section shapes are connected to create the full member shape. The lines connecting consecutive sections are assumed to be straight lines. This method uses the relationship between curvature in the fabric K, tensile force in the fabric T and hydrostatic pressure P from the wet concrete to develop a walking-out procedure from the bottom of the section to create the shape.

It is assumed that the fabric consists of infinitesimally small straight fabric segments as shown in 4.12 and the hydrostatic pressure of the wet concrete acts perpendicular to the fabric. From the in-plane forces vector shown, the equation between the tension force in the fabric and the fluid pressure at any point on the fabric perimeter is given as:

$$\delta\theta = \frac{\rho g z \delta L}{T} \qquad (4.25)$$

Where $\delta\theta$ is the angle between two consecutive segments, ρ is the density of the wet concrete, g is the gravitational acceleration, z is the hydrostatic height, δL is the length of fabric segments and T is the tensile force in the fabric.

Based on the above relationship, the coordinates of a number of equally spaced points on the perimeter of the fabric are found and these points are connected to define the hydrostatic cross-section shape. A number of assumption to derive the form-finding equations are made which are:

1) The tensile force in the fabric is constant along the fabric perimeter.

2) The strain in the fabric is negligible.

3) The selfweight of the fabric is negligible.

4) Out-of-plane stiffness of the fabric is negligible.

The walking out procedure starts from the point of origin ($x_1 = 0, y_1 = 0$) which is the lowest point of the fabric mould as indicated in Figure 4.12. Since the hung fabric shape is symmetric about the y-axis, only half of the perimeter is taken into consideration. The coordinates of point (x_{i+1}, y_{i+1}) is found as follows:

$$x_{i+1} = x_i + \delta L \cos\left(\sum_{j=0}^{i} \delta\theta_j\right) \tag{4.26}$$

$$y_{i+1} = y_i + \delta L \sin\left(\sum_{j=0}^{i} \delta\theta_j\right) \tag{4.27}$$

The angle $\delta\theta$ at each point on the perimeter can be found using equation (4.15). Since there are two unknowns, $\delta\theta$ and T, an iterative trial and error procedure is needed to find the correct value of T which produces the correct cross-section shape based on the given boundary condition. In this case the boundary condition is that the coordinate of the final point on the perimeter converges to ($x_n \approx \frac{b}{2}, y_n \approx d$), where n is equal to the number of coordinates taken on the perimeter. A simple goal-seeking algorithm was designed in Matlab to find the solution of the given problem by iterating the value of T. For quicker convergence to sufficiently accurate results, an initial guess of T can be selected.

The lower bound value of W can be taken as the weight of the rectangular bd per unit length z, where z is the out-of-plane dimension of the hung perimeter. The value of T is then increased gradually and for each value of T a curve is created.

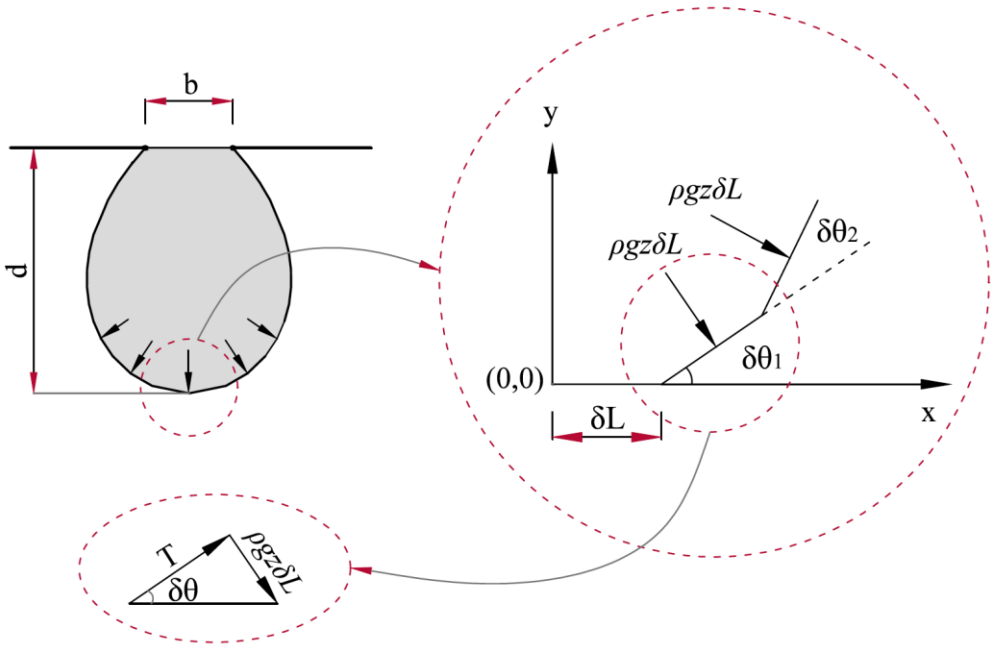

Figure 4.12: In-plane forces acting on a fabric mould

Assuming that the fabric in vertical at the hanging points, the total weight of the concrete in the fabric mould is equal to $2T$ as indicated in Figure 4.13.

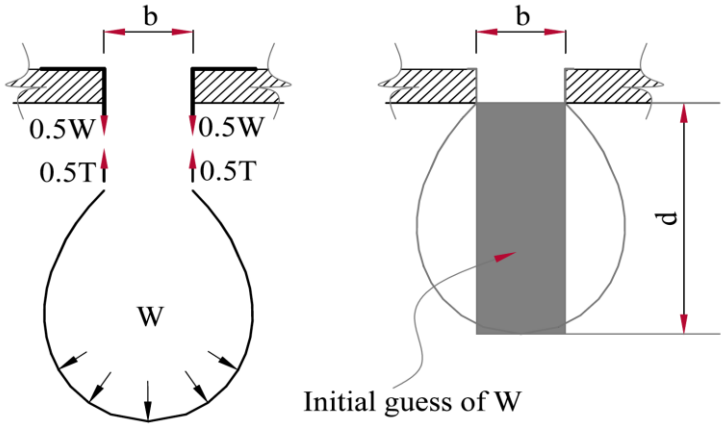

Figure 4.13: Selecting the initial input guess for the form-finding goal-seeking algorithm

4.9 Summary

In this chapter, the methods developed to optimise statically determinate and indeterminate concrete beams for strength and serviceability are presented. In the following chapter, the experimental program undertaken to validate these methods along with the prediction methods presented in Chapter Three is discussed.

[Blank Page]

Chapter Five

Experimental methods

5.1 Preface

To verify the theoretical methods developed in this work to analyse the behaviour and to optimise flexibly-formed concrete beams as described in Chapter Three and Chapter Four an experimental program was carried out. Five beam specimens were manufactured and tested. They were designed for different limit states based on their verification targets. Two of the specimens were simply supported concrete beams and the other three were continuous concrete beams. The design, manufacturing and testing process of the test specimens are described in this Chapter.

5.2 Design of test beams

Both statically determinate and indeterminate beams are considered in this thesis. Since different analysis and optimisation methods are used for these two classes of beams, two separate test programs were undertaken. The iterative design procedure of optimised flexibly-formed concrete beams includes two main parts as discussed in Chapter Three and Chapter Four; prediction of behaviour and improvement of behaviour (optimisation). Therefore, the whole design methodology can be assessed through validating the prediction methods only. If the prediction methods developed for non-prismatic beams are valid, the optimisation methods can too be considered valid since they ultimately rely on the prediction methods to indicate how the optimisation should be achieved.

5.2.1 Test parameters

The theoretical methods to be verified by the experimental program are prediction methods and optimisation methods developed in this work. The prediction methods consist of; 1) the combined-interaction method and the register-eliminate algorithm developed to predict the crack width, cracking pattern and deflections of non-prismatic beams, and 2) the sectional-segmental stiffness method to analyse and predict the behaviour of statically indeterminate concrete beams. The optimisation methods are; 1) point-of-maximum-curvature method to optimise statically determinate concrete beams for serviceability and 2) point-of-maximum influence method to optimise statically indeterminate beams for serviceability.

The form-finding method adopted in this work and different construction techniques for fabric-formed beams described in Chapter Two have previously been used for simply supported beams. For continuous beams, the radius of curvature of the longitudinal profile of the beam maybe smaller than that of simply supported beams, especially in the hogging region. Since the form-finding method is section-based, the out-of-plane forces due to two-dimensionally woven fabric are not considered which they may affect the final shape of the beam and predictions based on the current form-finding method. On the other hand, construction of such beams is challenging because increased curvature of the longitudinal profile adds difficulty to reinforcing and can cause wrinkles in the fabric while casting which affects the surface quality of the member. The fabric layout then, and the physical boundaries defined by the rigid formwork and fabric restraining may require modification to the method of construction. Therefore, the form-finding method and construction of fabric-formed continuous concrete beams are taken into account in this experimental program.

In order to design a rigorous test matrix to create the right specimens to verify the above methods, a number of test parameters are indicated to measure the performance of the specimens and assess the results achieved from the methods. Figure 5.1 shows the selection procedure of the test parameters.

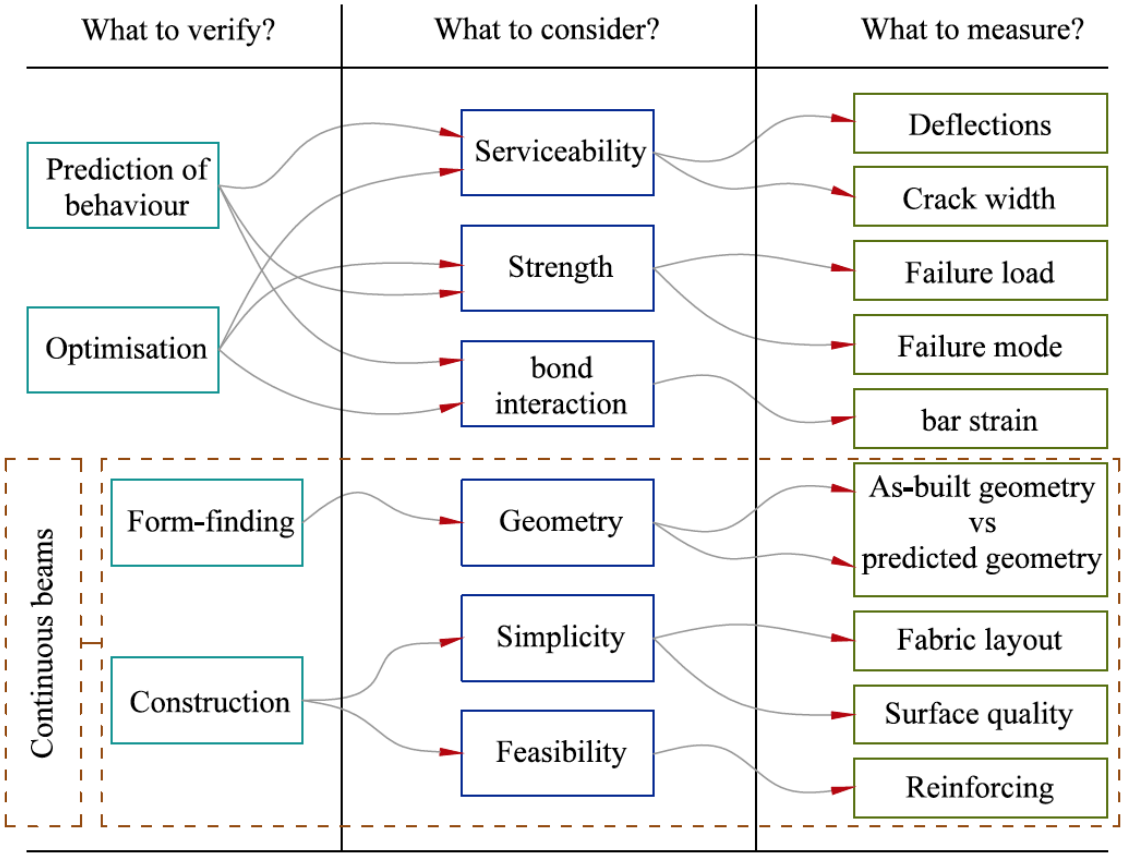

Figure 5.1: Selection of test parameters

At member level, prediction of the global behaviour of concrete beams at serviceability is assessed through measuring deflections and crack widths of test specimens. At the ultimate limit state, failure load and failure mode (shear or flexure) are indicators of the global behaviour of the beam. At section level, measuring the strain in the reinforcing bars at different stages of loading can be used as an indicator of the nature of concrete-reinforcement bond interaction. Since the three methods used in this work (full-interaction, partial-interaction and the combined-interaction) are mainly dependent on how the concrete and reinforcing bars interact at the bond interface, the strain in the reinforcing bars is selected as a test parameter to further check the performance of the mentioned methods against the test data.

Presented in Figure 2.3, is the convention used to name the specimens based on type, geometry and optimisation targets. For instance, in beam T-OSS-S, letter T stands for T-section, OSS for optimised for strength and serviceability and S is for simply supported.

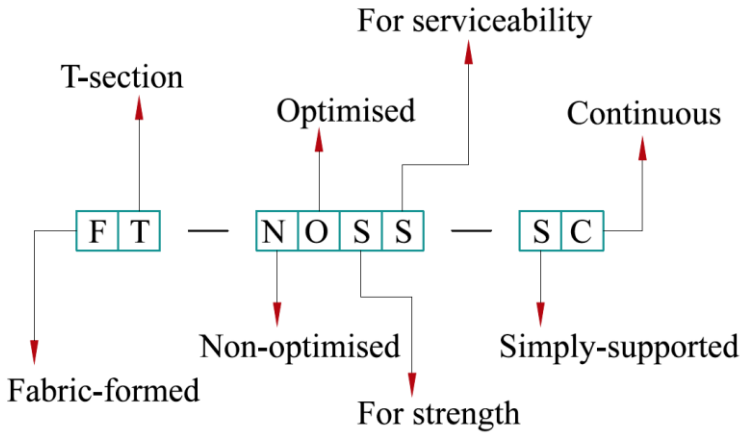

Figure 5.2: Naming convention for the specimens

5.2.2 Test matrix

The test specimens are selected based on the new methods developed in this thesis and the test parameters described in the preceding section. Figure 5.3 explains how each test specimen is chosen and which method each specimen is designed to verify. Two T-section simply supported beams were designed; one of them was optimised for strength only and the other was optimised for both strength and serviceability. These beams were aimed at verifying the methods developed for simply supported beams. Beam one, denoted as T-OS-S, is designed to verify the combined-interaction method (see § 3.3.3) and optimisation for strength method (§4.6.1). Beam two, denoted as T-OSS-S, is designed to verify the combined-interaction method, point-of-maximum-curvature method to optimise for serviceability (topology optimisation) (§4.6.2) and optimisation for strength method (shape optimisation) (§4.6.1). Apart from different optimisation targets, these beams are expected to have different cracking patterns at serviceability as explained in Chapter Four.

Three continuous beams were also designed and tested. The first beam, named T-N-C was a prismatic double-span continuous beam intended to verify the combined-interaction method and segmental-sectional stiffness method for statically indeterminate prismatic beams (Figure 5.3). It is worth mentioning that, a prismatic simply supported beam was not included in the test matrix because applying the combined-interaction method to these beams would converge to the same results as the partial-interaction method which has already been investigated by other researchers as explained in Chapter Two. However, the combined- and the partial-interaction methods would give different results for prismatic continuous beams because these beams are not experiencing ever-decreasing bending moment when moving away from the point of maximum moment (where the initial crack forms) (see §3.3.2).

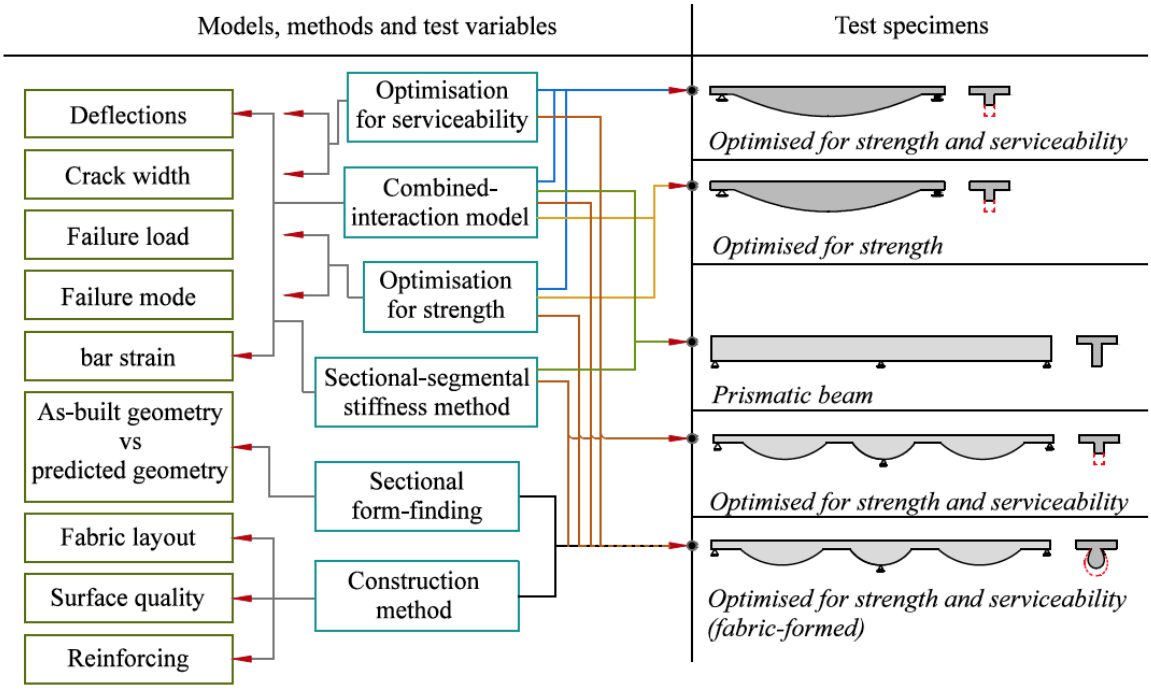

Figure 5.3: Choosing test specimens

The second continuous beam, denoted as T-OSS-C was a non-prismatic T-section beam optimised for both strength and serviceability aimed at verifying the sectional-segmental stiffness method, combined-interaction method and optimisation methods for statically indeterminate non-prismatic concrete beams.

As explained in Chapter Three, the predictions achieved from the combined-interaction method are affected by the assumed tension area of concrete. For prismatic beams, the depth of this area is assumed to be 2 times the concrete cover according to CEB-FIP (2010). Assuming the same value of depth for the tension area for fabric-formed concrete beams as shown in Figure 5.4 may affect the results obtained from $P-\Delta$ and $M-\theta$ analysis and eventually predictions obtained from the combined-interaction method. This is because this area changes along the length of the beam depending on the hydrostatic height of the concrete-filled fabric bulb. Therefore, a continuous fabric-formed beam which was optimised for strength and serviceability was also tested. This beam was denoted as FF-OSS-C and, as the beam T-OSS-C, was aimed at verifying optimisation and prediction methods applicable to continuous beams but with the additional benefit of assessing the form-finding method and addressing construction aspects.

In the following sections, the details of all specimens, methods of testing, methods of construction and material properties are explained.

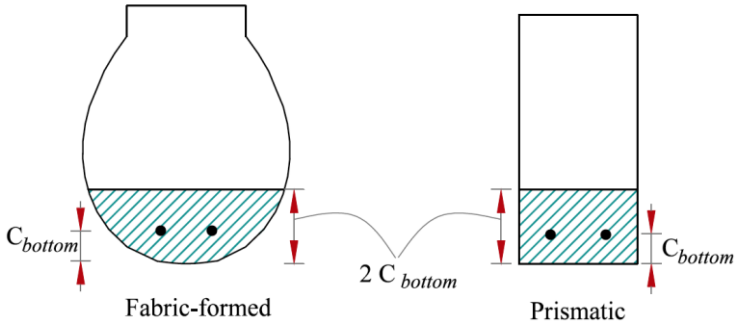

Figure 5.4: Tension area in prismatic and fabric-formed beams

5.2.3 Simply supported beams

Two simply supported beams were tested. Beam T-OS-S was optimised for strength only using the shape optimisation method described in §4.6.1. Beam T-OSS-S was also optimised for strength using the same method and then further optimised for serviceability using the topology optimisation method presented in §4.6.2. Both beams were identical in shear and flexural reinforcement layout, flange dimensions and web width, only their longitudinal profiles were different (i.e. beam depth). Saving in the web concrete material for beam T-OS-S and T-OSS-S was 33% and 17% respectively when compared to an equivalent strength prismatic web.

The beams were designed for the loading arrangement shown in Figure 5.(a). Since the beams were lab sized specimens, applying the loading conditions and the limit states of a real structure would not be appropriate. Therefore, the desired maximum dimensions of the beam were defined first, then a loading arrangement that produces specimens within the range of those predefined geometric boundaries was selected and finally, scaled-down serviceability limit state values were defined.

The main purpose behind this experimental program is to examine the validity of the proposed theoretical methods rather than designing based on specific codified limit states. Therefore, selection of any of serviceability limit state can be appropriate as far as the main serviceability optimisation goals are achieved which in this case is a reduction in deflections and crack widths.

In light of this, beam T-OSS-S was optimised for a reduction in the maximum deflection value and average crack width compared to beam T-OS-S. The limit states values used to design the beams are given in Table 5-1.

Table 5-1: Design limit state values for beams T-OS-S and T-OSS-S

Beams	*Failure mode*	*Failure load (kN)*	*Service load (kN)*	*Maximum deflection (mm)*	*Average crack width (mm)*	*Total number of cracks under service loads*
T-OS-S	Flexure	105	51	2.6	0.13	16
T-OSS-S	Flexure	105	51	2.1	0.10	13

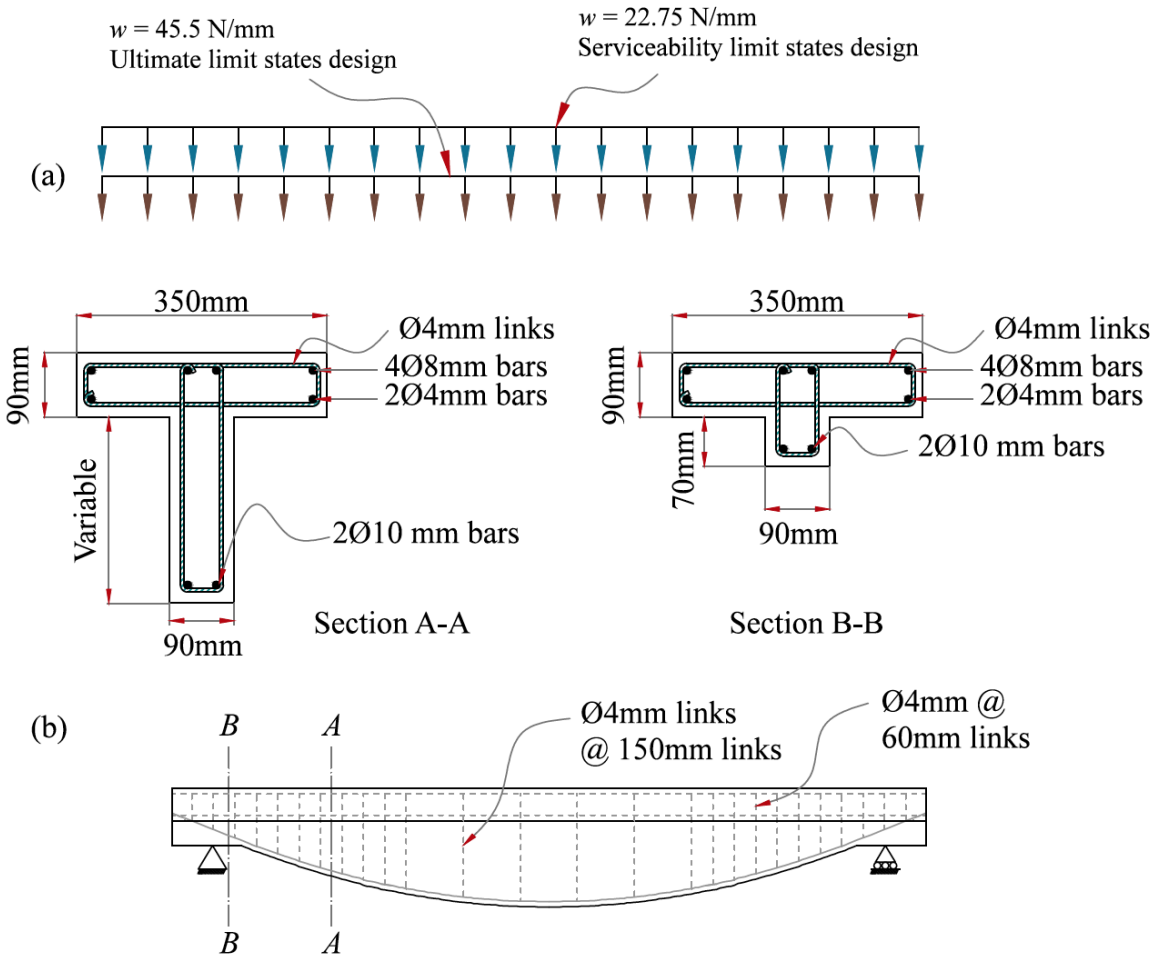

Figure 5.5: (a) Design loading arrangement, (b) reinforcement details

The beams were moderately reinforced, the maximum flexural reinforcement ratio which occurs in the smallest section (end of the beam) is equal to 0.014 and 0.01 in the compression and tension side of the cross-section respectively. These reinforcement ratios are below the balanced steel ratio, allowing ductile behaviour of all sections along the beam. The minimum tension and compression reinforcement ratio, calculated in the largest section, are 0.006 and 0.007 respectively. The cross-sectional dimensions and reinforcing details are shown in Figure 5.5.

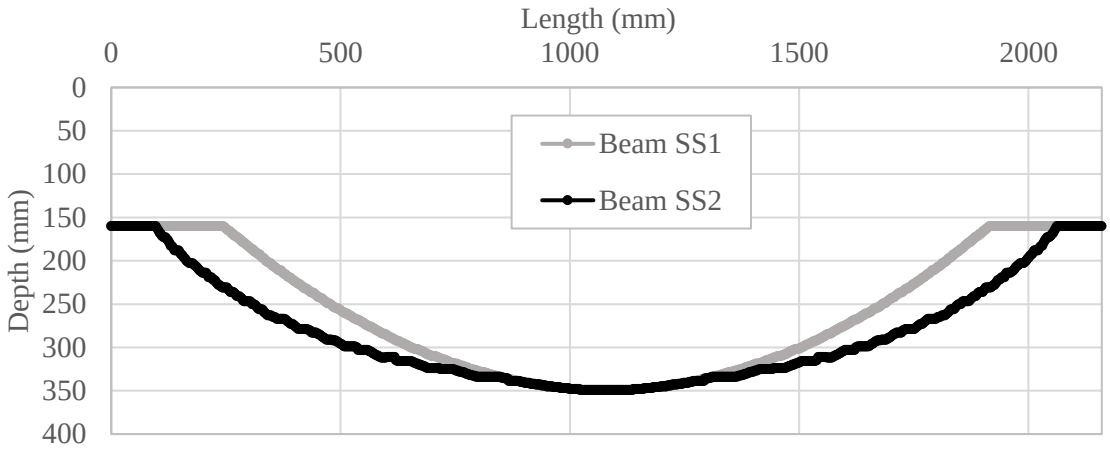

Figure 5.6: Longitudinal profiles of the simply supported beams

Figure 5.7: Beam T-OSS-S

Figure 5.8: Beam T-OS-S

Due to the variable section depth and variable applied shear stresses along the beam, the design produces a non-uniform spacing between the shear links. The spacing was therefore unified over three regions as shown in Figure 5.5 to simplify the manufacturing process.

The total span length of the beams was 2160mm, the minimum depth was 160mm to resist shear, and the maximum depth at mid-span was 350mm for both beams. The actual as-cast longitudinal profiles of the two beams are shown in Figure 5.6. The beams T-OSS-S and T-OS-S after casting are shown in Figure 5.7 and Figure 5.8 respectively.

5.2.3.1 Strain gauging

To measure strains in the longitudinal reinforcing bars at all stages of loading, strain gauges were installed on the bars at sixteen locations (eight on each side) for each beam as indicated Figure 5.9. The strain gauges were 6mm long and had an elongation capacity in excess of 5%. Prior to the application of the strain gauges, the surface of the steel bars at the specified locations were ground and smoothened as shown Figure 5.10 so that full interaction between the bars and the gauges is assured. The strain gauges were then glued to properly cleaned surfaces. To protect the gauges from any harm or damage while casting, a special coating agent (microcrystalline wax) was used to cover the gauges before it is bounded by a piece of a flexible rubber pipe and wrapped with electric tape.

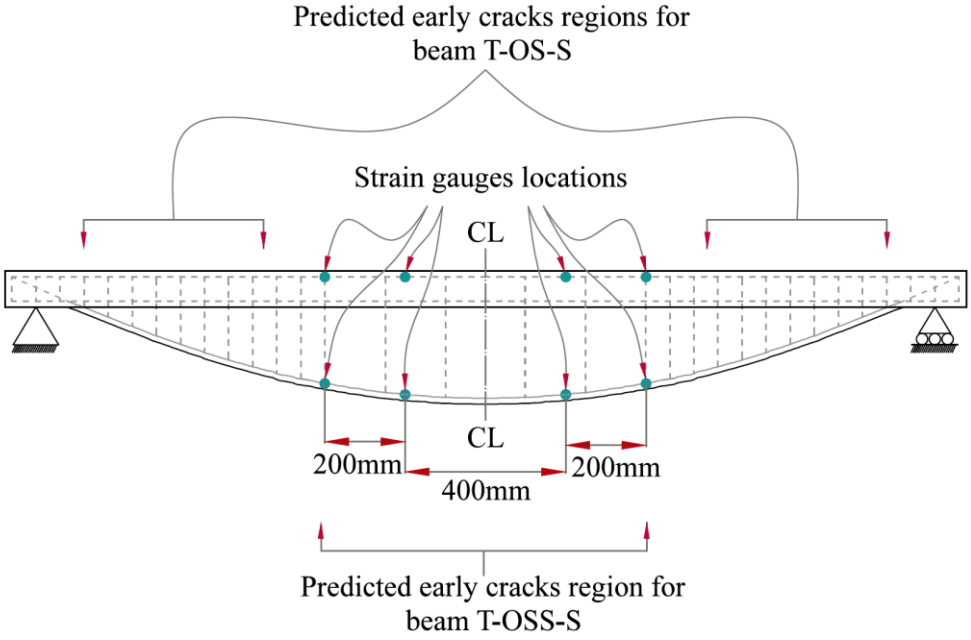

Figure 5.9: Strain gauge locations on the simply supported beams

Figure 5.10: Installation of the strain gauges

The locations of the strain gauges were chosen based on the predicted cracking pattern at the early stages of cracking. The strain gauges were intended to capture the strain data in the bars for the longest possible loading history in both full-interaction and partial-interaction regions. As explained

in Chapter Four (§4.6.2), for the beam T-OS-S, the cracks are expected to appear at regions near the supports as indicated in Figure 5.9. Therefore, the mid-span region stays as a full-interaction region for a longer loading period until at later stages of loading cracks form over the whole beam length. Conversely, considering beam T-OSS-S, early cracks are expected to form in the mid-span region. Therefore, a partial-interaction region forms in the mid-span region after cracking and continues to exist up until the failure of the beam. For these reasons, installing the strain gauges in the mid-span region is expected to allow following of the full and partial steel-concrete interaction through recording strains in the steel bars.

5.2.3.2 Test set-up

Since the beams were designed for uniformly distributed loading case, the beams were tested under a nine-point-load system shown in Figure 5.12 at equal distances apart from each other so as to simulate the design loading arrangement. The design and test bending moment diagrams are presented in Figure 5.11. The loads were applied by hydraulic jacks (Figure 5.13) at total load increments of 3kN. The loads were transferred from the jacks to the beam by means of pins and thick steel plates shown in Figure 5.13(right) to ensure distribution of the loads across the width of the beam. This technique was used for all the specimens. At each stage of loading, measurements of crack widths and deflections were taken. A high definition crack microscope with a precision equal to 0.02mm was used to measure the crack widths at each load interval at the level of the reinforcement. To follow the development of cracking at every loading step, the extent of each crack was indicated with a line next to it and the load at which it occurred. Deflection transducers were fixed under each point load as shown Figure 5.12.

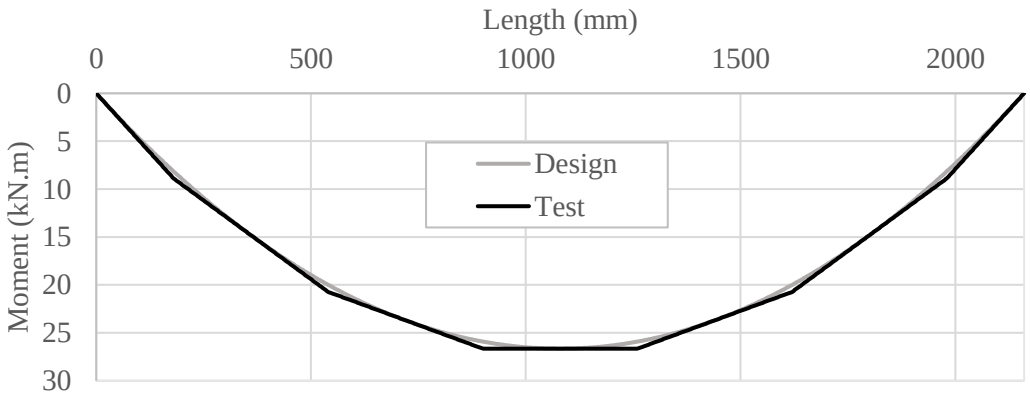

Figure 5.11: Test versus design bending moment diagram at failure

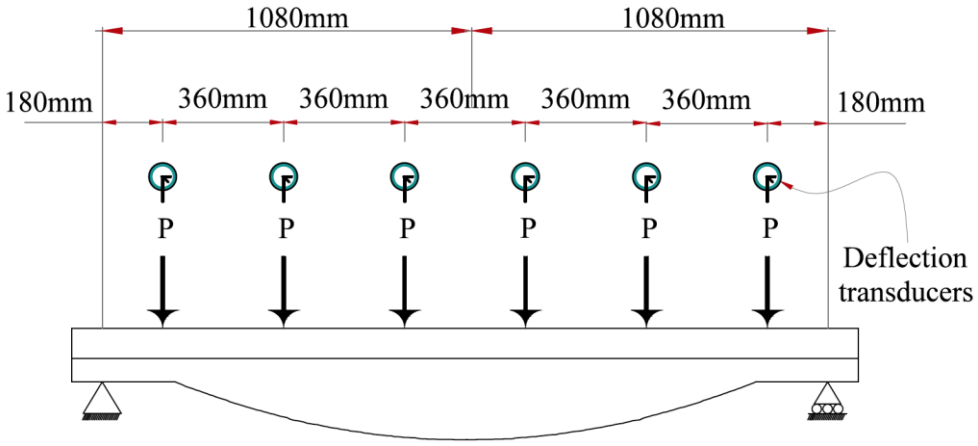

Figure 5.12: Test loads on the simply supported beams

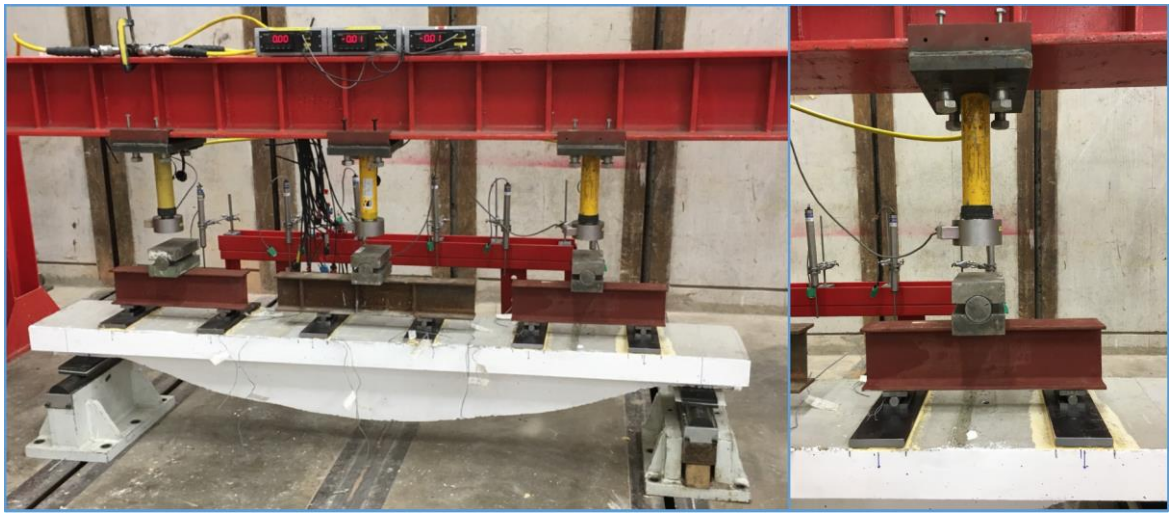

Figure 5.13: Test set-up of beam T-OS-S

5.2.4 Continuous beams

5.2.4.1 Beam T-N-C

A continuous prismatic concrete beam denoted as T-N-C was designed to verify the prediction methods developed in this work for prismatic continuous beams which are the combined-interaction method and the segmental-sectional analysis method as explained in the preceding sections. The beam consisted of two spans, each span was 2.4m long, and was designed for the failure mode two described in §4.7.1.2 (Moment redistribution from the hogging region to the sagging region was considered). Reinforcement details of this beam are shown in Figure 5.14. In order to avoid discontinuity in the reinforcement which would result in complications in the optimisation calculations, the longitudinal reinforcement layout was made constant along the beam.

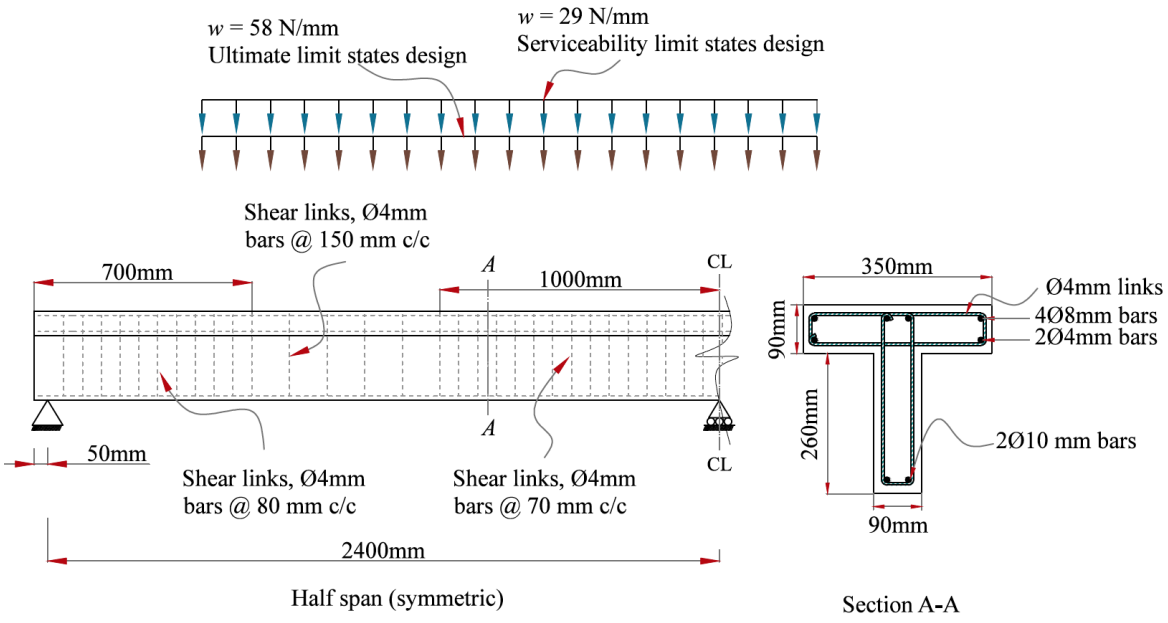

Figure 5.14: Geometric and reinforcing details of beam T-N-C

Figure 5.15: Beam T-N-C before and after casting

5.2.4.2 Beam T-OSS-C

Beam T-OSS-C was optimised for strength using the 'stable state method' and optimised for serviceability using the shape optimisation method described in § 4.7.2.1. This beam had a T-shape cross-section with variable depth and constant web width and flange dimensions along its length. It also had an identical flexural reinforcement in the positive and negative moment regions as shown Figure 5.16.

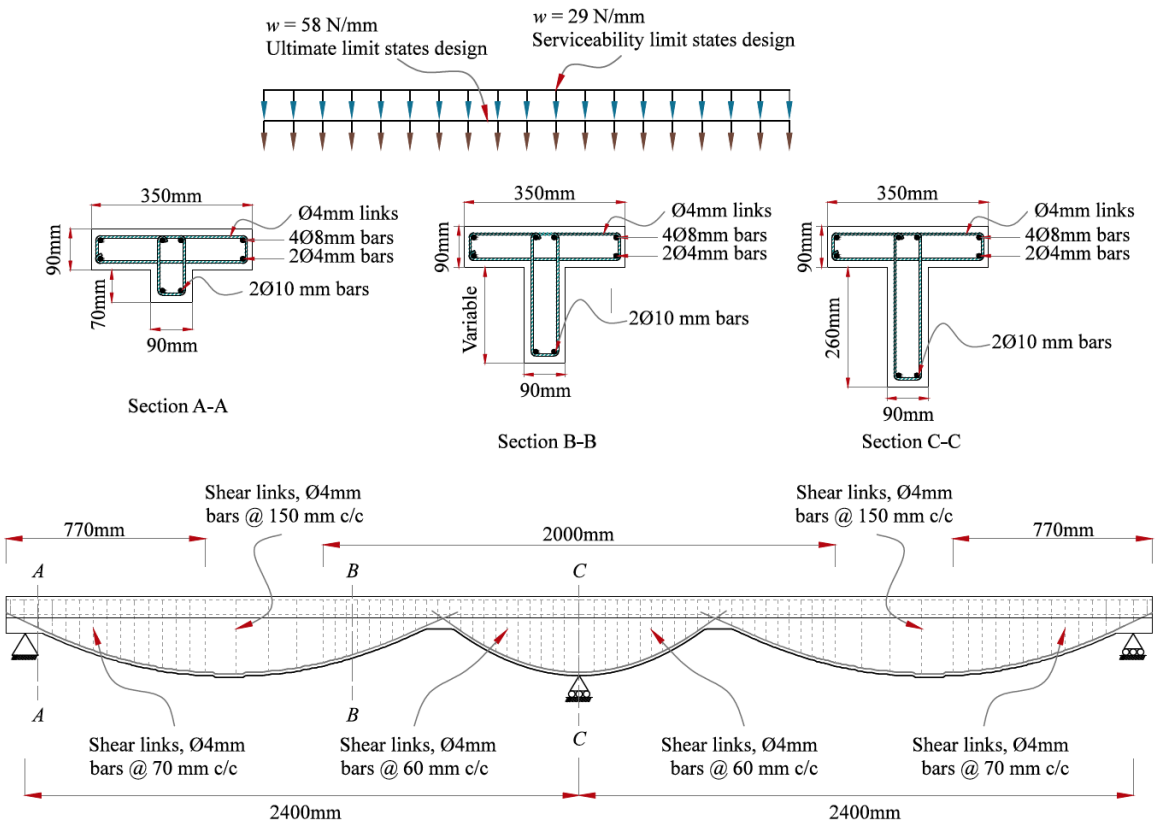

Figure 5.16: Geometric and sectional details of beam T-OSS-C

5.2.4.3 Beams FF-OSS-C

Beam FF-OSS-C was designed based on the same methods the same loading arrangement used for beam T-OSS-C. This beam was fabric-formed and its hydrostatic shape was found using the form-finding method presented in §4.8. The reinforcement details are shown in Figure 5.17 which is identical to that of beam T-OSS-C. The construction methods adopted to cast this beam are explained in details in the coming sections.

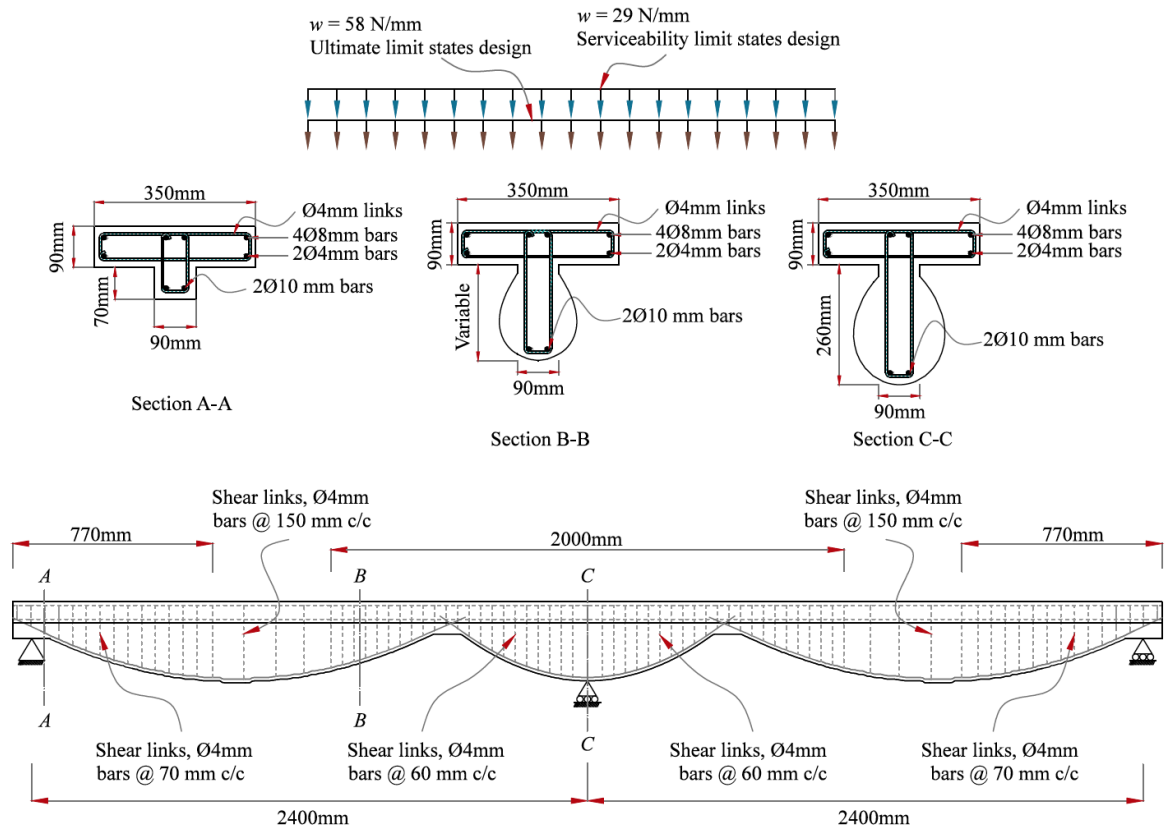

Figure 5.17: Sectional and longitudinal details of beam FF-OSS-C

The design ultimate and serviceability limit state values are shown in Table 5-2.

Table 5-2: Ultimate and serviceability limit state values for the continuous beam specimens

Beams	*Failure mode*	*Failure load (kN)*	*Service load (kN)*	*Maximum deflection (mm)*	*Average crack width (mm)*	*Total number of cracks under service loads*
T-N-C	Flexure	305	160	2.2	0.07	19
T-OSS-C	Flexure	305	160	3.8	0.10	23
FF-OSS-C	Flexure	305	160	3.7	0.10	23

5.2.4.4 Test set-up

The continuous beams were tested under an eleven-point load system. The loads were applied at equal intervals as shown in Figure 5.18 and Figure 5.19 to simulate the uniform loading arrangement used in designing the beam. The moment distribution pattern for the design and testing loading

arrangement at the ultimate limit states are shown in Figure 5.20 and Figure 5.21 for beam T-N-C and beams T-OSS-C and F-OSS-C respectively.

Six deflection transducers were used to monitor deflections and a load cell to calculate the reaction force was placed under the mid-support. Crack width values were recorded and crack trajectories were indicated on the beam at any loading step. The loads were applied by means of four hydraulic jacks and four steel I-beams in order to transfer the loads to the beam at eight points (Figures 5.22 & 5.23).

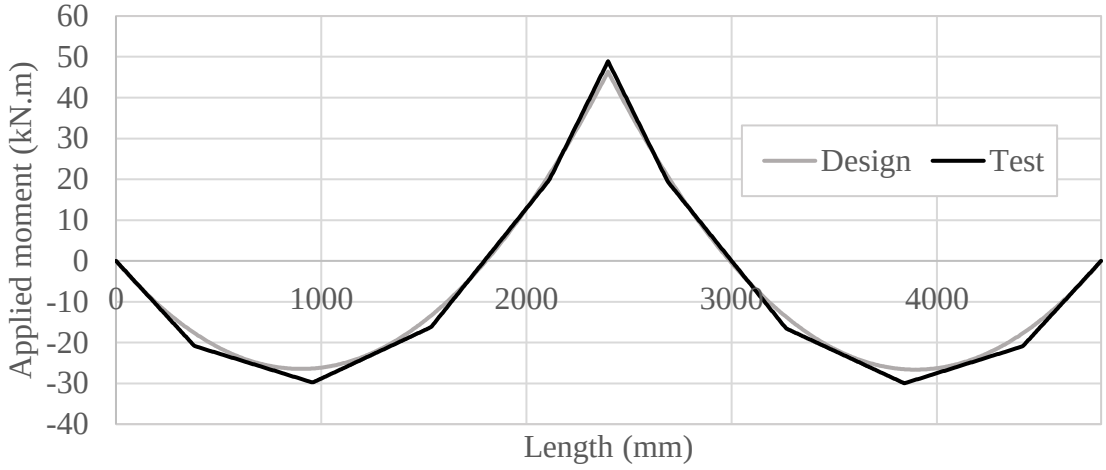

Figure 5.18: Design and test bending moment distribution for beam T-N-C

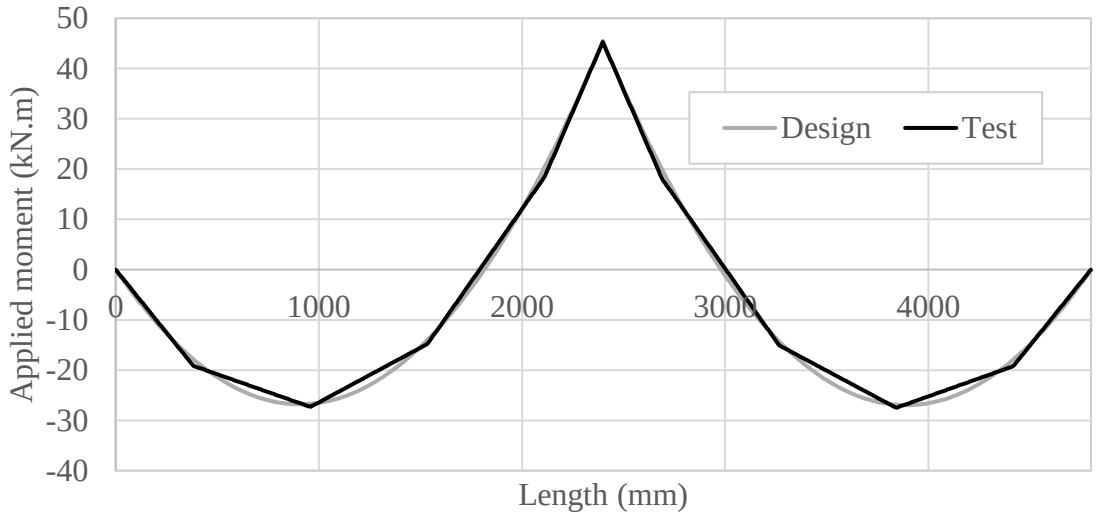

Figure 5.19: Design and test bending moment distributions for beams T-OSS-C and FF-OSS-C

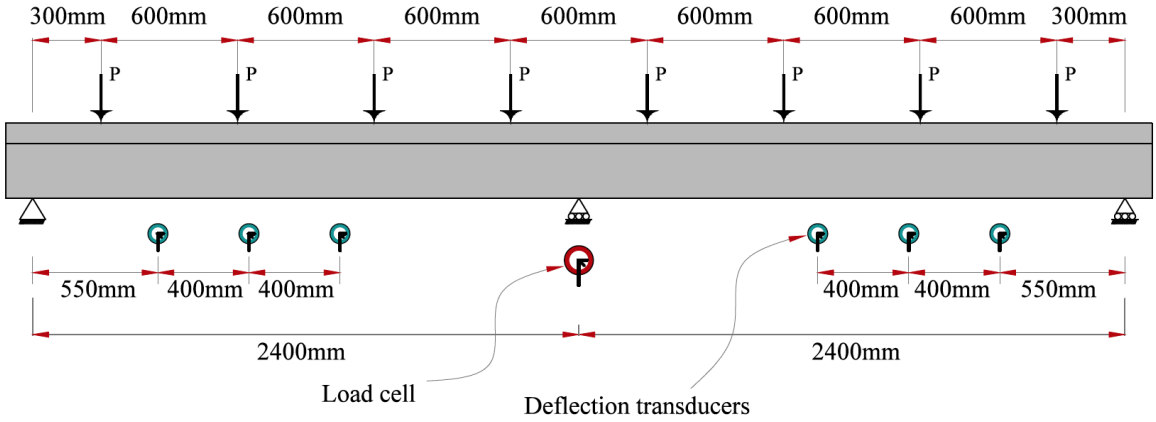

Figure 5.20: Test set-up for beam T-N-C

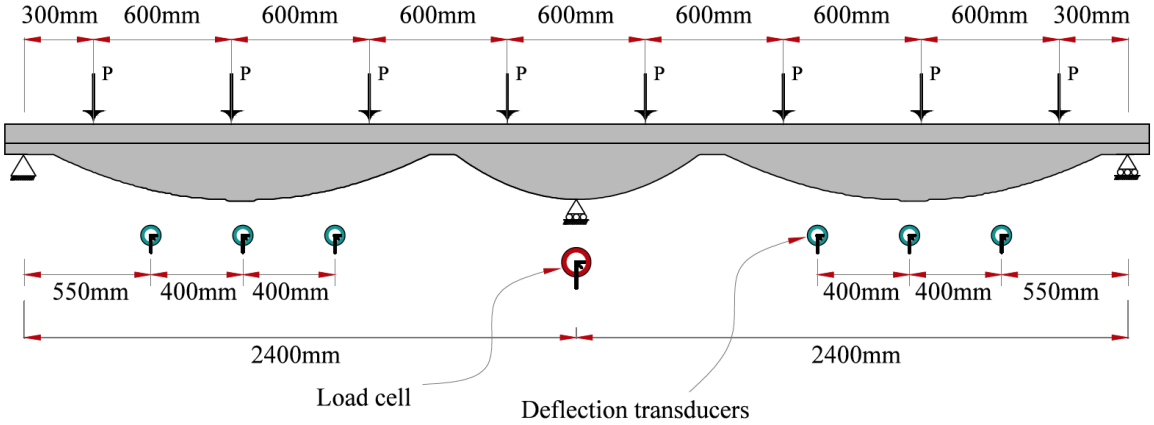

Figure 5.21: Test set-up for beams T-OSS-C and FF-OSS-C

Figure 5.22: Beam T-N-C at testing

Figure 5.23: Beam T-OSS-C at testing

5.2.4.5 Strain gauge locations

On each continuous beam, Twenty-four strain gauges were installed. For all beams, the highly utilised locations were selected in the design and these regions were used for locating strain gauges for all three beams for the sake of comparison. Eight strain gauges were installed in the sagging region near mid-span (four on each side) and the other eight strain gauges were located on hogging region on each side. The strain gauges were applied to both tension and compression bars. Figure 5.24 shows the strain gauge locations and distances for all continuous beams tested in this experimental program. The installation procedure described in §5.2.3.1 was used to apply the strain gauge to ensure functioning of the gauging.

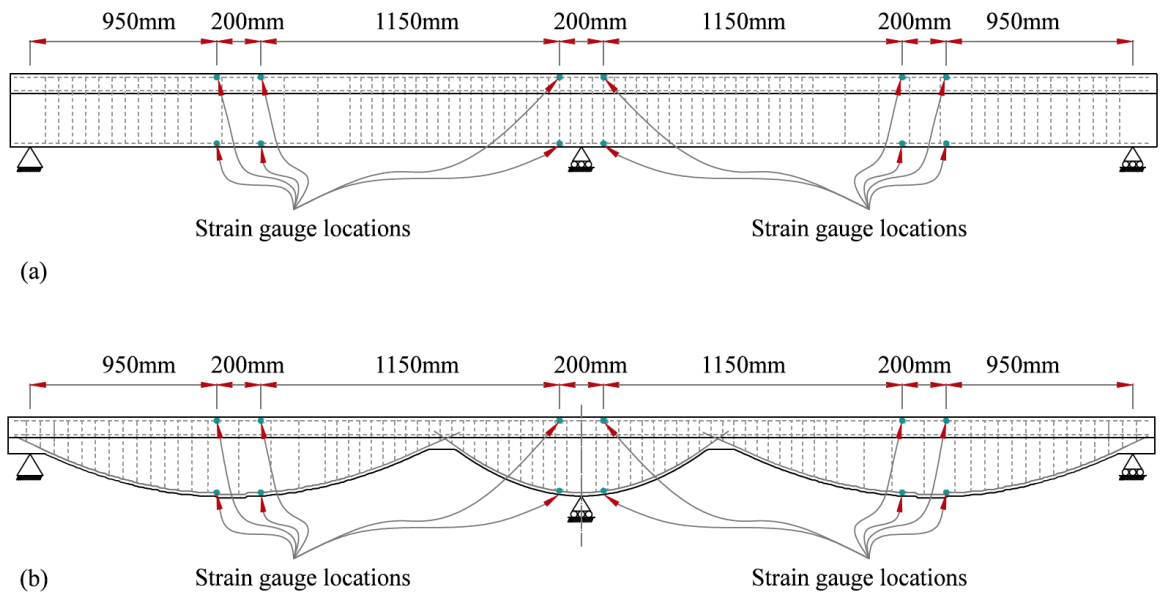

Figure 5.24: Strain gauge locations (a) beam T-N-C, (b) beams T-OSS-C and FF-OSS-C

5.3 Materials

5.3.1 Concrete

The concrete stress-strain behaviour used in the prediction methods developed in this work is a general relationship valid for a wide range of compressive strengths (normal and high strength concrete) (BS EN 1992-1-1, 2004). A target 30 MPa compressive strength was chosen to carry out the mix design according to Neville (1996). The water/cement ratio was slightly increased from the design value in order to improve workability. Table 5-3 shows the concrete mix ratios used for each specimen.

Table 5-3: Concrete mix proportions

Quantities in (kg) per 1 m3					*Slump*
Cement	*Crushed coarse aggregate*	*Fine aggregate*	*Water*	*w/c*	*(mm)*
375	768	930	225	0.5	90

Both beams were cast at the same time using concrete from the same batches. The compressive strength tests of concrete were undertaken by using 100mm cubes according to (BS EN 12390-1, 2000). The split tensile test was carried out on 100X200mm cylinders the tensile strength values achieved were converted to axial tensile strength according to (BS EN 1992-1-1, 2004) as follows:

$$f_{ct} = 0.9 f_{ct,sp} \qquad (5.1)$$

Where f_{ct} is the axial tensile strength and $f_{ct,sp}$ is the split tensile strength of concrete.

Eight cube samples were taken to test the compressive strength and six cylinders were taken for the split tensile strength test (Table 5-4). All specimens were tested on the day of testing the concrete beams.

Table 5-4: Properties of the test specimens

Beam	*Based on 8 cubes*		*Based on 6 cylinders*		*Age at testing (day)*
	f_c *(MPa)*	*SD*	f_{ct} *(MPa)*	*SD*	
T-OS-S	31.7	1.27	2.65	0.12	33
T-OSS-S	32.6	1.81	2.89	0.15	30
T-N-C	28.18	2.66	2.43	0.27	29
T-OSS-C	32.25	1.62	2.78	0.21	34
FF-OSS-C	27.16	1.01	2.53	0.11	37
f_c *is the compressive strength at testing date; SD: standard deviation*					

5.3.2 Reinforcement

For the longitudinal reinforcement of the specimens described in the previous sections, 10mm and 8mm ribbed steel bars were used, 4mm smooth steel bars were used to construct the shear links. The properties of the steel bars are given in Table 5-5.

Table 5-5: Properties of the steel bars

Bars	*Surface*	*Yield strength (MPa)*	*Rupture strength (MPa)*	*Use*
10 mm	Deformed	569	594	Flexural reinforcement
8 mm	Deformed	541	616	Flexural reinforcement
4 mm	Smooth	618	726	Shear links

5.3.3 Fabric

The fabric used as part of the formwork for the fabric-formed continuous concrete beam was a single layer polypropylene white sheet shown in Figure 5.25. This type of fabric is specially manufactured for casting marine concrete structures and it has the same elongation capacity in both warp and weft directions. This makes the fabric preferable as there is less tendency to wrinkle when stretched in different directions under the weight of the wet concrete, as explained in Chapter Four.

Figure 5.25: Polypropylene fabric used to cast beam FF-OSS-C

The specifications of the fabric are given in Table 0-2 as given by the manufacturer, Proserve Ltd.

Table 0-2: Fabric specifications

Composition	*Weave*	*Weight (gsm)*	*Tensile Strength (N/mm)*		*Extension at break (%)*		*Tear strength (N)*		*Pore opening size (mm)*
			Warp	*Weft*	*Warp*	*Weft*	*Warp*	*Weft*	
White polypropylene	Plain single weave fabric	220	60	54	25		900 (min)		0.25

5.4 Construction method

Depending on the formwork type, two different methods of construction were used in this experimental work, timber-foamboard formwork and fabric-formwork. As explained in the preceding sections, beam FF-OSS-C was cast in fabric-formwork and the rest of the test specimens were cast in timber-foamboard formwork.

5.4.1 Timber-foamboard

Since only the cross-section depth varies along the length of the first four beams, the formwork was relatively simple. An ordinary prismatic timber mould was built first as shown in Figure 5.26. A layer of foamboard with a thickness equal to the width of the beam web was cut as per the longitudinal profile of the beam and installed at the bottom of the timber mould. A layer of aluminium sheet was placed on the top of the foamboard so as to prevent absorption of the wet concrete by the foamboard. To prevent lateral movement of the timber mould parts due to the pressure exerted by the wet concrete, timber braces were applied at equal intervals along the mould.

Constructing the shear links was time-consuming and relatively difficult because each link has different dimensions as the cross-sectional depth of the beams vary.

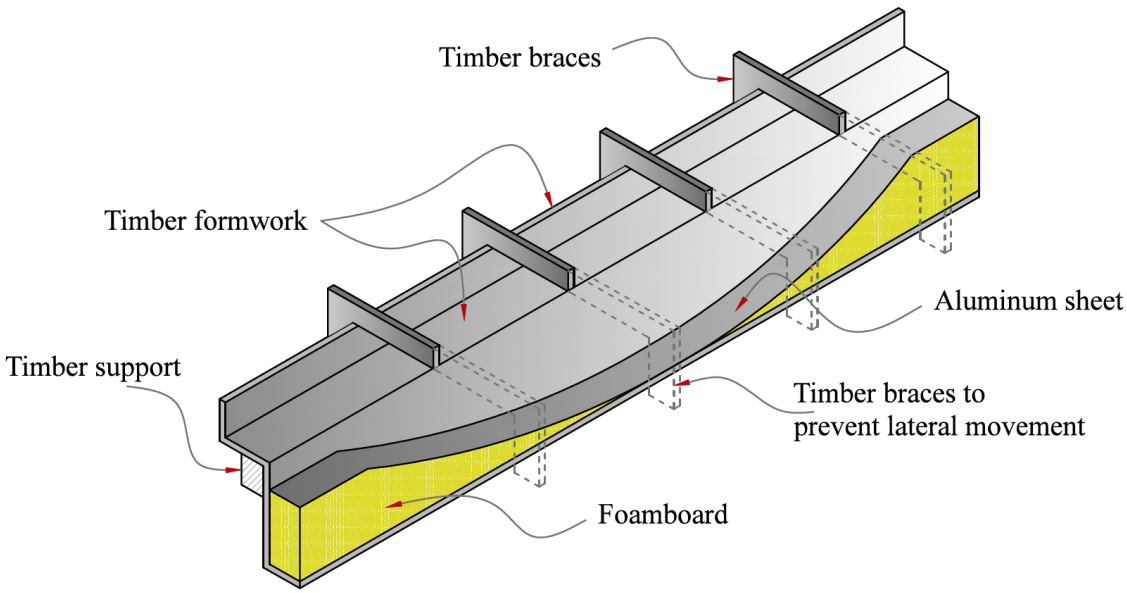

Figure 5.26: A longitudinal section of the timber-foamboard formwork

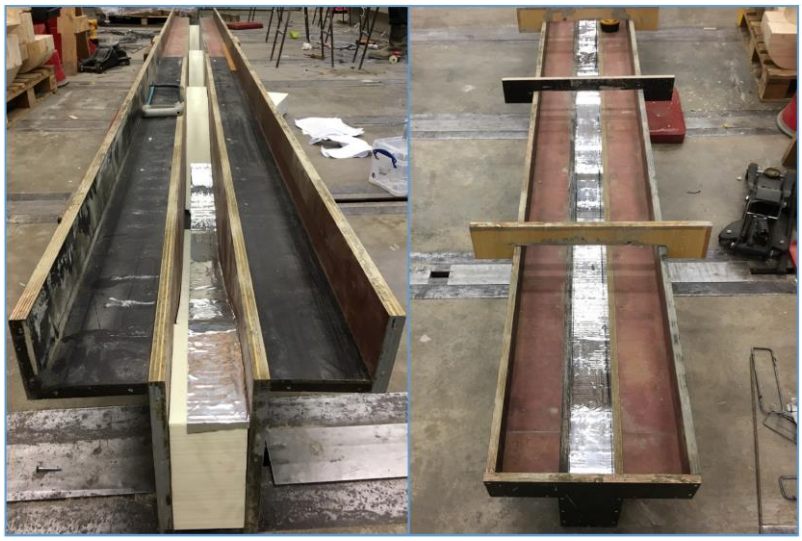

Figure 5.27: The timber-foamboard formwork

5.4.2 Fabric-formwork

The fabric formwork prepared in this work for beam FF-OSS-C, shown in Figure 5.28, consisted of two main parts; a rigid timber frame to carry the weight of the concrete-filled fabric mould and the fabric sheet stitched to the timber frame at both sides of the web opening. The rigid boundaries of the wooden form table and the layout of the fabric are of the two main factors defining the final shape of a fabric-formed beam. Therefore, a careful design of the formwork and the correct layout of the fabric is essential.

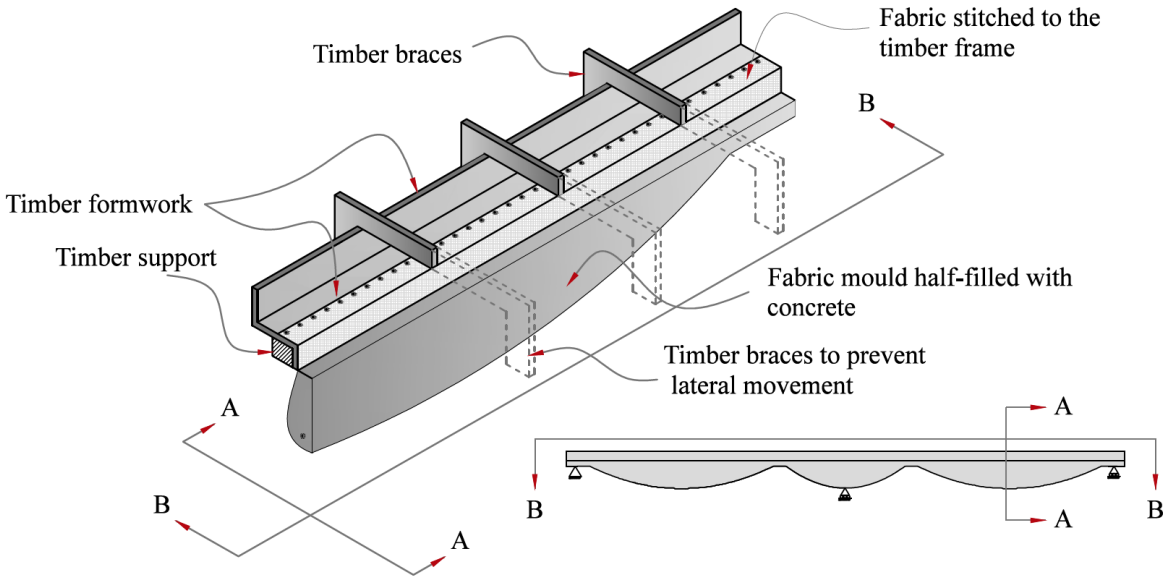

Figure 5.28: Fabric formwork details

5.4.2.1 Timber frame

The timber frame is the rigid part of the fabric formwork and is designed to carry the vertical gravity loads of the fabric mould filled with wet concrete and the lateral hydrostatic loads on the sides of the formwork. The whole timber frame can be divided into two parts; 1) a timber table form which defines the boundaries of the concrete flange and which supports the fabric web, and 2) a supporting timber frame which carries the loads of the concrete-filled mould, as shown in Figure 5.29 and 5.30.

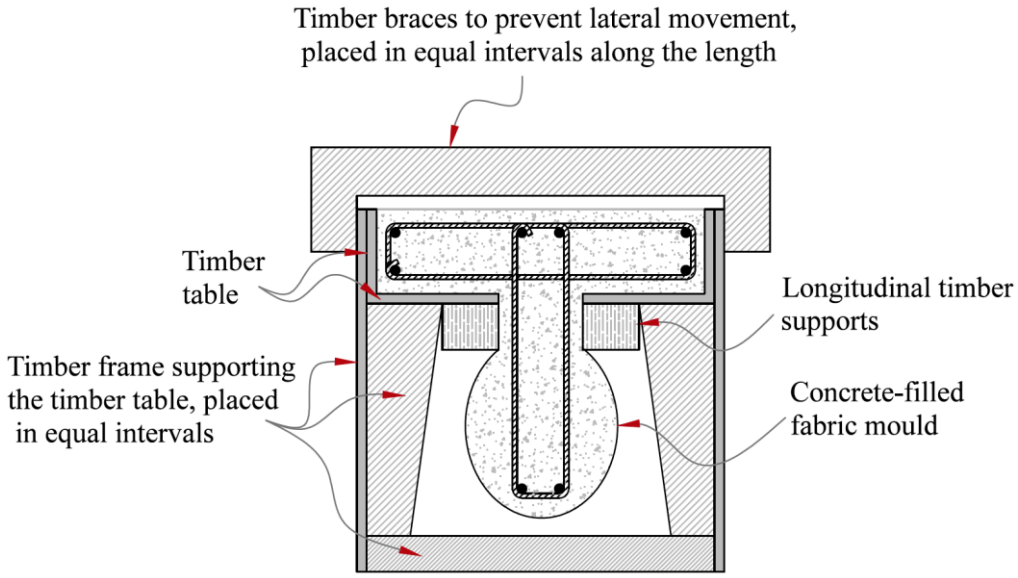

Figure 5.29: Cross-section of the formwork used

Figure 5.30: Beam FF-OSS-C prior to casting

5.4.2.2 Fabric layout

In this experimental work, the fabric layout and fixing to the timber form was attempted in two ways. In the first attempt, the fabric was marked according to the longitudinal profile of the beam as presented in Figure 5.31. At any point along the length, the distance between the two marked lines is equal to the perimeter of the cross-section of the beam at that point. The fabric was then fixed to the timber table along the indicated lines.

However, this method was not successful as the designed cross-sectional depths not achieved due to numerous transverse and longitudinal wrinkles and folds which occurred in the fabric after fixing the fabric to the timber frame as shown Figure 5.32. This might be due to two reasons. First, beam FF-OSS-C has a high longitudinal curvature especially in the mid-span region and this leads to differential extension of the fabric as its stiffness is not the same in all directions. Second, to fix the fabric to the table form along a straight line, the fabric has to be pulled according to the required depth in order to match with the lines that indicate the longitudinal profile. This changes the direction of fabric threads and therefore diagonal tension forces develop in the fabric due to pulling while fixing it to the timber frame, as explained in Figure 5.33(a), and folds and wrinkles form between the stretched and non-stretched fabric parts.

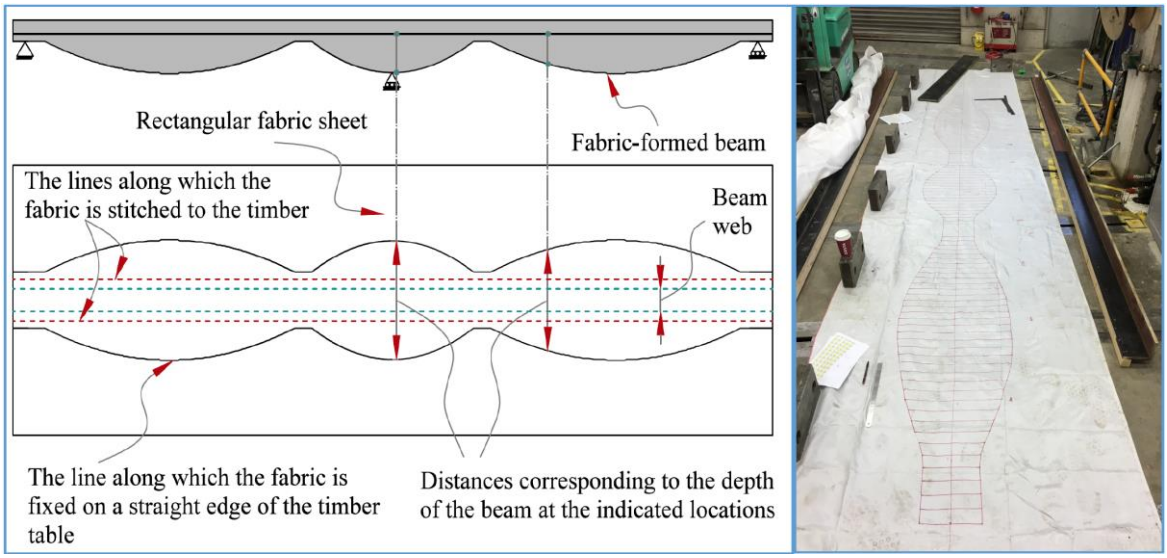

Figure 5.31: Fabric layout in the first attempt

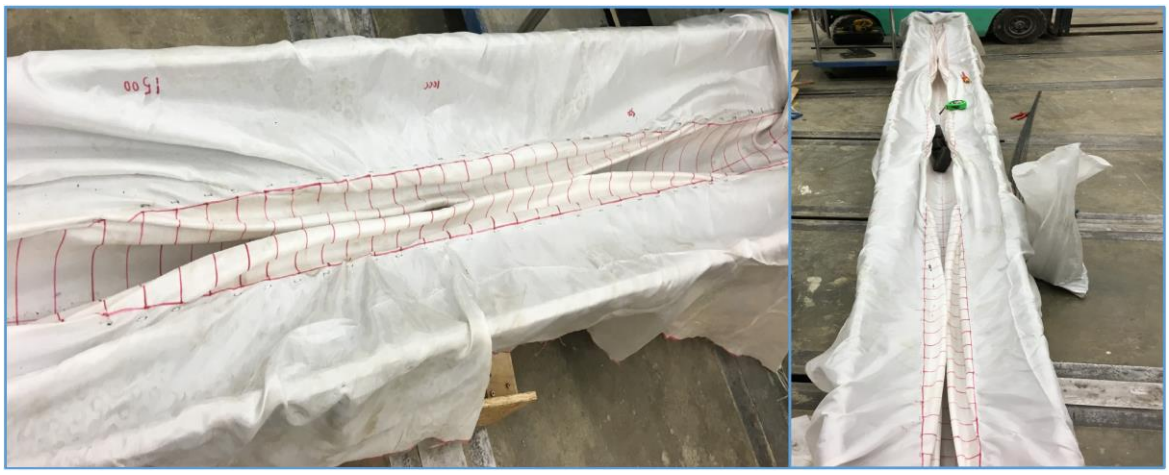

Figure 5.32: Folds and wrinkles in the fabric in the first attempt

In the second attempt, the profile of the beam was created by sewing two halves of the fabric together as shown in Figure 5.33 (b). This was done to avoid longitudinally pretensioning the fabric while fixing it to the timber table. It also ensured that the directions of the fabric threads are approximately aligned with the vertical and horizontal principal tensile forces in the fabric due to the weight of the wet concrete and the lateral hydrostatic pressure respectively.

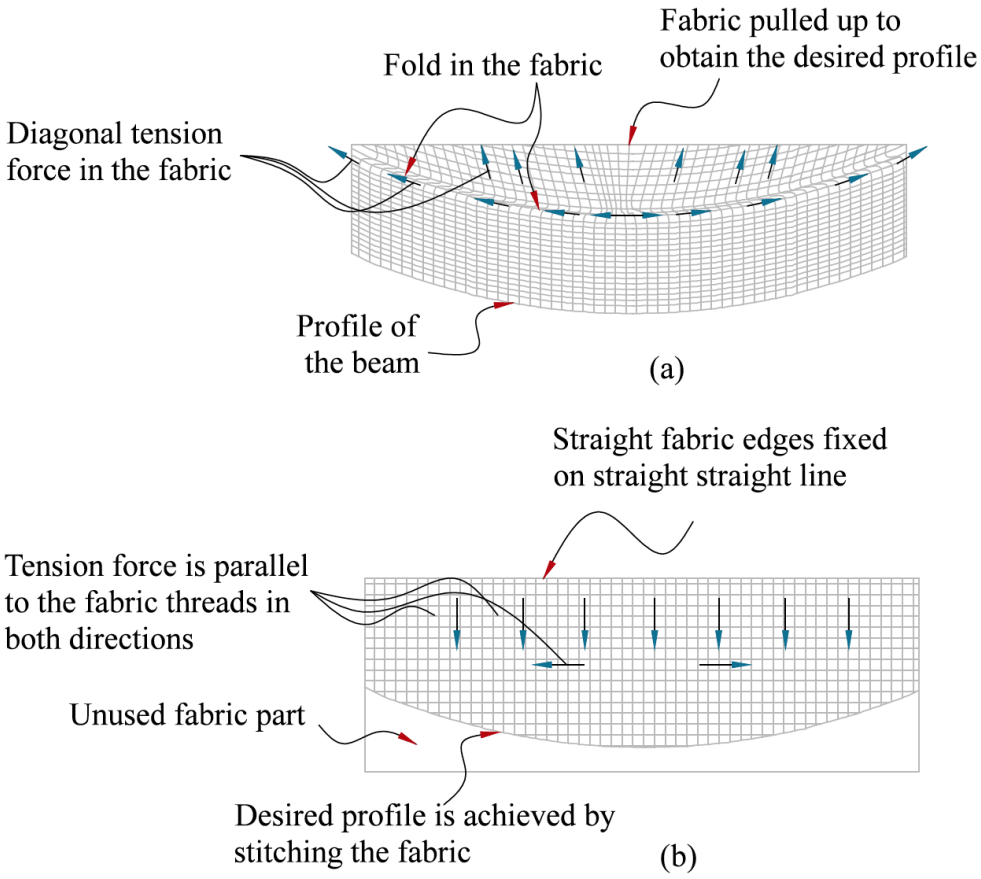

Figure 5.33: Fabric layout (a) first attempt, (b) second attempt

The second attempt allowed a successful layout of the fabric without big folds or noticeable number of wrinkles. This layout of the fabric also allowed easy installation of the reinforcement cage and the correct cross-section depths were achieved easily after casting. The casting process of this beam had some minor difficulties due to the relatively small web size of the beam. Compaction while placing the concrete by means of vibrators needed to continue for a longer period of time in the small sections near the supports. Figure 5.34 through Figure 5.36 show fabric layout, fabric-formed mould preparation, casting process and the demoulding of beam FF-OSS-C.

It should also be mentioned that, there was some difficulty in constructing the reinforcement cages as the longitudinal bars had to be bent according to the longitudinal profile. For beams with usual sizes this problem is minor because the longitudinal curvature of the beam is larger.

Figure 5.34: Fabric layout in the second attempt

Figure 5.35: Casting of beam FF-OSS-C

Figure 5.36: Demoulding beam FF-OSS-C

5.5 Summary

In this chapter, the experimental program undertaken to verify the theoretical methods developed in this thesis was presented. A test matrix was designed based on the test parameters required to verify the methods. In Chapter Six, the test results and discussion of all tests are presented.

[Blank Page]

Chapter Six

Experimental results and discussion

6.1 Preface

The results of the experimental program presented in Chapter Five are discussed in this chapter along with the numerical calculations carried out to predict the behaviour of the test specimens. The models proposed to predict the behaviour of the beams are first validated by comparing their performance to the experimental data. The optimisation models are then assessed by analysing the behaviour of the beam specimens designed to meet different optimisation targets.

6.2 Simply supported beams

6.2.1 Overview of the tests

The simply supported beams were tested under eight-point loading at 3kN load increments according to the method described in §5.2.3.2. Upon loading, the first cracks were noticed at 27 kN and 29 kN for beams T-OS-S and T-OSS-S respectively. Since both simply supported beams were designed to fail in flexure of the steel bars, the strain gauge readings were considered at late stages of loading to monitor the failure of the beams.

6.2.1.1 Failure modes

Both beams failed in flexure as predicted. Beam T-OS-S showed a number of wide local cracks which were distributed approximately uniformly over the length of the beam. Since this beam was optimised for strength only, all sections along the beam are expected to fail theoretically at the same load level. The strain gauge readings indicated that the tensile steel bars yielded at all locations along the beam at within a small loading interval (103.2kN to 106.8 kN), as explained later in §6.2.3.

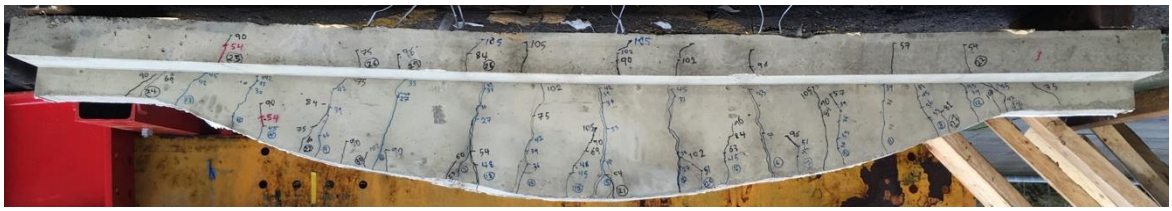

Figure 6.1: Beam T-OS-S after failure

The cracks for beam T-OSS-S at failure were wide local cracks at midspan region where extra material has not been added while optimising for serviceability. The cracks in the side regions, where material was topologically added to optimise the beam for serviceability, were smaller cracks and closely spaced compared to that of the midspan region. The ultimate failure of the beam was reached and the beam was not capable of carrying higher loads when the tensile steel bars in the midspan region yielded (at 107.3 kN). Unlike beam T-OS-S, this beam had higher sectional moment capacity than the applied moment at failure due to increase of depth in the serviceability optimisation procedure. Therefore, the tensile steel bars did not yield in this region, as explained later in §6.2.3.

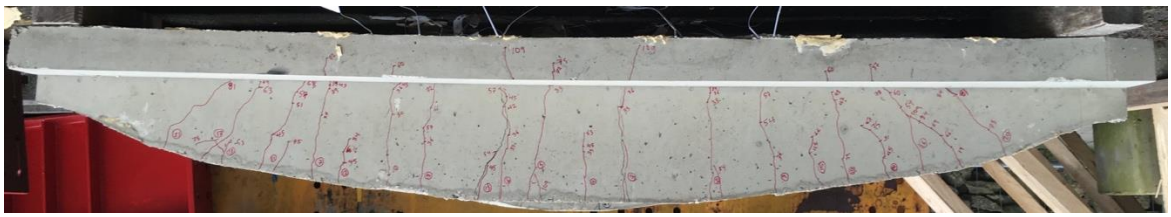

Figure 6.2: Beam T-OSS-S after failure

6.2.2 Prediction of behaviour

Three prediction models were presented in Chapter Three. These models are 1) the partial-interaction model which simulates post-cracking deflection and crack widths for concrete beams, 2) the full-interaction model which predicts the deflections and the ultimate flexural capacity of concrete beams and 3) the combined-interaction method (CI) which was developed in this thesis to predict crack widths, deflection and sectional moment capacity of concrete beams.

The test results against the predictions made by each of the mentioned models are presented and comparisons between results of these models are shown.

6.2.2.1 Cracking behaviour

The crack width values and crack locations were recorded for the simply supported beams at every stage of loading. The models that are based on discrete crack approach, the partial-interaction and the CI method, are considered in comparison of the test and predicted cracking data. Due to the non-linear behaviour and non-homogenous nature of concrete material, predicting the width of individual cracks is not possible. Therefore, the average values of crack width, crack spacing and the maximum crack width were considered in presenting the test data and comparing it to the predictions.

For beam T-OS-S (the details are shown in §5.2.3), experimental crack width values and locations are presented against the cracking data predicted by the combined and partial-interaction models in Figure 6.3 through Figure 6.5. The cracking data at three stages of loading is considered, as presented in Table 6-1, in order to consider the cracking process at the initiation of cracking at 30 kN, propagation of cracks at 36 kN and serviceability at 51 kN. At a total load of 30 kN, a number of cracks formed in the beam. The PI method, which allows cracks to form solely by bond-stress transfer, predicted only two cracks (the initial cracks) compared to eight actual cracks as shown in Figure 6.3. This means the applied moment at the initial cracks is smaller than the moment needed to produce further cracks according to the PI method. The CI method on the other hand, which allows cracks to form through full and partial bond interaction, predicted twelve cracks with a reasonably accurate prediction of the average and maximum crack width values (Table 6-1). It is therefore clear that, depending on the geometric and material properties of the beam, the PI method does not provide a reasonable prediction of cracking pattern for non-prismatic beams but the CI method developed in this work can be used as a suitable alternative model.

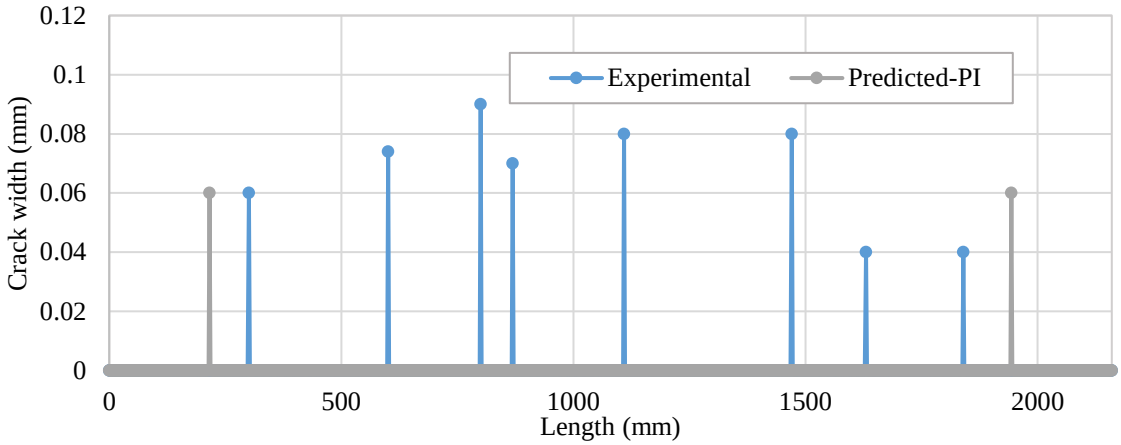

Figure 6.3: Experimental and predicated (PI) crack width values and locations at load 30 kN for beam T-OS-S

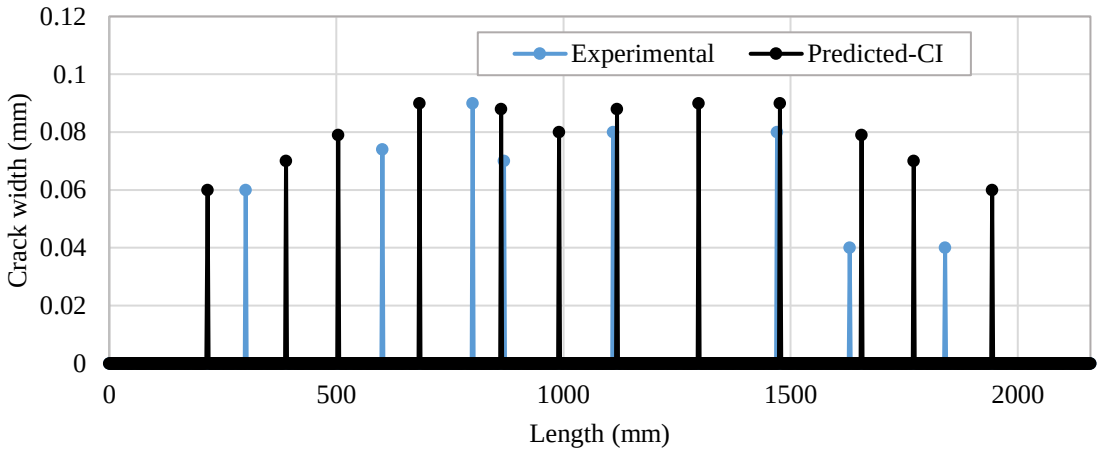

Figure 6.4: Experimental and predicted (CI) crack widths and locations at load 30 kN for beam T-OS-S

At the service load level of 51 kN, nineteen cracks occurred in the beam. As presented in Figure 6.5, the PI method predicted twenty cracks which mostly are equally spaced from each other because the PI method allows a crack to form at a certain distance from an existing crack. The CI method has predicted a more realistic cracking distribution as the crack spacing varies along the beam depending on the interaction nature between the steel bars and the concrete in different regions.

Generally, the CI method provided a good indication of the actual cracking behaviour of beam T-OS-S. Although some predictions obtained from the PI method had a close agreement with the experimental data, the model is unsuitable for non-prismatic concrete beams because the full bond interaction mechanism (which is not accounted for in the PI method) may govern the cracking process for beams with different geometry, reinforcement layout and material characteristics.

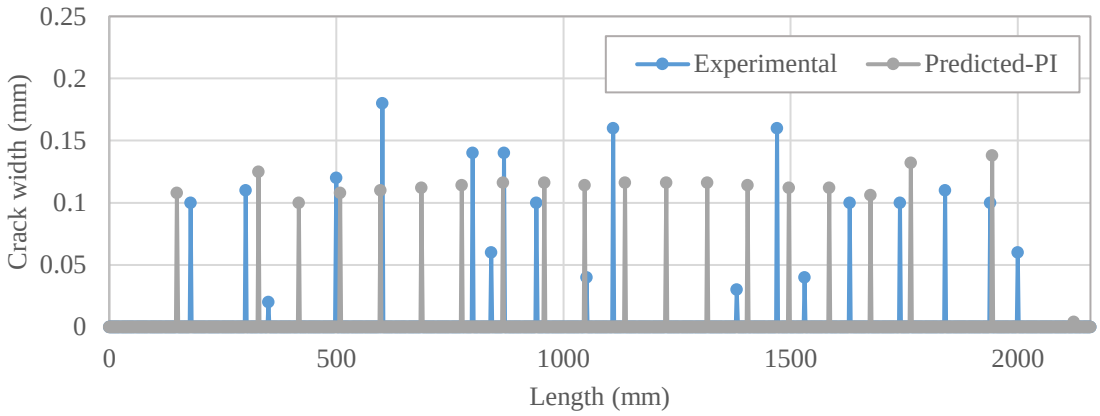

Figure 6.5: Experimental and predicted (PI) crack widths and locations at load 51 kN for beam T-OS-S

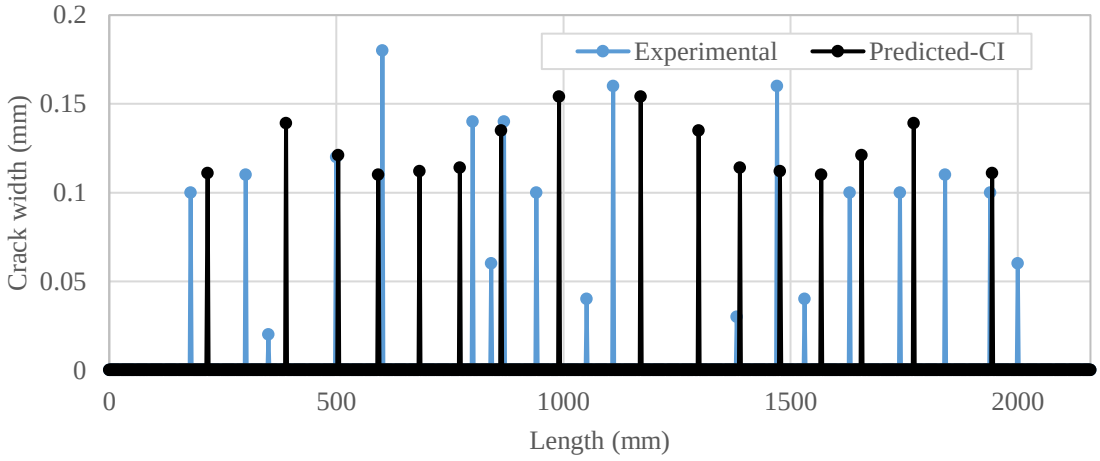

Figure 6.6: Experimental and predicted (CI) crack widths and locations at load 51 kN for beam T-OS-S

Considering beam T-OSS-S now, similar cracking patterns were predicted by both PI and CI methods at 33 kN as Figure 6.7 and Figure 6.8 indicate. Both models over predicted the crack width and cracks number values. The PI method, as for the CI method, predicted nine equally spaced cracks compared to six experimental cracks. The close agreement between the two models, in this case, is attributable to the fact that, cracking capacity from full bond interaction is close to that of the partial bond interaction in the cracking region. Seven out of nine cracks at this stage of loading were discovered through bond stress transfer in the CI method and therefore the model converged to a cracking pattern similar to the PI method. This again indicated the dependence of the PI method on the beam properties, making this model fail to serve as a general-purpose tool to predict the cracking behaviour of non-prismatic beams.

Table 6-1: Experimental and predicted crack width and cracks number values for beam T-OS-S

Load	*Average crack width (mm)*			*Maximum crack width (mm)*			*Number of cracks*		
	Exp.	Pred.		Exp.	Pred.		Exp.	Pred.	
		CI	PI		CI	PI		CI	PI
30	0.07	0.08	0.06	0.09	0.12	0.06	8	12	2
39	0.09	0.10	0.12	0.16	0.13	0.14	12	14	11
51	0.10	0.13	0.11	0.18	0.15	0.14	19	16	20

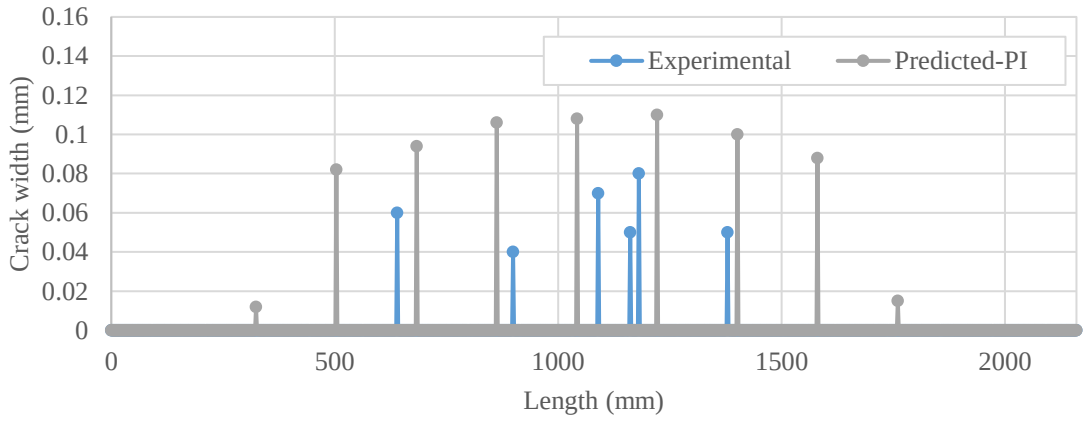

Figure 6.7: Experimental and predicted (PI) cracking pattern for beam T-OSS-S at 33 kN

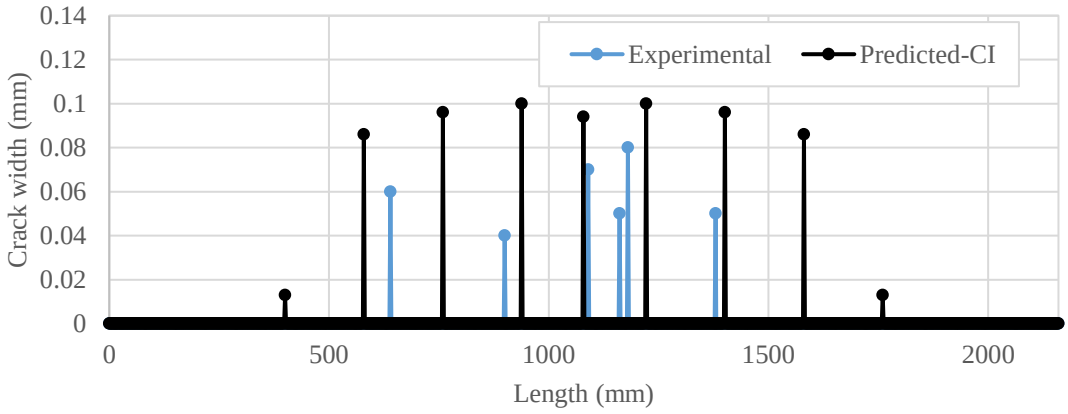

Figure 6.8: Experimental and predicted (CI) cracking pattern for beam T-OSS-S at 33 kN

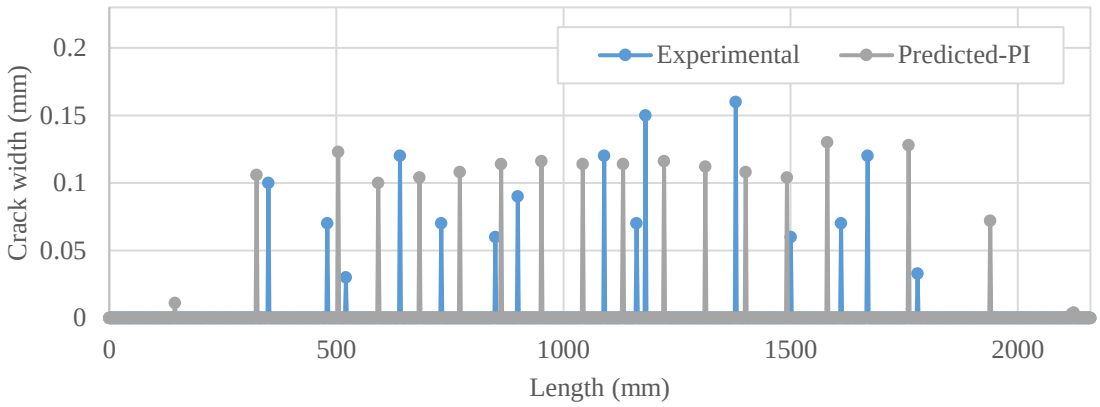

Figure 6.9: Experimental and predicted (PI) crack width values for beam T-OSS-S at 51 kN

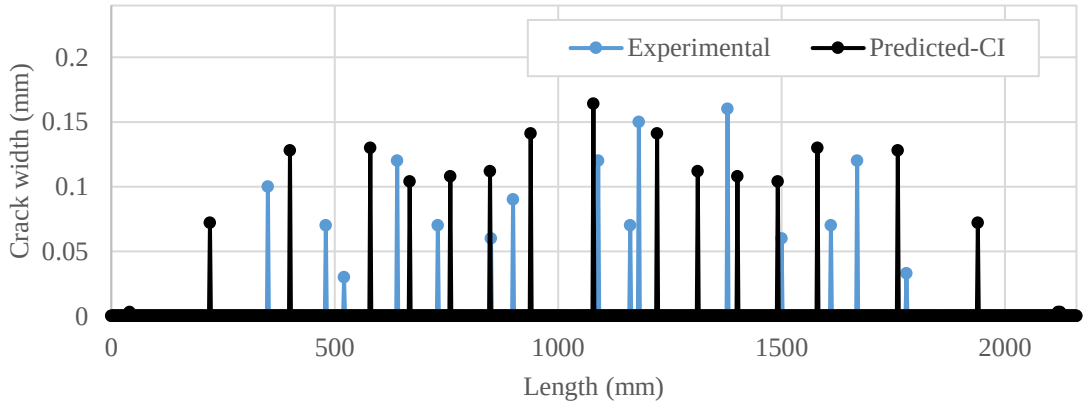

Figure 6.10: Experimental and predicted (CI) crack width values for beam T-OSS-S at 51 kN

At the load level 51 kN, cracks scatter over larger regions. Depending on the applied moment value, wider crack spacing leads to higher crack width values as higher bond stress transfer is achieved over longer distances (see §3.32). The crack spacing predicted by the PI method is constant over large cracking regions as can be noted from Figure 6.9 and Figure 6.10, unlike those predicted by the CI method which change along the cracking interval. Therefore, the CI method produced a better prediction of the maximum and average crack width values than the PI method at all stages of loading (Table 6-2) because it allows for variation in crack spacing depending on the bond interaction.

Table 6-2: Predicted and experimental cracking data of beam T-OSS-S

Load	*Average crack width (mm)*			*Maximum crack width (mm)*			*Number of cracks*		
	Exp.	Pred.		Exp.	Pred.		Exp.	Pred.	
		CI	PI		CI	PI		CI	PI
33	0.06	0.07	0.08	0.08	0.10	0.11	6	9	9
39	0.08	0.10	0.10	0.12	0.13	0.14	10	11	11
51	0.09	0.10	0.10	0.16	0.16	0.13	15	17	18

6.2.2.2 Load-deflection behaviour

The deflection values for the simply supported beams are collected at six points. However, the average deflection value of the two middle points, which are equally distanced from the centre of the beam on the right and left sides, is considered here.

Presented in Figure 6.11 and Figure 6.12, respectively are the experimental load deflection response of beam T-OS-S and T-OSS-S plotted against the predicted load deflection relationships obtained from the full-, partial- and CI methods. Since the PI method accounts for deflection mainly through rigid body rotation at the cracks and ignores deflection due to curvature within the cracking region, a return in the value of deflection can be seen just after the initial crack(s) forms in beam T-OS-S. Only two initial cracks form (Figure 6.3) at the onset of cracking but curvature values between these cracks over a large region of the beam are neglected when calculating deflections according to PI theory. A similar return in load-deflection response cannot be seen for beam T-OSS-S when cracking initiates because a higher number of cracks form (Figure 6.7) and their contribution to deflections is higher than the effect of the neglected curvature values.

The full-interaction model slightly overpredicted deflection values for loads lower than the service load. This might be due to tension-stiffening effect which is not simulated by this model. The combined interaction model shows closest agreement with the test data compared to the other models because it accounts for the tension-stiffening effect and full and partial bond-slip mechanism in different regions of the beam.

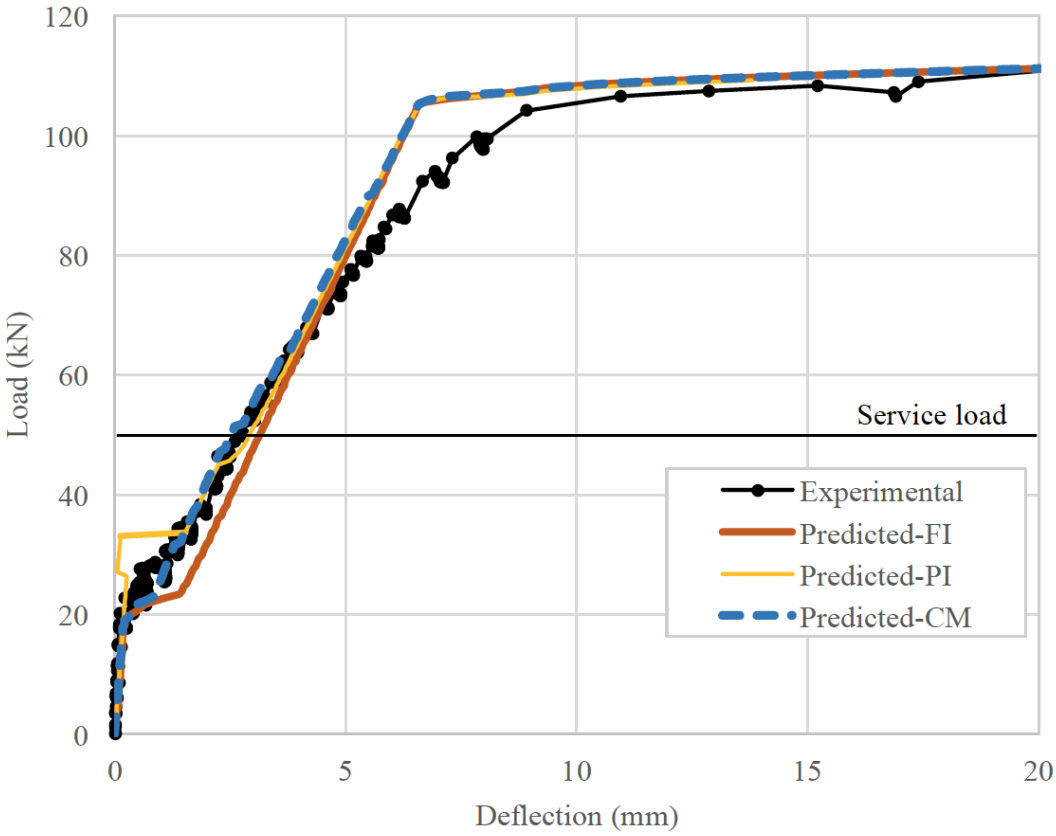

Figure 6.11: Predicted and experimental load-deflection response of beam T-OS-S

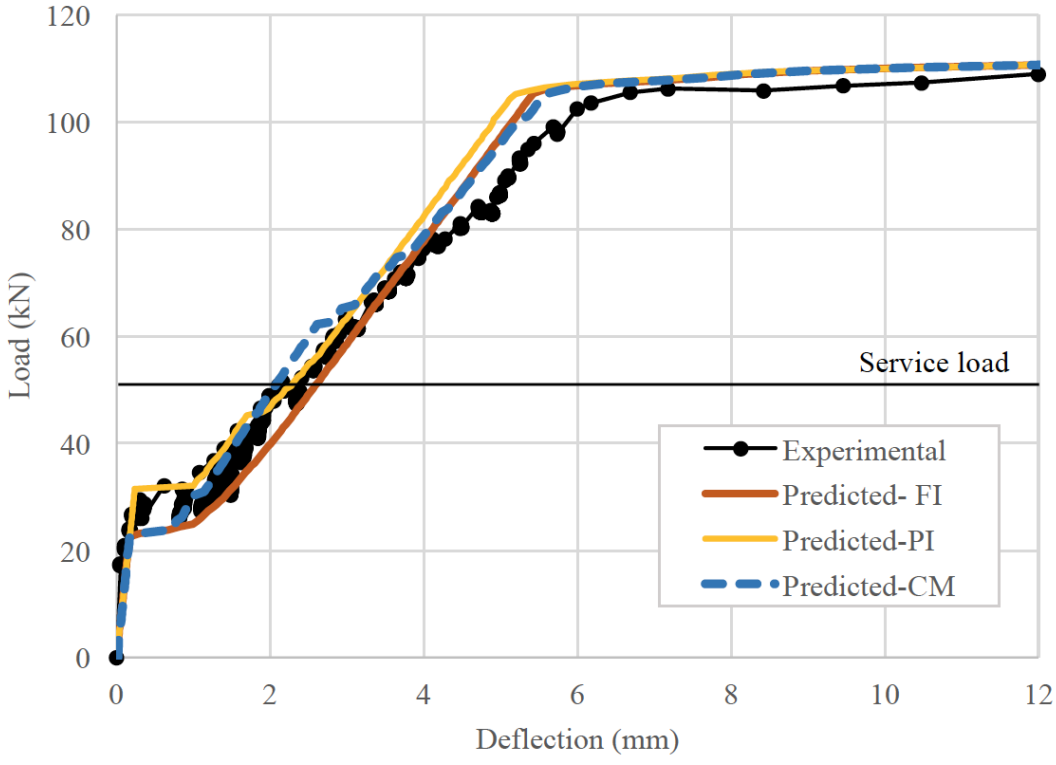

Figure 6.12: Experimental and predicted load-deflection response for beam T-OSS-S

At later stages of loading, after the service load level, larger regions of the beam crack and cracking governs the behaviour of the beam. Therefore, all models overestimate deflection values because the behaviour of a highly-cracked beam is governed by a more complicated cracking mechanism and the assumption of plane sections may no longer be valid. However, as the main purpose behind this work is dealing with serviceability, the accuracy of prediction at higher loads than the service load is not of primary importance.

6.2.2.3 Sectional behaviour

The performance of the proposed prediction models for the behaviour of the beams at section level was assessed by monitoring strain values on the steel bars. The locations and designations of the strain gauges are shown in figure 6.13. Unfortunately, due to technical problems, some of the strain gauges did not work. For beam T-OS-S, strain gauges A1, A3, A4, A6, A7, A8 and B5 worked and the recorded test strains are plotted on Figure 6.14 through Figure 6.20 against the predicted data. For beam T-OSS-S, only strain gauges A2 and A3 recorded data successfully.

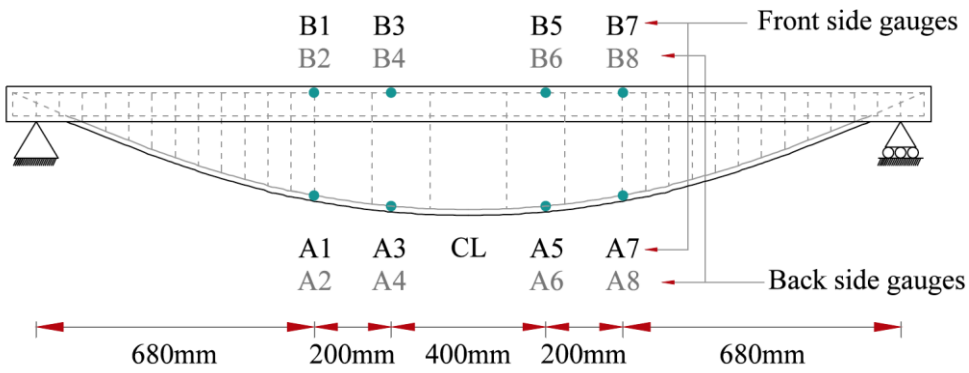

Figure 6.13: Strain gauges names and locations on the simply supported beams

Generally, all models showed a good agreement with the experimental data at the post-cracking and pre-yielding stages. However, the proposed CI method performed better than the other two models at all stages of loading in most cases. The FI method tends to slightly overestimate the strain values as it can be seen in Figure 6.14, Figure 6.15 and Figure 6.17, which might be due to neglecting the effect of tension-stiffening by this model.

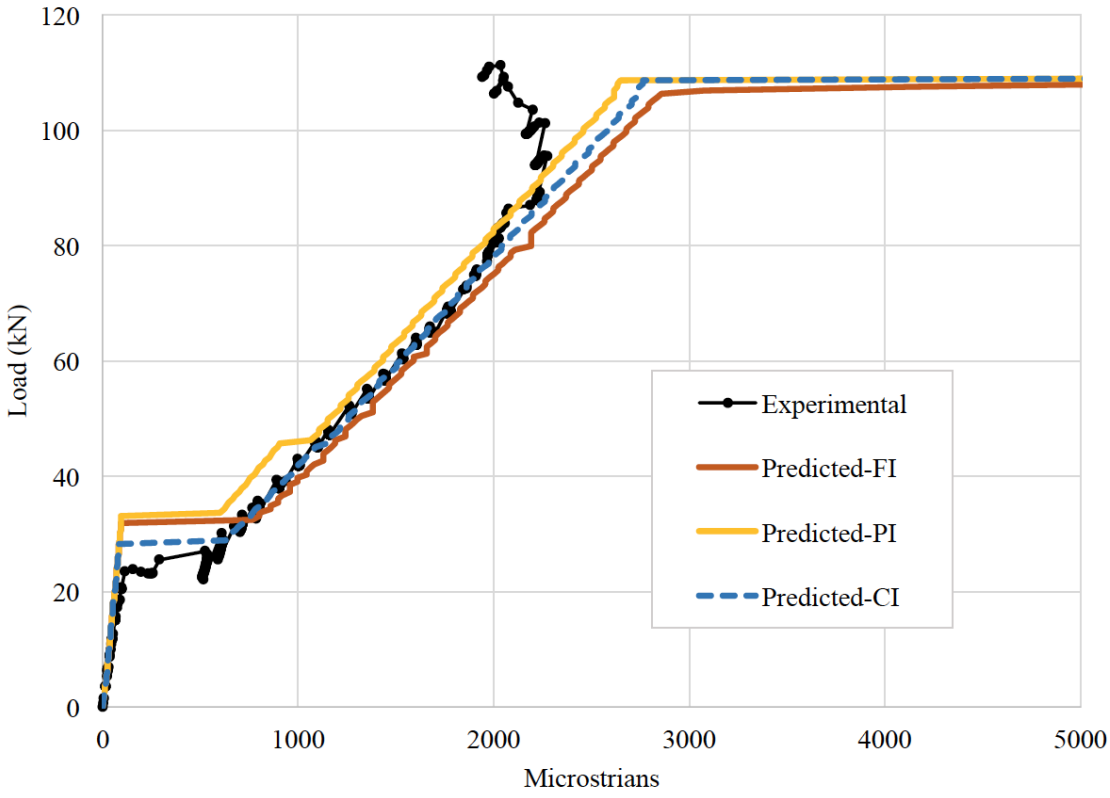

Figure 6.14: Experimental and predicted bar strains at point A1 for beam T-OS-S

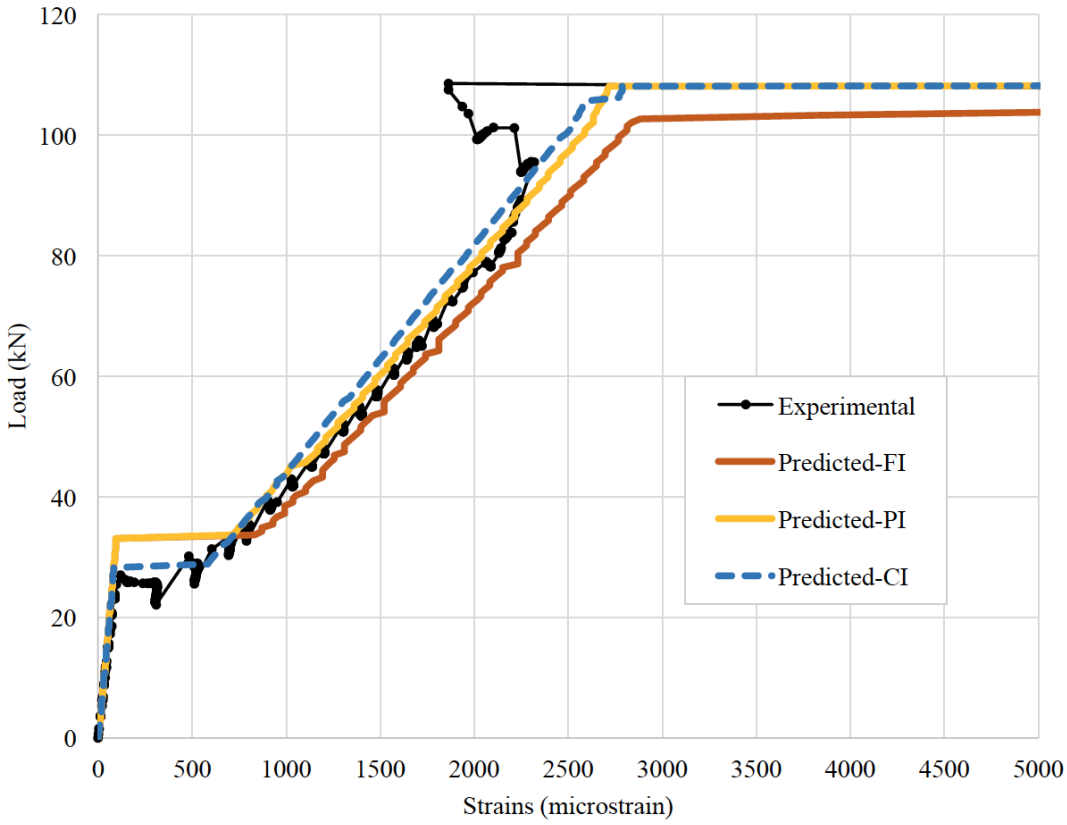

Figure 6.15: Experimental and predicted bar strains at point A3 for beam T-OS-S

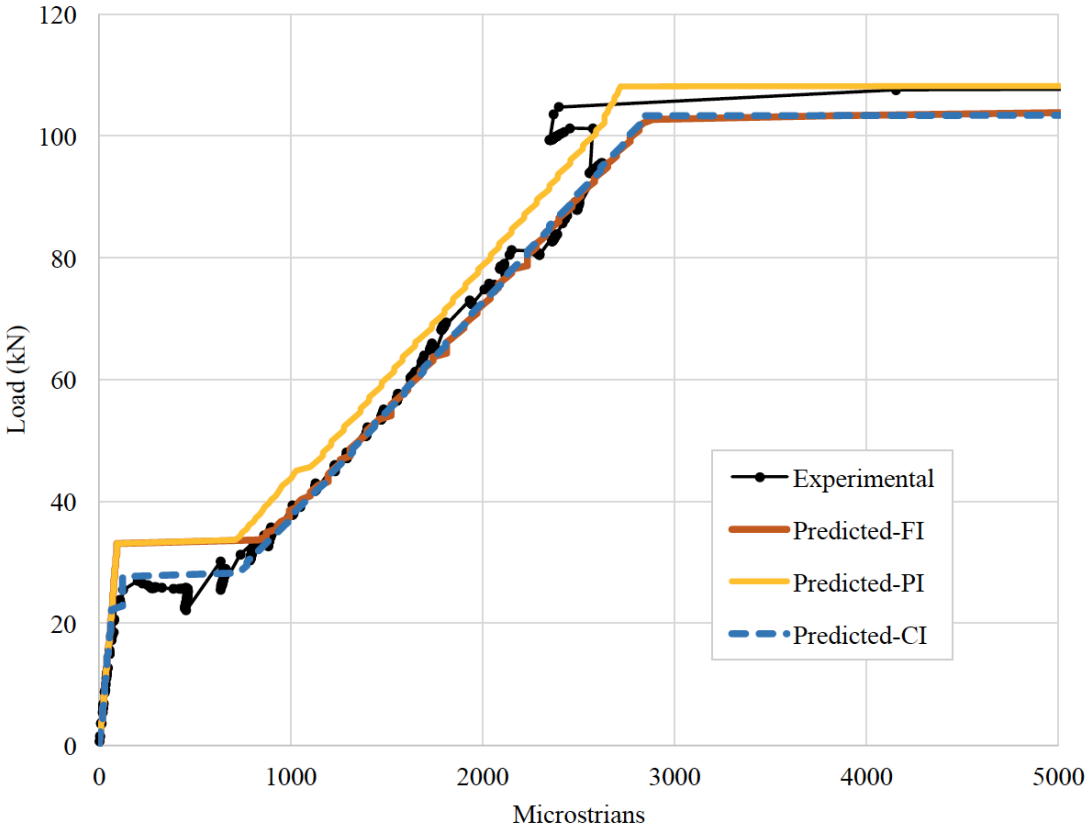

Figure 6.16: Experimental and predicted bar strains at point A4 for beam T-OS-S

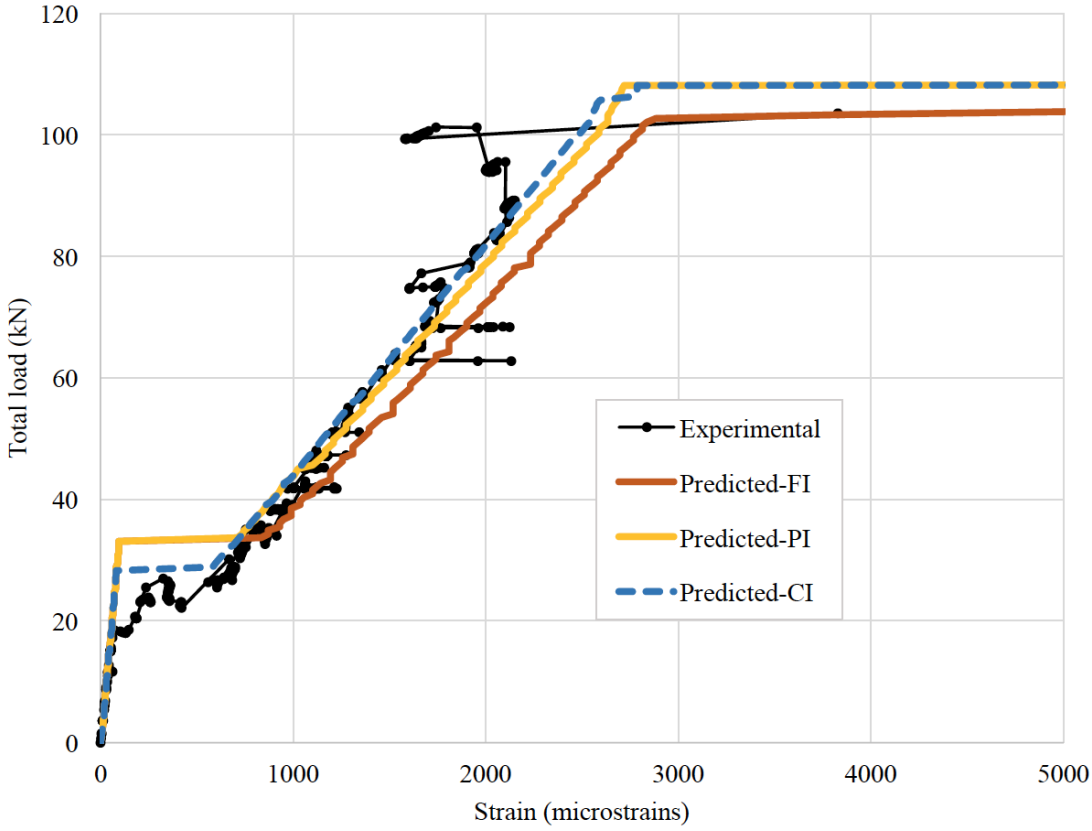

Figure 6.17: Experimental and predicted bar strains at point A6 for beam T-OS-S

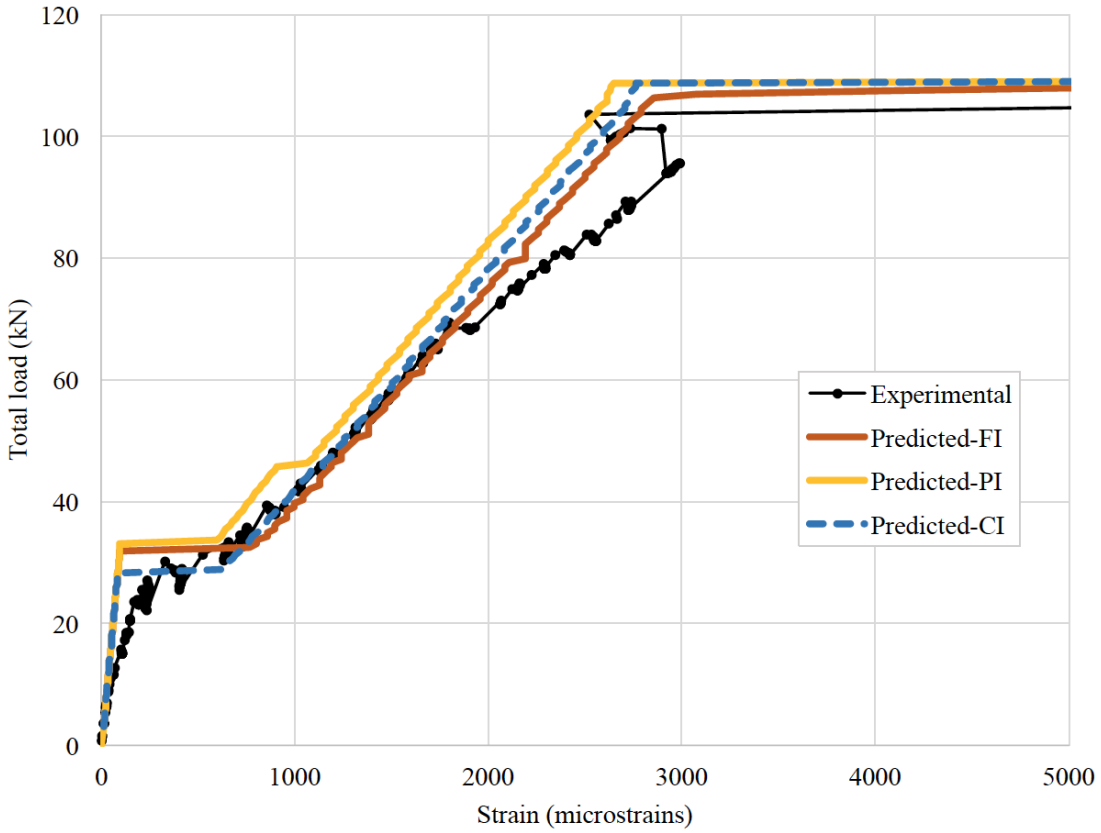

Figure 6.18: Experimental and predicted bar strains at point A7 for beam T-OS-S

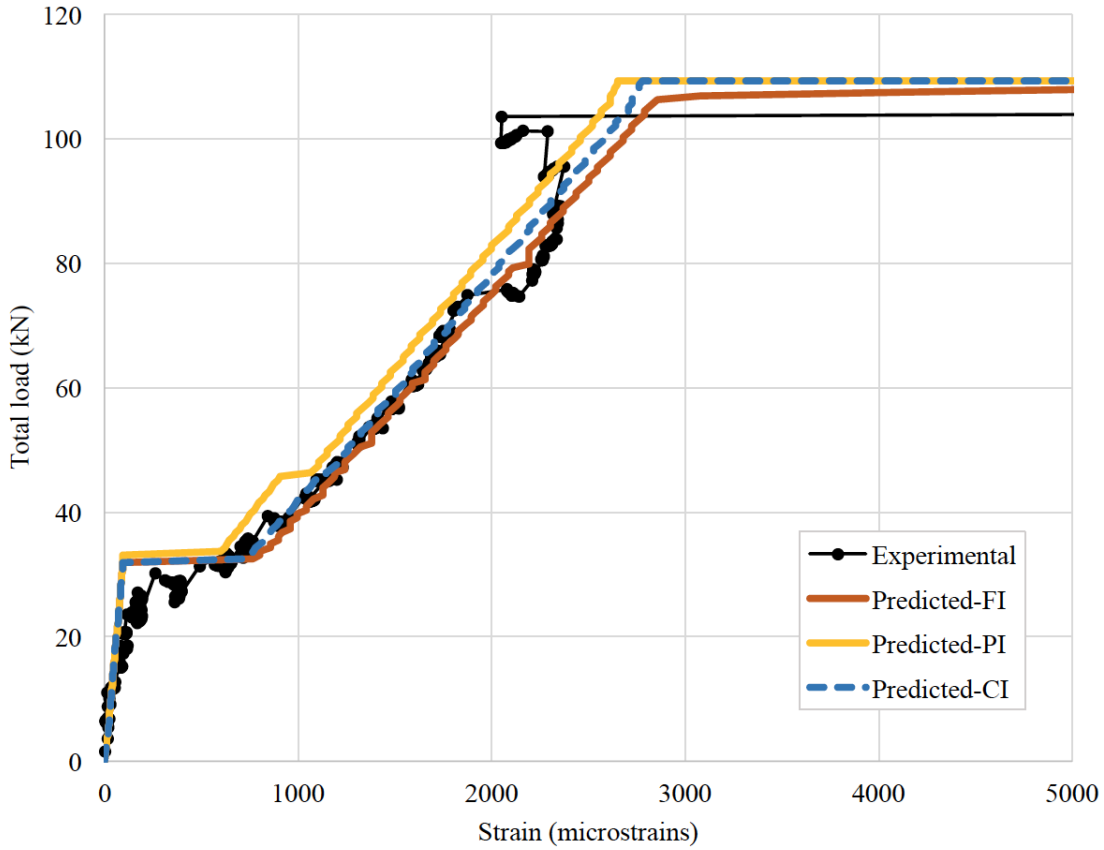

Figure 6.19: Experimental and predicted bar strains at point A8 for beam T-OS-S

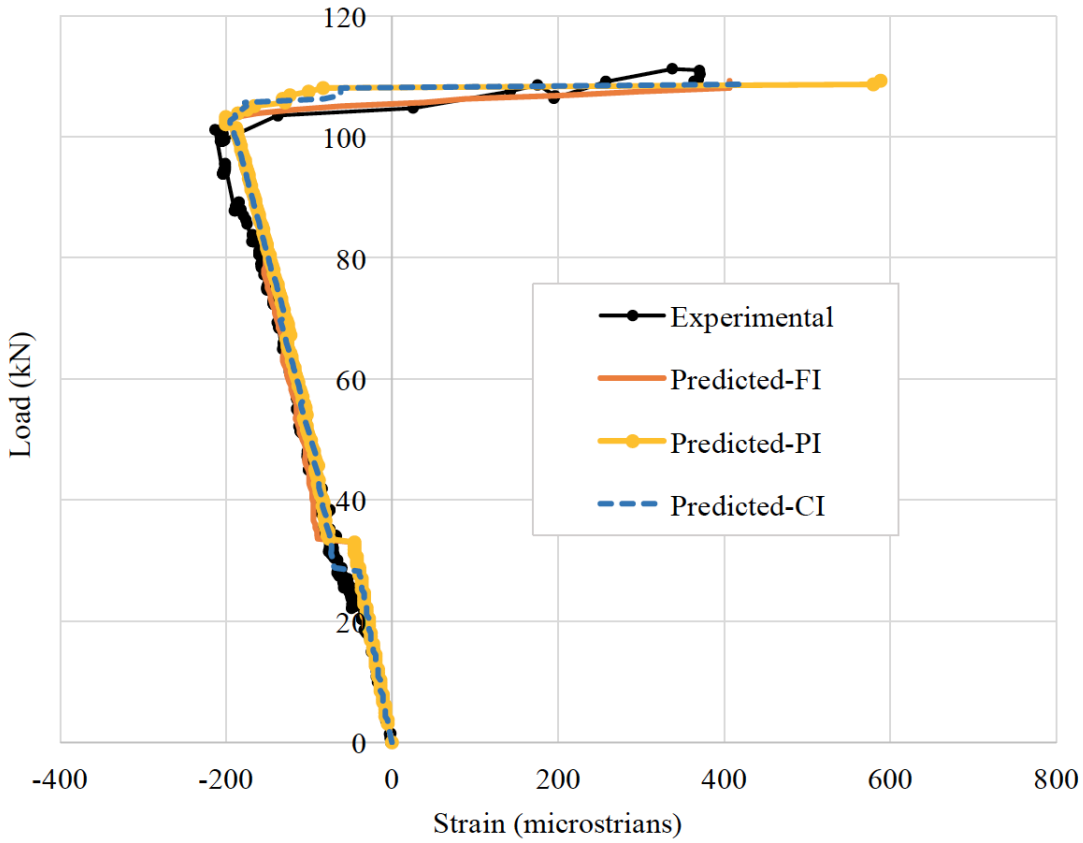

Figure 6.20: Experimental and predicted bar strains at point B5 for beam T-OS-S

The PI method overestimates the strain value of the bars at the initiation of cracking. This can clearly be seen in all cases for beam T-OS-S. The reason behind this is that the PI method predicts cracks which occur by the partial-interaction mechanism whilst a number of cracks form in this beam in the full-interaction regions prior to the PI-predicted cracks.

The strain values achieved from the discrete crack models, the PI and the combined interaction models, are dependent on the actual crack locations with respect to the location of the strain gauge considered. The strain in the reinforcing bar varies between two subsequent cracks. Therefore, since the actual crack locations are not precisely predicted by the models, the prediction accuracy of the strain values is slightly affected by the difference between the actual and predicted crack locations. For instance, the PI method overestimates the strains and predict higher strain values than the CI method in most situations. However, at locations A6 and A8 in Figure 6.17 and Figure 6.19 respectively, smaller strain values from the PI method than the CI method can be seen possibly due to different distances of the strain gauge location from an actual crack according to both models.

Prior to yielding of the steel bars, two changes in the experimental load-strain response at all tensile strain gauge locations were not accurately picked up by any of the prediction methods. First, in Figure 6.14 and at point A1, the experimental strain value at the ultimate load is close to, but does not reach the yield strain, in contrast to that is predicted by the models. Second, a decrease in the

tensile strain can be seen in beam T-OS-S in Figure 6.14 through Figure 6.19 possibly because the neutral axis reaches points beyond the level of the compression steel bars changing their state from compression to tension and decreasing the tensile force in the tensile bars. This is not predicted by the models possibly due to a slight change in the location of the steel bars during the construction process.

Figure 6.20 shows the experimental and predicted strain values of the compressive steel bars. As for the tensile bars, the PI and FI methods, overestimate the cracking strain while the CI method indicates a fairly accurate agreement. The load level at which the neutral axis exceeds the compressive steel bars is accurately predicted by all models.

For beam T-OSS-S, the tensile bars at locations A1, A2, A7 and A8 were not expected to yield because material was added to these regions during the optimisation for serviceability and therefore they should exhibit higher moment capacity (at yielding) than the applied moment, unlike beam T-OS-S which was optimised to fail simultaneously by yield of the bars anywhere along the moment-shaped beam portion. Figure 6.21 and Figure 6.22 demonstrate this point clearly as it can be noted both experimental and predicted load-strain values indicate that when the beam fails the bars in location A3 yield but those at location A2 do not.

Underestimation of the strain values by all models can be seen in Figure 6.22 but the strains were overestimated at late stages of loading at point A2 for beam T-OSS-S. However, a reasonably good prediction at serviceability was achieved.

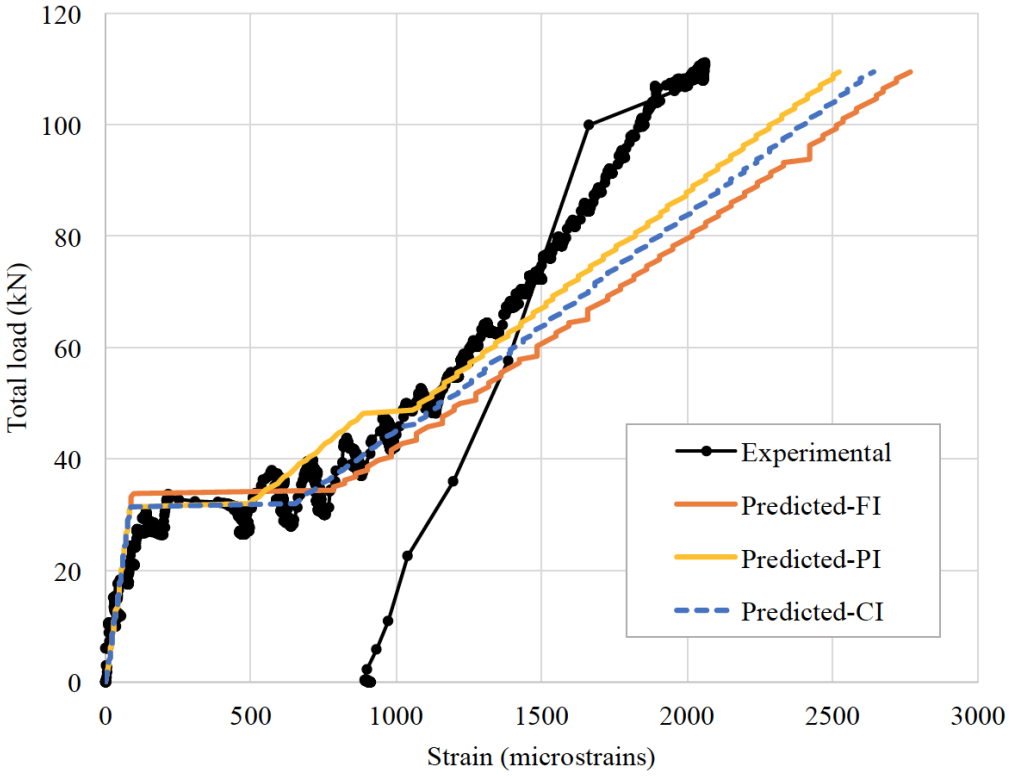

Figure 6.21: Experimental and predicted bar strains at point A2 for beam T-OSS-S

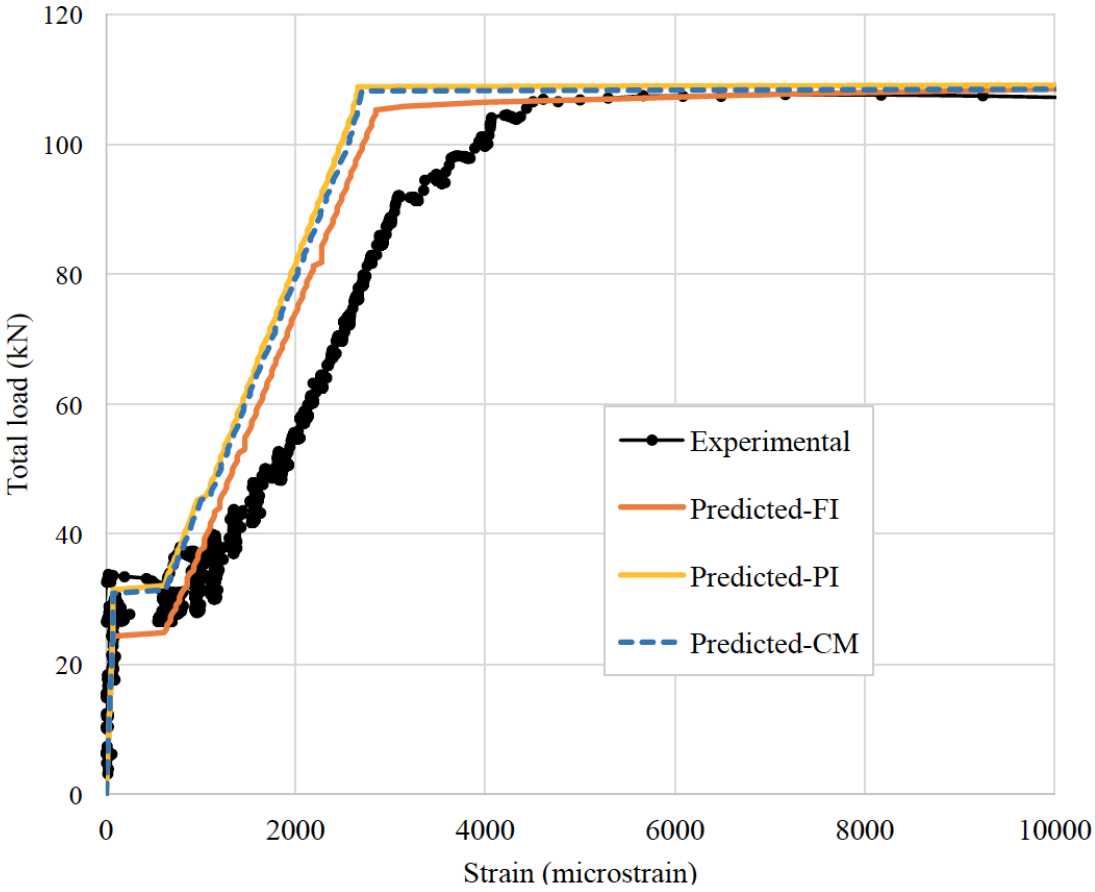

Figure 6.22: Experimental and predicted bar strains at point A3 for beam T-OSS-S

6.2.3 Optimisation

6.2.3.1 Optimisation for strength

Both simply supported beams tested in this experimental program were designed to fail in flexure by yielding of the steel bars. Beam T-OS-S, which was optimised for strength only, had theoretical critical sections anywhere along the beam apart from its flat. According to the sectionwise strength-optimisation model used in this work, the tensile steel bars should reach the yield strain anywhere along the moment-shaped part of the beam at approximately the same loading level. To confirm this, the load-strain relationships collected from the tensile strain gauges are compared in Figure 6.23. Generally, the bars yielded at the indicated locations within a relatively close loading interval, apart from point A1, where the steel does not seem to have yielded at failure as explained earlier. At location A3, the steel bar reached the yield point at a relatively higher load than the bars at locations A4, A6, A7 and A8.

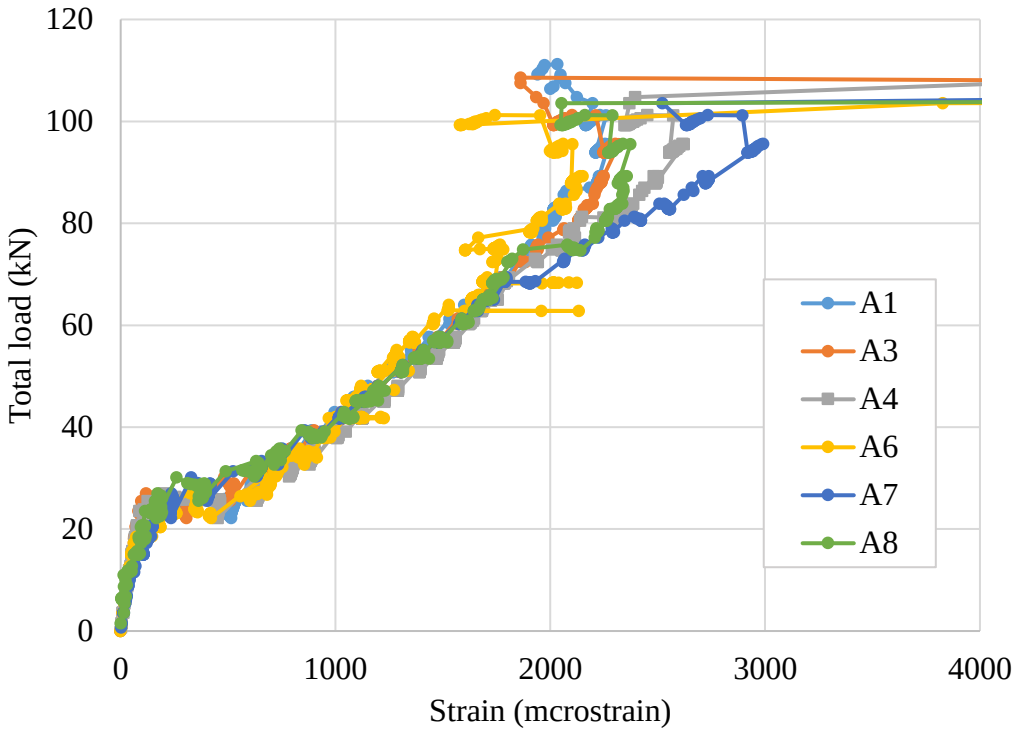

Figure 6.23: Experimental tensile strain values on steel bars for beam T-OS-S

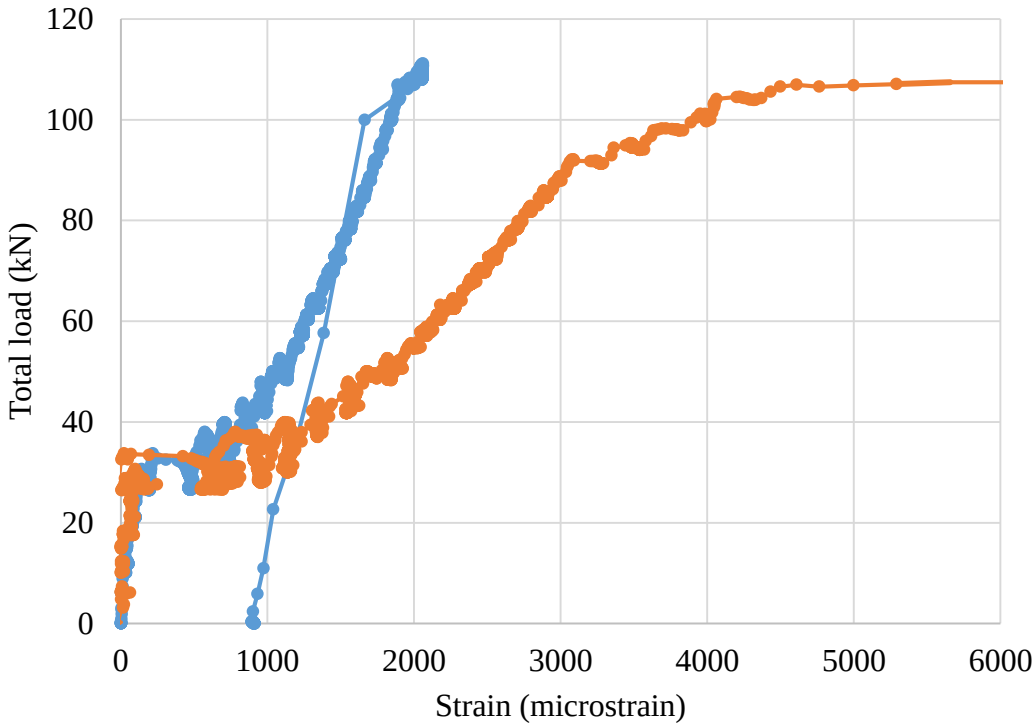

Figure 6.24: Experimental bar strain values of beam T-OSS-S at locations A2 and A3

Strain gauges at points A2 and A3 on beam T-OSS-S are located in different optimisation regions. In Figure 5.6 (§5.2.3), it can be seen that the middle portion of the beam is optimised for strength only and no material is added to this region for further serviceability optimisation. Point A3 is located inside this region and so the steel bars at this point are expected to yield at failure, which is in agreement with the test results (Figure 6.24). Point A2 on the other hand, is located in a region where extra material is added to the initially strength-optimised sections while optimising for serviceability. Therefore, the sectional moment capacity at this point has been increased to a value higher than the corresponding applied moment. The steel bars, hence, did not yield at the ultimate failure load of the beam, indicating a good agreement between the predictions and the experimental data.

The sectional analysis procedure used in this model, which was based on the full-interaction theory, showed a fairly good indication of cross-sectional moment capacity of the beams. The load-deflection responses in both beams (Figure 6.11 and Figure 6.12) and the load-strain relationships (Figure 6.14 through Figure 6.22) show the close agreement of the predicted and experimental failure loads despite some slight overestimation in some cases.

6.2.3.2 Optimisation for serviceability

6.2.3.2.1 Deflections

In order to gauge how the serviceability optimisation model performed, two aspects of the calculated and test data can be considered. First, since the CI method which was used to predict the performance of the beams as part as the whole optimisation procedure showed reasonably good predictions, the designated performance and optimisation targets can be considered to have been closely met.

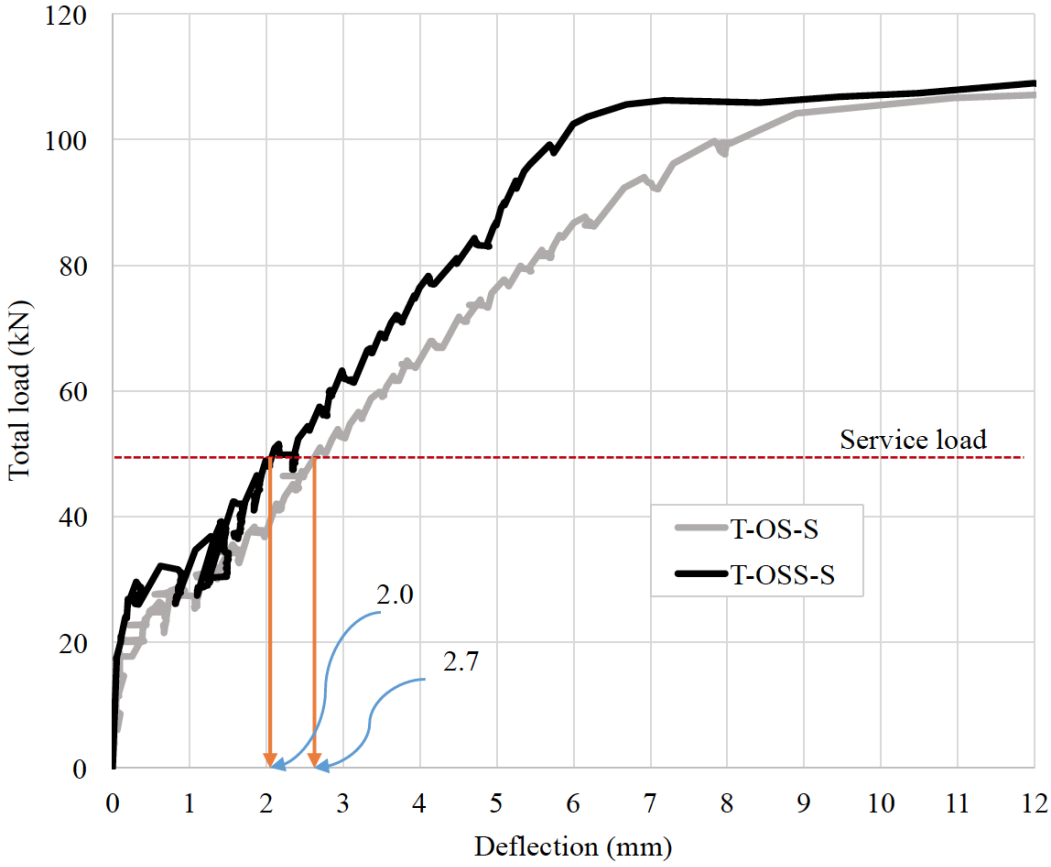

Figure 6.25: Experimental load-deflection relationships for beams T-OS-S and T-OSS-S

Second, the load-deflection relationships of beam T-OS-S was compared with that of beam T-OSS-S, shown in Figure 6.25. It can be seen that an increased flexural stiffness has been attained, especially at higher loading. The design deflection values for beams T-OS-S and T-OSS-S at serviceability (see Table 5-1, §5.2.3) are 2.1mm and 2.6mm respectively and are in a good agreement with the corresponding experimental deflection values of 2.0 mm and 2.7mm as indicated on Figure 6.25.

The response of beam T-OS-S at later stages of loading experiences higher softening rate than that of beam T-OSS-S due to the occurrence of a higher number of cracks over larger cracking intervals. Such an improvement in the behaviour of beam T-OSS-S after optimising for serviceability over

beam T-OS-S, which was optimised for strength only, importantly indicates how the optimisation model performed in limiting cracking (as explained below) and reducing deflections.

6.2.3.2.2 Cracking

The topology optimisation procedure used in this thesis to optimise the beams for cracking works on reducing the crack width values by changing the cracking pattern and the rate at which cracks occur. As explained in §4.6.2.2, the cracks in a simply supported beam optimised for strength only (beam T-OS-S in this case) are expected to scatter over a wide region at serviceability loading, thus allowing crack spacing to be relatively wide and so crack widths to be wide too. The topology optimisation procedure is aimed at limiting the crack interval and thus reducing crack spacing and crack width values at service load levels. The average and maximum crack width values and the number of cracks presented in Table 6-1 and Table 6-2 clearly indicate significant improvement in the cracking behaviour of beam T-OSS-S compared to beam T-OS-S. In order to show the extent of reduction in the crack width values achieved by the optimisation procedure, the experimental cracking data of both beams are tabulated at two load levels, 36 kN and 51 kN (Table 6-3). Since the topology optimisation procedure attempts to minimise crack widths by changing the cracking pattern at early stages of cracking, the experimental and predicted cracking behaviour at 36kN is also considered along with that at the service load level of 51kN.

Figure 6.26 illustrates the observed crack patterns of both beams at a load of 36kN. The number on each crack indicates the order of formation of the crack. As predicted, beam T-OS-S cracked over a large region with relatively widely spaced cracks, whilst beam T-OSS-S exhibited a smaller number of more closely spaced cracks which are distributed over a smaller cracking interval.

Table 6-3: Experimental cracking data for the simply supported beams

Beam	Crack width and cracks number values					
	At 36kN			At 51kN		
	Av.	Max.	No.	Av.	Max.	No.
T-OS-S	0.09	0.14	11	0.12	0.18	16
T-OSS-S	0.07	0.11	9	0.09	0.16	13

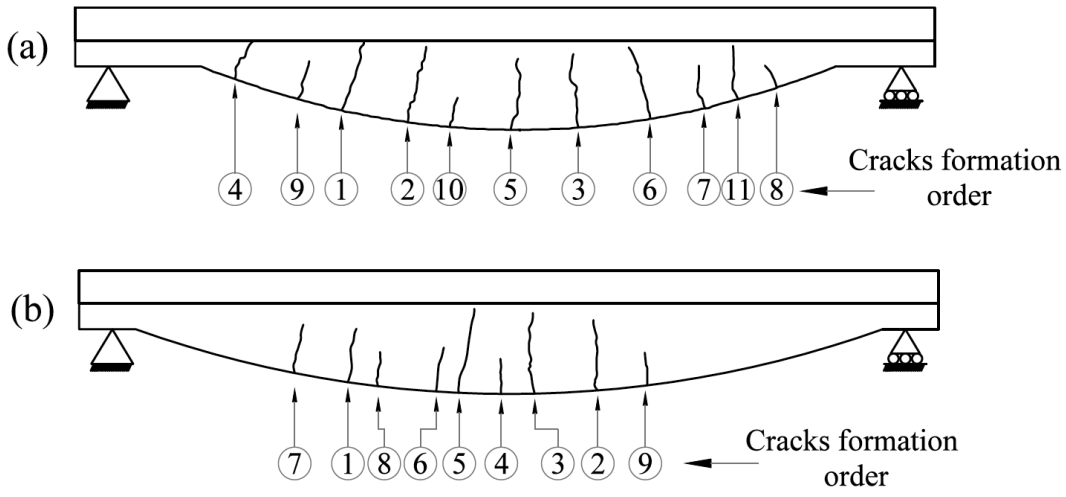

Figure 6.26: Cracking pattern at 36 kN for (a) beam T-OS-S, (b) beam T-OSS-S

6.3 Continuous beams

6.3.1 Over view of the test

As described in §5.2.4.4, the continuous beams were tested under eleven-point loading system. Upon gradual increase of loads, the data from the deflection transducers on both sides of the beam showed close agreement at the elastic stage, confirming correct setup of the beam. In Beam T-N-C, the first cracks start to appear at a load level of about 88 kN in 96 kN in the hogging and sagging regions respectively. Beams T-OSS-C and FF-OSS-C, which where both optimised for strength and serviceability, had approximately the same cracking capacity in hogging and sagging regions. The first crack appeared in beam T-OSS-C in the hogging region at load 60 kN, however, beam FF-OSS-C cracked in the sagging region first at load 80 kN.

6.3.1.1 Failure modes

Gradual loading at 4 kN load increments were continuous until the specimen was unable to carry any increase of loads. All beams failed in flexure as the failure pattern and readings from the strain gauges suggested. Beam T-N-C failed at a total load level of about 318 kN by yield of the tensile steel bars in the sagging region. This led to wide local cracks in this region as shown in Figure 6.27. At earlier stages of loading, the tensile bars in the hogging region yielded and moment redistribution occurred from hogging to sagging region, as explained later in §6.3.2.3. At failure, slight crushing in the compression side in the concrete was noticed which may indicate that, the tensile bars in the sagging region and the compressive concrete in the hogging region reached their ultimate capacity at nearly the same load level.

Figure 6.27: Beam T-N-C after failure

Figure 6.28: Cracks in the hogging region of beam T-N-C after failure

The cracking patterns of beams T-OSS-C and FF-OSS-C were different from that of the prismatic beam at failure. For the optimised beams, a high number of evenly distributed cracks scattered over the sagging regions. However, only a few wide local cracks formed over the middle support (hogging region) in all beams as shown in Figures 6.28, 6.30 and 6.31. Beam T-OSS-C failed prematurely at the total load of about 275 kN due to spalling of the concrete cover and possibly buckling of the compression steel bars as shown in Figure 6.29 (explained later in §6.3.3). The total applied load at which beam FF-OSS-C failed was about 300 kN when the tensile bars in the sagging region reached yield. The strain gauge readings indicate a short loading period over which moment redistribution from the hogging to the sagging region occurred. This further explained in §6.3.2.3.

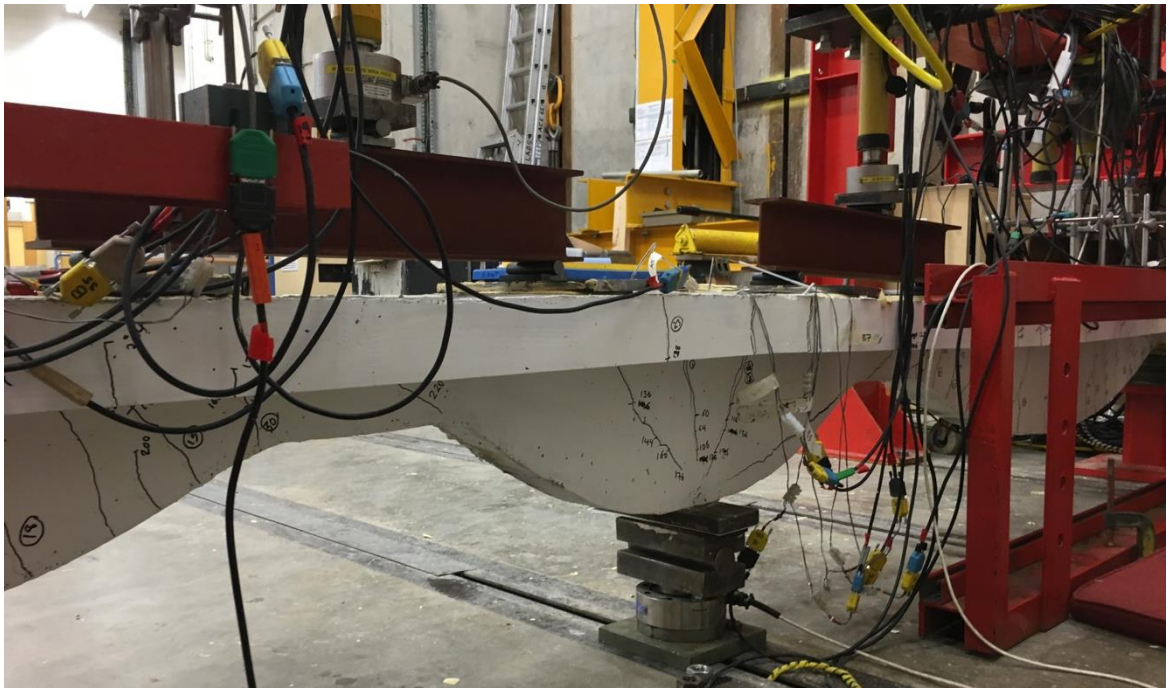

Figure 6.29: Beam T-OSS-C at failure

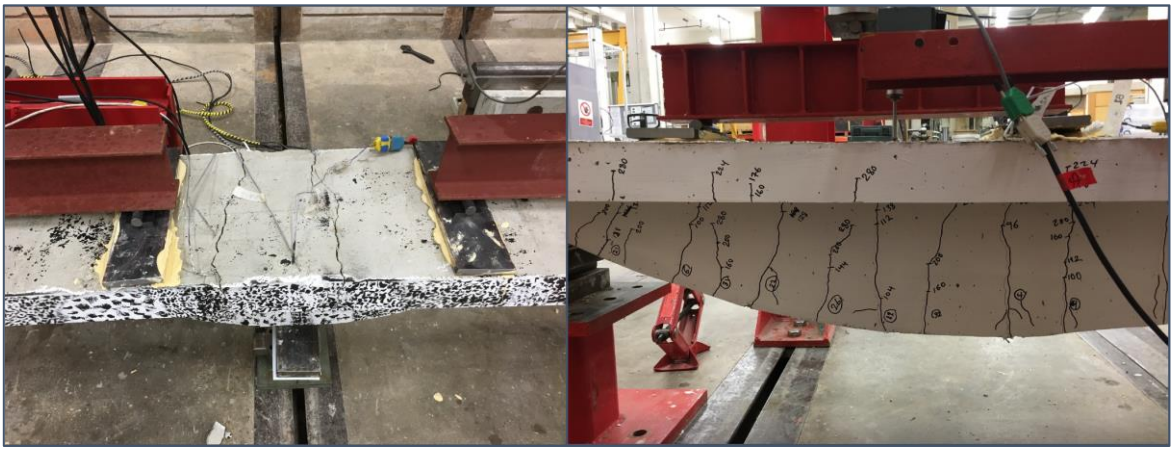

Figure 6.30: Cracking in the hogging and sagging regions of beam T-OSS-C at failure

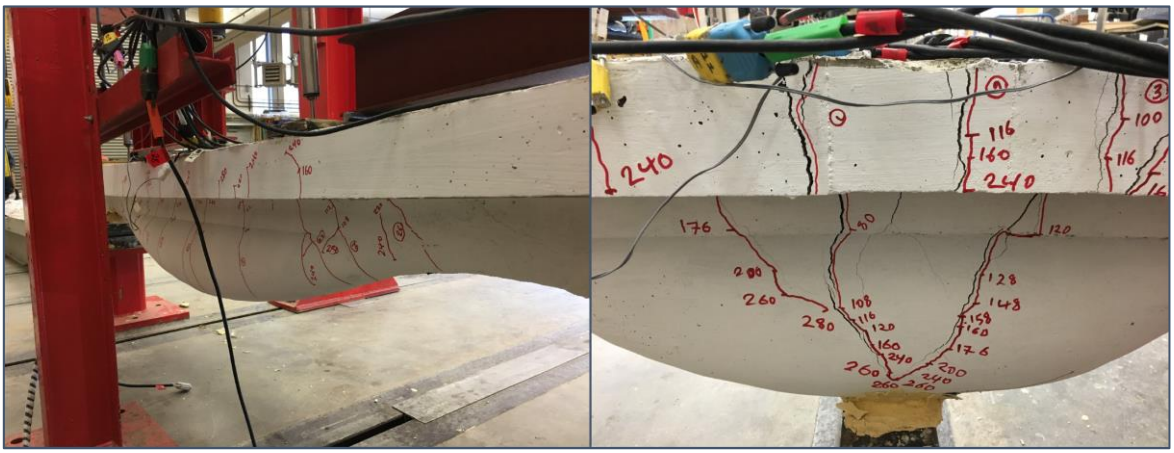

Figure 6.31: Beam FF-OSS-C at failure

6.3.2 Prediction of behaviour

6.3.2.1 Cracking behaviour

The crack width values and crack locations are recorded for the continuous beams at serviceability. The cracking data predicted by the CI method is compared to the experimental data at three stages of loading, 104 kN, 136 kN and 160 kN in Table 6-4 and Figure 6.32 through Figure 6.38. These load levels are chosen to consider the cracking behaviour of the beam at equal load intervals from the initiation of cracking to the service load level (which was taken as 160 kN). Starting from beam T-N-C, which was a prismatic continuous beam, the prediction of the cracking pattern by the CI method is good generally. At the load level of 104 kN, when the initial cracking stage occurred, crack width values were underestimated. However, a closer agreement between the experimental and predicted crack width values (average and maximum crack widths) can be seen at later stages of loading.

The number of predicted cracks at all stages of loading showed a close match with the experimental results. If hogging and sagging regions are considered separately, a balance between the crack widths and cracks number can be seen for both experimental and predicted cracks. For instance, in the hogging and sagging regions shown in Figure 6.33 and 6.34, there are fewer experimental cracks than predicted, but experimental crack widths are larger than the predicted ones on average. This is satisfactory as a good prediction of overall behaviour is the main purpose behind this work.

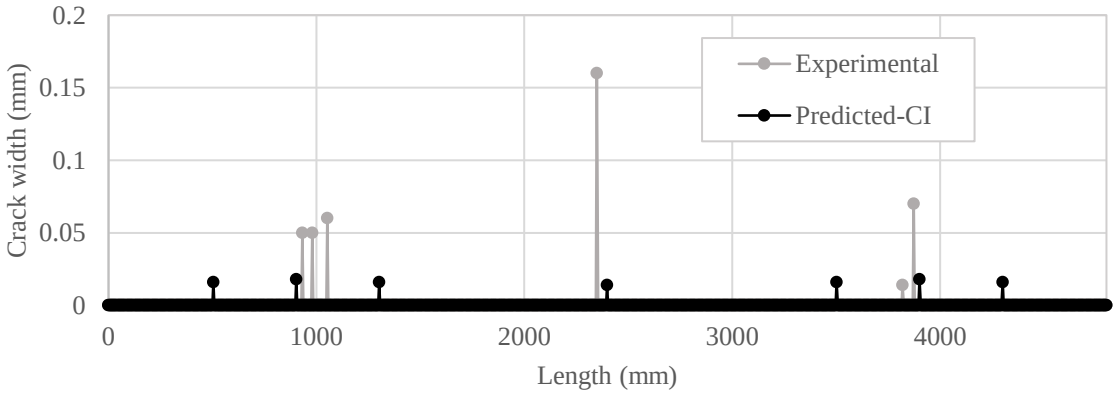

Figure 6.32: Experimental and predicted crack width and crack locations for beam T-N-C at 104 kN

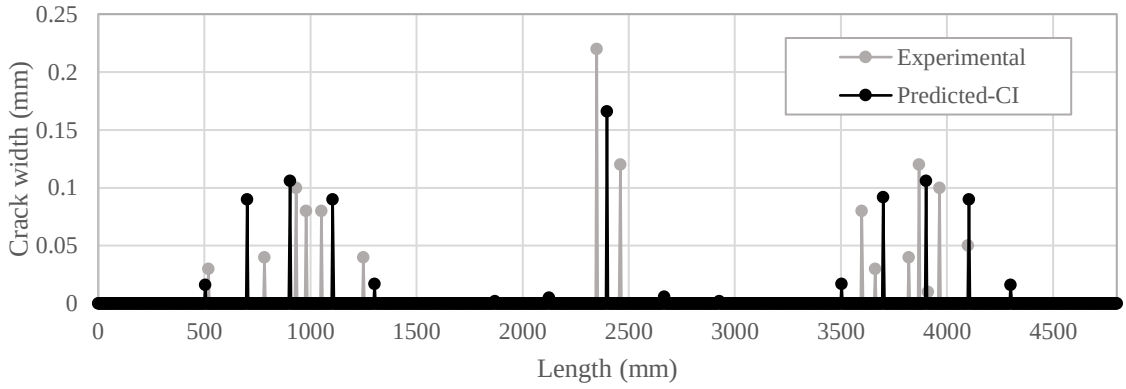

Figure 6.33: Experimental and predicted crack width and crack locations for beam T-N-C at 136 kN

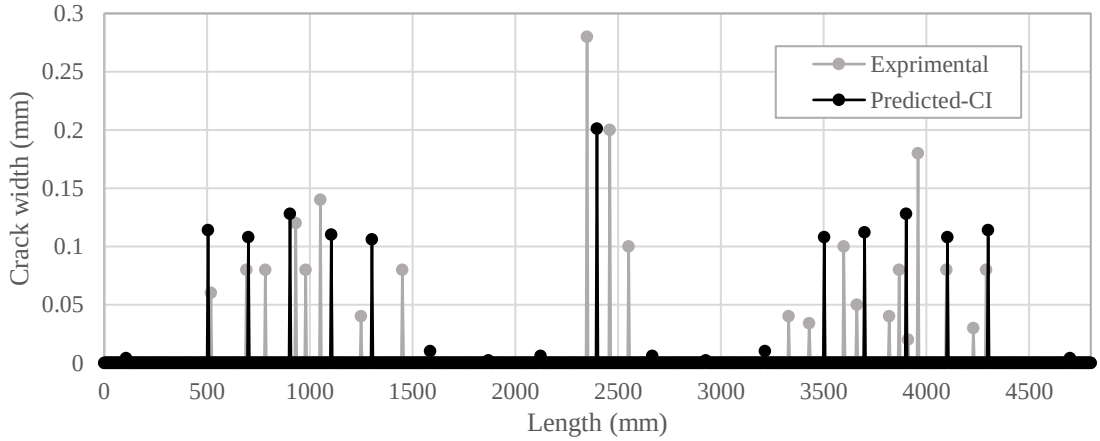

Figure 6.34: Experimental and predicted (CI) crack width and crack locations for beam T-N-C at 160 kN

Table 6-4: Experimental and predicted crack widths and cracks number of beam T-N-C

Load (kN)	*Average crack width (mm)*		*Maximum crack width (mm)*		*Number of cracks*	
	Exp.	Pred.	Exp.	Pred.	Exp.	Pred.
104	0.07	0.02	0.16	0.02	6	7
136	0.08	0.05	0.22	0.17	15	15
160	0.08	0.07	0.28	0.20	21	19

Considering beam T-OSS-C, Figures 6.35, 6.36 and 6.37 show experimental crack widths and crack locations versus the corresponding predicted values at the total load levels 104 kN, 136 kN and 160 kN respectively. Overall, the cracking pattern, the variation in crack width values, and the way cracks are scattered over different regions are predicted reasonably well, especially at later stages of loading. A higher number of cracks in the hogging region was predicted compared to the test results but maximum crack width value was underestimated 104 kN. Over a specific cracking region, a higher number of closer spaced cracks leads to a shorter bond-stress transfer length and therefore closer crack widths (see §3.3.3).

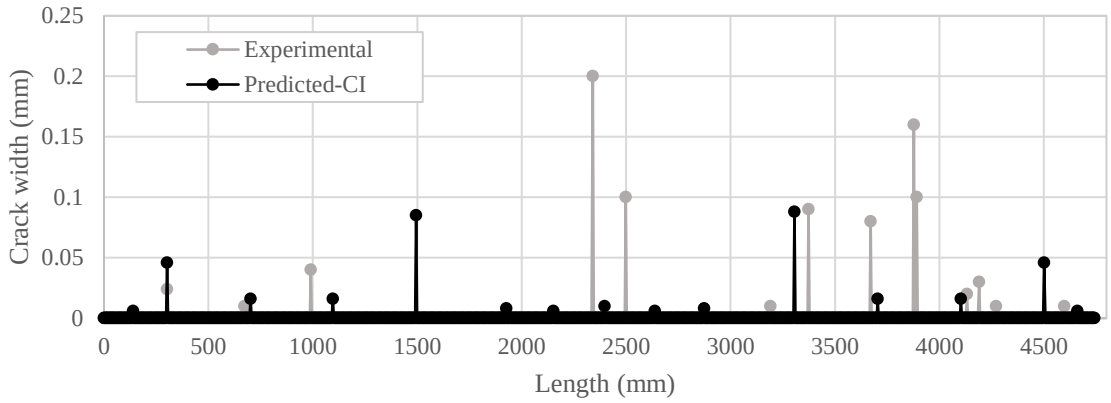

Figure 6.35: Experimental and predicted (CI) crack width and crack locations for beam T-OSS-C at 104 kN

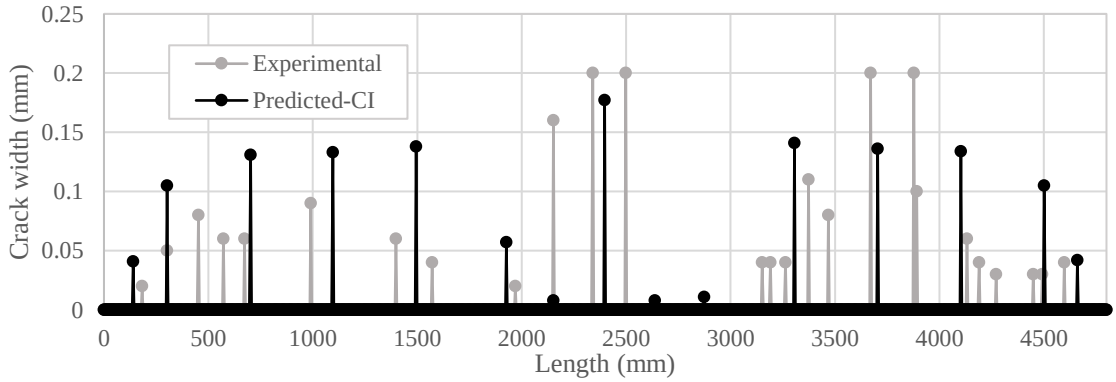

Figure 6.36: Experimental and predicted (CI) crack width and crack locations for beam T-OSS-C at 136 kN

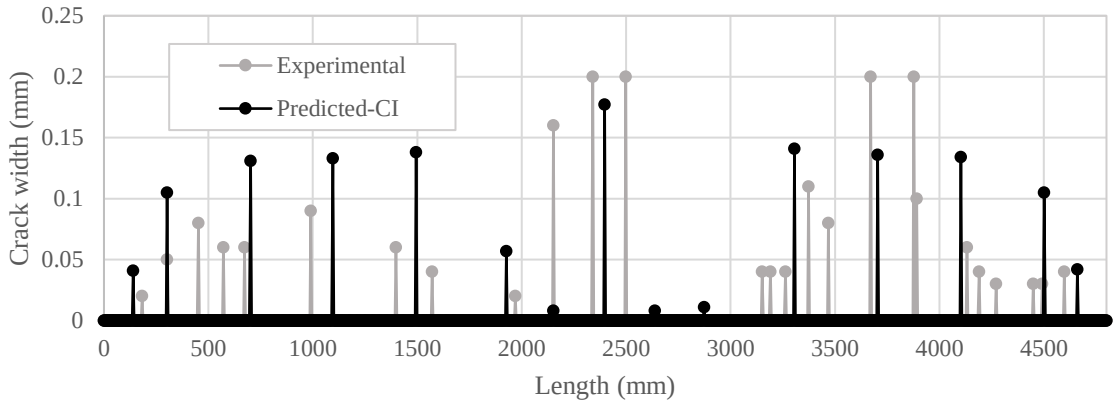

Figure 6.37: Experimental and predicted (CI) crack width and crack locations for beam T-OSS-C at 160 kN

In Table 6-5, which shows predicted cracking data versus the experimental values, average crack width values are shown to be estimated at all load levels fairly accurately. However, the maximum crack width values were underestimated, possibly because experimental cracks than the predicted cracks in the hogging region has led to higher bond-stress transfer and wider cracks for the same reason as mentioned previously.

Figure 6.38 through Figure 6.40 present cracking patterns of the fabric-formed beam, beam FF-OSS-C, at all formerly indicated load levels. For the load levels of 104kN and 136kN, tested and predicted cracking patterns and crack width variation were in a moderately close agreement despite some underestimation of crack widths in the hogging regions. This underestimation becomes more obvious at the total load value of 160 kN as shown in Figure 6.40. The assumed of tension prism area A_c (see §3.3.2) in deriving the partial-interaction crack-widening rules for a fabric-formed beam may be the reason behind such underprediction of crack widths. As demonstrated in §5.2.2, the effective tension area considered here is based on the value defined for prismatic concrete beams by CEB-FIP (2010) which might not be valid for fabric-formed beams.

Table 6-5: Experimental and predicted (CI) crack width and cracks number values for beam T-OSS-C

Load (kN)	*Average crack width (mm)*		*Maximum crack width (mm)*		*Number of cracks*	
	Exp.	Pred.	Exp.	Pred.	Exp.	Pred.
104	0.06	0.06	0.2	0.14	14	19
136	0.08	0.08	0.2	0.18	27	23
160	0.08	0.1	0.28	0.21	32	23

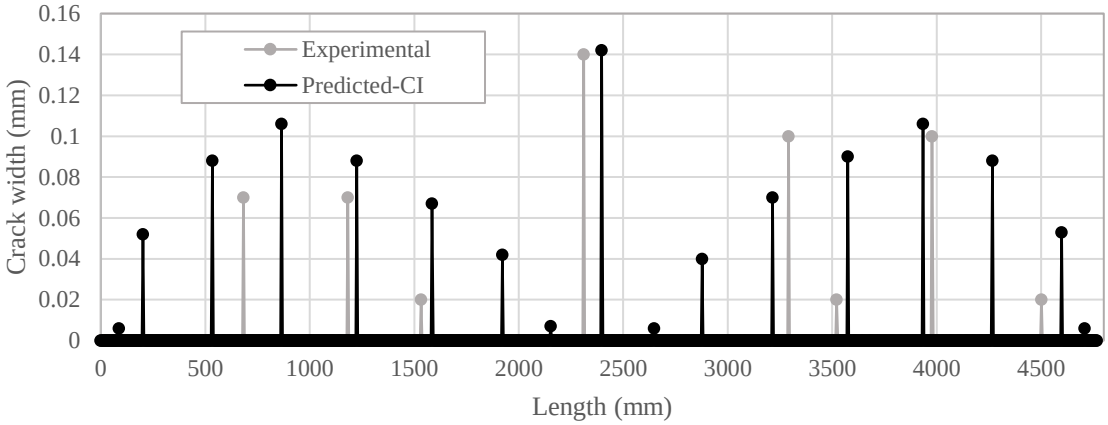

Figure 6.38: Experimental and predicted cracking pattern at load level 104kN for beam FF-OSS-C

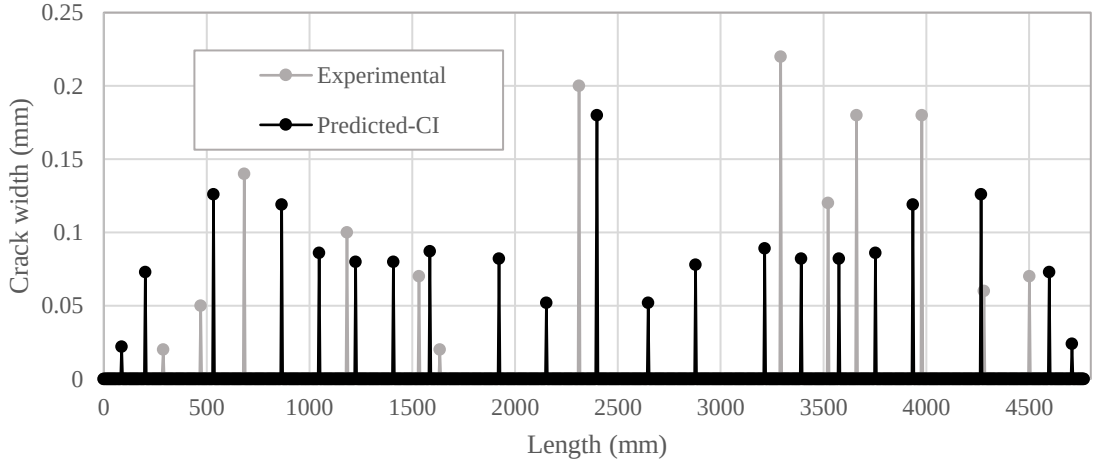

Figure 6.39: Experimental and predicted cracking pattern for beam FF-OSS-C at load level 136kN

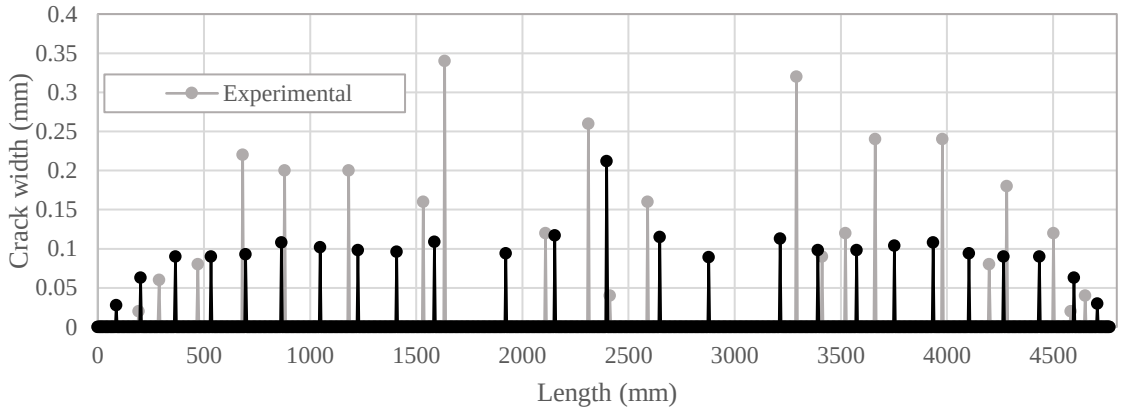

Figure 6.40: Experimental and predicted cracking pattern at load level 160kN for beam FF-OSS-C

Table 6-6 shows that, the proposed CI method produced fairly good predictions for the average and maximum crack width values at load levels 104kN and 136kN. However, the number of cracks was overestimated by the model. In contrast, the crack width predictions diverge from the experimental data at the load level 160kN but a close match of the number of cracks can be seen.

Table 6-6: Experimental and predicted cracks data for beam FF-OSS-C

Load (kN)	*Average crack width (mm)*		*Maximum crack width (mm)*		*Number of cracks*	
	Exp.	Pred.	Exp.	Pred.	Exp.	Pred.
104	0.06	0.06	0.14	0.14	8	17
136	0.12	0.09	0.22	0.18	14	21
160	0.15	0.1	0.32	0.21	22	23

Overall, the proposed CI method showed moderate to good predictions of the cracking behaviour for the continuous concrete beams, given that accurate predictions may not be achievable as cracking in concrete is governed by a complicated mechanism and highly affected by the non-homogeneity of concrete (Neville, 1996).

6.3.2.2 Load-deflection behaviour

The experimental load-deflection responses for the continuous concrete beams are plotted against the predicted load-deflection relationships in Figures 6.41 to 6.42. Among the six deflection transducers placed on the beams (Figure 5.19 and Figure 5.20), the data from the middle transducer in each span only is presented because some of the other transducers did not successfully record data. The middle deflection transducers were close to the point of maximum deflection. The prediction models used are the FI and the CI methods. At the pre-cracking stage, deflection values are calculated based on the FI method only in both cases. However, at the post-cracking stage, the CI method employs the FI method at certain regions along the beam only where slip is predicted to be zero. For all the specimens, deflection values were underestimated in the pre-cracking stage. The full-interaction model also overestimates stiffness in the post-cracking stage. Therefore, this model and the assumptions related to it such as the perfect bond between the reinforcement and the concrete may not be an accurate assumption for statically indeterminate concrete beams even in the elastic stage. The CI method on the other hand, resulted in a reasonably accurate prediction of load-deflection behaviour for all specimens.

At the final stages of loading the deflection values predicted by the CI model diverge from the experimental values due to prediction of a higher number of cracks. Crack propagation is affected by many factors. For instance, the cracks are assumed to develop perpendicular to the longitudinal axis of the beam but the actual cracks incline in areas near the supports at high loading levels. This misrepresentation of the cracking behaviour affects the prediction of moment redistribution and may cause even further inaccuracy in predicting cracking and deflection behaviour.

In Figure 6.41, lines A and B indicate the total load level at which the tensile steel bars in the hogging region are predicted to yield by the FI and CI models respectively. The reason for this difference is; there is a significant different between the moment distribution predicted by those models. This is explained further later in §6.3.1.3. It is now clear that the accuracy of any of the interaction models used in combination with the stiffness model to find deflections depends not only on how accurately the concrete-reinforcement bond interaction is simulated but also how precisely sectional stiffness values are determined (which affects the predicted moment distribution).

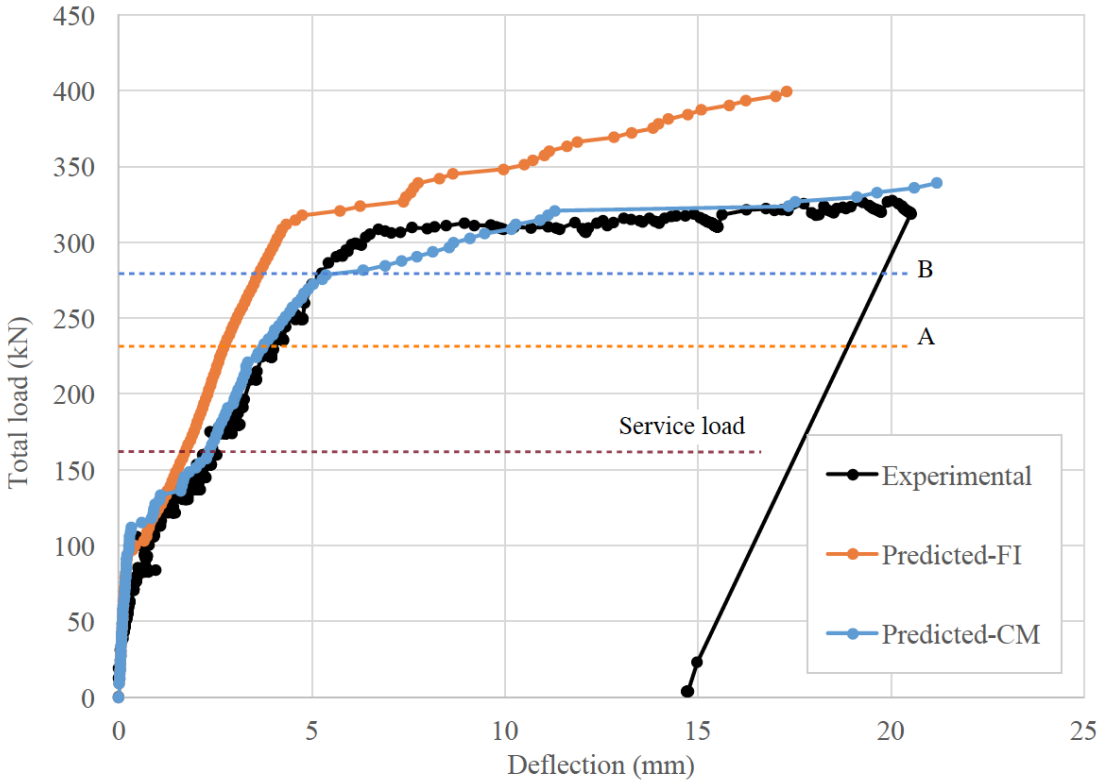

Figure 6.41: Predicted and experimental load-deflection relationships for beam T-N-C

For beam T-N-C, the initial cracking stage was predicted by the CI model to occur at a slightly higher load level compared to the experimental value and that predicted by the FI method. However, for beams T-OSS-C and FF-OSS-C, the initiation of cracking was predicted more precisely by the CI than the FI method. Despite the fact that the initial crack in both methods is predicted by the full-interaction model, a set of cracks following the initial crack occur in the sagging region of the optimised beams which are discovered through the partial-interaction mechanism. The moment distribution achieved from the FI method is characterized by lower applied moment values in the sagging regions than that obtained from the CI method. Therefore, cracks scatter over the hogging and sagging regions at the early stages of loading for beams T-OSS-C and FF-OSS-C according to the combined-model, in agreement in what is seen with the experiments (Figure 6.35 and Figure 6.37).

For the optimised beams, beams T-OSS-C and FF-OSS-C, accurate prediction of deflections by the CI model can be seen at serviceability. The FI method considerably overpredicts stiffness at all stages of loading.

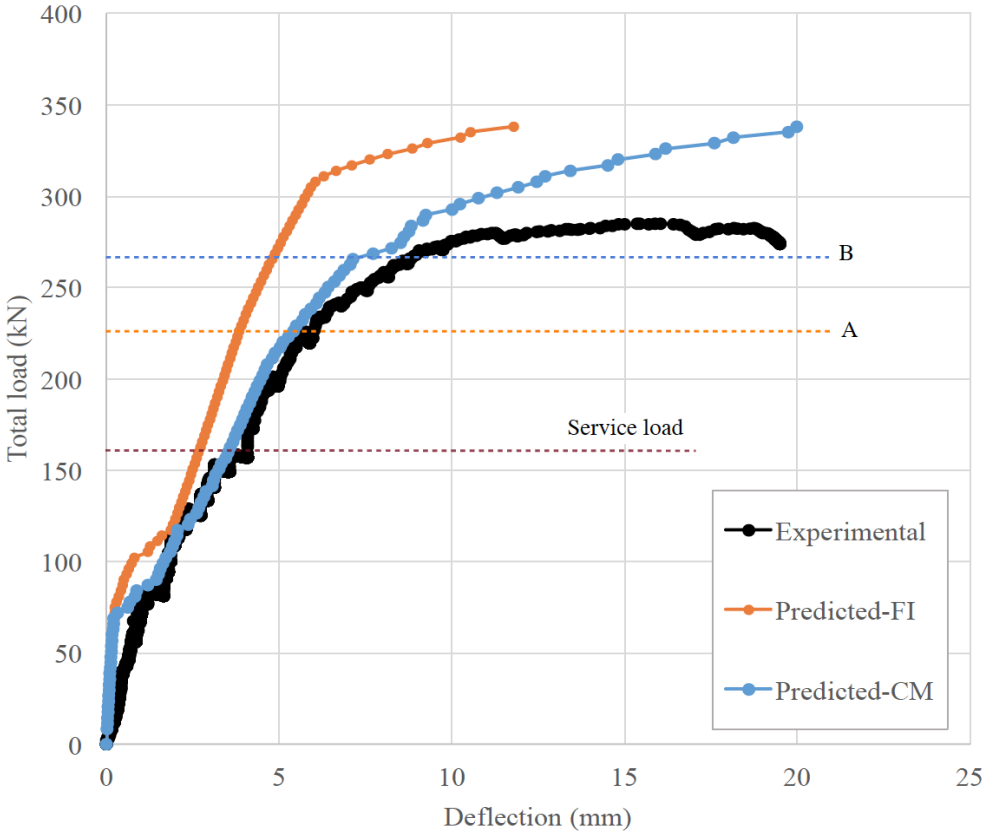

Figure 6.42: Predicted and experimental load-deflection relationships for beam T-OSS-C

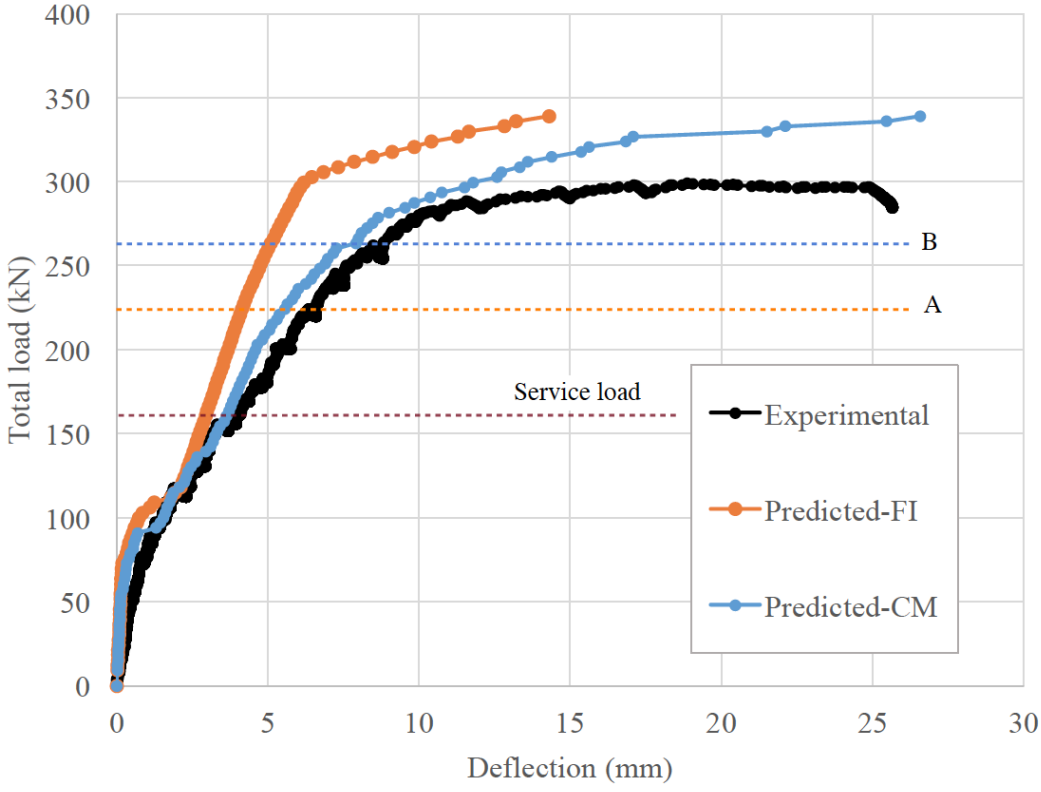

Figure 6.43: Predicted and experimental load-deflection relationships for beam FF-OSS-C

6.3.2.3 Cross-sectional behaviour

The cross-sectional behaviour of the continuous beams and the strain of the steel bars was monitored using strain gauges at different locations in both hogging and sagging regions. The names and positions of the strain gauges are shown in Figure 6.44.

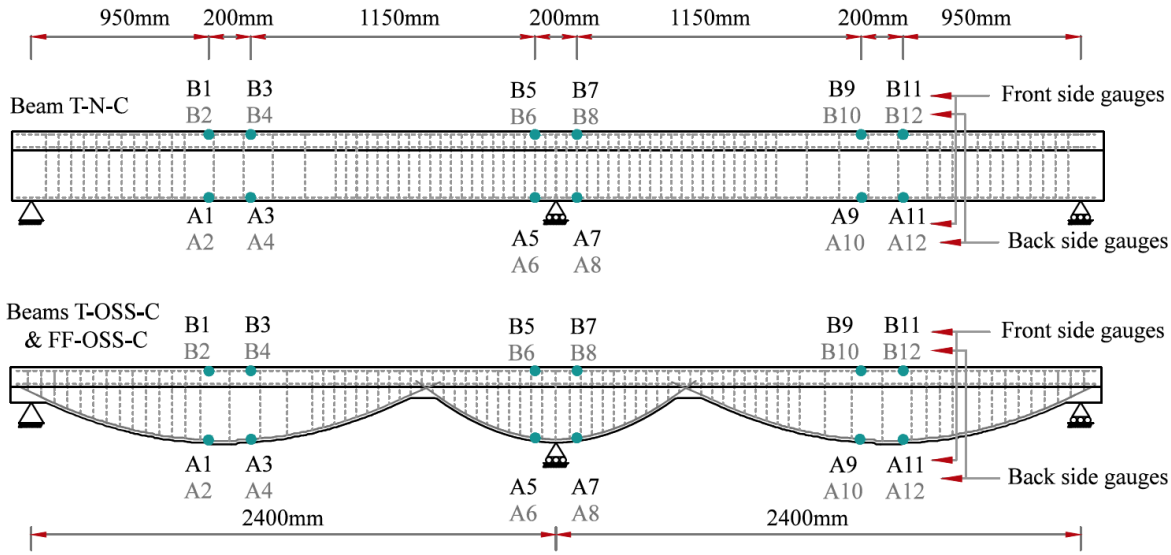

Figure 6.44: Strain gauge locations and names for the continuous beams specimens

The load-strain relationships of bars in beam T-N-C is shown in Figures 6.46 to 6.53 at locations A1, A4, A8, A11, B3, B4, B6 and B9 where the strain gauges successfully recorded data. In the hogging region slight underestimation of tensile strain can be seen in Figure 6.46 and Figure 6.47 and this overestimation becomes more apparent at location A11. The difference between the actual and predicted moment distribution might have caused this. Both FI and CI methods produced similar predictions in all strain gauge locations in the sagging regions prior to yield of the steel bars. At the initiation of cracking, the models predict a short fluctuation due to a minor moment redistribution effect caused by cracking. This is with a good agreement with the experimental load-strain pattern at locations A1, A8 and B6.

The prediction of the yield strain by the FI method varies from good predictions at locations A1 and A11 to a considerable overestimation at location A4. Again, failure of this model to accurately predict the moment distribution plays a key role in this. Despite some slight underestimations, the CI method results in a better estimation of the yield strain in the sagging regions.

In the hogging region, only two of the strain gauges worked, at locations A8 and B6. According to the FI method, the tensile bars in this region yield (indicated by line B in Figure 6.52) at a much lower load level than the failure load of the beam at which the steel bars at that location seem to have yielded (line A in Figure 6.52). This is because the applied moment value calculated by this

model at the hogging part of the beam is higher than the actual moment value (see Figure 6.45). The bars do not yield however, according to the CI method, at location B6.

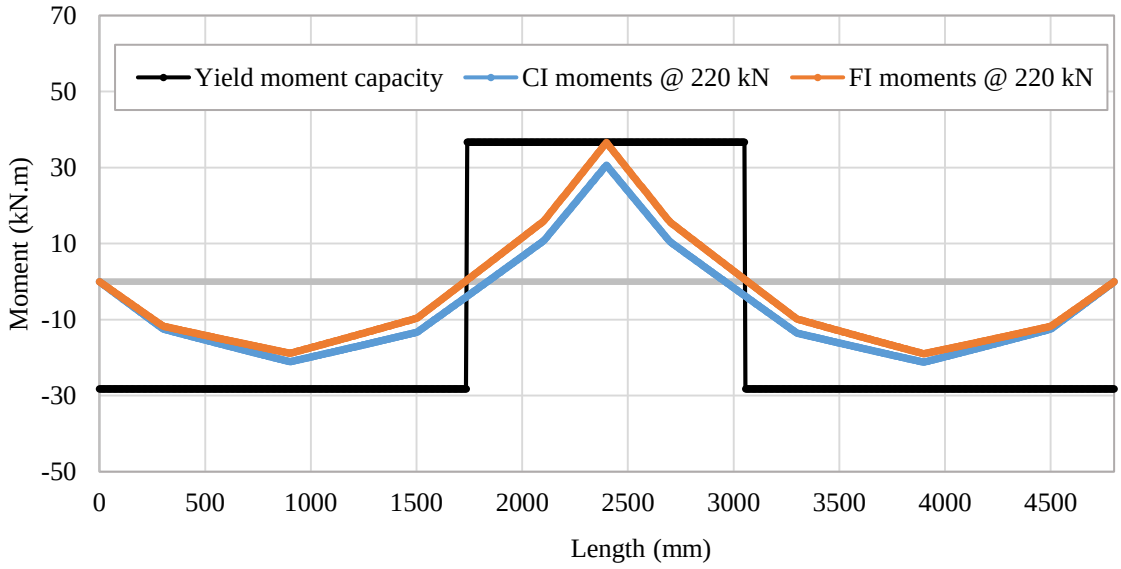

Figure 6.45: Applied moment values determined from the interaction models at 220 kN compared to the yield moment values

Additionally, the FI method predicts that the neutral axis lies above the compression bars at the total load of 207 kN and so the compressive strain changes to tensile strain as indicated by line B in Figure 6.48 (in contrast with the experimental data (line A) and what was predicted by the CI method (line C)).

The combined model overestimates the compressive strain values at A8 at load levels beyond serviceability. It should be noted that the sensitivity of the analysis is affected by the small values of compressive strains. Even a small misprediction of the behaviour may cause large deviation of the predictions from the experiments when considering compressive strains.

At locations B3, B4 and B9, the prediction of compressive strain values by the CI method were fairly accurate at all stages of loading. The load level at which the neutral axis moves up to above the compressive steel bars (indicated by line A in Figure 6.50, Figure 6.51 and Figure 6.53) were accurately predicted by this model whilst the FI method significantly overestimates it (line B).

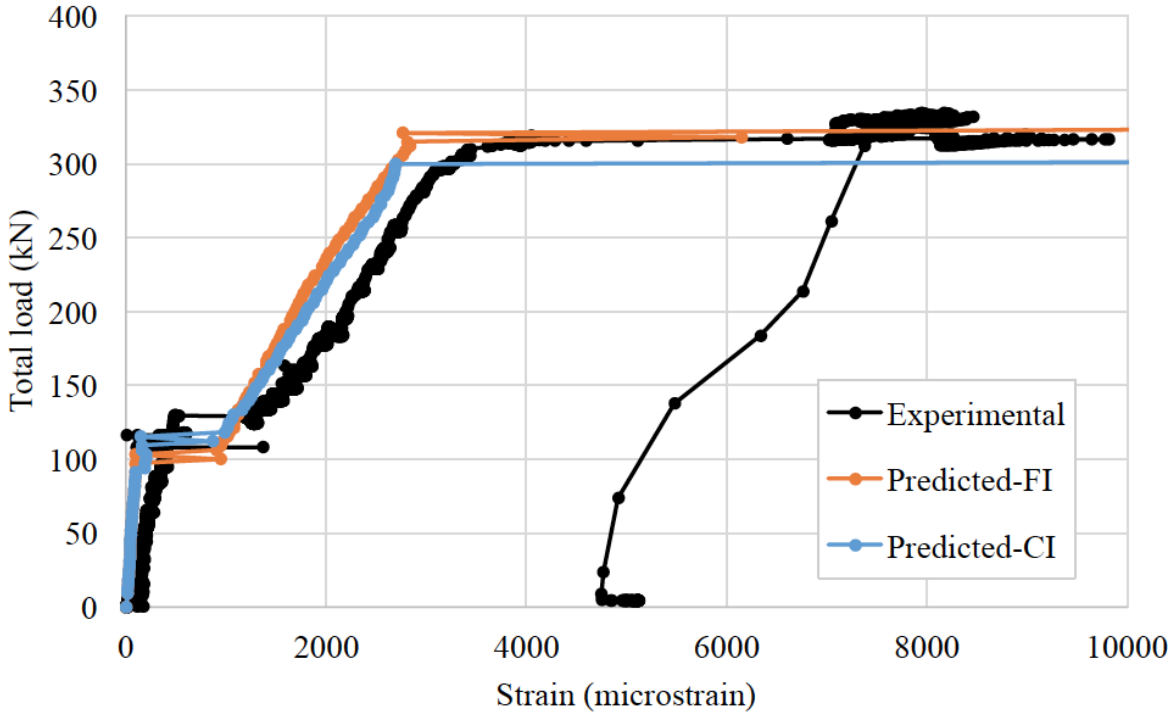

Figure 6.46: Load-strain relationship of the tensile bars in beam T-N-C at location (A1)

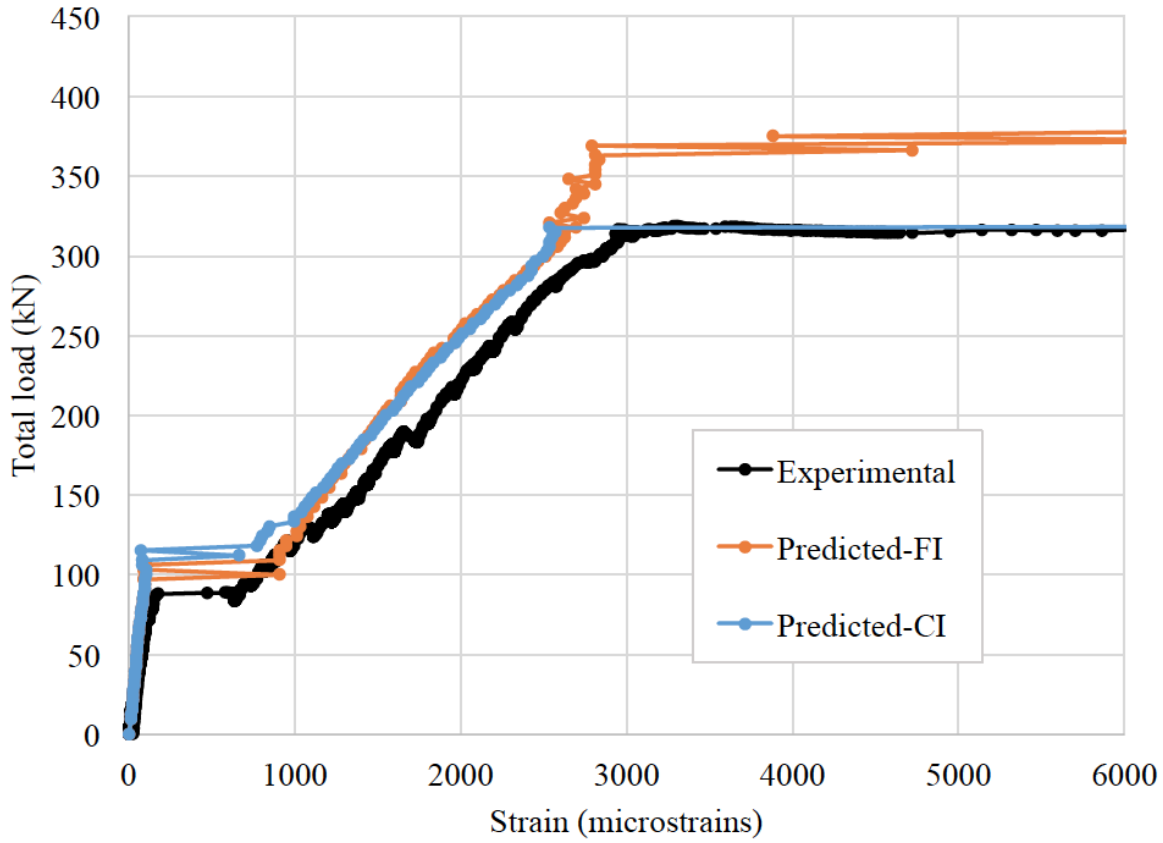

Figure 6.47: Load-strain relationship of the tensile bars in beam T-N-C at location (A4)

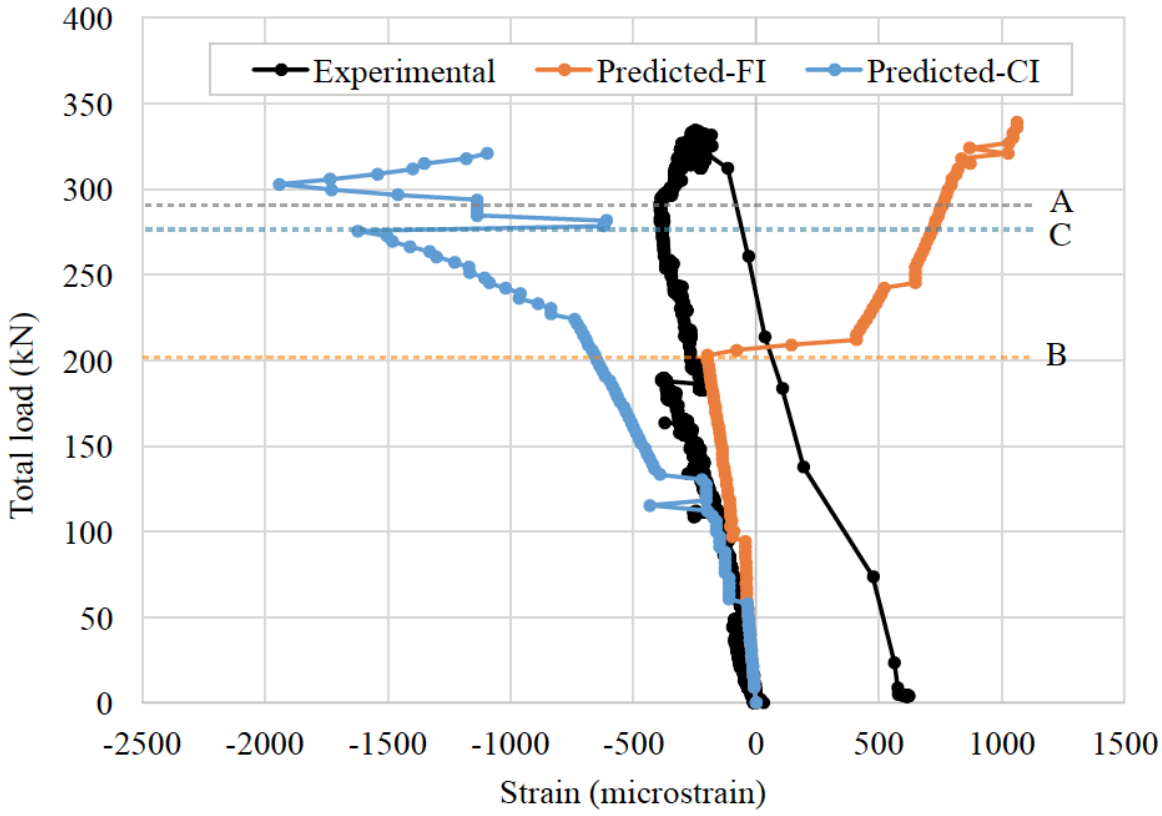

Figure 6.48: Load-strain relationship of the compressive bars in beam T-N-C at location (A8)

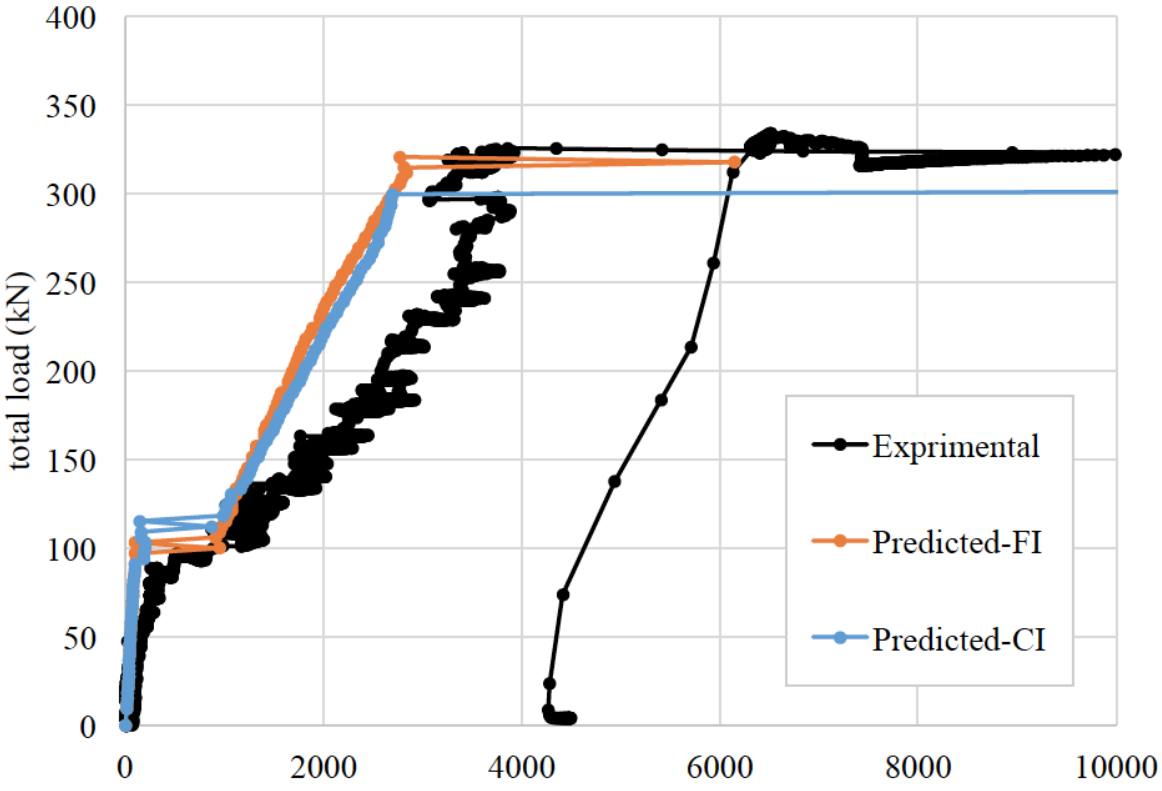

Figure 6.49: Load-strain relationship of the tensile bars in beam T-N-C at location (A11)

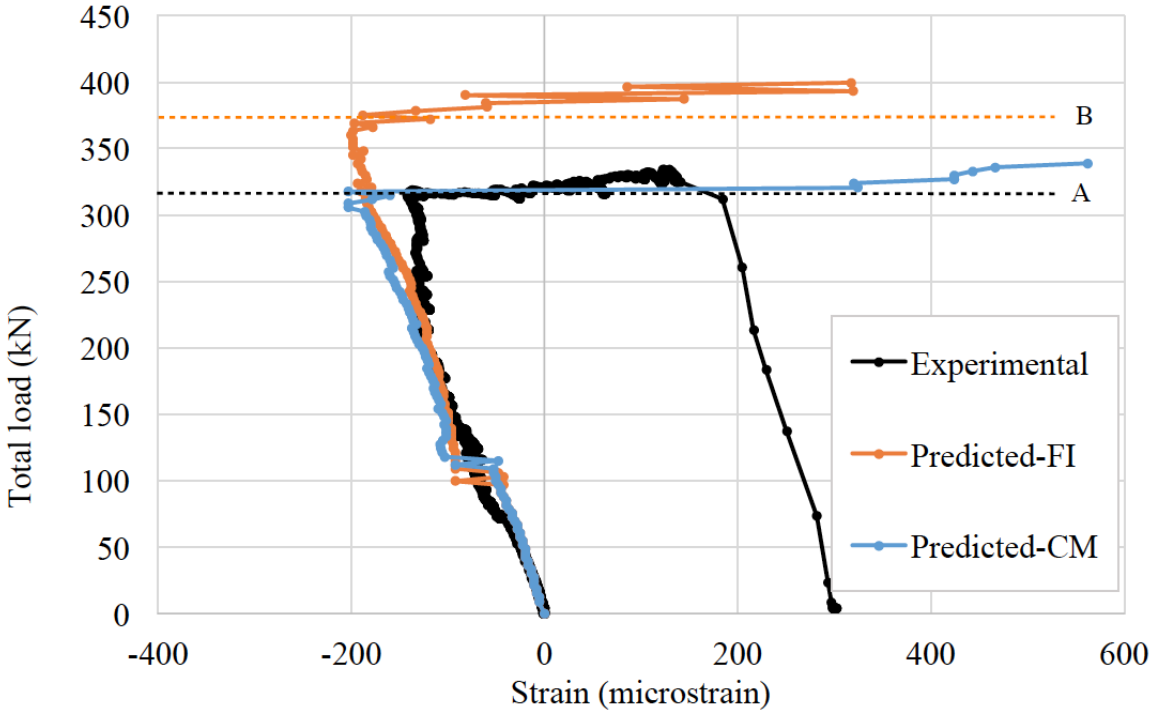

Figure 6.50: Load-strain relationship of the compressive bars in beam T-N-C at location (B3)

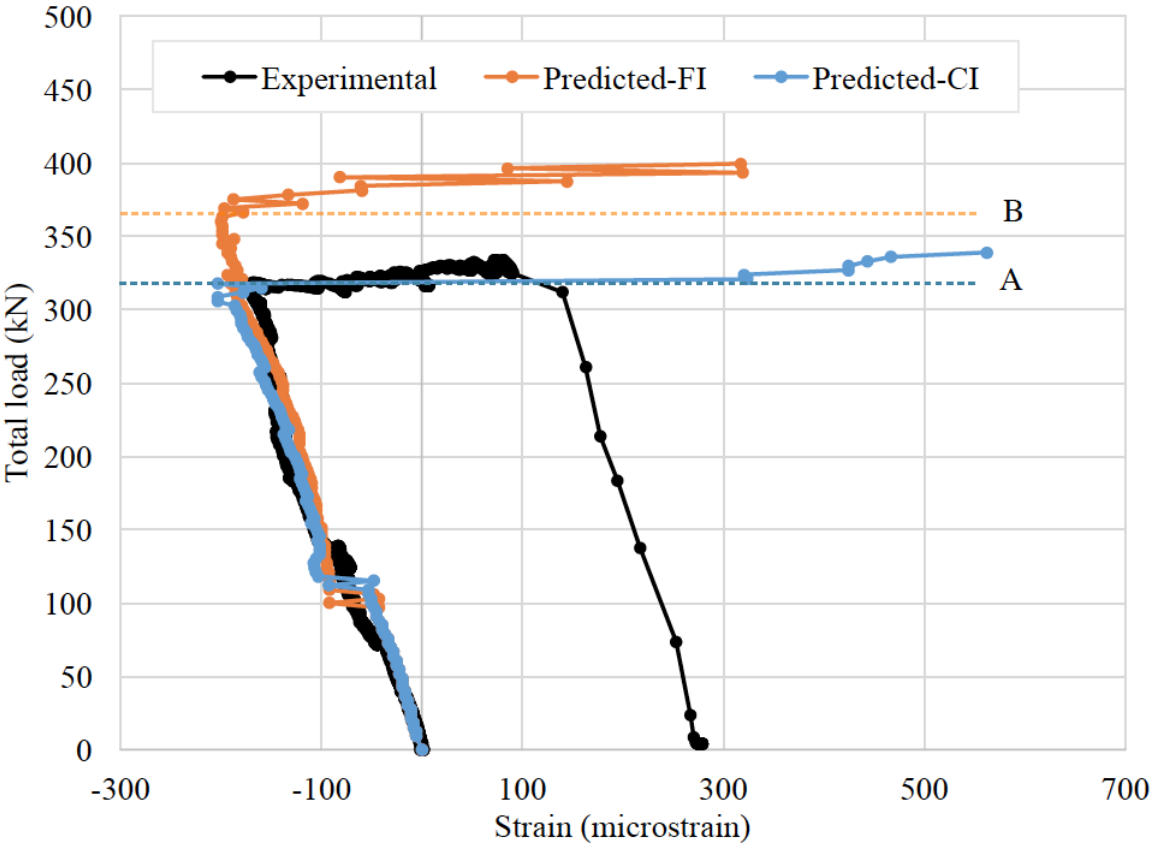

Figure 6.51: Load-strain relationship of the compressive bars in beam T-N-C at location (B4)

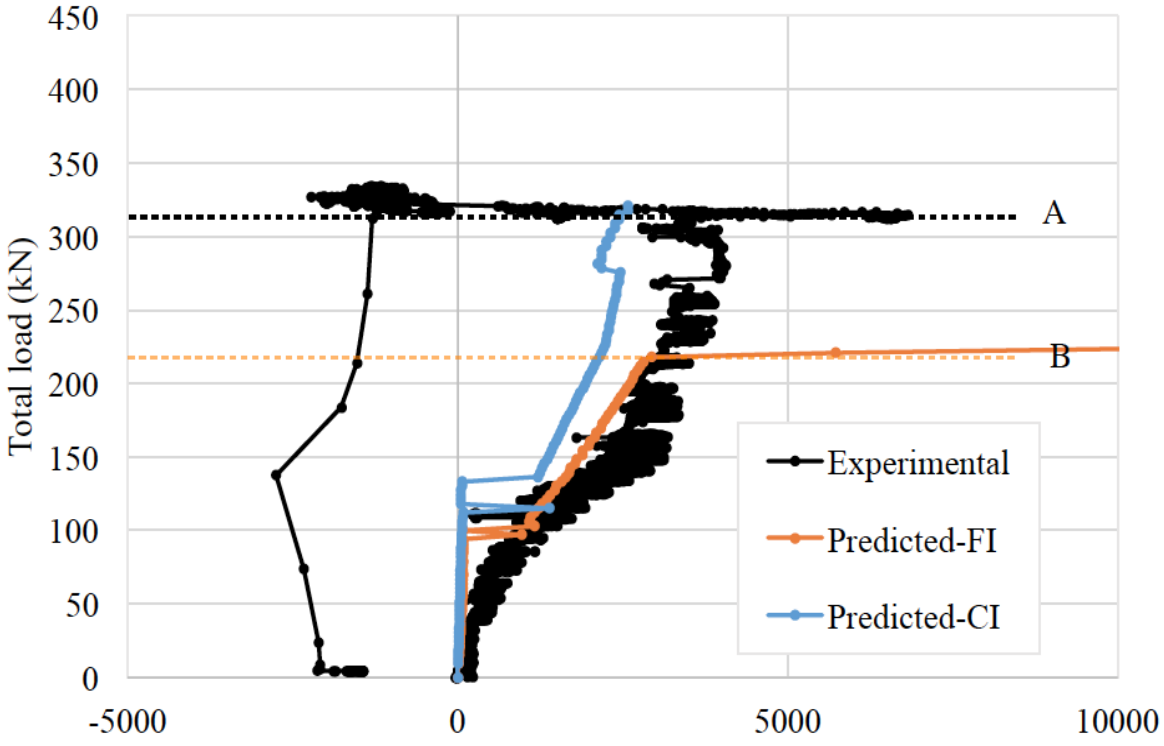

Figure 6.52: Load-strain relationship of the compressive bars in beam T-N-C at location (B6)

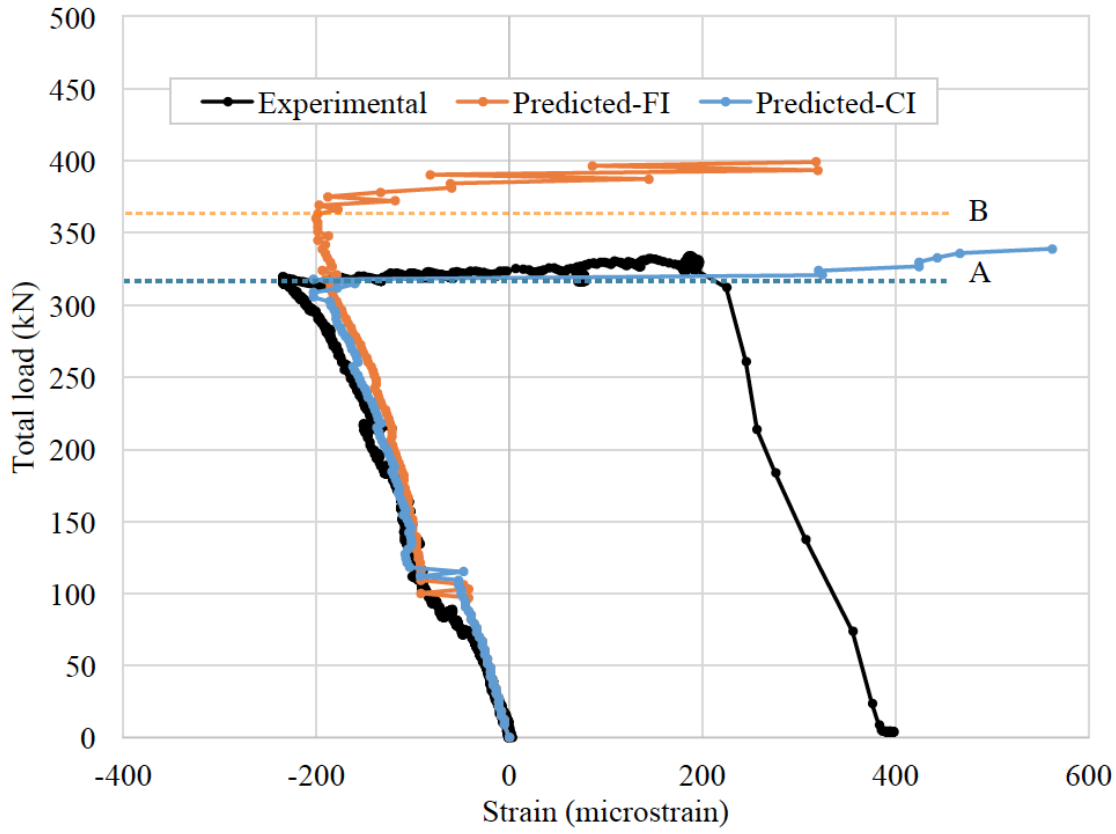

Figure 6.53: Load-strain relationship of the compressive bars in beam T-N-C at location (B9)

Generally, the CI method shows a closer agreement between the experimental and predicted load-strain relationships indicating that this model is successful in simulating the concrete-reinforcement bond interaction behaviour and ultimately the performance of the beams at the cross-section level for prismatic continuous beams (beam T-N-C).

For beam T-OSS-C, unfortunately only two of the strain gauges worked at locations B1 and B6. The compressive strains in the sagging region at point B1 (Figure 6.54) was underestimated by both models although accurate prediction was achieved in the elastic range. The total load at which the compressive strain changes to tensile strain (line A) when the neutral axis rises above the bar was accurately determined by the CI method (line C) but overestimated by the FI method (line B).

At point B6, where the tensile strain in the hogging region is recorded, the FI method underpredicts the yield strain owing mainly to differences between the actual and calculated moment distributions. In Figure 6.56, the applied moment values calculated from the FI and CI methods are shown at load levels of 205kN and 275kN at which the tensile steel bars yield according to both models respectively.

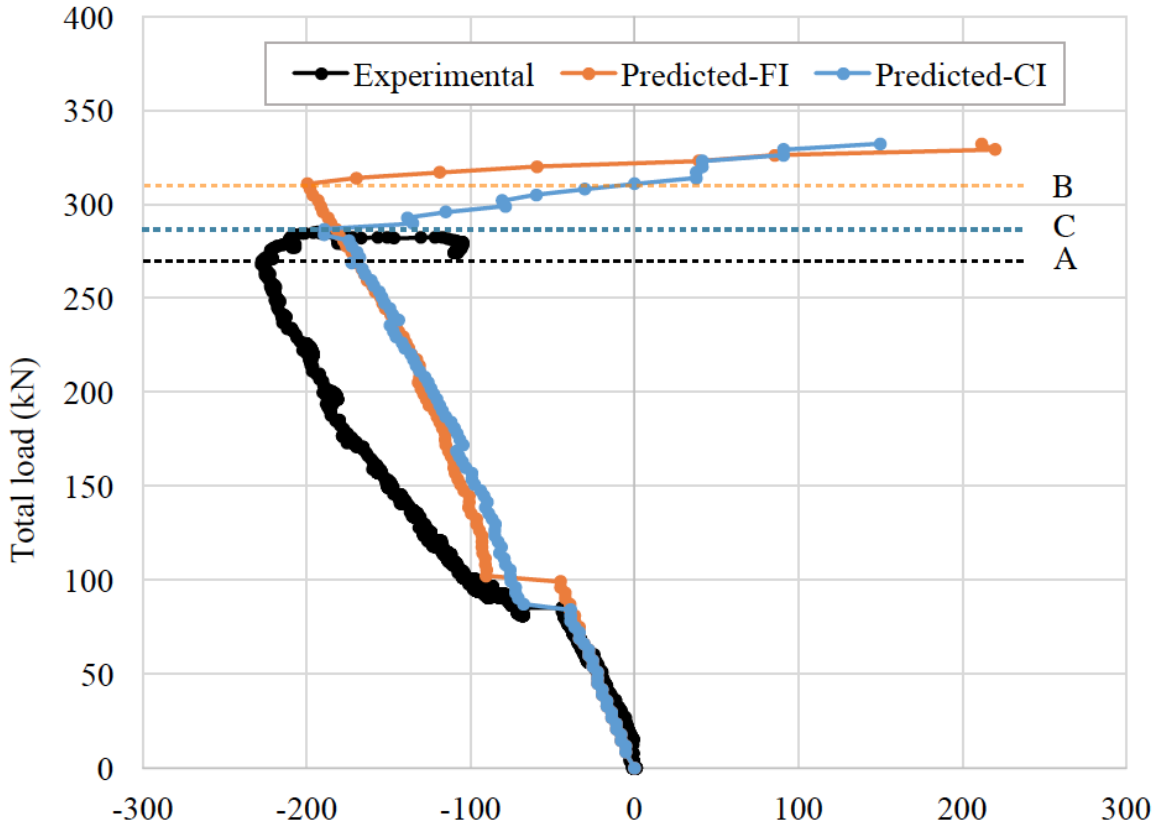

Figure 6.54: Experimental and predicted load-strain values of steel bars in beam T-OSS-C at location B1

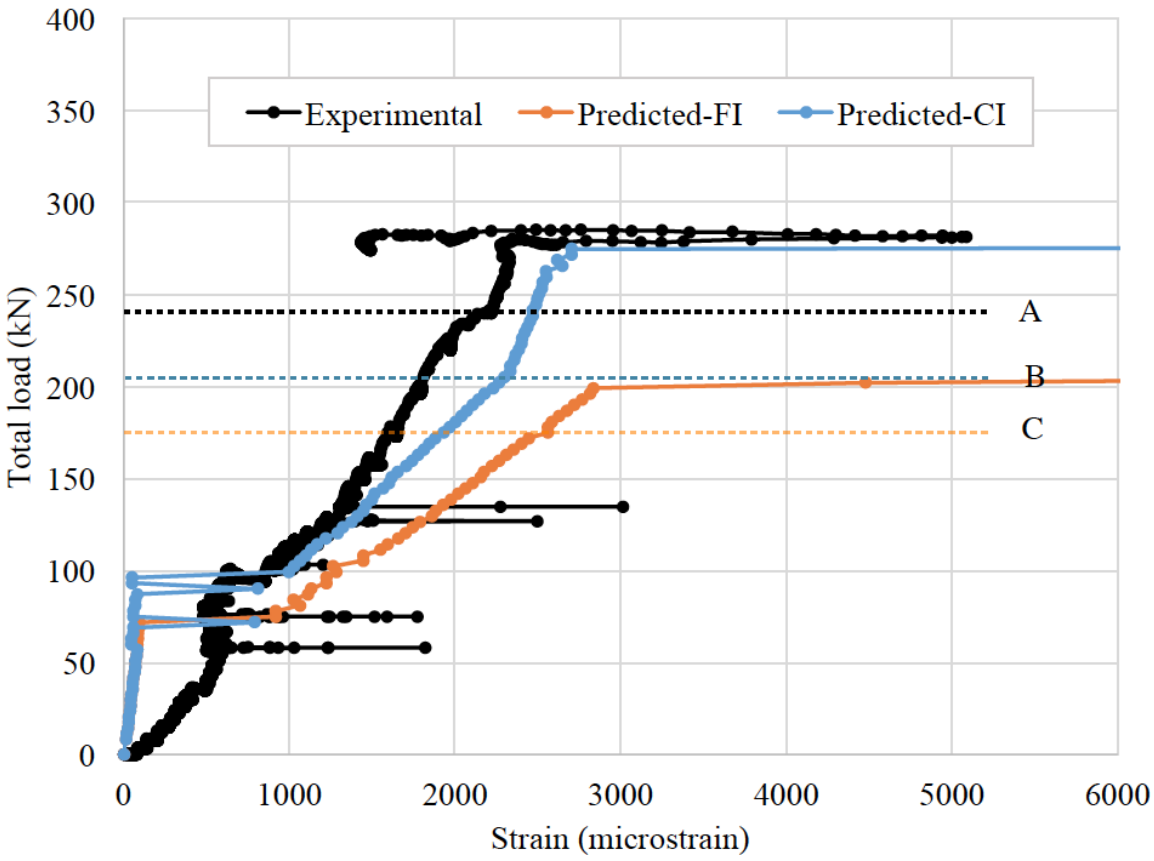

Figure 6.55: Experimental and predicted load-strain values of steel bars in beam T-OSS-C at location B6

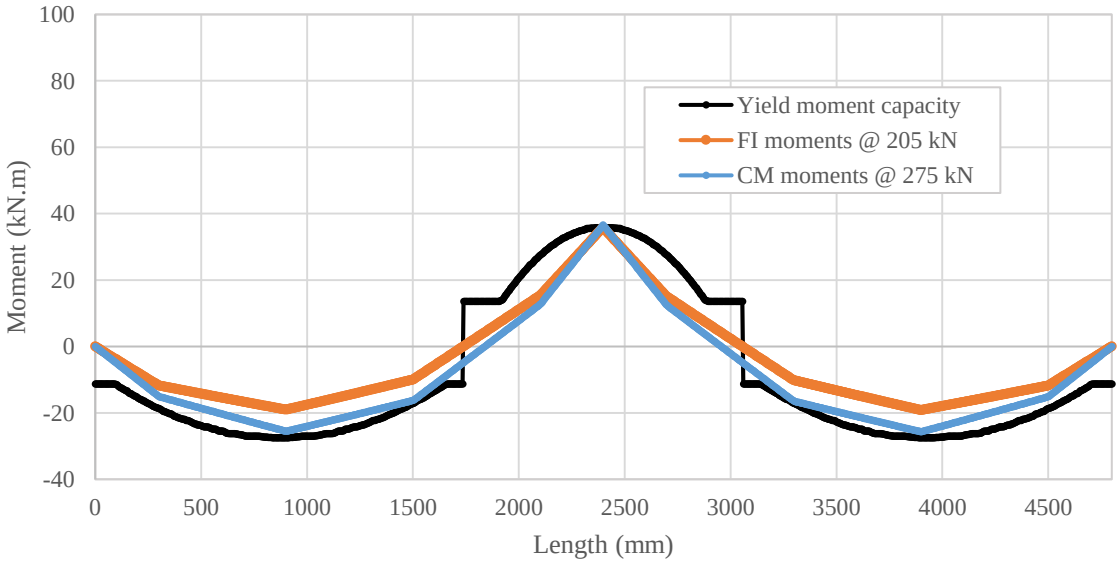

Figure 6.56: Applied moment values found from the interaction models and compared to the yield moment capacity of beam T-OSS-C

In Figure 6.55, lines A, B and C indicate the total load level at which moment redistribution starts from the hogging region to the sagging region on the experimental (line A), FI (line C) and CI (line B) load-strain relationships respectively. Since the strain gauge at location B6 is not located at the

point of maximum moment within the hogging region, the steel bar yields after moment-redistribution has started. Although both models underestimated the initiation of moment redistribution, the CI method produces a closer match.

Figures 6.57 to 6.67 show the experimental and predicted load-strain responses of beam FF-OSS-C. Both full- and CI methods accurately predict the pre-cracking tensile strains and yield strain values in the sagging regions (locations A1 and A2 in Figure 6.57 and Figure 6.58 respectively). At the post-cracking stage, the models overestimate the strain values. Since both models returned similar strain values in this stage, the choice of concrete-reinforcement bond interaction may not be the reason behind this overestimation but rather the distance of the strain gauge from the adjacent cracks. The distance between the point where strain values are collected and a nearby crack affects the strain values because the force in the reinforcement varies from a crack face along the bar depending on the bond interaction behaviour (partial-interaction theory). Therefore, when the CI method is applied, the accuracy in finding the actual crack locations affect the prediction of bar strain values.

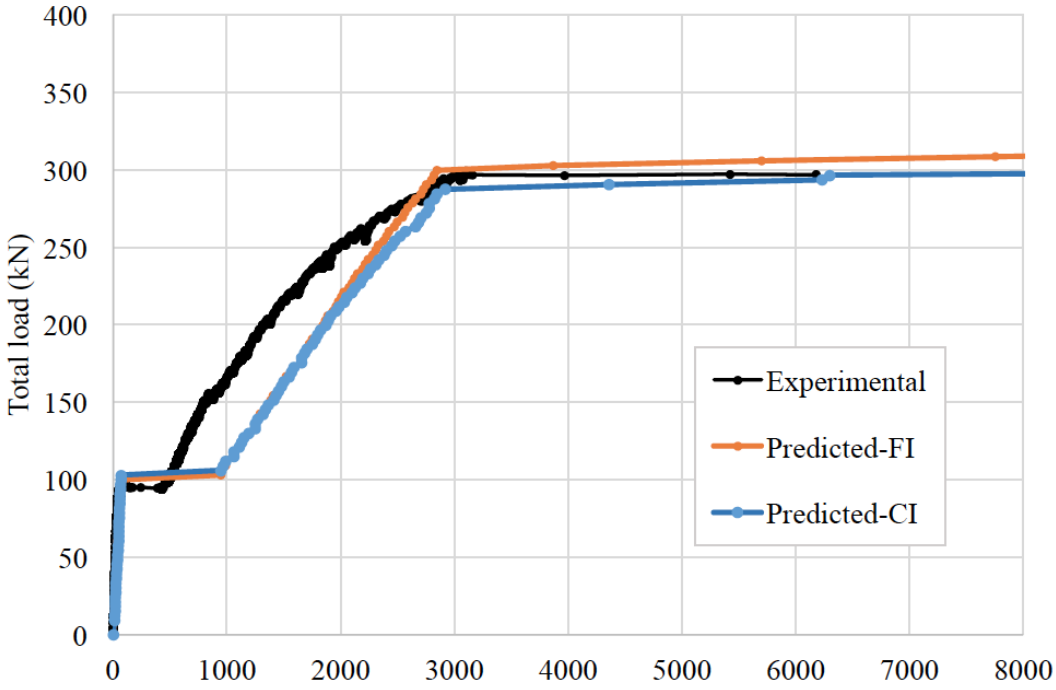

Figure 6.57: Load-strain behaviour of steel bars in beam FF-OSS-C at location A1

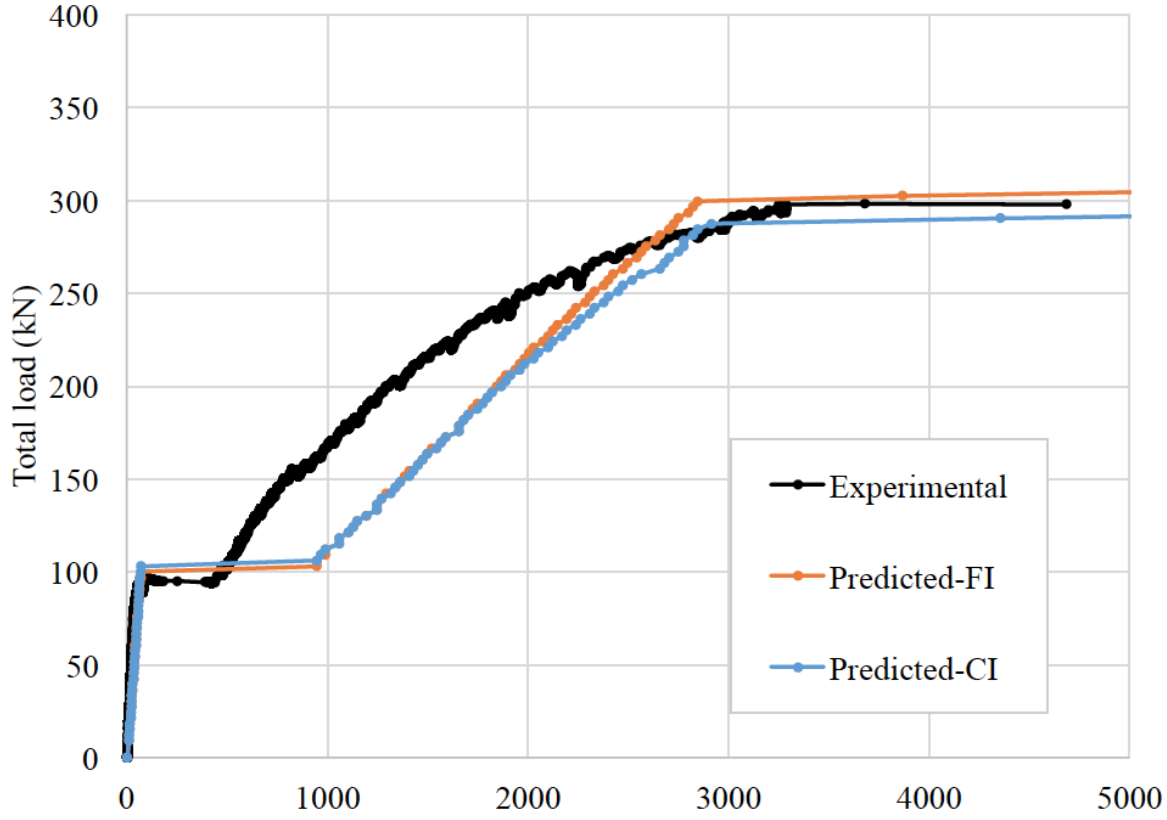

Figure 6.58: Load-strain behaviour of steel bars in beam FF-OSS-C at location A2

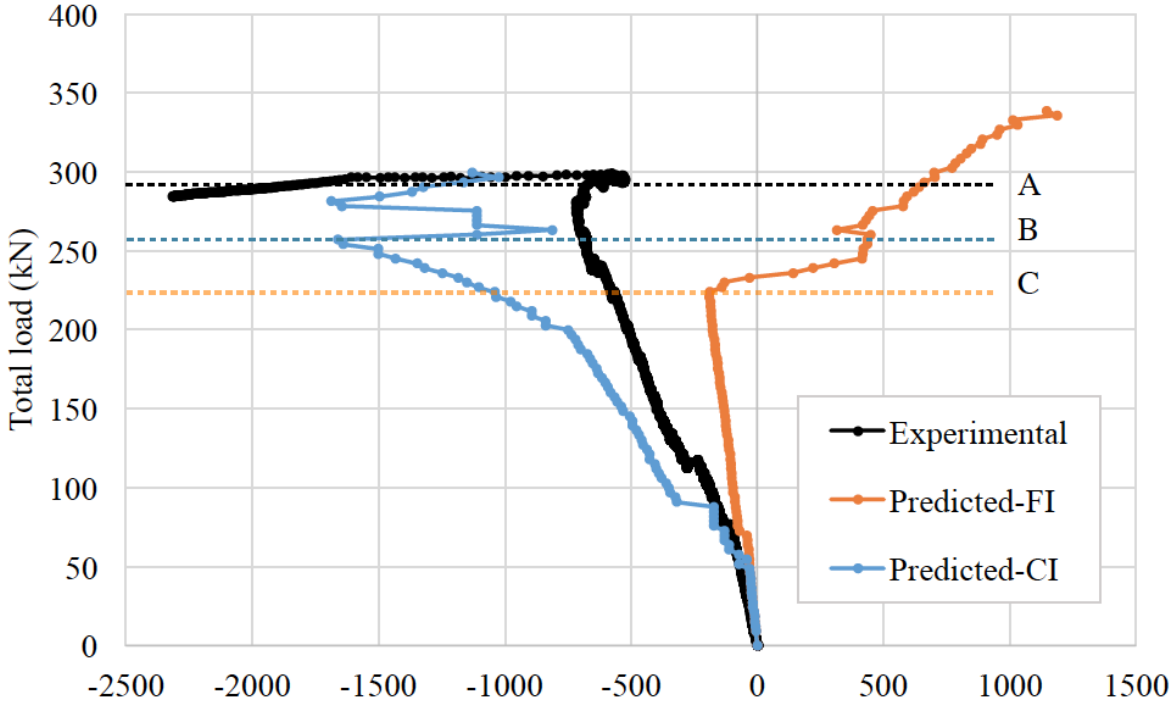

Figure 6.59: Load-strain behaviour of steel bars in beam FF-OSS-C at location A6

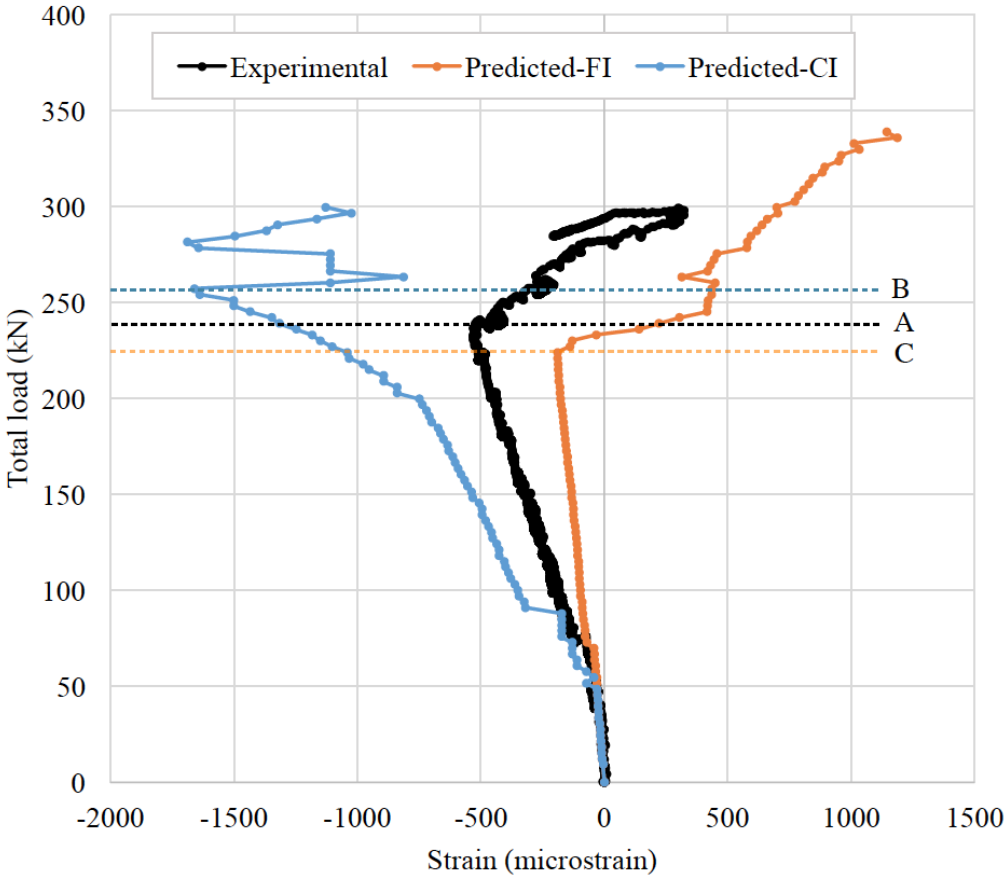

Figure 6.60: Load-strain behaviour of steel bars in beam FF-OSS-C at location A7

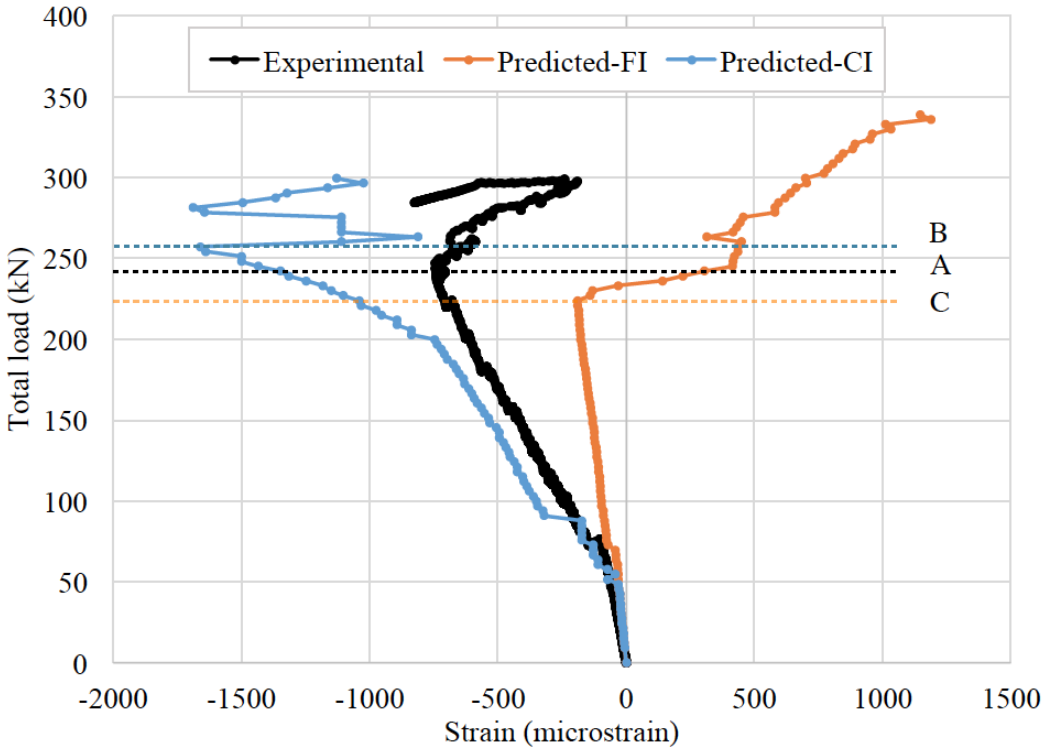

Figure 6.61: Load-strain behaviour of steel bars in beam FF-OSS-C at location A8

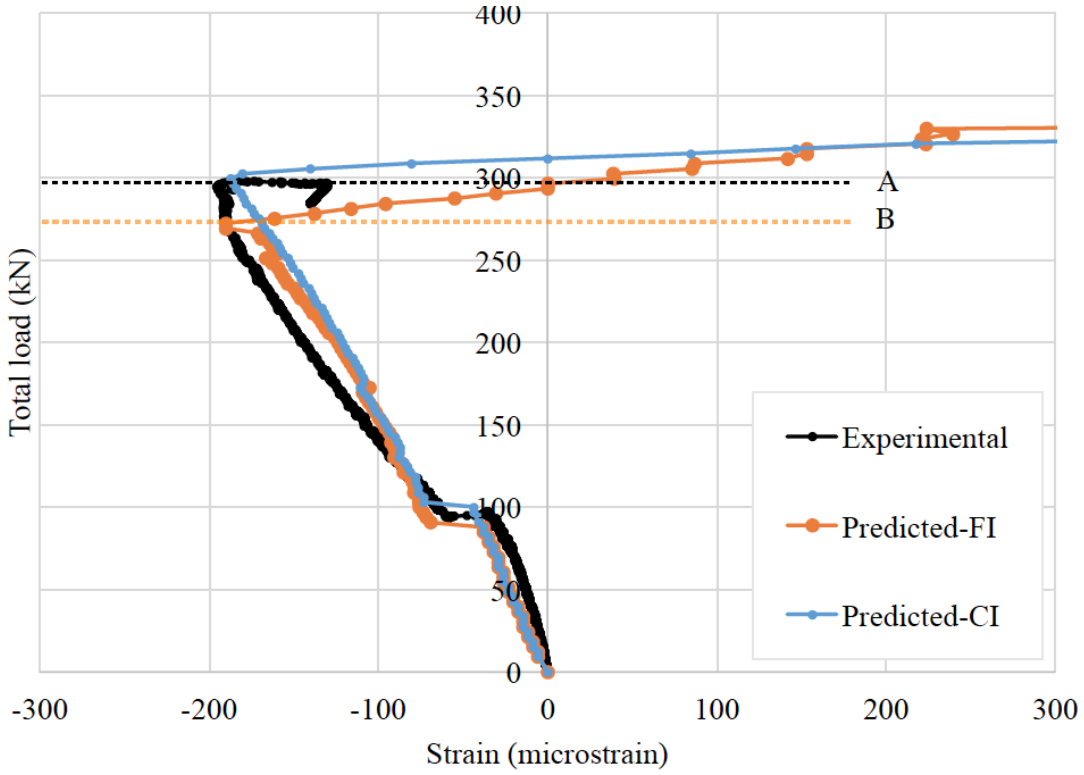

Figure 6.62: Load-strain behaviour of steel bars in beam FF-OSS-C at location B1

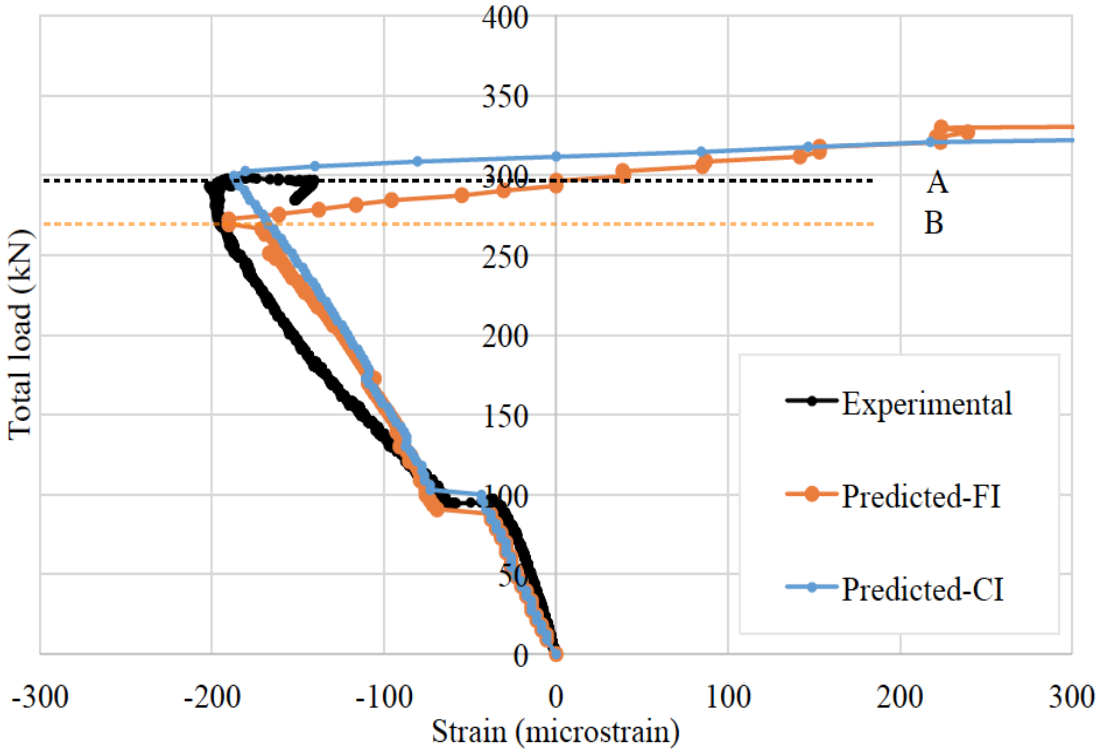

Figure 6.63: Load-strain behaviour of steel bars in beam FF-OSS-C at location B2

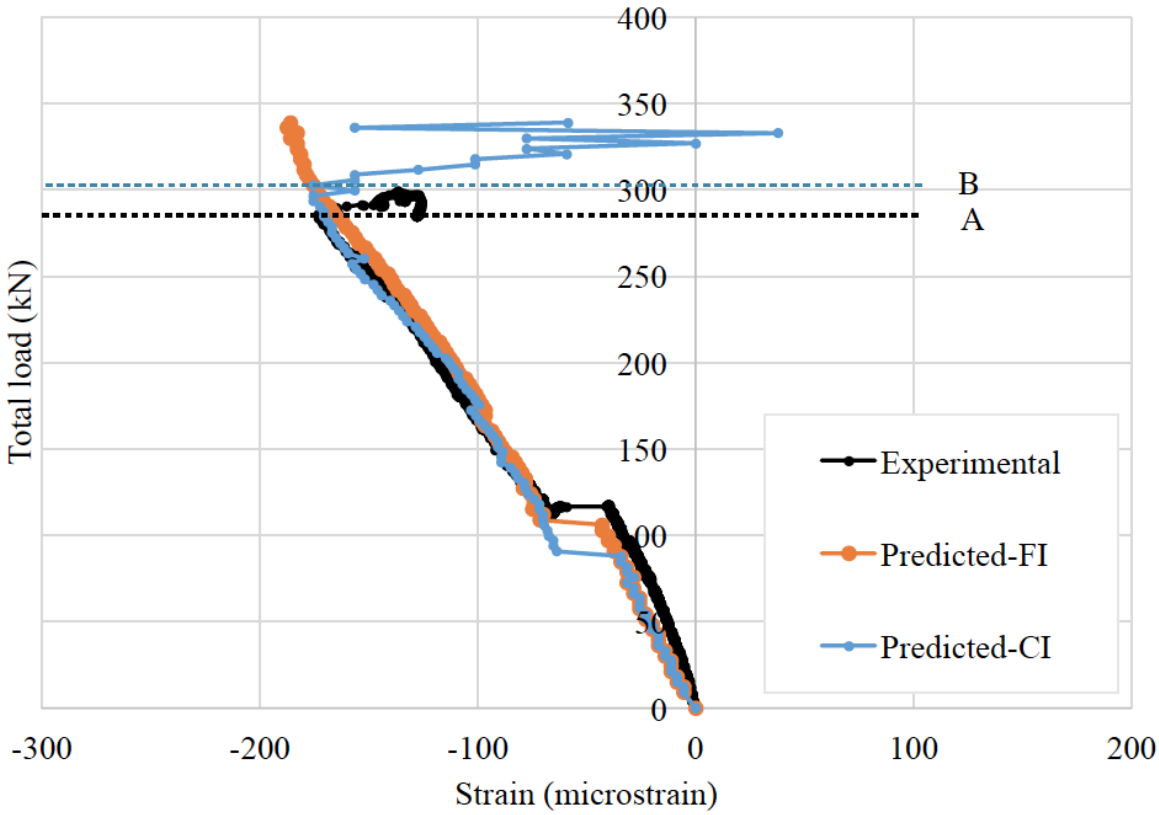

Figure 6.64: Load-strain behaviour of steel bars in beam FF-OSS-C at location B3

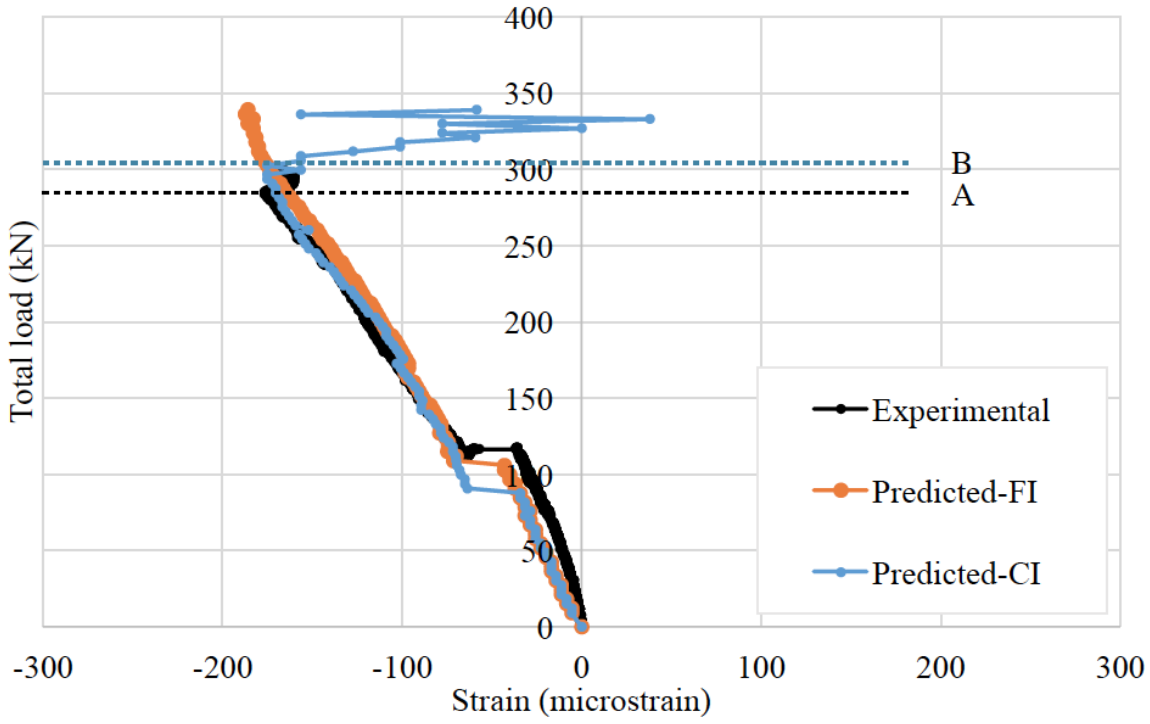

Figure 6.65: Load-strain behaviour of steel bars in beam FF-OSS-C at location B4

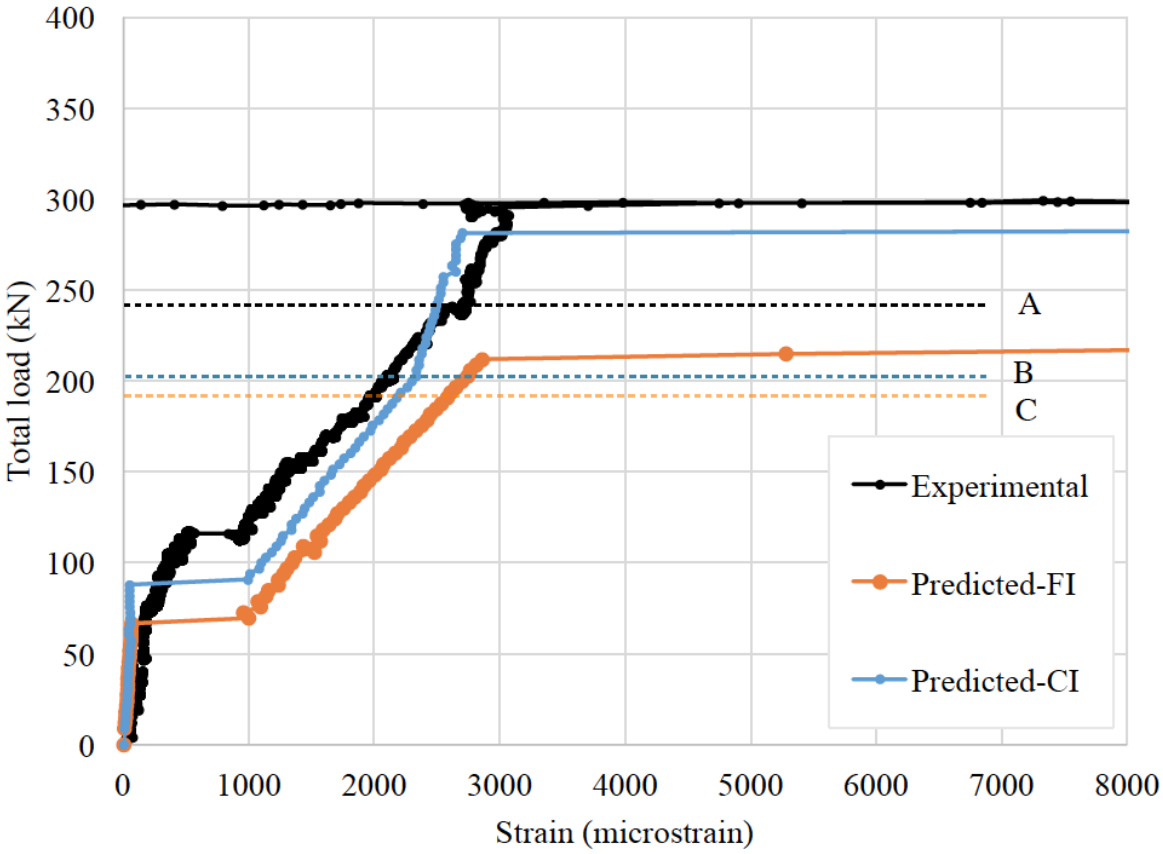

Figure 6.66: Load-strain behaviour of steel bars in beam FF-OSS-C at location B6

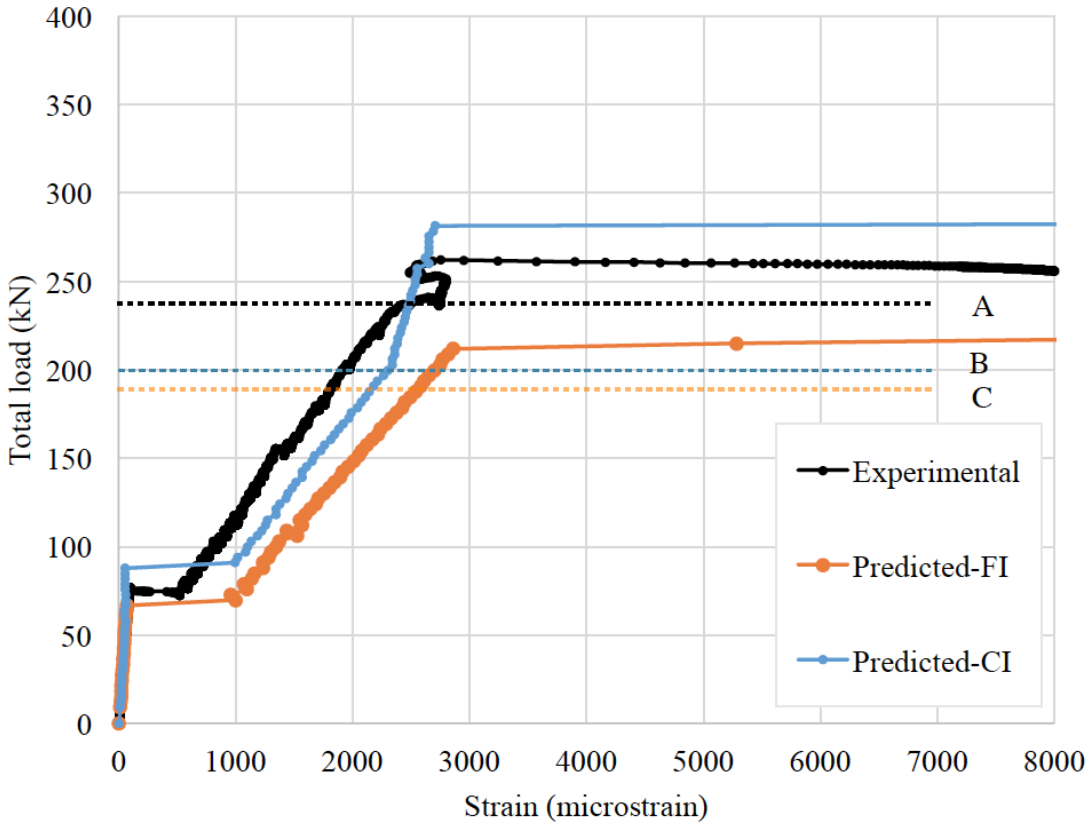

Figure 6.67: Load-strain behaviour of steel bars in beam FF-OSS-C at location B7

The compressive strain values in the hogging region at locations A6, A7 and A8 are shown in Figure 6.59, Figure 6.60 and Figure 6.61 respectively. The FI and the CI methods under- and overestimate strains at these locations respectively with a closer prediction to the experimental data seen from the CI method. As explained earlier in §6.3.1.2 for beams T-N-C and beam T-OSS-C, this is due to the difference between the experimental and predicted applied moment values on one hand and the accuracy of the interaction model on the other hand (considering the sensitivity of the analysis at these locations).

Lines A in Figure 6.59 through Figure 6.65 specify the experimental total load value at which the neutral axis location shifted up above the level of compression steel bars. In most cases, this load level predicted by the CI method (indicated by line B), agrees well with the experimental value.

The relationship between the tensile strains and the total applied load in the hogging region is presented in Figure 6.66 and Figure 6.67 at strain gauge locations B6 and B7. Indicated by line A is the load level at which the actual moment redistribution started in the experiments. Both models underestimated this load but the total load corresponding to the yield of steel bars is predicted better by the CI method than the FI method.

Generally, for all continuous beam specimens, the CI method generated reasonably accurate predictions for the load-strain values. This indicates that, the model adopted for the load-slip analysis and the proposed combined bond interaction model were successful in simulating the cross-sectional behaviour of the beams.

6.3.3 Optimisation

6.3.3.1 Optimisation for strength

All continuous beams were designed based on the second model of failure described in §4.7.1.2 according to which the tensile steel bars in the hogging part of the beam yield first to allow moment redistribution to the sagging parts and the ultimate failure of the beam is considered to be reached when the tensile steel bars in the sagging regions yield. This section, examines whether this condition is met or not, and what level of strength-utilisation of the beams is.

Figure 6.68 show the moment distribution of beam T-N-C versus the yield moment values and ultimate failure moment values corresponding to the crushing point of the concrete. Since beams T-OSS-C and FF-OSS-C had the same reinforcement ratio and flange dimensions and different only in their web shape and size (which is mostly cracked at failure), both beams had approximately the same calculated yield, failure and applied moment values shown in Figure 6.69.

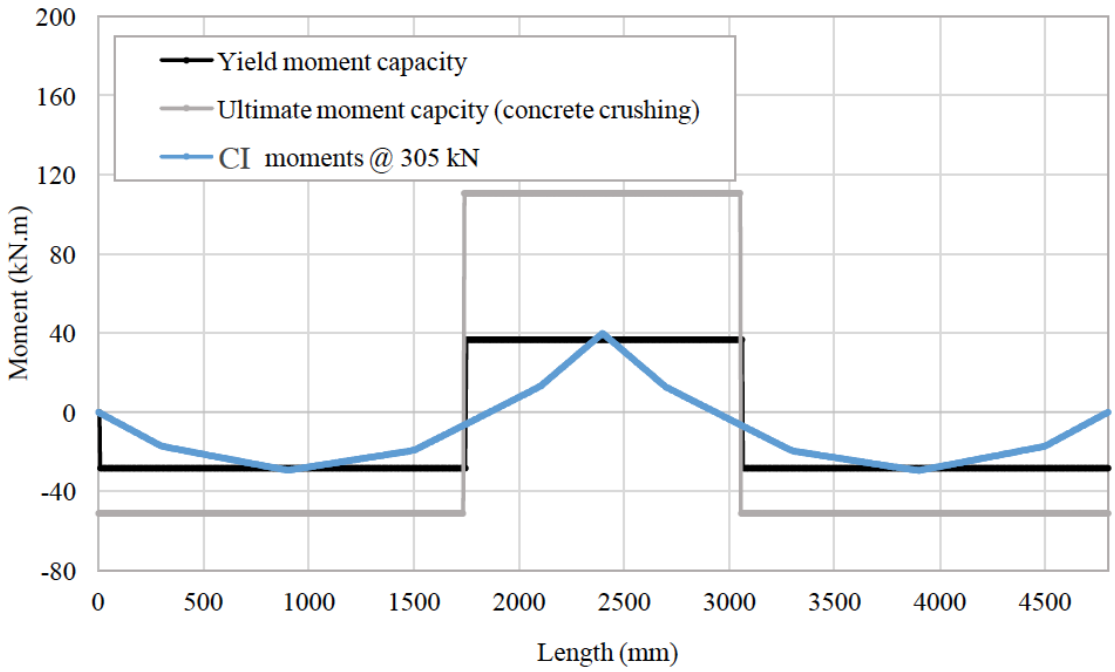

Figure 6.68: Moment distribution values determined from the full- and CI methods compared to the ultimate and yield moment capacities of beam T-N-C

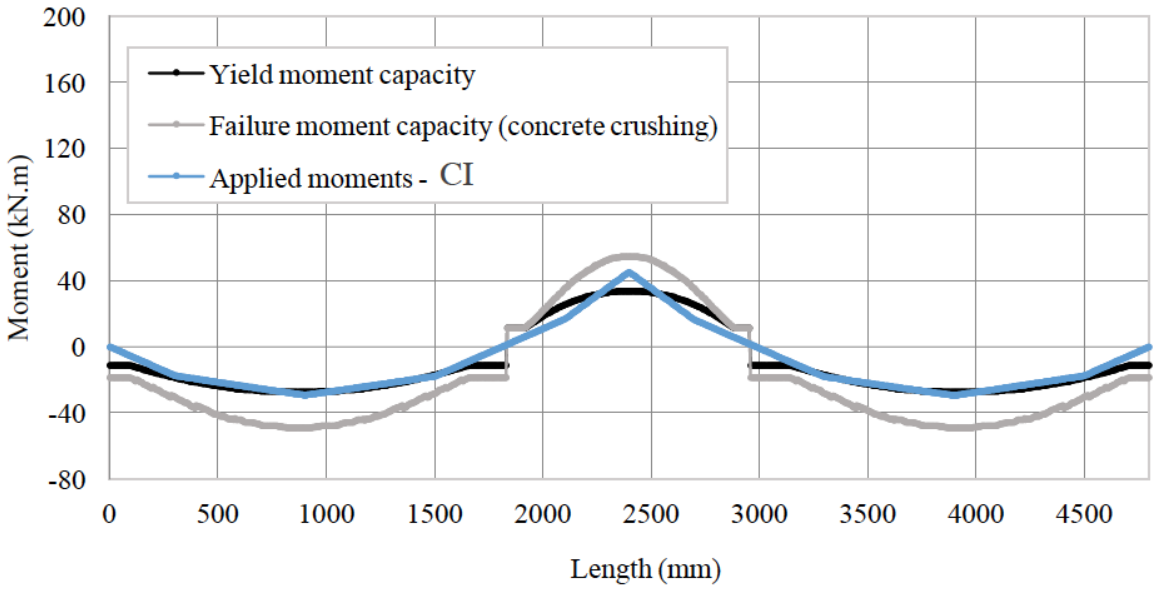

Figure 6.69 Moment distribution values determined from the full- and CI methods compared to the ultimate and yield moment capacities of beams T-OSS-C and FF-OSS-C

All beams were designed to fail in flexure at a total load of 305 kN. Beam T-N-C was designed to be equivalent in strength to beams T-OSS-C and FF-OSS-C (refer to §5.2.2). For the maximum strength utilisation of the optimised beams to be achieved, the tensile bars in the sagging regions at the critical sections should reach yield at nearly the same load as the equivalent prismatic beam. For all beams, the theoretical critical section locations in the sagging regions are approximately located at the strain gauge locations A1, A2, A11 and A12. Therefore, the total yield load of the steel bars

at these location is considered to indicate the level of strength-utilisation of the optimised beams compared to the equivalent strength prismatic beam. The load-deflection relationships presented previously are used to indicate the ultimate load capacity of the beams.

As it can be noted in Figure 6.41 and Figure 6.43, beams T-N-C and FF-OSS-C showed slightly higher and lower ultimate failure load values respectively. However, beam T-OSS-C failed at a considerably lower load than the designed failure load. The beam could have failed due to arching effect of the compression bars in the hogging region and buckling of the bars. At the final stages of loading, spalling of the concrete cover along the direction of the compression reinforcement was seen as indicated by the arrows in Figure 6.70. To avoid this sort of failure and achieve highest degree of capacity utilisation, the radius of curvature of the longitudinal profile of the beam may need to be considered as a design variable and minimum allowable limits may need to be specified. The smaller the radius of curvature, the higher the difficulty in bending the bars and achieving the correct placement on one side and the higher the arching effect on the other side. For the beams tested in this program, increasing the radius of curvature in the hogging region was not possible because of the relatively short span lengths. However, for larger (usually-sized) beams a proper longitudinal profile may automatically be achieved by using the proposed strength optimisation method.

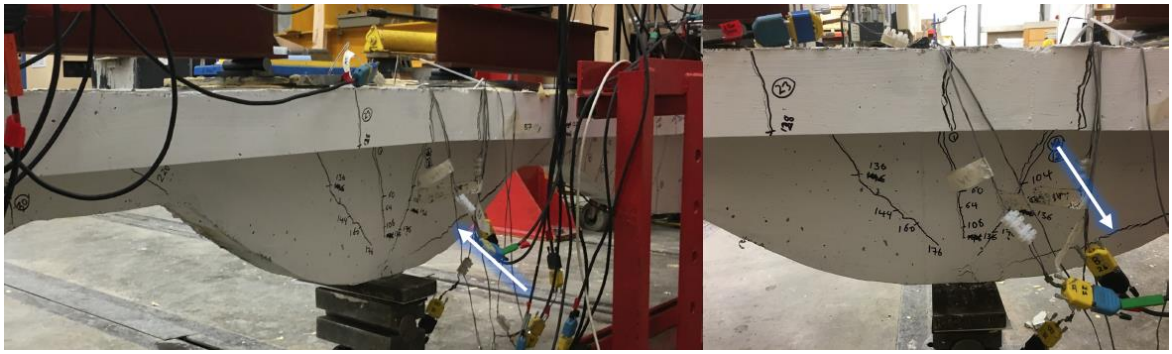

Figure 6.70: Spalling due to arching effect of the compression bars in beam T-OSS-C

As hown in Figure 6.46, Figure 6.47 and Figure 6.49, tensile bars in the sagging regions of beam T-N-C yielded at an average total load value of 318kN. For beam T-OSS-C, none of the strain gauges installed on the tensile bars in this region worked (damaged probably during casting). The tensile bars at locations A1 and A2 for beam FF-OSS-C yielded at 300kN as presented in Figure 6.57 and Figure 6.58. This indicates that the optimised fabric-formed beam exhibited an ultimate capacity equal to 98% of the design capacity.

In summary, the performance of the fabric-formed beam implies that, continuous concrete beams can be optimised for strength based on the proposed optimisation method (the stable state method)

to resist the same loads as an equivalent prismatic beam but use a smaller amount of concrete material.

6.3.3.2 Optimisation for serviceability

The method developed in this thesis is to optimise statically indeterminate concrete beams simultaneously for both for strength and serviceability. Therefore, unlike the simply supported beams tested in this experimental program, both of the optimised continuous beams tested in this work were optimised for strength and serviceability. It was therefore intended to verify the optimisation methods through assessing the validity of the prediction models rather than comparing specimens that have different optimisation targets.

The models proposed in this thesis to analyse and predict the behaviour of continuous concrete beams generated reasonably good predictions for both crack widths and deflections at serviceability. Therefore, the pre-assigned optimisation target can be assumed to have been met and the optimisation models can be regarded as verified.

In order to support this statement further, the values of the crack widths and deflections for the continuous beams under service loads (assumed to be 160 kN) are compared, Table 6-7. The limits on crack width and deflections are based on the provision of BS EN 1992-1-1 (2004) for all possible exposure classes from normal to aggressive environmental conditions. It can be noted that all serviceability limit state values for the optimised beams fall below the allowable limits and are not considerably larger than those of the prismatic beam. In fact, the average and maximum crack width values for beam T-OSS-C is equal to that of the prismatic beam (T-N-C). It should also be noted that the codified deflection limits are significantly larger than the actual deflections for the beams because the specimens tested in this experimental program are lab-sized beams. However, it has been shown later in Chapter Seven that beams with larger spans exhibit a deflection value larger than the allowable limit in many cases.

The above results indicate that it is possible to use the prediction and optimisation methods proposed in this thesis to design continuous concrete beams which are optimised for strength and serviceability and by which a significant amount concrete may be saved.

Table 6-7: Serviceability limit state values and codified limits for the continuous beam specimens

Beam	Serviceability limit states				
	Crack widths (mm)			Deflection (mm)	
	Av.	Max.	Limit	Max.	Limit
T-N-C	0.08	0.28	0.3-0.4	2.4	9.6
T-OSS-C	0.08	0.28	0.3-0.4	3.8	9.6
FF-OSS-C	0.15	0.32	0.3-0.4	3.9	9.6

6.4 Conclusion

In this chapter, the results collected from the testing program described in Chapter Five have been presented. The methods described in Chapter Three to predict the behaviour of statically determinate and indeterminate concrete beams are used to generate predictions of the behaviour of the test specimens. Comparing the experimental and predicted data indicates that the CI method proposed in this thesis is reasonably accurate in predicting cracking, deflections and bar strains. The optimisation methods were successful in producing concrete beam shapes that met the specified optimisation targets. In some cases, the predicted and the experimental data diverge.

[Blank Page]

Chapter Seven

Parametric Analysis

7.1 Preface

This chapter presents a parametric analysis conducted to assess the performance of the optimisation methods presented in Chapter Four in terms of reduction in the concrete material used for concrete beams. The optimisation parameters introduced in Chapter Four are considered here as variables. These parameters are the cross-section shape of the beams, span length, support conditions, and cross-section depth. The main purpose behind this parametric study can be stated as: 1) to show whether or not the beams optimised for strength only satisfy the serviceability criteria (i.e. if further optimisation for serviceability is needed) using the prediction methods developed in this work; 2) to show how much material can be saved to optimise for both ultimate and serviceability limit states compared to an equivalent prismatic beam using the optimisation methods developed in this work. Therefore, only a specific range of geometric parameters are selected as optimisation parameters and all other cross-sectional properties (such as reinforcement ratio and type), loading type and load intensity are taken to be constant.

7.2 Optimisation parameters

7.2.1 Loading arrangement

The loading arrangements and the values of actions selected for this parametric study are chosen based on the provisions of BS EN 1990:2002 +A1 (2005) and BS EN 1991-1-1:2002 (2004) respectively. The types of loads considered in this study are permanent actions which consists of the selfweight of the member and variable actions which is selected based on the type of structure taken into account. The equations of the fundamental combination of actions is as below:

$$L_d = \sum_{j \geq 1} \gamma_{G,j} G_{k,j} + \gamma_{Q,1} Q_{k,1} \qquad (17)$$

Where L_d is the design load, G_k and Q_k are characteristic permanent and variable loads on the beams respectively, j is the number of permanent actions, γ_G and γ_Q are partial factors taken as 1.35 and 1.5 respectively according to BS EN 1990:2002 +A1 (2005) when optimising for the ultimate limit state and both taken as 1 when serviceability limit states are considered.

7.2.2 Selected cross-section shapes

The cross-section shapes considered in this analysis are divided into two types, concrete beams with and without a flange. Both types of beams are frequently seen in concrete structures. A number of cross-section shapes from each category have then been selected based on feasibility of construction and potential to save the highest possible amount of concrete material. The cross-section shapes selected are shown in Figure 7.1. The T-section and rectangular cross-section shapes are chosen because they are considered to be easier to construct using rigid forms. The T-keyhole shape combines the benefits of flexible formwork, such as easier achievement of curved longitudinal profile. The bulb cross-section shape characterises a fully flexibly-formed beam shape whilst the keyhole cross-section shape facilitates lower material consumption compared to the bulb shape but involves partial use of rigid formwork.

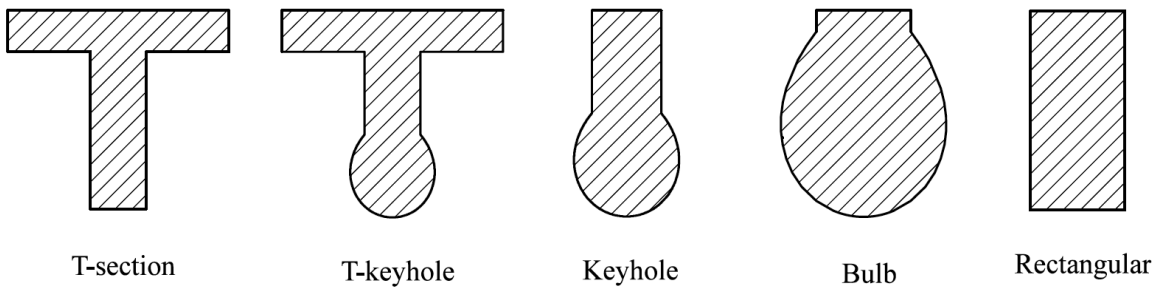

Figure 7.1: Cross-section shapes used in the parametric study

The permanent load on all beams was assumed to be the self-weight of the member only but the variable load is taken as 2.5 kN/m^2 for office use according to BS EN 1991-1-1:2002 (2004). The beams were assumed to be steel reinforced. The total factored load of 23 kN/m and unfactored load of 15 kN/m were used for the ultimate and serviceability limit state design respectively, plus the self-weight which varies along the beam.

7.3 Simply supported beams

The span length of a beam affects which limit state governs the final shape and the design. Strength optimised beams with shorter span length tend to show lower deflection (compared to span) and crack widths at serviceability than those with longer spans. In order to clarify this further, a set of simply-supported beams consisting of five beams with the five cross-section shapes presented in §7.2.1 were optimised. The span length of the beams was assumed to vary but all beams were subjected to the same loading conditions, same number of compression and tension steel bars and same material properties. The beams were assumed to be reinforced with steel bars with the strength characteristics given in Table 5-4. The concrete strength properties are taken as those of beam T-OS-S as given in Table 5-3. The cross-section details and beam names are shown in Figure 7.2. The beams were optimised in two phases.

7.3.1 Phase one

In phase one, the beams were optimised for strength (see §4.6.1) only and in phase two the beams were optimised for both strength and serviceability (§4.6.2). Figure 7.3 shows the amount of material saved in phase one depending on the span length while keeping the applied load, reinforcement ratio, cross-sectional properties constant (apart from the depth which changes during the optimisation procedure). It can be clearly seen that the cross-section shape and span length have a significant effect on the amount of material saved. The longer the span the higher the amount of material saved for beams T-S1 and R-S1. For beam B-S1 which has a bulb cross-section shape, the increase in span length increases the cross-section depths required along the beam and, hence, the bulb width. At some point, this increase in size outweighs the amount of material saved by varying cross-sectional depth and the size of the optimised shape becomes larger than that of an equivalent strength prismatic beam.

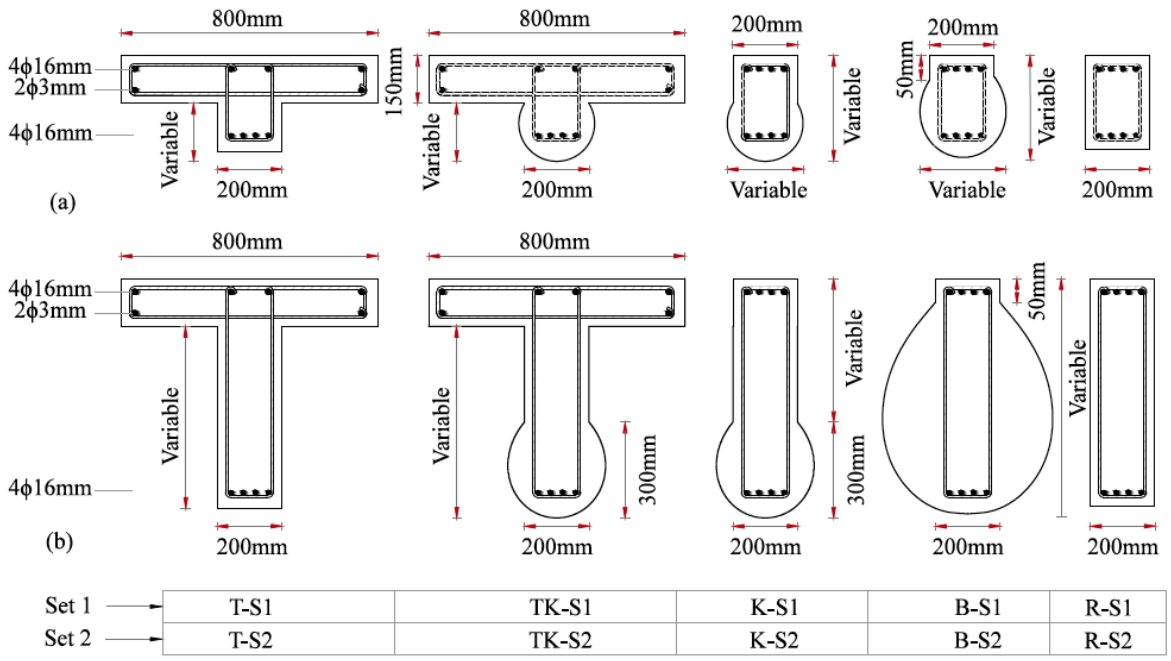

Figure 7.2: Cross-section details of beams in set one and two (a) Sections near supports, (b) Sections near mid-span

For beams TK-S1 and K-S1, which are partially fabric-formed, there is a specific span length beyond which the amount of reduction in material by optimisation starts to decrease.

The maximum deflection values of each beam under service loads and at the first phase of optimisation compared to the allowable limit which was taken as span/250 (according to BS EN 1992-1-1 (2004)) is shown in Figure 7.4. It is clear that the maximum deflection value for all beams are larger than the allowable limit in most cases and therefore optimisation for serviceability is essential, although, for larger spans (beyond 10-12 m), the beams seem to exhibit smaller deflection values than the allowable limit. This signifies the importance and necessity of serviceability optimisation model and shows how in many cases serviceability governs the design of non-prismatic concrete beams.

In some cases, the maximum deflection value of the equivalent prismatic beam was also larger than the allowable limit. Since this limit is provided for the sake of explanation only in this work, the larger of the maximum serviceability deflection of the equivalent prismatic and the allowable limit (span/250) was considered as the target while optimising for serviceability.

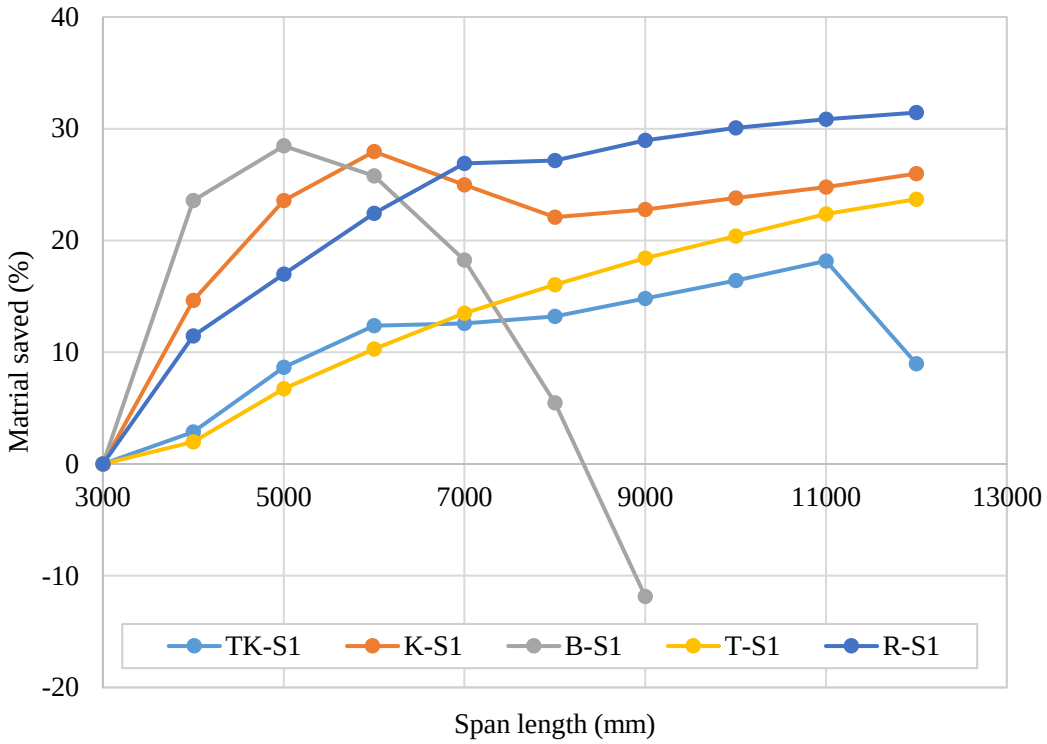

Figure 7.3: Relation between the amount of material saved and span length in phase one of the optimisation

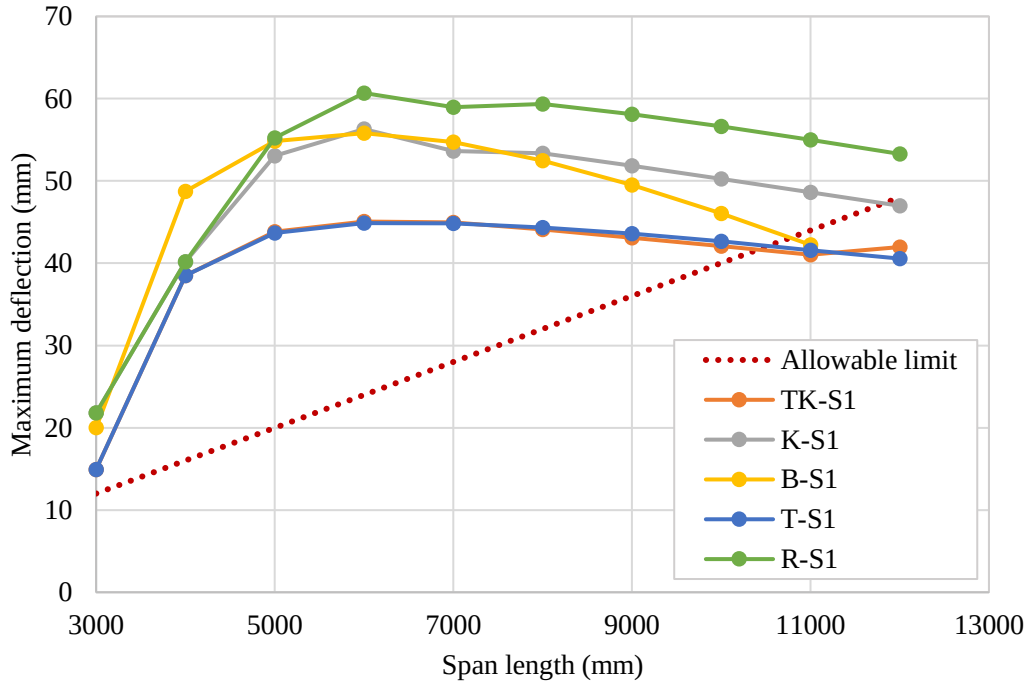

Figure 7.4: Maximum deflection value versus span length for beams in set one and phase one of optimisation

For crack width control, the maximum crack width value was considered for all optimised beam shapes in the first and second phases of optimisation (Figure 7.5). The allowable crack width value

was taken as 0.3mm according to the provisions of BS EN 1992-1-1 (2004) although this limitation may vary depending on the type of structure and the function of the structural element. For beams T-S1 and TK-S1, the maximum crack width values are below the allowable limit and so no optimisation to reduce crack width values is necessary. The rest of the beams needed further optimisation for crack widths alongside deflections in most cases.

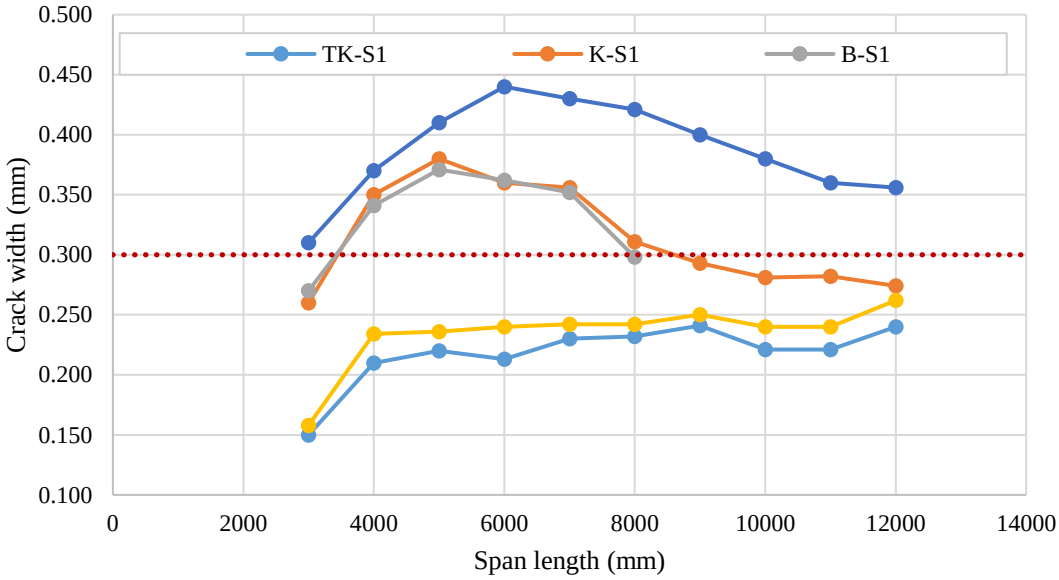

Figure 7.5: Maximum crack width values for beams in set one in the first phase of optimisation

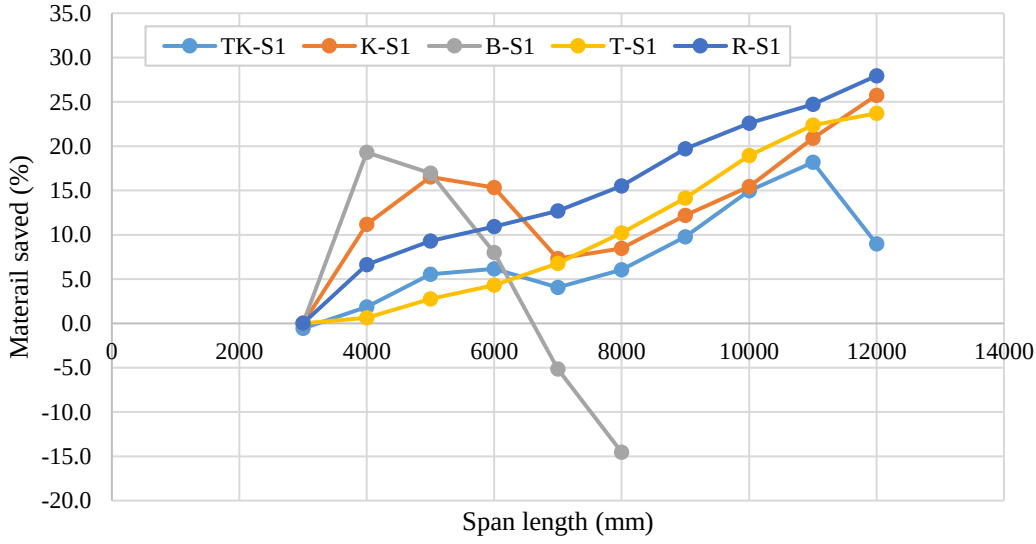

Figure 7.6: Material reductions per span length for beams in set one in the second phase of optimisation

Phase two

In the second phase of optimisation, material is added back topologically to those beams which failed to satisfy either of the serviceability limit states in the first phase. Optimisation was carried out simultaneously for crack widths and deflections as per the topology optimisation method described in §4.6.2. Generally, the longer the span, the higher the amount of saving in concrete material compared to and equivalent prismatic beam as presented in Figure 7.6

In order to compare the amount of material saved in both phases of the optimisation and show what ratio of material is added back to the strength optimised beam in each case, the output of the optimisation procedure is presented in Table 7-1. It is clear that the larger the deflection and crack width values the higher the amount of material which is need to be added back. For beam spans equal to 3m or less, a minimum allowable depth along the beam provides sufficient strength and stiffness under the given loading arrangement. Therefore, the amount of material saved in these cases is zero. The beams with a flange tend to show less reduction in concrete material than the beams without flange, which can be seen by comparing beam T-S1 to R-S1 or TK-S1 to K-S1. The beam with a rectangular cross-section shape showed highest saving in concrete material of about 28% after optimisation for both strength and serviceability compared to a prismatic concrete beam.

In order to compare the beam shapes produced by the first and second phases of optimisation and to show the longitudinal material layout given by the topology optimisation, the output shapes of beams T-S1 (which has a flange) and R-S1 (which is without a flange) are shown in Figure 7.7 and Figure 7.8.

For the same reinforcement ratio and total cross-sectional depth, a T-section has a higher moment capacity than a rectangular beam. However, the cross-sectional depths of beam R-S1 are smaller than that of beam T-S1 for the same span length and under the same loading conditions. The reason behind this is the higher selfweight of the T-beam compared to that of the rectangular beam which play an important role for beams with longer spans.

Table 7-1: The amount of material saved per span length in phases one and two of optimisation for beams in set one

	Material saved (%)									
Beam	**R-S1**		**B-S1**		**K-S1**		**TK-S1**		**T-S1**	
Phase / **Span (mm)**	*Ph1*	*Ph2*	*Ph1*	*Ph2*	*Ph1*	*Ph2*	*Ph1*	*Ph2*	*Ph1*	*Ph2*
4000	12	7	24	19	15	11	3	2	2	1
5000	17	9	29	17	24	17	9	6	7	3
6000	22	11	26	8	28	15	12	6	10	4
7000	27	13	18	-5	25	7	13	4	13	7
8000	27	16	6	-15	22	9	13	6	16	10
9000	29	20	-12	-	23	12	15	10	18	14
10000	30	23	-36	-	24	15	16	15	20	19
11000	31	25	-	-	25	21	18	18	22	22
12000	31	28	-	-	26	26	9	9	24	24

The volume of the optimised beams is larger than an equivalent-in-strength prismatic beam.

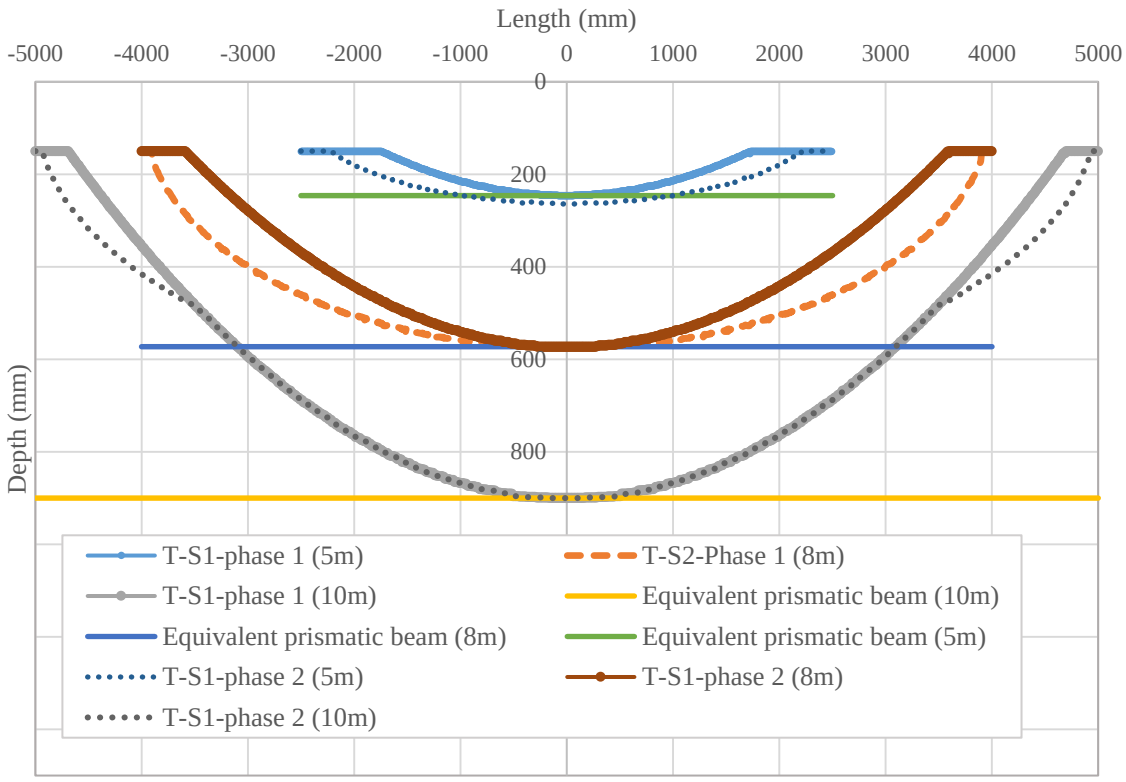

Figure 7.7 Optimised shapes for beam T-S1 for different span lengths

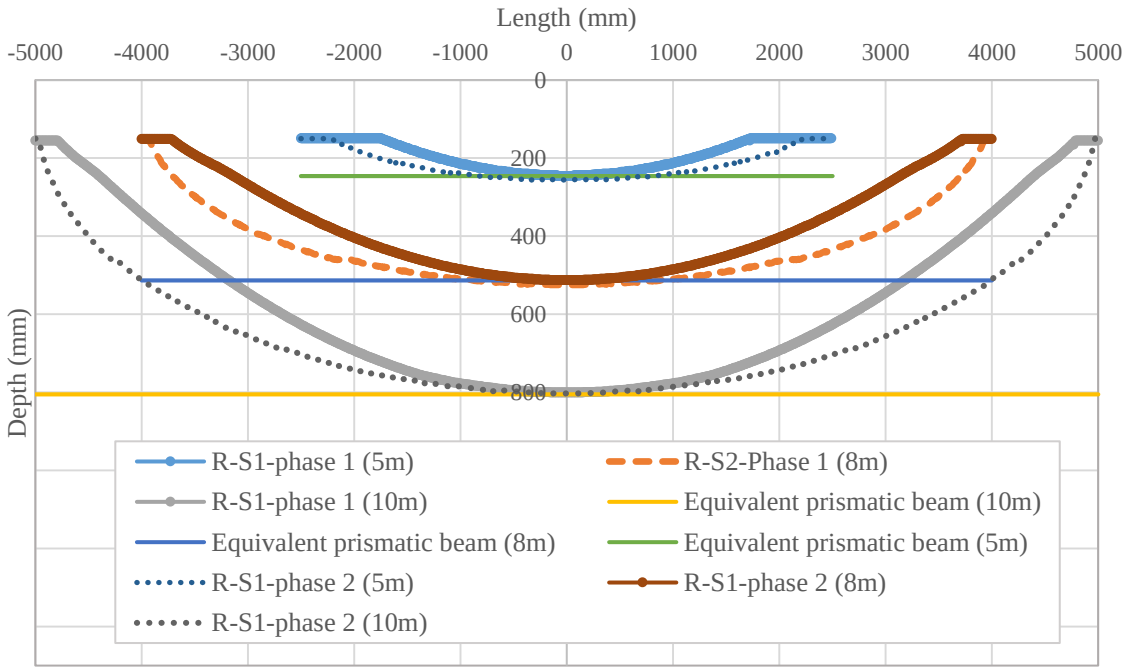

Figure 7.8 Optimised shapes for beam R-S1 for different span lengths

The addition of material in the serviceability optimisation procedure starts from regions near the supports. Depending on the amount of material needed to be added back to the beam optimised initially for strength, the location of maximum curvature (where material is added) moves towards the mid-span. The effect of this can clearly be seen in the case of beam T-S1 with a span length of 10 meters where added material is accumulated near the supports. The irregular profile of the beam caused by this has minimal effect in terms of appearance and construction as this situation only occurs in long beams (over 8m). However, this can be corrected by fitting the bottom profile of the beam into a curve that smooths the shape without significant effect on the optimisation outcome. Figures 7.9 and 7.10 show 3D models for beams T-S and TK-S1 after the second optimisation phase.

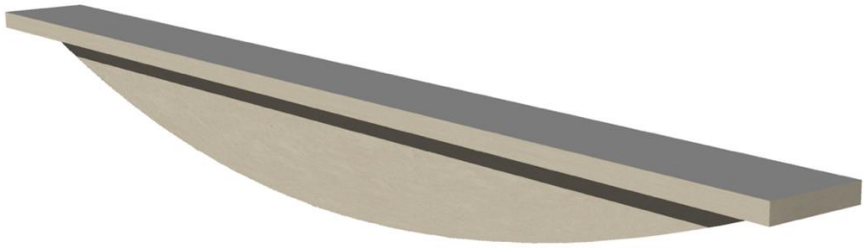

Figure 7.9: 3D model of beam T-S1 (10m)

Figure 7.10: 3D model of beam TK-S1 (10m)

7.4 Continuous beams

Another set of continuous beams (set two) were designed in the same two optimisation phases as the simply supported beams described in the previous section. Five beams with the cross-section shapes shown in Figure 7.2 were considered. The reinforcing steel area, material properties and applied load were the same for all beams and taken as those for beams in set one.

7.4.1 Phase one

In the first phase, in which the beams were optimised for strength only using the 'stable state' method described in §4.7.2, various levels of material saving were achieved. The amount of material reduced from an equivalent strength prismatic beam for the beams in phase one gradually increases with the increase of span length, until beyond a specific span length (depending on the section layout and material properties) the reduction in material starts to reduce as shown in Figure 7.13. For beam B-S2, this decrease starts for relatively shorter spans and for beam spans longer than 8m the size of the optimised beams becomes larger than that of the equivalent strength optimised beam.

It can be seen in Figure 7.14 that, the beams failed to meet the maximum deflection conditions in most cases. The beams with smaller spans (smaller than about 6m) satisfied the crack width criteria as shown in Figure 7.15. Combining the deflection and cracking serviceability limit states, the majority of the beams optimised in phase one need further optimisation for serviceability.

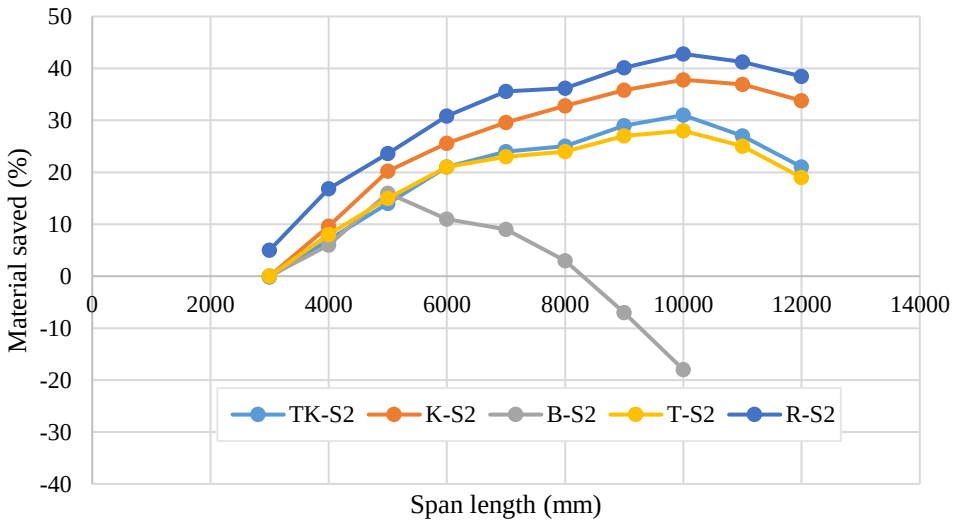

Figure 7.13: Material reduction in phase one of optimisation for beams in set two per span length

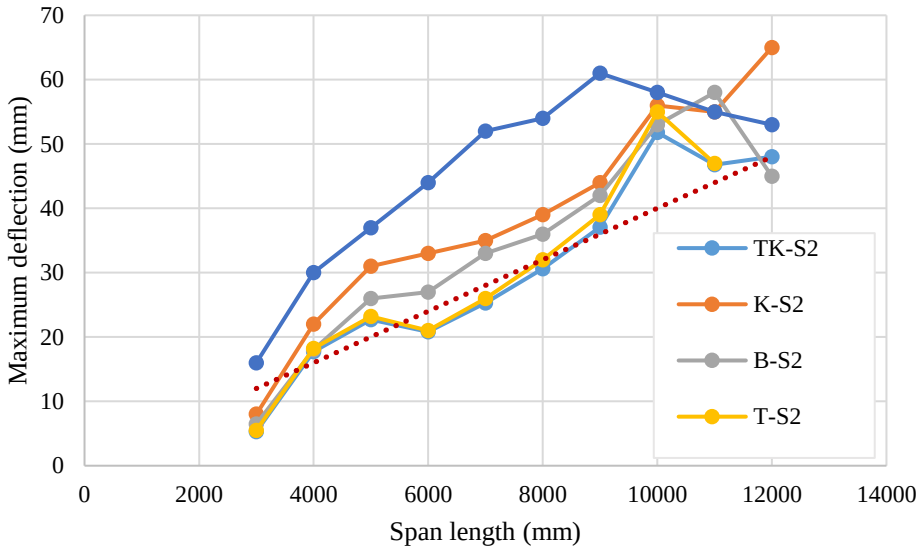

Figure 7.14: Maximum deflection values for beams in set one after optimisation for strength

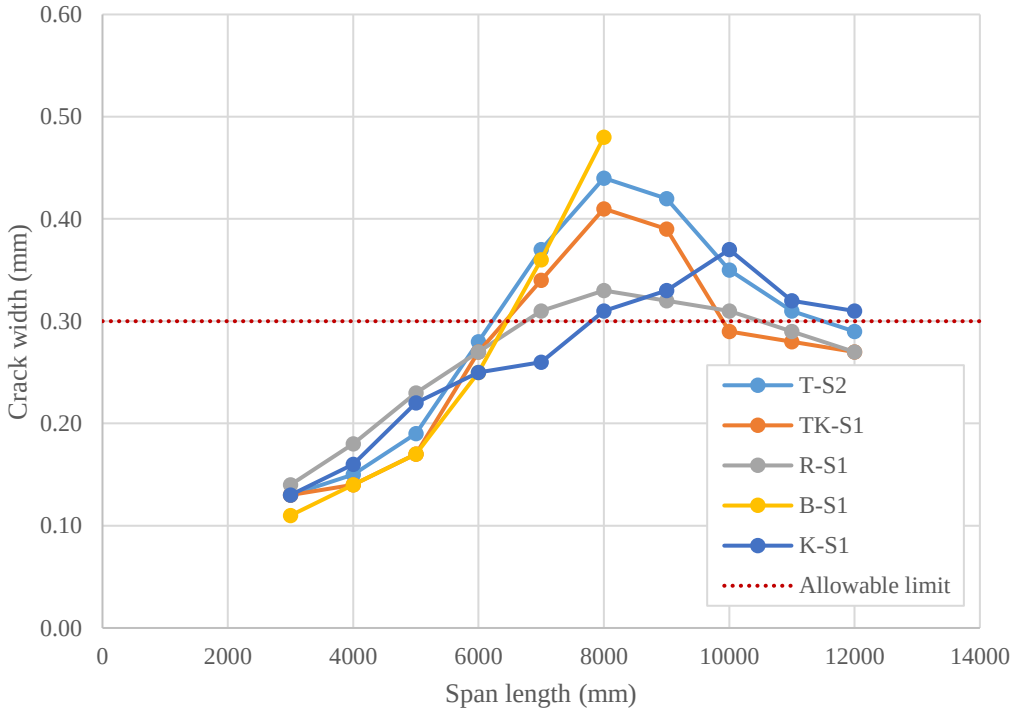

Figure 7.15: Maximum crack width values for beams in set two in the first phase of optimisation

7.4.2 Phase two

In the second phase of optimisation, the shape optimisation method described in §4.7.2.1 was used to add material back to the beams so as to satisfy the serviceability limit states.

In Table 7.2, a summary of the amount of material saved in both optimisation phases is shown. The dependence of reduction in the amount of material used on the shape of the cross-section and span length can be seen. To arrive at the most optimum solution for a specific beam problem, not only is optimisation for material layout along the beam necessary, but also a topology optimisation procedure that can choose the best combination of cross-sectional shape and layout, span length (if possible), support conditions (simply supported or continuous) and shape of the longitudinal profile (shape optimisation) is required.

Table 7.2: The amount of material saved per span length in phases one and two of optimisation for beams in set two

	Material saved (%)									
Beam	**R-S2**		**B-S2**		**K-S2**		**TK-S2**		**T-S2**	
Phase / **Span (mm)**	*Ph1*	*Ph2*	*Ph1*	*Ph2*	*Ph1*	*Ph2*	*Ph1*	*Ph2*	*Ph1*	*Ph2*
3000	4	1	0	0	0	0	0	0	0	0
4000	17	11	6	4	10	7	6	4	8	5
5000	23	16	16	13	20	15	14	11	15	11
6000	31	20	11	6	26	19	21	21	21	21
7000	35	21	9	-8	29	23	25	20	23	18
8000	35	16	3	-17	34	26	26	18	24	17
9000	40	20	-6	-	36	26	29	19	27	16
10000	43	24	-19	-	37	21	31	20	28	19
11000	41	23	-	-	36	21	26	22	25	21
12000	38	22	-	-	34	17	21	21	19	19

The volume of the optimised beams is larger than an equivalent-in-strength prismatic beam.

The optimised shapes of two of the continuous beams and their equivalent strength prismatic beam are shown in Figure 7.16 and Figure 7.17 before and after the application of both phases of optimisation.

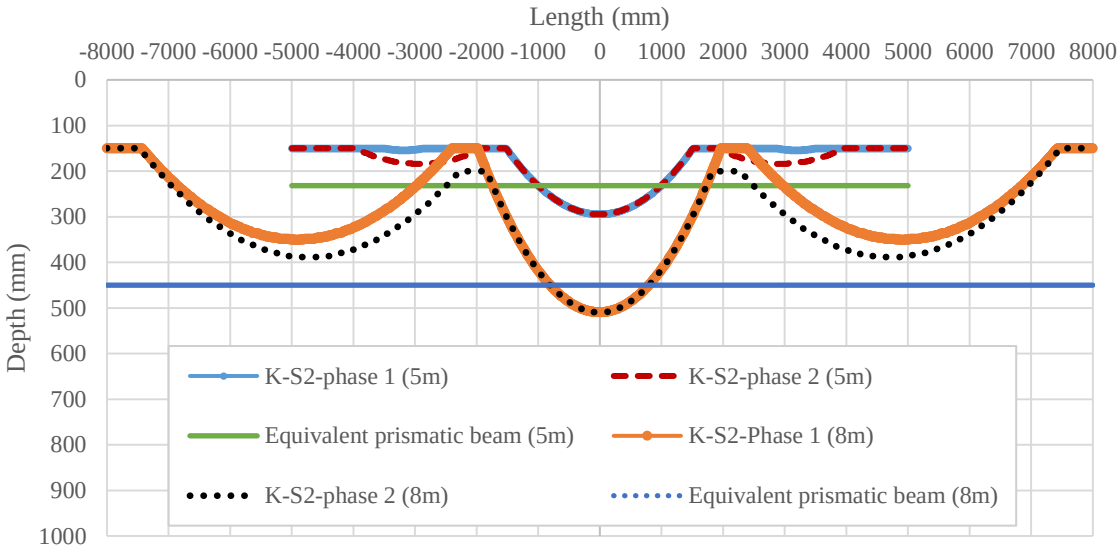

Figure 7.16: Keyhole section beam in both phases of optimisation for span lengths 5m and 8m

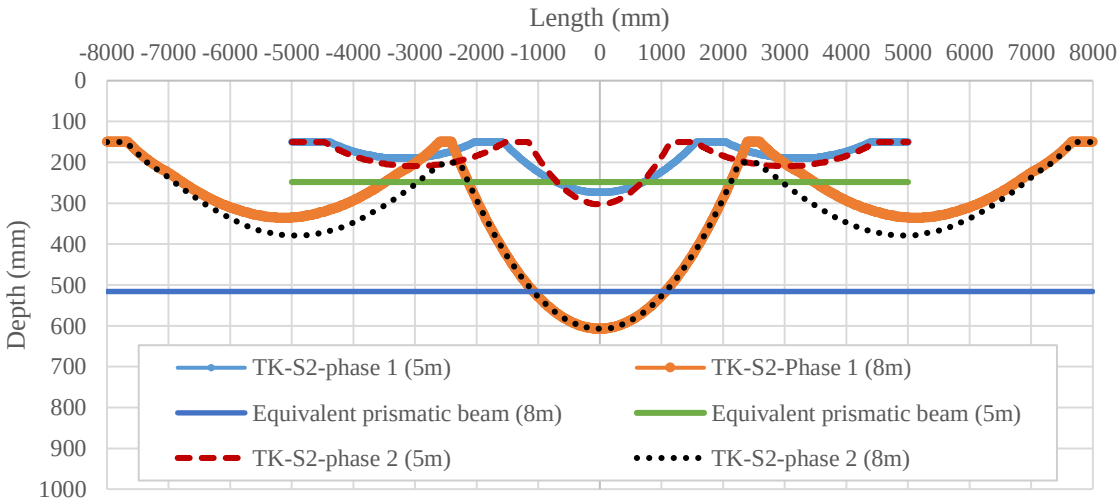

Figure 7.17: T-keyhole section beam in both phases of optimisation for span lengths 5m and 8m

For beam K-S2, which has no flange, additional material in the serviceability optimisation procedure was added to both hogging and sagging regions (5m). This was done based on choosing the region where adding material offers highest level of improvement in stiffness. All beams had a cross-section in the hogging region deeper than that of equivalent prismatic beam. The reason behind this is the difference between the applied moment distribution (including redistributed moments) for the optimised and equivalent prismatic beams.

7.5 Conclusion

In this chapter, a parametric study conducted to show the performance of the optimisation methods is presented. Both statically determinate and indeterminate beams were considered. The results showed that, the amount of material saved when optimising for strength, the necessity for further optimisation for serviceability and the amount of material saved after optimisation for serviceability are highly dependent on the cross-sectional shape and layout, and span length of the beam. A maximum reduction of material of 28% was achieved for simply supported beams (rectangular section shape) and 26% for continuous beams (keyhole section shape) after optimisation for both strength and serviceability compared with equivalent prismatic beams.

[Blank Page]

Chapter eight

Conclusions and future work

8.1 Introduction

This research has been carried out to investigate the behaviour and optimisation of statically determinate and indeterminate fabric-formed concrete beams. Two methods developed to predict the serviceability behaviour of non-prismatic concrete beams; the combined-interaction method and the sectional-segmental stiffness method. The combined-interaction method accounts for different full and partial bond interaction regions between the reinforcement and concrete and simulates the cracking behaviour. The 'register-eliminate' algorithm to support the combined-interaction method was developed to find the location of cracks based on the highest cracking index which represents the highest possibility of occurrence of cracks. The sectional-segmental stiffness method, in conjunction with the combined-interaction method, was developed to analyse and predict the behaviour of statically indeterminate concrete beams.

Three methods were developed to optimise statically determinate beams for serviceability, and statically indeterminate beams for both serviceability and strength: 1) the maximum curvature method which optimises simply supported concrete beams for deflections and crack widths; 2) the stable state method which optimises continuous beams for strength; and 3) the point-of-maximum-influence method to optimise continuous concrete beams for serviceability.

8.2 Main conclusions

1. In this work, a novel method developed to predict the serviceability behaviour (cracking and deflections) of non-prismatic concrete beams which was successful in achieving reasonably accurate results.

2. A new topology optimisation method was developed in this work which can successfully optimise statically determinate concrete beams for both strength and serviceability with up to 30% reduction in concrete material compared to an equivalent prismatic beam.

3. The optimisation models developed in this work where successful in producing statically indeterminate concrete beams which are optimised for both strength and serviceability with a reduction in concrete material compared to an equivalent prismatic beam.

4. This work successfully transforms flexible-formwork research into the realms of fully form-found (structurally optimised) structures which satisfy both strength and serviceability. It also opens up the possibility for fabric-formed concrete structures to be used with confidence.

8.3 Predictions of behaviour

8.3.1 Statically determinate beams

In Chapter Three, the prediction methods mentioned in the previous section were presented. In Chapters Five and Six, an experimental program which was carried out to verify those methods was described and a discussion of the results was given. The main conclusion of the results obtained from the work are outlined as below:

1. A sectional analysis procedure is found to be a suitable method to analyse concrete beams; it is comparatively simple, accurate, and compatible with the other prediction and optimisation methods implemented in this work for fabric-formed concrete beams (prediction of behaviour, optimisation and form-finding).

2. In the experimental program performed in this work, the proposed combined-interaction method offered reasonably good predictions for crack patterns and crack widths for the simply supported beams. However, the predictions made by the partial-interaction method varied significantly depending on the loading level and specimen type.

3. The full- and partial-interaction methods address the serviceability behaviour of simply supported concrete beams according to different concrete-reinforcement bond interaction

methods. However, neither method is capable of simulating the cracking behaviour of non-prismatic concrete beams.

4. The partial-interaction method, which is based upon a discrete crack approach, predicts cracks through bond-stress transfer only and so ignores the cracks which may form in the full-interaction regions. This makes the accuracy of this method highly dependent on the geometry, cross-sectional layout and material properties of the analysed beam.

5. The full-interaction method does not account for the effect of tension-stiffening and therefore an overestimation of deflections can be seen at serviceability compared to the predictions made by the combined-interaction method which considers the tension-stiffening effect on increasing the stiffness of the beams.

6. The combined-interaction method, which finds deflections from the contribution of crack rotations (in the partial-interaction regions) and curvature (in the full-interaction regions), exhibited fairly good predictions for deflections at serviceability. This indicates that, this method has been successful in simulating the reinforcement-concrete bond interaction over different regions along the beam.

7. At final stages of loading beyond the service load level, all three interaction methods showed similar predictions for deflection and overestimated stiffness. The reason may be that at the final loading stages, cracks are widely spread and the basic assumptions made to derive these methods may no longer be valid. These assumptions for instance are: plane section are assumed to stay plane after bending, and the crack trajectories are assumed to develop perpendicular to the longitudinal axis of the beam.

8. The partial- and full-interaction methods overpredict the bar strain in the reinforcement at the cracking stage whilst the predictions made by the combined-interaction are close matches of the experimental values. This shows that the proposed combined-interaction method is capable of accurately predicting bond interaction behaviour between the concrete and reinforcing bars and the behaviour of concrete beams at section level.

9. Generally, it can be seen that there is fairly close agreement between the experimental bar strains and those predicted by the combined-interaction and full-interaction methods after cracking. The partial-interaction method, however, overestimated the experimental values in many cases. This is because the partial-interaction method underestimates the number of cracks and ignore the contribution of curvature to deflections at this stage.

8.3.2 Statically indeterminate beams

1. The average and maximum crack width values for the prismatic continuous beam was slightly underestimated by the combined-interaction method. However, the cracking pattern which characterizes the cracking spacing, variation in crack widths along the length of the specimen and the number of cracks was predicted reasonably accurately at serviceability loading.

2. For the optimised continuous beams, the accuracy of prediction for crack widths and cracks number varied from moderate to good predictions depending on the load level and beam specimen. Generally, the predictions were acceptably accurate.

3. Inaccurate predictions by any of the methods for finding the cross-sectional moment-curvature (or moment-rotation) stiffness values would affect the values of the calculated applied moments. This will in turn lead to further inaccuracy in predicting the behaviour of statically indeterminate concrete beams.

4. The smeared cracks approach (full-interaction) appears to be highly inaccurate for continuous concrete beams because the sectional stiffness values (EI) achieved from this method produce a moment distribution that does not match the actual values. This makes this method considerably overestimate deflections.

5. The experimental pre-cracking stiffness was overestimated by both the combined-interaction and full-interaction methods for all continuous beams because both methods rely on the full-interaction mechanism to find stiffness at the elastic stage.

6. The load-deflection response predicted by the combined-interaction method was in a good agreement with the experimental data at serviceability. This indicates that the model was successful in predicting the interaction behaviour between the concrete and reinforcing bars and the actual stiffness distribution for continuous beams.

7. The initial cracking load was over-predicted by the full-interaction method for the optimised continuous beams whilst the combined-interaction method showed good predictions.

8. The relationship between the strain in the steel bars and the total load was shown to be in a reasonably good agreement with the combined-method predictions for the prismatic continuous beam.

9. The actual and predicted load-strain responses in all continuous beams indicated that using the combined-interaction method in conjunction with the stiffness method to calculate the applied moments yielded a more accurate moment distribution than when the full-interaction method was used with the stiffness method.

10. The total load at which the steel bars yield predicted by the combined-interaction method was shown to be in a good agreement with the experimental values. The full-interaction method overpredicted this value in the sagging regions and underpredicted it in the hogging region due to the difference between the actual moment values and those predicted by this method (in combination with the stiffness method).

11. The cross-sectional behaviour of the beams is governed by the behaviour of the concrete and reinforcing bars. Accurate predictions of the bar strains by the combined-interaction method implies that the method can successfully simulate the behaviour of reinforced concrete beam sections.

8.4 Optimisation

The optimisation methods developed in this thesis are described in Chapter Four. In parallel with verifying the prediction models, the experimental program and test results described in Chapters Five and Six were also aimed at assessing the optimisation targets. The main conclusions are briefly given below.

8.4.1 Statically determinate beams

1. The proposed serviceability optimisation method (topology optimisation) was successful at increasing the overall flexural stiffness of the simply supported beam optimised for strength and serviceability compared to the beam which was optimised for strength only.

2. For the small lab-sized simply supported concrete beams, the proposed optimisation methods successfully achieved a concrete beam shape which uses 17% less concrete material in the web than a strength-equivalent prismatic concrete beam without compromising the serviceability limit states.

3. The topology optimisation procedure proposed in this work was successful in altering the cracking pattern so that cracks are scattered over closer intervals with smaller crack width values.

4. The serviceability optimisation method was successful in reducing average and maximum crack widths and also the number of cracks at serviceability.

5. The proposed combined-interaction method was reasonably accurate in predicting the cross-sectional behaviour and the total load at which the tensile bars yield. Therefore, this method can be considered as a good method to base the strength optimisation on.

6. The results from the parametric analysis conducted in this work show that the amount of material saved for simply supported beams after optimisation for both strength and

serviceability increases with the increase of span length. A maximum reduction in concrete material of 28% was achieved for rectangular beams for a 12m span beam.

8.4.2 Statically indeterminate beams

1. The failure load of the prismatic and fabric-formed continuous beams tested in the experiments carried out in this work were in a good agreement with the design failure load. Both beams were designed according to failure mode two (see §4.7.1.2) and failed as predicted. This implies that, continuous concrete beams can confidently be optimised for strength using the proposed method.

2. The T-section optimised continuous beam (T-OSS-C), which was also designed according to failure mode two, exhibited a premature failure at a load equal to about 92% of the design load. This is possibly due to buckling of the compression bars.

3. The failure mode of the T-section beam indicates that the compression bars in the hogging region may start to buckle outwards, cause spalling of the concrete cover and result in premature failure of the beam. Therefore, a minimum radius of curvature of the longitudinal profile in the hogging region should be specified as an optimisation constraint in the strength optimisation procedure.

4. Assessing the cross-sectional behaviour through monitoring strain in the reinforcing bars showed a good agreement between the experimental and predicted data using the proposed combined-interaction method. In most cases, a high level of sectional strength utilisation indicates successful implementation of the strength optimisation method in conjunction with the combined-interaction method.

5. Reasonably accurate predictions achieved for the crack widths and deflections by the combined-interaction method allows using this method in combination with the serviceability optimisation methods for continuous beams with confidence.

6. The experimental crack width values of the optimised beams were close to those of the equivalent strength prismatic beam in most cases. This confirms that the serviceability optimisation method has been successful in limiting crack width values.

8.5 Future work

The research work conducted in this thesis has aided developing of appropriate methods to optimise statically determinate and indeterminate concrete beams for both strength and serviceability. This work has also helped developing prediction methods which can accurately simulate the serviceability behaviour of non-prismatic and fabric-formed concrete beams, both statically determinate and indeterminate. However, there are still many aspects that requires thorough investigation and research.

8.5.1 Analysis of behaviour of non-prismatic concrete beams

The combined-interaction method developed in this thesis offers relatively good predictions of serviceability behaviour of non-prismatic concrete beams. However, the prediction can be improved and the method needs further verification against a broader range of possibilities to ensure that it is a robust and reliable method to predict the serviceability behaviour of non-prismatic concrete beams. Two aspects for further research work in this area are presented below.

8.5.1.1 The area of tension prism

The area of the tension prism A_c presented in §3.3.2 was assumed to be twice as the concrete cover times the width of the beam. This assumption was originally made for prismatic concrete beams by CEB-FIP (2010). For fabric-formed beams, the cross-section shape is different from that of a prismatic beam. In addition, the total section depth varies along the beam and so the actual area of the tension prism area may vary too depending on the nature of interaction between the concrete and reinforcing bars. Therefore, further research work in this area may be needed to address this aspect.

8.5.1.2 Reinforcement type

The experimental program carried out in this thesis deals with concrete beams reinforced with steel bars. The methodology developed in this thesis is applicable to concrete beams reinforced with other types of reinforcement such as FRP bars, if the relevant bond-slip relationship is available. However, experimental verification is required to assess the validity of the methods when a reinforcement type other than deformed steel bars is used.

8.5.2 Optimisation of concrete structures

In this work, shape and topology optimisation methods for fabric-formed concrete beams were presented which can successfully reduce the amount of concrete material needed without compromising serviceability limit states. Although a high number of possibilities were considered in the parametric analysis carried out in Chapter Seven, such as different steel ratio, span length, supporting conditions and applied loads, only cross-sectional depth was taken as the optimisation variable. A cost- or material- optimisation for concrete members needs to look at different

combinations of cross-sectional and material properties to arrive at an optimum final design. For instance, different steel ratios per section area can be used to gauge the flexural strength and flexural stiffness values to achieve a specific beam shape, especially in case of continuous concrete beams. This often requires a probabilistic optimisation method which varies several geometric and material variables simultaneously until an optimum design in terms of minimum cost, material, or embodied carbon is achieved. Such a probabilistic optimisation method can be combined with the proposed shape or topology optimisation methods to achieve the highest possible level of optimisation on both member and structure level.

8.5.3 Prediction of behaviour and optimisation of fabric-formed concrete slabs

Slabs are usually make up a high amount of the concrete material in a typical concrete structure. Therefore, optimisation of such members will bring about a high level of reduction in embodied carbon energy. The optimisation methods presented in this thesis deal with concrete beams in which out of plain stresses are ignored. For concrete slabs, stresses in different planes play important roles in articulating behaviour depending on the support conditions. Investigation in this area to develop shape optimised fabric-formed concrete slabs is suggested. The construction of such slabs in fabric forms may also need experimental and theoretical research work to arrive at a feasible, cost-effect method of forming.

[Blank Page]

[Blank Page]

References

A

ACI 318-08, 2008. *Building Code Requirements for Structural Concrete and Commentary*, American Concrete Institute, Miami, ACI Committee 318.

ACI Committee 435, 2000. *Control Of Deflection In Concrete Structures*, *ACI 435R-95.*

Ashby, M. F., 2013. *Materials And The Environment* : *Eco-informed Material Choice*. Elsevier, 2012.

Bagge, N., et al., 2014. *Moment Redistribution in RC Beams – A Study of The Influence of Longitudinal and Transverse Reinforcement Ratios and Concrete Strength,* Engineering Structures 80: 11-23.

B

Bailiss, J., 2006. *Fabric-Formed Concrete Beams Design and Analysis*, Architecture and Civil Engineering, University of Bath. MEng.

Bazant, Z. P. and Oh, B. H., 1984. *Deformation of Progressively Cracking Reinforced Concrete Beams,* ACI Journal 81(3): 268-278.

Bendose, M. P. and Sigmound, O., 2003. *Topology Optimisation: Theory, Methods and Applications*, Springer.

Browne, P. A., 2013. *Topology Optimization of Linear Elastic Structures*. Department of Mathematical Sciences, University of Bath. PhD.

BS 8110-1, 1997. *Structural Use of Concrete, Code of Practice for Design and Construction*, UK, British Standards Institution.

BS EN 1990:2002 +A1, 2005. Eurocode - *Basis of Structural Design.*

BS EN 1991-1-1:2002, 2004. Eurocode 1: *Actions on Structures.*

BS EN 1992-1-1, 2004. Eurocode 2: *Design of Concrete Structures.*

BS EN 12390-1, 2000. *Testing Hardened Concrete*.

C

Camp, C. V. and Huq, F., 2013. *CO2 and Cost Optimization of Reinforced Concrete Frames Using a Big Bang-Big Crunch Algorithm,* Engineering Structures 48: 363-372.

CAST, 2007. *The Centre for Architectural Structures And Technology (C.A.S.T),* Retrieved 14/07/2016, 2016, from http://www.arrodesign.org/fabric-formed-concrete/f-f-concrete-for-structures/.

CEB-FIP, 2010a. *Model Code,* Switzerland International Federation for Structural Concrete (fib).

CEB-FIP, 2010b. *Model Code,* Switzerland, International Federation for Structural Concrete (fib).

Chandler, A. and Pedreschi, R., 2007. *Fabric Formwork,* London, RIBA Publishing.

D

Degertekin, S. O., 2007. *A Comparison of Simulated Annealing and Genetic Algorithm for Optimum Design of Nonlinear Steel Space Frames,* Structural and Multidisciplinary Optimization 34(4): 347-359.

Ding, Y., 1986. *Shape Optimisation Of Structures: A Literature Survey*, Computers & Structures 24(6): 985-1004.

Du, J. S., et al., 2016. *Deflection of Unbonded Partially Prestressed Concrete Continuous Beams,* Engineering Structures 118: 89-96.

Dundar, C., et al., 2015. *Prediction of Load–Deflection Behaviour of Multi-Span FRP and Steel Reinforced Concrete Beams,* Composite Structures 132: 680-693.

E

El-Mogy, M., et al., 2009. *GFRP-Reinforced Continuous Beams*, The Second Official International Conference of International Institute for FRP in Construction for Asia-Pacific region. Seoul, Korea.

F

Fedghouche, F. and Tiliouine, B., 2012. *Minimum Cost design of Reinforced Concrete T-beams at Ultimate Loads Using Eurocode2*, Engineering Structures 42: 43-50.

Ferreira, C. C., et al., 2003. *Optimal Design of Reinforced Concrete T-sections in Bending*, Engineering Structures 25(7): 951-964.

Foster, R., 2010. *Form Finding and Analysis of Fabric Formed Concrete Beams*, Architecture and Civil Engineering, University of Bath. MEng.

G

Galileo, 1638. *Dialogues: Concerning Two New Sciences*.

Garbett, J. and Ibell, T., 2008. *Bone Growth Analogy for Optimising Flexibly Formed Concrete Beams*, Department of Architecture and Civil Engineering, University of Bath. MEng.

Ghaib, M. A. A. and Gorski, J., (2001). *Mechanical Properties of Concrete Cast In Fabric Formworks*, Cement and Concrete Research 11: 1459-1465.

Ghasemzadeh, F., et al., 2016. *Predicting long-term compressive creep of concrete using inverse analysis method*, Construction and Building Materials 124: 496-507.

Gilbert, R. I., 2011. *The Serviceability Limit States in Reinforced Concrete Design*, Procedia Engineering 14: 385-395.

Govindaraj, V. and Ramasamy, J. V., 2005. *Optimum Detailed Design of Reinforced Concrete Continuous Beams Using Genetic Algorithms*, Computers & Structures 84(1-2): 34-48.

Gribniak, V., et al., 2013. *Deflection Prediction of Reinforced Concrete Beams by Design Codes and Computer Simulation*, Engineering Structures 56: 2175-2186.

H

He, Z., et al., 2007. *The Trilinear Moment vs. Curvature Relationship of Concrete Beams Reinforced with Fiber Reinforced Polymer (FRP) Rebars*, Composite Structures 77(1): 30-35.

I

Iosilevskii, G., 2010. *Shape of a Soft Container Under Hydrostatic Load*, Journal of Applied Mechanics 77(1): 014501.

K

Kalkan, I., 2010. *Deflection Prediction for Reinforced Concrete Beams Through Different Effective Moment of Inertia Expressions,* Int.J.Eng. Research & Development 2(1): 72-80.

Kara, I. F. and Dundar, C., 2009. *Effect of Loading Types and Reinforcement Ratio on an Effective Moment of Inertia and Deflection of a Reinforced Concrete Beam,* Advances in Engineering Software 40(9): 836-846.

Karihaloo, B. L. and Kanagasundaram, S., 1987. *Optimum Design Of Statically Indeterminate Beams Under Multiple Loads,* Computers & Structures 26(3): 521-538.

Kostova, K., et al., 2013. *Sustainable Concrete Construction Using Fabric Formwork,* Future Build.

Kripka, M., et al., 2015. *Use of Optimization for Automatic Grouping of Beam Cross-Section Dimensions in Reinforced Concrete Building Structures,* Engineering Structures 99: 311-318.

Kwak, H.-G. and S.-P. Kim, 2002. *Non-Linear Analysis of RC Beams Based Of Moment-Curvature Relation,* Computers & Structures 80: 615-628.

L

Lamberton, B. A., 1968. *Method of Forming Concrete Bodies,* U.S Patent Office. 3396545.

Landry, C., 2012. *The Art of City Making,* Rutledge.

Lee, D. S.-H., 2011. *Study of Construction Methodology and Structural Behaviour of Fabric-Formed Form-Efficient Reinforced Concrete Beam,* The University of Edinburgh. PhD.

Lepš, M. and Sejnoha, M., 2003. *New Approach to Optimization of Reinforced Concrete Beams,* Computers & Structures 81(18-19): 1957-1966.

Lilienthal, L. W. G., 1899. *Fireproof Ceiling,* U.S Patent Office.619769.

Long, G., et al., 2015. *Designing More Sustainable and Greener Self-Compacting Concrete,* Construction and Building Materials 84: 301-306.

Lou, T., et al., 2016. *Response of Continuous Concrete Beams Internally Prestressed with Unbonded FRP and Steel Tendons,* Composite Structures 154: 92-105.

M

Malvar, L. J. and Fourney, M. E., 1990. *A Three Dimensional Application of the Smeared Crack Approach,* Engineering Fracture Mechanics 35(1/2/3): 251-260.

Meyer, C., 2009. *The Greening of The Concrete Industry,* Cement and Concrete Composites 31(8): 601-605.

Miller, D., et al., 2015. *Concrete Slab Comparison and Embodied Energy Optimisation for Alternate Design and Construction Techniques,* Construction and Building Materials 80: 329-338.

Muhamad, R., et al., 2013. *Discrete Rotation Deflection Of Reinforced Concrete Beams At Serviceability,* Proceedings of the Institution of Civil Engineers - Structures and Buildings 166(3): 111-124.

N

Neville, A. M., 1996. *Properties of Concrete*.

Ng, P. L., et al., 2011. *Effects of Concrete-to-Reinforcement Bond and Loading Conditions on Tension Stiffening*, Procedia Engineering 14: 704-714.

O

Oehlers, D. J., et al., 2013. *Serviceability Flexural Ductility of FRP RC Beams: a Discrete Rotation Approach,* Construction and Building Materials 49: 974-984.

Orr, J., 2012. *Flexible Formwork for Concrete Structures*, Architecture and Civil Engineering, University of Bath. PhD.

Orr, J., et al., 2012. *Optimisation and Durability in Fabric Cast Double T-Beam*, Second International Conference on Flexible Formwork (icff2012).

Orr, J., et al., 2011. *Concrete Structures Using Fabric Formwork,* The Structural Engineer 89: 97-105.

P

Pronk, A. D. C., et al., 2013. *Rigid Inflatable Structures, a Production Method for Optimised Structures",* Proceedings of the International Association for Shell and Spatial Structures (IASS) Symposium 2013, Beyond The Limits of Man, Poland.

Purnell, P., 2013. *The Carbon Footprint of Reinforced Concrete,* Advances in Cement Research 25(6): 362-368.

R

Rath, D. P., et al., 1999. *Shape Optimisation of RC Flexural Members,* Journal of Structural Engineering 125(12): 1439-1447.

Reynolds, C. E., et al., 2007. *Reinforced Concrete Designer's Handbook.*

S

Sakai, K. and Noguchi, T., 2012. *The Sustainable Use of Concrete.*

Sancho, J. M., et al., 2007. *An Embedded Crack Model for Finite Element Analysis of Concrete Fracture*, Engineering Fracture Mechanics 74(1-2): 75-86.

Shams, S., et al., 2011. *A Comparative Analysis of Building Materials for Sustainable Construction with Emphasis on CO2 Reduction,* International Journal of Environmental and Sustainable Development 10(4): 364-374.

Shepherd, B., A. and Richens, P., 2012. *Intuitive Interactive Form-finding of Optimised Fabric Cast Concrete,* Second International Conference on Flexible Formwork (icff2012). University of Bath.

T

Thirion, C., 2012. *Putting Material to The Right Place: Investigations Into the Sustainable Use of Structural Materials to Reduce the Embodied Environmental Impact of Building Structures,* University College London.

U

USGS, 1996. *Minerals Information,* Retrieved 29/07, 2016, from http://minerals.usgs.gov/minerals/pubs/commodity/cemen.

V

Veenendaal, D., 2008. *Evolutionary Optimization Of Fabric Formed Structural Elements*, Delft University of Technology. Master's degree.

Veenendaal, D., et al., 2011. *Design and Optimization of Fabric-Formed Beams and Trusses: Evolutionary Algorithms and Form-Finding,* Structural Concrete 12(4): 241-254.

Veenendaal, D., et al., 2011. *History and Overview of Fabric Formwork: Using Fabrics for Concrete Casting,* Structural Concrete 12(3): 164-177.

Visintin, P., et al., 2013. *Partial-Interaction Short Term Serviceability Deflection of RC Beams,* Engineering Structures 56: 993-1006.

W

Waller, J. H. D. W., 1934. *Method of Building with Cementitious Material Applied to Vegetable Fabrics*, U.S Patent Office.1955716.

West, M., 2001. *Fabric-Formed Concrete Structures*, First International Conference on Concrete and Development, Tehran, Iran.

Y

Yang, Z. J. and Chen, J., 2005. *Finite Element Modelling of Multiple Cohesive Discrete Crack Propagation in Reinforced Concrete Beams*, Engineering Fracture Mechanics 72(14): 2280-2297.

Z

Zhong, Y. and Wu, P. 2015. *Economic sustainability, environmental sustainability and constructability indicators related to concrete- and steel-projects*, Journal of Cleaner Production 108: 748-756.

[Blank Page]

[Blank Page]